THE MOLECULAR BASIS OF DIABETIC CARDIOMYOPATH

Ahmed Salaheldin Mustafa Ali Sultan

DOCTORATE DISSERTATION NO. 2022:16

College of Medicine and Health Sciences

THE MOLECULAR BASIS OF DIABETIC CARDIOMYOPATHY

Ahmed Salaheldin Mustafa Ali Sultan

September 2022

United Arab Emirates University

College of Medicine and Health Sciences

THE MOLECULAR BASIS OF DIABETIC CARDIOMYOPATHY

Ahmed Salaheldin Mustafa Ali Sultan

This dissertation is submitted in partial fulfilment of the requirements for the degree of Doctor of Philosophy in Biomedical Sciences

September 2022

Cover: Zucker Diabetic rats in their cage

(Photo: By Ahmed Salaheldin Mustafa Ali Sultan)

Declaration of Original Work

I, Ahmed Salaheldin Mustafa Ali Sultan, the undersigned, a graduate student at the United Arab Emirates University (UAEU), and the author of this dissertation entitled "*The Molecular Basis of Diabetic Cardiomyopathy*", hereby, solemnly declare that this dissertation is my own original research work that has been done and prepared by me under the supervision of Professor Frank Christopher Howarth, in the College of Medicine and Health Sciences at UAEU. This work has not previously formed the basis for the award of any academic degree, diploma or a similar title at this or any other university. Any materials borrowed from other sources (whether published or unpublished) and relied upon or included in my dissertation have been properly cited and acknowledged in accordance with appropriate academic conventions. I further declare that there is no potential conflict of interest with respect to the research, data collection, authorship, presentation and/or publication of this dissertation.

Student's Signature: _____

Date: 14/9/22

Advisory Committee

1) Advisor: Prof. Frank Christopher Howarth

Title: Professor

Department of Physiology

College of Medicine and Health Sciences

2) Co-advisor: Prof. Anatoliy Shmygol

Title: Professor

Department of Physiology

College of Medicine and Health Sciences

3) Member: Prof. Ernest Adeghate

Title: Professor

Department of Anatomy

College of Medicine and Health Sciences

4) Member: Dr. Starling Emerald

Title: Associate Professor

Department of Anatomy

College of Medicine and Health Sciences

Approval of the Doctorate Dissertation

This Doctorate Dissertation is approved by the following Examining Committee Members:

1) Advisor (Committee Chair): Prof. Frank Christopher Howarth

   Title: Professor

   Department of Physiology

   College of Medicine and Health Sciences

   Signature: Date: 14/9/22

2) Member: Prof. Ernest Adeghate

   Title: Professor

   Department of Anatomy

   College of Medicine and Health Sciences

   Signature: Date: 14/9/22

3) Member: Prof. Mauro Pessia

   Title: Professor

   Department of Physiology

   College of Medicine and Health Sciences
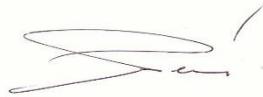
   Signature: Date: 14/9/22

4) Member (External Examiner): Prof. Saadeh Suleiman

   Title: Professor

   Department of Physiology, Faculty of Health Sciences

   Institution: University of Bristol, UK
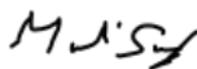
   Signature: Date: 14/9/22

This Doctorate Dissertation is accepted by:

Acting Dean of the College of Medicine and Health Sciences: Professor Juma Al Kaabi

Signature _____
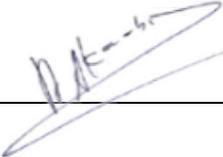
Date 06/October/2022

Dean of the College of Graduate Studies: Professor Ali Al-Marzouqi

Signature ___ Ali Hassan ___

Date _____ 06/10/2022 ___

Abstract

Diabetes mellitus (DM) is a major and worsening global health problem. Type 2 diabetes mellitus (T2DM) accounts for more than 90% of DM and the global epidemic of obesity largely explains the dramatic increase in the incidence and prevalence of T2DM over the past 20 years. Cardiovascular complications are the major cause of morbidity and mortality in diabetic patients. The electrocardiogram (ECG) of diabetic and obese patients is frequently disturbed. The aim of this project was to characterize and clarify the molecular basis of electro-mechanical dysfunction in the hearts of type 2 diabetic and type 2 diabetic/obese rats. Experiments were performed in Zucker diabetic fatty (ZDF), Zucker fatty (ZF) and Zucker lean (ZL) rats. *In vivo* biotelemetry experiments were performed to establish how the ECG was altered by diabetes and diabesity. Experiments were also carried out in isolated heart to further investigate how diabetes and diabesity affects the electrical conduction system of the heart. Cell imaging was employed to assess ventricular myocyte shortening. Fluorescence photometry and whole-cell patch-clamp techniques were used to assess the effects of diabetes and diabesity on ion channel currents. Molecular biology and electron microscopy techniques were employed to assess proteins and structures associated with cardiac muscle contraction. Heart rate (HR) was reduced by ageing and by diabesity in the absence of changes in physical activity and body temperature. Reductions in heart rate variability linked with altered sympathovagal drive may partly underlie disturbed HR in the ZDF rat even in the absence of autonomic nervous system control in the isolated perfused heart. Amplitude of shortening is generally well preserved in ZDF myocytes. There was evidence of altered time course of the Ca^{2+} transient and shortening in ventricular myocytes from ZDF rat. Molecular and structural defects in the ZF and ZDF rat heart were observed. The results suggest that sarcoplasmic reticulum (SR) Ca^{2+} handling as well as energy utilization are compromised in ZDF and ZF myocytes. Myocyte contraction and relaxation may also be affected in the ZDF and ZF rat due to protein and ventricular structural defects. Isoprenaline was less effective at generating an increase in the AMP of shortening in ZDF and ZF compared to ZL myocytes and defects in Ca^{2+} signaling, and in particular SR Ca^{2+} transport, might partly underlie these abnormalities.

Title and Abstract (in Arabic)

الأساس الجزيئي لاعتلال عضلة القلب السكري

الملخص

مرض السكري (DM) هو مشكلة صحية عالمية رئيسية وتزداد سوءًا. يمثل داء السكري من النوع 2 (T2DM) أكثر من 90٪ من DM ، ويفسر وباء السمنة العالمي إلى حد كبير الزيادة الهائلة في حدوث وانتشار T2DM على مدار العشرين عامًا الماضية. مضاعفات القلب والأوعية الدموية هي السبب الرئيسي للمراضة والوفيات في مرضى السكري. كثيرًا ما يُضطرب مخطط كهربية القلب (ECG) لمرضى السكري والسمنة. كان الهدف من هذا المشروع هو توصيف وتوضيح الأساس الجزيئي للخلل الوظيفي الكهروميكانيكي في قلوب مرضى السكري من النوع 2 والسكري من النوع 2 / السمنة. أجريت التجارب على جرذان زوكر المصابة بداء السكري (ZDF) وفئران زوكر الدهنية (ZF) وفئران زوكر الخالية من الدهون (ZL). أجريت تجارب القياس الحيوي في الجسم الحي لتحديد كيفية تغيير تخطيط القلب بسبب مرض السكري والسمنة السكرية. وأجريت التجارب أيضًا في القلب المنعزل لمزيد من التحقيق في كيفية تأثير مرض السكري و السمنة السكرية على نظام التوصيل الكهربائي للقلب. تم استخدام التصوير الخلوي لتقييم تقصير الخلايا العضلية البطينية. تم استخدام تقنيات قياس الضوء الفلوري ومشبك الخلية الكاملة لتقييم آثار مرض السكري و السمنة السكرية على القنوات الأيونية. تم استخدام تقنيات البيولوجيا الجزيئية والمجهر الإلكتروني لتقييم البروتينات والهياكل المرتبطة بانقباض عضلة القلب. انخفض معدل ضربات القلب (HR) مع التقدم في السن والسكري مع عدم وجود تغيرات في النشاط البدني ودرجة حرارة الجسم. قد تكمن التخفيضات في تقلب معدل ضربات القلب المرتبطة بمحرك الودي المهبلي المتغير جزئيًا وراء اضطراب الموارد البشرية في الجرذ ZDF حتى في غياب التحكم في الجهاز العصبي اللاإرادي في القلب المعزول المروي. يتم حفظ سعة السمن جيدًا بشكل عام في الخلايا العضلية ZDF. كان هناك دليل على المسار الزمني المتغير لـCa^{2+} عابر وتقصير في الخلايا العضلية البطينية من الفئران ZDF. لوحظت عيوب جزيئية وتركيبية في قلب الجرذان ZF و ZDF. تشير النتائج إلى أن معالجة الشبكة الساركوبلازمية Ca^{2+}(SR) وكذلك استخدام الطاقة تتعرض للخطر في الخلايا العضلية ZDF و ZF. قد يتأثر تقلص الخلايا العضلية واسترخائها أيضًا في الجرذان ZDF و ZF بسبب عيوب البروتين والعيوب البطينية الهيكلية. كان Isoprenaline أقل فعالية في توليد زيادة في AMP للتقصير في ZDF و ZF مقارنة بالخلايا العضلية ZL والعيوب في إشارات Ca^{2+} ، وخاصة نقل Ca^{2+} SR ، قد تكمن جزئياً في هذه التشوهات.

مفاهيم البحث الرئيسية: القلب، السكري، السمنة، اعتلال عضلة القلب السكري، جرذ زوكر الدهني السكري، جرذ زوكر الدهني، الجرذ زوكر العجاف.

Author's Contribution

The contribution of Ahmed Sultan to the dissertation was as follows:

I. Participated in planning of the work, had main responsibility for the data collection and processing, and evaluation of results.

II. Participated in planning of the work, had main responsibility for the experimental work, data collection and processing, and evaluation of results.

III. Sole responsibility for planning the research and conducting the experiments.

Author Profile

Ahmed Sultan is a Research Associate currently working in the Physiology Department of the College of Medicine and Health Sciences at United Arab Emirates University in Al Ain. He is a Bachelor of Pharmacy degree holder from University of Sharjah in the UAE and M.Sc. of Pharmacology and Toxicology from UAEU. His current interest is the electrical and mechanical dysfunction of the diabetic heart.

He is a member of the Physiological Society, the largest network of physiologists in Europe which brings together over 4000 scientists from over 60 countries. Since its foundation in 1876, its members have made significant contributions to our knowledge of biological systems and the treatment of disease. Members of the Physiological Society have included numerous Nobel Prize winners from Ivan Pavlov to John O'Keefe.

He also has several publications as first author and a book chapter titled "Cellular and Molecular Effects of Obesity on the Heart" from the book titled "Cellular and Biochemical Mechanisms of Obesity".

Acknowledgements

Dedication

To my beloved parents, family, and most importantly my wife & children for their incredible love and support

Table of Contents

List of Tables

List of Figures

List of Abbreviations

ABSI	Body Shape Index
AET	Aerobic Exercise Training
AF	Atrial Fibrillation
AGTR2	Angiotensin II Receptor Type 2
AMI	Acute Myocardial Infarction
AMP	Amplitude
AMPK	Adenosine Mono Phosphate dependent protein Kinase
ANS	Autonomic Nervous System
AP	Action Potential
APD	Action Potential Duration
ATP	Adenosine Triphosphate
AVN	Atrioventricular Node
BMI	Body Mass Index
BP	Blood Pressure
BPM	Beats Per Minute
BSA	Bovine Serum Albumin
CAD	Coronary Artery Disease
CaMKII	Ca^{2+}/Calmodulin Dependent Protein Kinase II
CaMKIIδ	Ca^{2+}/Calmodulin Dependent Protein Kinase II Delta
CNS	Central Nervous System
CPM	Counts Per Minute
CREB	c-AMP Response Element-Binding protein
CV	Conduction Velocity
CVD	Cardiac Vascular Disease
C_x45	Connexin
DCM	Diabetic Cardiomyopathy
DEKA	Asp-Gly-Lys-Ala
DIO	Diet Induced Obesity
DM	Diabetes Mellitus
DNA	Deoxyribonucleic Acid
ECC	Excitation-Contraction Coupling

ECG	Echocardiogram
EDH	Endothelium Derived Hyperpolarization
ENS	Endosomal System
ET-1	Endothelin-1
FBG	Fasting Blood Glucose
FFFRs	Fructose-Fat Fed Sprague-Dawley rats
GAPDH	Glyceraldehyde 3-Phosphate Dehydrogenase
GD	Gestational Diabetes
GIRK	G-protein Couped Inwardly Rectifying K+ channels
GK	Goto-Kakizaki
Gln	Glycine
GLUT	Glucose Transporter
GSH	Glutathione
GTT	Glucose Tolerance Test
GyG	Glycine-Tyrosine-Glycine
HCN	Hyperpolarization Activated Cyclin Nucleotide Channels
HDL	High Density Lipoproteins
HF	Heart Failure
HFq	High Frequency
HR	Heart Rate
HRV	Hear Rate Variability
I_{CaL}	L-type Ca^{2+} Current
IDF	International Diabetes Federation
IFG	Impaired Fasting Glucose
IGEPAL	Octylphenoxypolyethoxyethano
I_{NCX}	Na^+/Ca^{2+} Exchanger Current
IPC	Ischemic Pre-Conditioning
IR	Insulin Resistance
IRK	Insulin Receptor Kinase
ISO	Isoprenaline
KATP	ATP sensitive K^+ Channels
LBB	Left Bundle Branch
LCFH	Long-Chain Fatty Acids

LepR	Leptin Receptor
LFq	Low Frequency
LVPV	Left Ventricular Pressure Volume
MENA	Middle East and North Africa
MG	Methlyglyoxal
MOPS	3-(N-morpholino) Propanesulfonic Acid
mRNA	messenger Ribonucleic Acid
NCX	Na^+/Ca^{2+} Exchanger
NE	Norepinephrine
NO	Nitric Oxide
NOS	Nitric Oxide Synthase
NT	Normal Tyrode
O-GlcNAc	O-Linked N-Acetylglucosamine
PBS	Phosphate-Buffered Saline
PKD	Protein Kinase D
PLB	Phospholamban
PMSF	Phenylmethylsulfonyl Fluoride
Pro	Proline
PSD	Power Spectral Density
PVDF	Polyvinylidene Fluoride
PVT	Perivascular Tissue
RBB	Right Bundle Branch
RBG	Random Blood Glucose
RCL	Resting Cell Length
RIPA	Radioimmunoprecipitation
RMP	Resting Membrane Potential
RNA	Ribonucleic Acid
RPM	Revolutions Per Minute
rRNA	ribosomal Ribonucleic Acid
RyR	Ryanodine Receptor
SAN	Sinoatrial Node
SCD	Sudden Cardiac Death
SDANN	Standard Deviation of the Average Normal-to-Normal HR

SDS	Sodium Dodecyl Sulfate
SEM	Standard Error of Mean
SERCA	Sarco/Endoplasmic Reticulum Ca^{2+}-ATPase
SMA	Small Mesenteric Artery
SR	Sarcoplasmic Reticulum
SrE	Strain rate Values in Early Diastole
SrIVR	Strain rate Values Isovolumic Relaxation
SrS	Strain rate Values in Systole
STE	Speckle Tracking Echocardiography
T1DM	Type 1 Diabetes Mellitus
T2DM	Type 2 Diabetes Mellitus
THALF	Time To Half
Tm	Tropomyosin
Tn	Troponin
TnC	Troponin C
TnI	Troponin I
TnT	Troponin T
TPK	Time To Peak
tRNA	transfer Ribonucleic Acid
VAs	Ventricular Arrythmias
VLDL	Very Low-Density Lipoproteins
VLDL-TG	Very Low-Density Lipoproteins-Triglyceride
WC	Waist Circumference
WHO	World Health Organization
ZDF	Zucker Diabetic Fatty
ZF	Zucker Fatty
ZL	Zucker Lean
β-AR	β-Adrenergic Receptor

Chapter 1: Introduction

1.1 Heart anatomy and physiology

The heart continuously beats to pump blood and circulate it around our body. The heart is a fibromuscular hollow organ that is shaped like an irregular cone. It is encased in the fibrous pericardium sac, occupying the center mediastinum. 1/3 of the heart rests to the right of the sagittal (or median) plane of the body and 2/3 to the left of this plane. It is resting in the center mediastinum, in the middle of the left and right pleural sacs, its long axis rests diagonally beside a line passing from the left mid-clavicular line anteriorly, to the right mid-scapular line posteriorly (Mahadevan, 2012). Looking into the pericardium sac itself, it is further composed of different layers, mainly three layers of muscles, the epicardium or the external layer, the middle layer or myocardium and the innermost layer or endocardium (Lockhart et al., 2014). The myocardium is responsible for ventricular contraction and consists of strong muscular tissue. The outmost layer, termed the "fibrous pericardium", which is a fibrous, tough, dense and rigid layer. The fibrous pericardium is fused inferiorly with the main tendinous part of the diaphragm, whereas anteriorly it is affixed to the rear exterior of the sternum by bands of connective tissue termed "sternopericardial ligaments" (Figure 1). Inside the fibrous pericardium is the "serous pericardium", which is comprised of two layers. The outer layer termed the "parietal layer" which is positioned to the inner surface of the fibrous pericardium. This layer is displayed over the bases of the great vessels to become permanent with the inner visceral layer (commonly named epicardium), which wraps the surface of the heart, and is securely connected to it. Amongst the visceral and parietal layers of the serous pericardium is the "pericardial cavity", which comprises a thin film of fluid which permits the pounding heart to slide frictionless within the pericardium. The pericardial cavity also has two important inlets: the "transverse sinus" and the "oblique sinus". The transverse sinus sits at the rear of the roots of the aorta and pulmonary trunk, where it is restricted posteriorly by the atrial chambers. While the oblique sinus, positioned at the rear of the left atrium, is constrained right-handedly by the right pulmonary veins and inferior vena cava, and left-handedly with the left pulmonary veins. The fibrous pericardium merges through the walls of the great

vessels (inferior and superior vena cava, pulmonary trunk, four pulmonary veins, and the ascending aorta) where these vessels pierce the fibrous pericardium (Mahadevan, 2012).
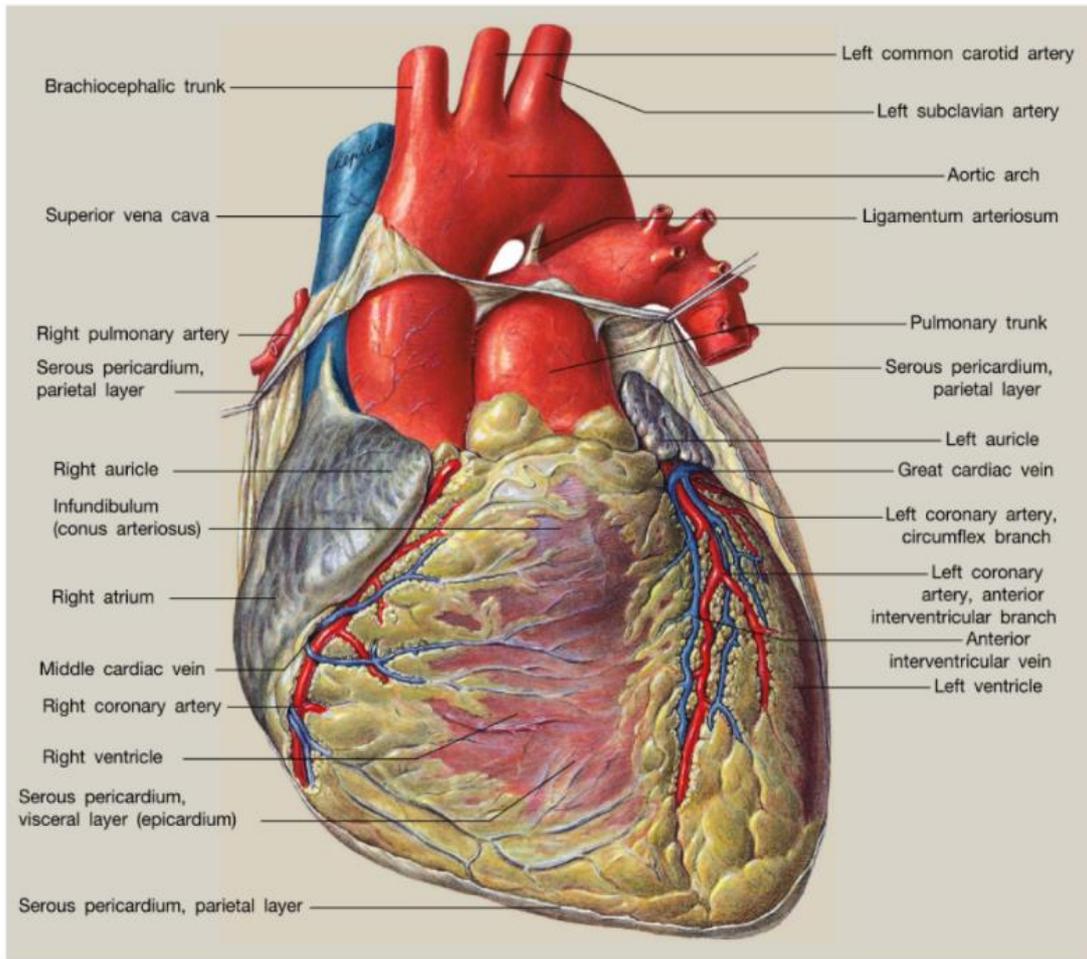
Figure 1: The heart and pericardium frontal view. Adapted from (Mahadevan, 2012).

1.2 Heart chambers and valves

The heart has a 'fibrous skeleton' composed of dense collagen that acts as an anchor for the cusps of the heart valves and for the myocardium of the cardiac chambers. The skeleton is a combination of four fibrous rings (equivalent to the left and right atrioventricular cavities, as well as the cavities of the pulmonary trunk and aorta) and the attached parts of the inter-atrial and inter-ventricular septal wall that separates these chambers (Figure 2). Collectively, the heart has four chambers: The right and left atrium as well as the right and left ventricle. It also has four cardiac valves that rest behind the body of the sternum alongside a nearly vertical line. They are the aortic valve, pulmonary

valve, mitral valve, and tricuspid valve. Normal heart sounds or beats are the outcome of rapid collocation of valve cusps at the time of valve closure and are simply recorded by auscultation. The right atrium is largely composed of a smooth interior. Part of the anterior wall and the atrial appendage have trabeculated interiors. There is a vertical ridge on the inner aspect of the anterior wall termed the "crista terminalis". Another parallel groove on the exterior wall is termed the "sulcus terminalis" while the posterior wall of the right atrium is the "interatrial septum". The openings of the inferior and superior vena cava are on the floor and roof, respectively. Towards the left of the inferior vena cava opening is the opening of the coronary sinus, which sends the majority of the venous return to the right atrium. To the left of the opening of the coronary sinus is the tricuspid opening (shielded by the tricuspid valve), heading to the right ventricle. Directly over the opening of the coronary sinus, in the adjoining portion of the interatrial septum, is the atrioventricular node (AVN). The intersection of the sulcus terminalis and superior vena cava indicates the position of the sinoatrial node (SAN). The left atrium is composed of smooth walls apart from within the left atrial appendage. Penetrating the posterior wall of the left atrium, on either side, are the subsequent lower and upper pulmonary veins. The inferior part of the left atrium holds the mitral opening (protected by the mitral valve) leading towards the left ventricle (Dal-Bianco & Levine, 2013; Mahadevan, 2012; Mori et al., 2016).
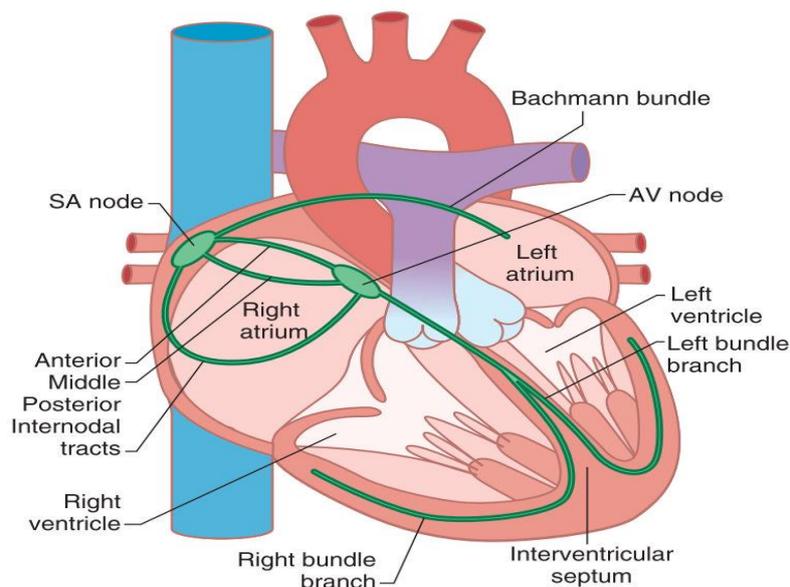
Figure 2: Heart Anatomy. Adapted from (Marks, 2019).

1.3 Cardiac myocytes

These striated muscle cells are the essential components of heart muscle, and their primary role is to produce mechanical tension (Figure 3). Myocytes are enclosed by a lipid membrane called the "sarcolemma", which separates the cell exterior from the interior compartments. Myocytes may have one or more nuclei which are usually located at the center. Moreover, they contain mitochondria, myofibrils, the sarcoplasmic reticulum (SR), the sarcomeres and the cytoskeleton, that provides anchoring for the different organelles. The intracellular space is filled with the sarcoplasm, an aqueous solution containing lipids, various ion species, carbohydrates and proteins. The plasma membrane (sarcolemma) of one cardiac cell is joined tightly with its neighbor by intercalated disks, which contain gap junctions that permit the rapid passage of electrical impulses in the form of ions from one cell to the next. The intercalated disks allow cells of the myocardium to work together in a coordinated manner as a functional syncytium. Moreover, the sarcolemma forms membrane-lined channels, which penetrate the cell and develop into transverse (T) tubules. The T-tubules permit extracellular fluid and ions to disperse close to intracellular structures. T-tubules, which contain a high density of voltage-gated L-type calcium channels, are located in close proximity to the SR, the primary internal Ca^{2+} store. Sarcomeres form myofibrils, which are responsible for contraction upon Ca^{2+} release. The Golgi apparatus serves as the "loading dock" and the microtubules serve as "highways", to deliver ion channels to certain subdomains on the plasma membrane. Mitochondria provide the energy needed for the contraction of cardiomyocytes. Intercalated discs found at the ends of each ventricular cardiomyocyte facilitate the cell-to-cell propagation of action potentials (APs) (Hong & Shaw, 2017).
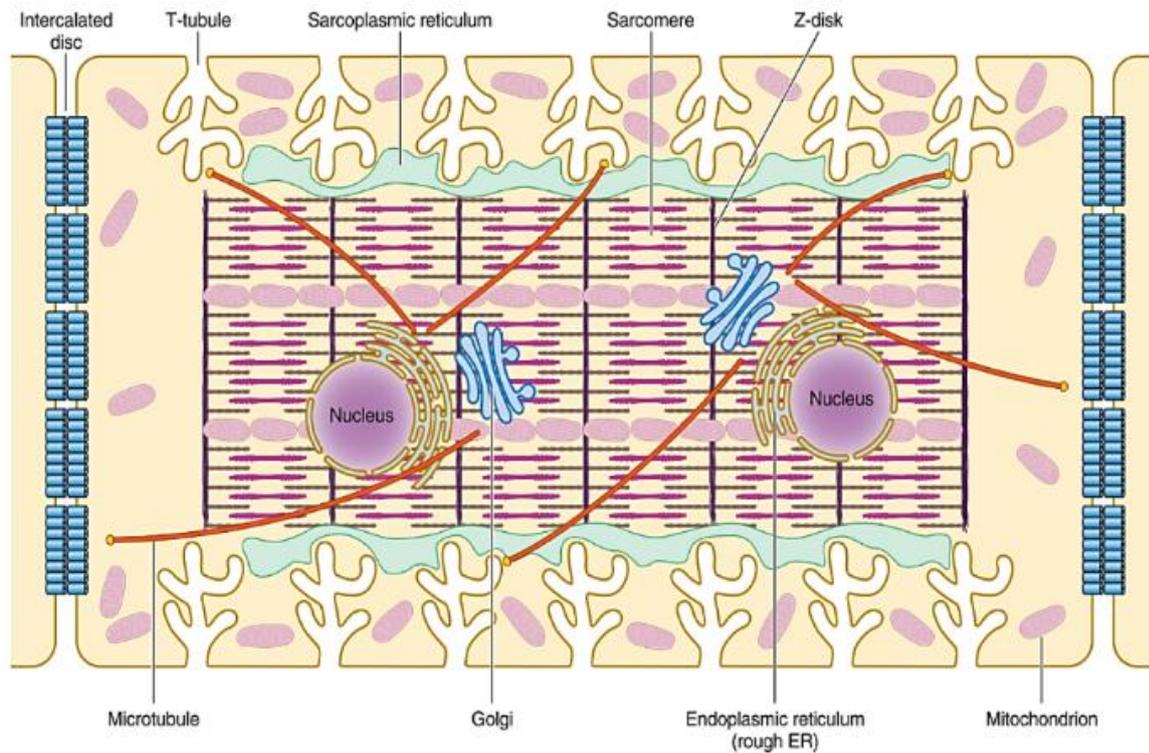
Figure 3: Cardiac Myocyte. Adapted from (Hong & Shaw, 2017).

1.4 Sarcomeres

The basic components of the sarcomeres are the myofilaments and, they are the fibers that generate contraction. They are composed of titin filaments and repeating units of thin and thick filaments (Figure 4). Titin, an intracellular anchor protein, works as a spring both at rest and during contraction. Thin filaments are comprised of actin and the regulatory proteins tropomyosin (Tm) and troponin (Tn), while thick filaments are comprised of myosin and accessory proteins. Rod domains of myosin heavy chains consist of the backbone, and globular heads called cross-bridges protrude outward from that backbone. Light chain accessory proteins bound to the myosin globular heads deliver structural reinforcement of cross-bridges but in some contractile systems, particularly smooth muscles and non-muscle systems, provide a regulatory function. The interaction of myosin cross bridges with actin generates contractile force (Golob et al., 2014).
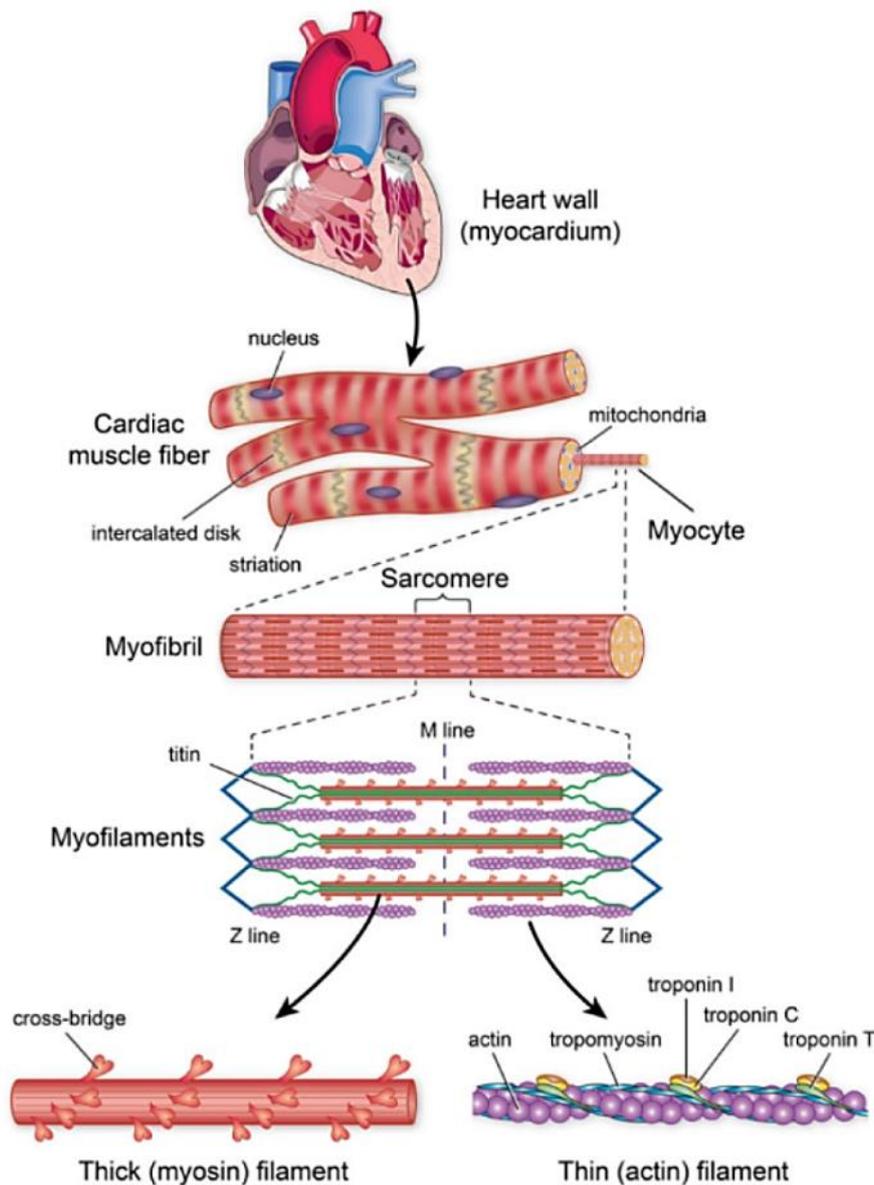
Figure 4: Sarcomere structure. Adapted from (Golob et al., 2014).

1.5 Electrical system of the heart

The heart is a four chambered pump that functions to distribute blood to all the organs in the body. It is comprised of left and right atria and left and right ventricles. The right side of the heart pumps blood through the pulmonary circulation and the left side of the heart pumps blood through the systemic circulation. The contraction of atria and then the ventricles proceed in an orderly manner and is controlled by a specialized electrical conduction system comprising the SAN, the AVN, left and right bundle branches and the Purkinje fibers (Figure 5).
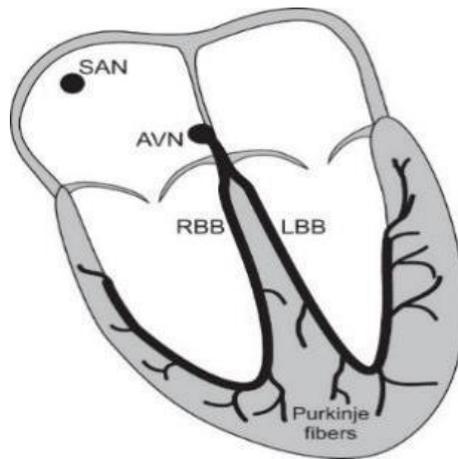
Figure 5: Diagram showing pacemaker site and conduction pathways within the heart. Sinoatrial node (SAN), atrioventricular node (AVN), left bundle branch (LBB), right bundle branch (RBB). Adapted from (Martín et al., 2015).

Electrical activity of the heart is initiated by specialized cells in the SAN which is located in the upper part of the wall of the right atrium. SAN cells have the ability to spontaneously generate APs (Crawford et al., 2009).

APs generated by SAN cells are rapidly conducted across the atria and then, after a brief delay in the AVN, are conducted rapidly across the ventricles. APs in SAN cells, as in other conducting and muscle cells of the heart, are caused by changes of ion conductance in specialized ion channels (Martín et al., 2015). Typical SAN and atrial muscle APs are shown in Figure 6.
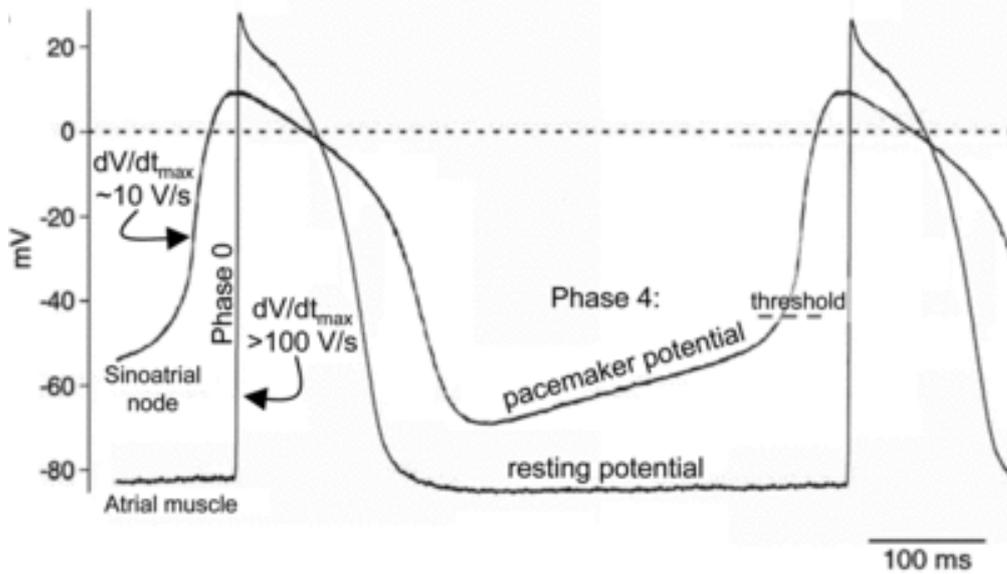
Figure 6: Diagram showing the action potentials from the SAN and atrial muscle of rabbit heart. Adapted from (Boyett, 2009).

1.6 Sinoatrial node action potential

SAN cells are able to generate spontaneous APs which allow them to set the normal electrical rhythm and rate in a healthy heart (Boyett, 2009; Kashou & Kashou, 2018). SAN cells have unstable resting membrane potentials (RMPs) (Phase 4). During phase 4 of the SAN AP hyperpolarization-activated cyclic-nucleotide (HCN) channels or "funny current (I_f)" channels open and there is an inward current carried by Na^+ and K^+. Opening of these channels leads to a small depolarization of the SAN membrane potential. L-type and T-type Ca^{2+} currents also contribute to phase 4 of the SAN AP (Figure 7). When the membrane potential reaches threshold, an AP is generated in each myocyte of the heart. L-type Ca^{2+} current (I_{CaL}) is largely responsible for phase 0. Closure of L-type Ca^{2+} channels and opening of K^+ channels, including the delayed rectifier K^+ channels (I_{Kr}) and (I_{Ks}) repolarize the cell giving rise to phase 3 of the AP (Bartos et al., 2015; Boyett, 2009).
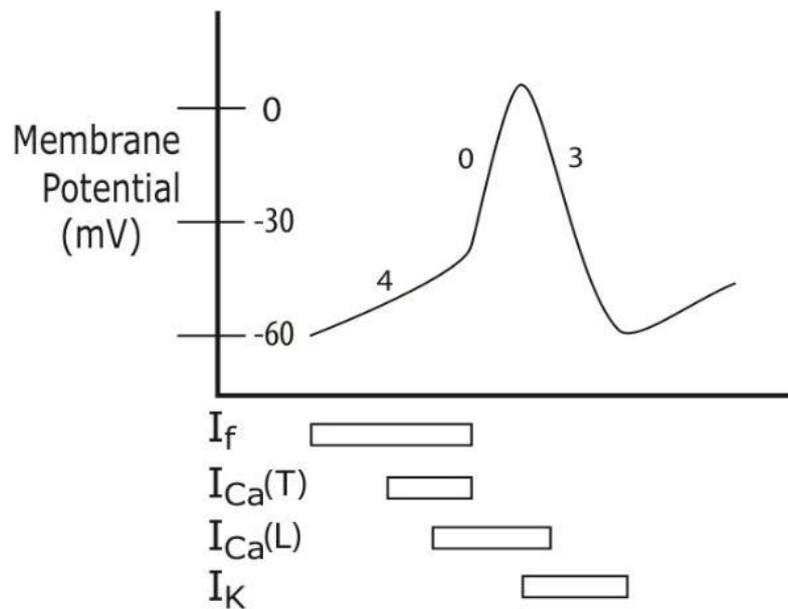
Figure 7: Diagram showing SAN depolarization. Adapted from (Czick et al., 2016).

1.7 Cardiac muscle action potential

The heart muscle AP contains five phases. Recording from a typical body surface electrocardiogram (ECG) and a ventricular AP are shown in Figure 8. APs generated in the SAN spread rapidly through the atria and stimulate contraction of the atria muscle. The P wave of the ECG represents depolarization of the atria. Electrical activity spreads from the atria to the AVN, where there is a short delay, before electrical activity quickly spreads through the ventricular myocardium. The QRS wave of the ECG represents ventricular depolarization and the T wave represents ventricular repolarization (Boyett, 2009; Kashou & Kashou, 2018).

The first phase of the AP (phase 0) is caused by the opening of fast Na^+ channels with high voltage sensitivity, and rapid regenerative influx of Na^+, which depolarizes the membrane from the RMP (-90 mV) to around +30 mV. The Na^+ channels are rapidly inactivated and a transitory opening of the K^+ channels causes a transitory early repolarization (phase 1). The plateau phase mainly results from activation of voltage-gated L-type Ca^{2+} channels (phase 2). The closure of the Ca^{2+} L-type channels and the opening of the K^+ voltage-gated channels results in cell repolarization (phase 3). Finally, the

membrane potential returns to resting levels (phase 4) (Pinnell et al., 2007; Shih, 1994) (Figure 8).
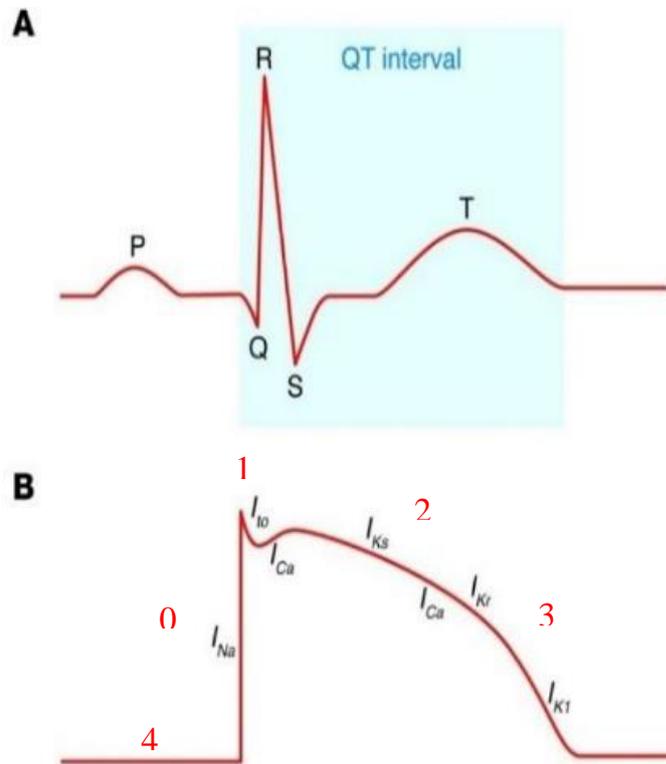
Figure 8: Diagrams showing action potentials of cardiac Myocyte. (A) Surface electrocardiogram and (B) ventricular action potential. Adapted from (George, 2013).

Once the APs have spread across the atria, they are conducted to the AVN. There is a short delay in AVN conduction before the APs are rapidly conducted across the ventricular myocardium. The AVN can be seen as a secondary heart pacemaker. The AVN is a subendocardial structure located in the lower posterior right atrium, in an anatomical region on the posterior border of the coronary sinus ostium, superiorly to the tendon of Todaro and anteriorly to the septal tricuspid valve annulus. This anatomic region is also commonly referred to as the "triangle of Koch". The AVN beats at a lower rate than the SAN, around 40-60 beats per minute. The delay in signal transmission in the AVN allows the atria to complete contraction before the ventricle chambers contract. After passing through the AVN the wave of depolarization quickly spreads to the his bundle branches, the Purkinje fibers , and through the myocardium (Bartos et al., 2015; Boyett, 2009; Hafeez & Grossman, 2018).

1.8 Excitation-contraction coupling

The excitation contraction coupling (ECC) process couples the electrical activity of the heart with mechanical contraction of the heart muscle (Figure 9). The generation of APs leads to the opening of L-type Ca^{2+} channels during phase 2 of the AP and a small influx of Ca^{2+}. This small influx of Ca^{2+} binds to ryanodine receptors (RYR) in the SR and prompts a large release of Ca^{2+} from the SR. This process is so called "Ca^{2+}-induced Ca^{2+} release". There follows a rise in cytoplasmic Ca^{2+} referred to as the Ca^{2+} transient. The Ca^{2+} binds to Troponin C (TnC) which in turn causes tropomyosin (Tm) to reveal the active binding site of the myosin myofilaments triggering a shift and binding of myosin to actin proteins producing muscle contraction. After the cycle ends, the muscles relax and Ca^{2+} is released from the myofilaments. The Ca^{2+} that was released from SR is returned to the SR by the Ca^{2+}-ATPase pump (SERCA) and the Ca^{2+} that entered the cell through the L-type Ca^{2+} channels is ejected, primarily by the Na^+/Ca^{2+} exchanger (NCX), but to a lesser extent by the cell membrane Ca^{2+} ATPase (Bers & Despa, 2013; Landstrom et al., 2017; Martín et al., 2015; Pfeiffer et al., 2014; Silverthorn et al., 2007).
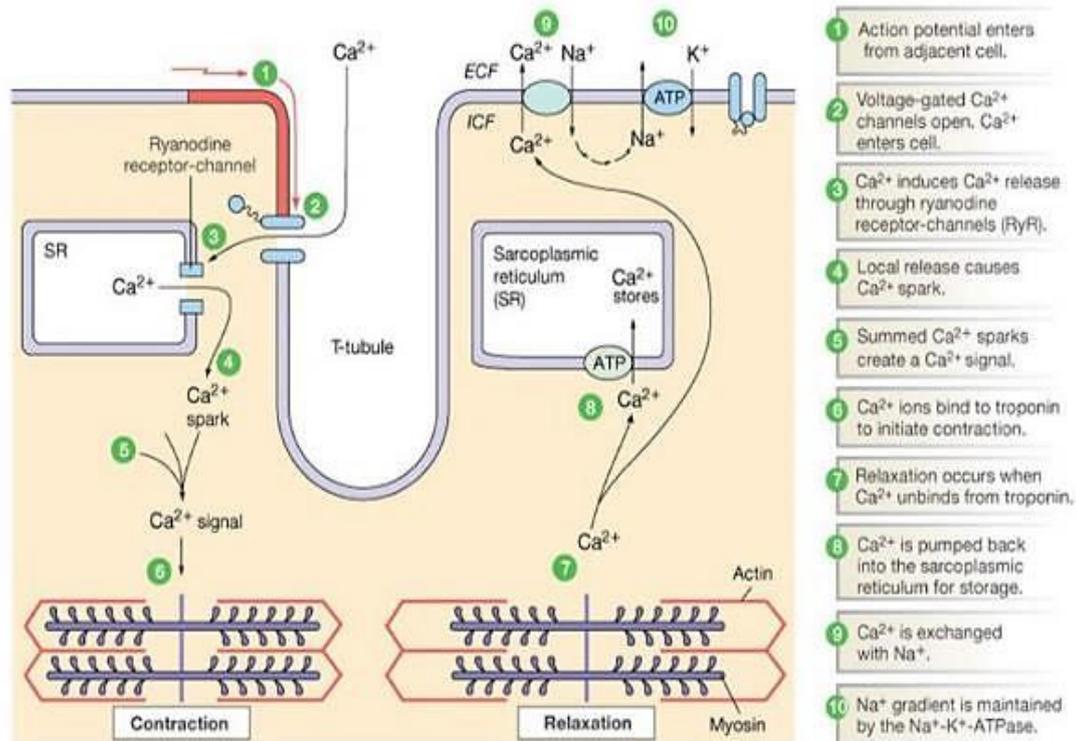
Figure 9: Illustration depicting the excitation-contraction coupling process in the heart. Adapted from (Silverthorn et al., 2007).

1.9 Voltage-gated channels of the heart

Since the spread of APs depends on the voltage-gated channel, it is helpful to discuss them in more detail. Voltage-gated ion channels are important transmembrane proteins that help control physiological processes such as cardiac muscle cell contraction and relaxation. In the heart, voltage-gated ion channels include Ca^{2+}, Na^+, K^+ and Cl^- channels. The voltage-gated Na^+ channels and the voltage-gated Ca^{2+} channels are usually present in the cell membranes of most excitable cells (Catterall, 2000, 2005; Hille, 1978; McGivern & Worley, 2007).

Voltage-gated Na^+ channels are composed of a single α subunit and one or two β subunits as shown in Figure 10. The α subunit consists of four homologous domain regions (I-IV) of six transmembrane spanning segments (S1-S6) and a pore forming loop. The segment S4 is the voltage sensor and a channel gate modulator. The pores that allow Na^+ ions to pass also have a fatty acyl chain that allows small hydrophobic inhibitors to pass. The pore forming Na^+ channel α subunit, is an "Asp-Glu-Lys-Ala" (DEKA) motif which controls Na^+ selectivity (Catterall, 2000, 2005; Hille, 1978; McGivern & Worley, 2007).

The voltage-gated Ca^{2+} channels [Ca_v1-3] are proteins that allow the passage of Ca^{2+} ions. These channels are hetero-oligomeric complexes of different subunits of α, β, γ and δ that assemble into 5 units, the pore forming α subunit (α1) and at minimum two accessory subunits α2δ and β, hence the term "hetero-oligomeric". So far 10 cloned α-subunits have been identified and make up three main families: 1) The most abundant [Ca_v1.x] L-type Ca^{2+} Dihydropyridine-sensitive (high voltage long or slow inactivation), 2) [Ca_v2.1] P/Q-type Ca^{2+} current Dihydropyridine-insensitive (High voltage-activated, moderate voltage-dependent inactivation), [Ca_v2.2] N-type Ca^{2+} current (High voltage-activated, moderate voltage-dependent inactivation), [Ca_v2.3] R-type Ca^{2+} current (moderate voltage-activated, fast voltage-dependent inactivation) and 3) [Ca_v3.x] T-type Ca^{2+} (Low voltage-activated, moderate voltage-dependent inactivation). The T-type and L-type Ca^{2+} channels variously contribute to pacemaker cell APs. Just like the voltage-gated Na^+ channels, each α-subunit is composed of four homologous regions (I-IV) of six transmembrane domains (S1-S6) where the S4 is responsible for the gating function. The α2δ and β subunits augment expression as well as regulate the voltage dependence and

gating kinetics of the α1 subunit. The Ca^{2+} channel α subunit four glutamate residues, "the EEEE motif", are responsible for Ca^{2+} selectivity (S. Alexander et al., 2013; Catterall, 2000; H. Huang et al., 2017).

Potassium (K^+) channels can be divided into three major groups differing in the channel structure formed by the pores. The first group of voltage-dependent K^+ currents (K_v) originated from six different families of channel proteins built upon *Drosophila melanogaster* nomenclature. The K^+ currents involved in this group consist of the Ca^{2+} activated K^+ channels, transient outward K^+ channels and KCNQ channels. Each form of tetrameric structure consists of six transmembrane segments S1-S6 subunits and cytoplasmic C- and N-termini. The segments S1-S4 shift in response to voltage changes and function as channel voltage sensors. The second group of K^+ channels comprises of two transmembrane segments S1–S2, conducting three inward K^+ currents which are: ATP-sensitive K^+ (KATP) channels, the inward-rectifying K^+ (K_{ir}) channels and G protein-coupled inwardly-rectifying K^+ (GIRK) channels (Snyders, 1999). The S1 and S2 segments are linked by a pore-forming P-loop. The third group of K^+ channels are the most abundant with more than 50 members. Each have a two-pore P1 and P2 structure with four transmembrane segments S1–S4. The glycine-tyrosine-glycine (GYG) motif is the key sequence for K^+ selectivity in the pore region. A gene called "KCNH2" codes for the Kv11.1 channel, recognized as the human Ether-à-go-go Related Gene (hERG), which carries the inward delayed rectifier K^+ current (I_{Kr}), a vital element of repolarization during the cardiac AP. Obstruction of I_{Kr} impedes cardiac repolarization, extending action potential duration (APD) and the QT interval of the ECG, and hypothetically increases the risk for the development of the cardiac arrhythmia such as: *Torsades de Pointes* (TdP). The molecular structures of the different cation channels are shown in Figure 10 (Chen et al., 2015; Gutman, 2005; H. Huang et al., 2017; Snyders, 1999).
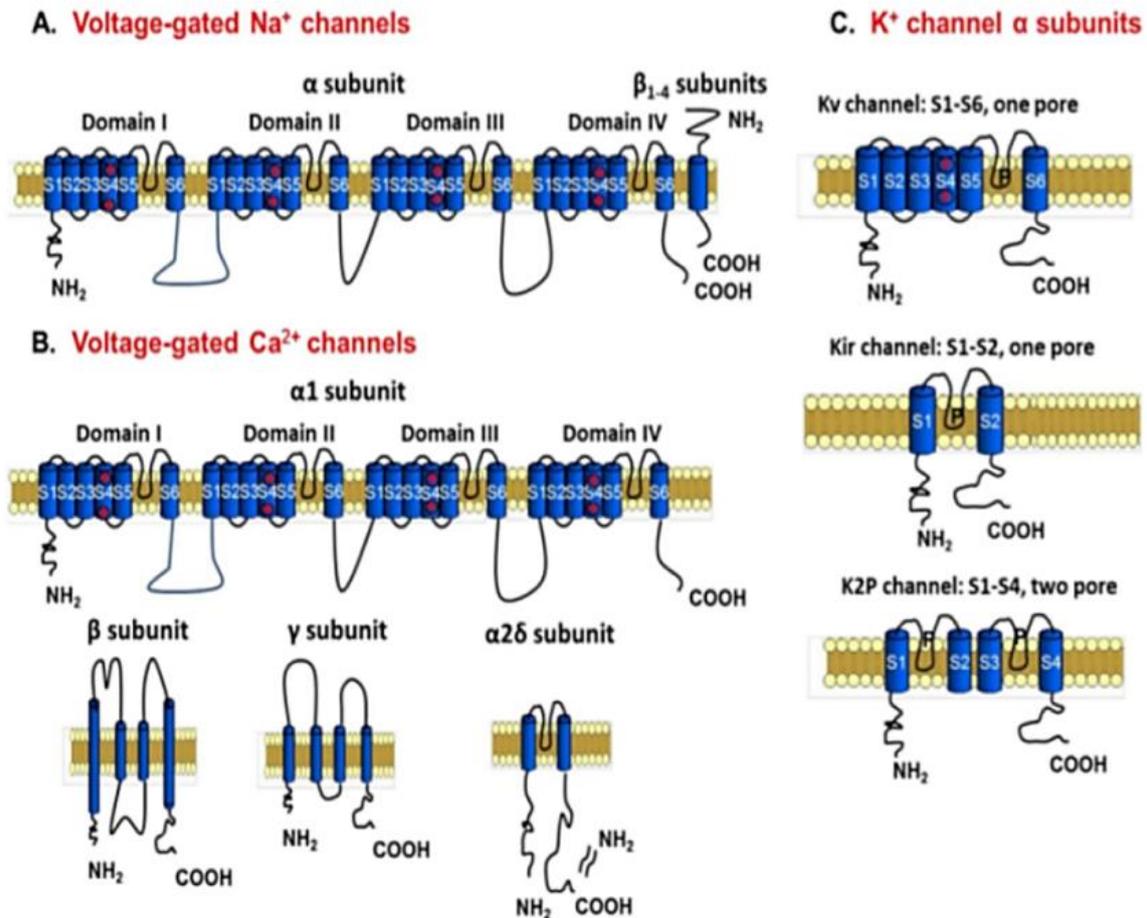
Figure 10: Structure of voltage-gated Na$^+$, Ca^{2+} and K$^+$ channels. Adapted from (H. Huang et al., 2017).

1.10 Molecular biology

The human body consists of cells which are the basic functional units of living organisms. An individual cell can carry out all the processes of life (Figure 11). All living organisms store genetic information within the cell nucleus as nucleic acids which are deoxyribonucleic acid (DNA) and ribonucleic acid (RNA) and transmit them to future generations of cells. Through the use of a common genetic code, the cell can transfer genetic information from DNA to RNA to protein, it can make use of proteins and some RNAs to catalyze chemical reactions. It can also synthesize proteins in ribosomes, derive energy by breaking down simple sugars and lipids, use adenosine triphosphate (ATP) as their energy currency, and separate their cytoplasm from the external environment by

means of phospholipid membranes containing pumps, carriers, and channels (Silverthorn et al., 2007; Thomas et al., 2017).
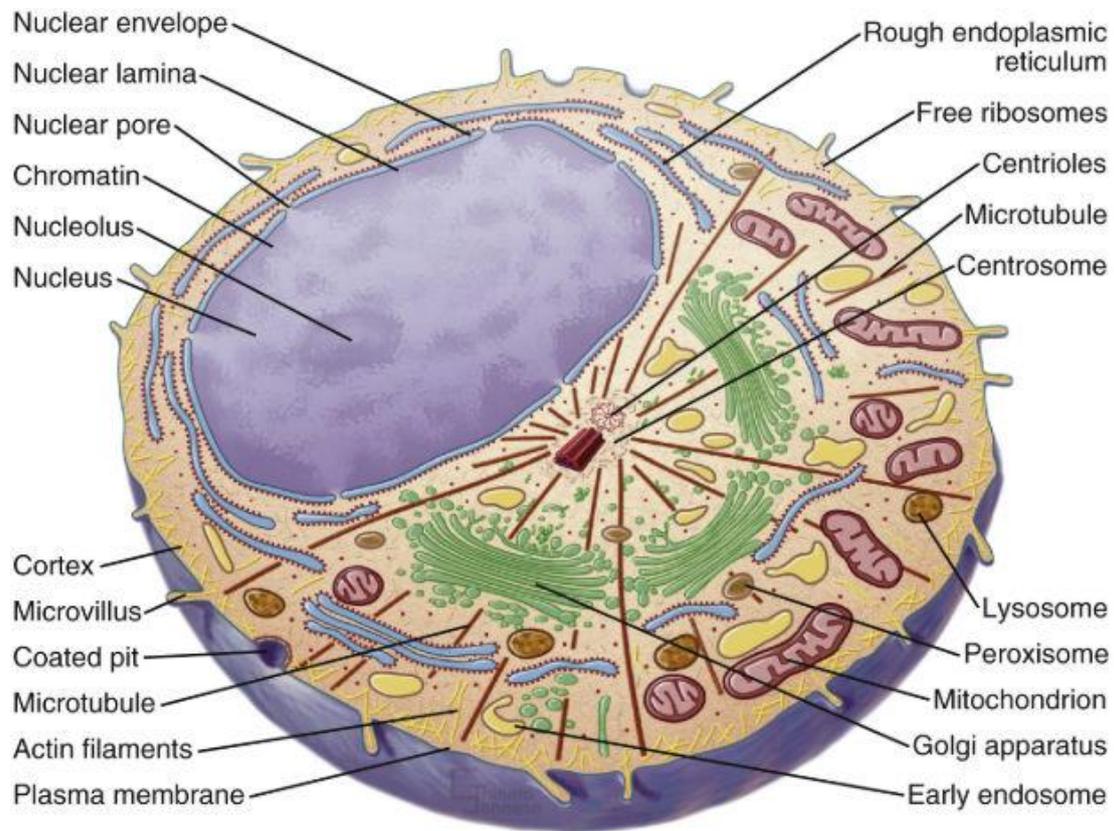
Figure 11: The Eukaryotic cell with internal components. Adapted from (Thomas et al., 2017).

Nucleic acids play an important role in many cell processes, including storage and transmission of genetic information and energy. A single nucleotide is a three-part molecule composed of one or more groups of phosphates, a five-carbon sugar and a carbon-nucleotide structure called a nitrogen base. Many millions of nucleotides are joined together to form DNA usually in the form of a double-stranded double helix. Each nucleotide contains one of the two possible sugars of either the 5-carbon sugar ribose or deoxyribose (ribose without oxygen). There are two types of nitrogen bases, purines and pyrimidines. The purines have a double ring structure while the pyrimidines have a single ring. There are two purines, adenine and guanine, and three pyrimidines, cytosine,

thymine, and uracil. The smallest nucleotides consist of the energy-transferring compounds ATP and adenosine diphosphate (ADP) (Silverthorn et al., 2007) (Figure 12).
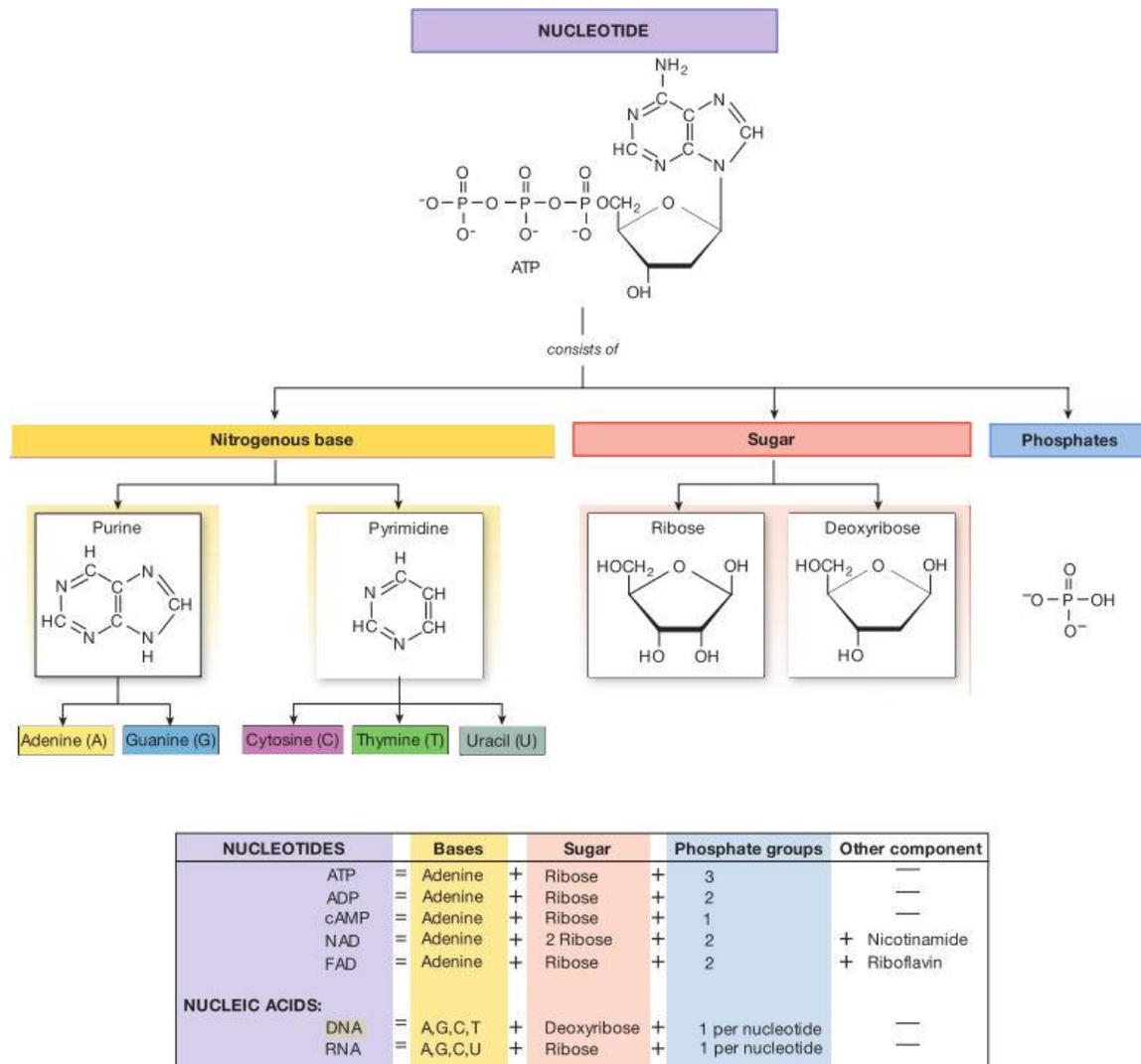
Figure 12: Nucleotides and nucleic acids. Adapted from (Silverthorn et al., 2007).

In order to be transmitted from one generation to the next, DNA must be replicated by special proteins (i.e. DNA polymerase) that unzip the DNA double helix and build new DNA by pairing new nucleotide molecules to the two existing DNA strands that results in two double-stranded DNA molecules (Silverthorn et al., 2007) (Figure 13).
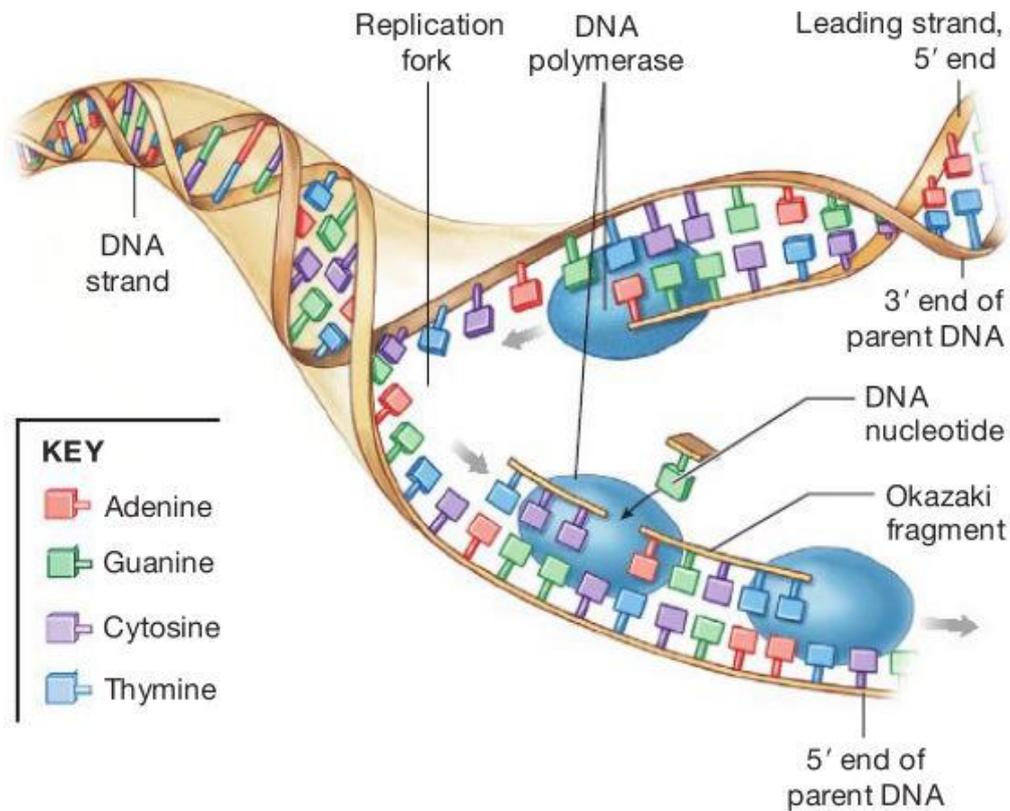
Figure 13: DNA replication. Adapted from (Silverthorn et al., 2007).

The general flow of information from DNA to RNA to protein is termed the "central dogma" of molecular biology (Figure 14). The copying process in which a DNA serves as a model for RNA synthesis is called transcription. In summary there are three major types of RNA that participate in the process of protein synthesis which are ribosomal ribonucleic acid (rRNA), transfer ribonucleic acid (tRNA), and messenger ribonucleic acid (mRNA). Transcription produces mRNAs that are translated into sequences of amino acids such as proteins or polypeptide chains. The main function of mRNA is to transmit genetic information from nuclear DNA to cytosols where it is used as a template for protein synthesis while rRNA is a component of the ribosomes. On the other hand tRNA serves as an "adaptor" molecule that carries a specific amino acid to the site of protein synthesis (Harvey & Ferrier, 2011).
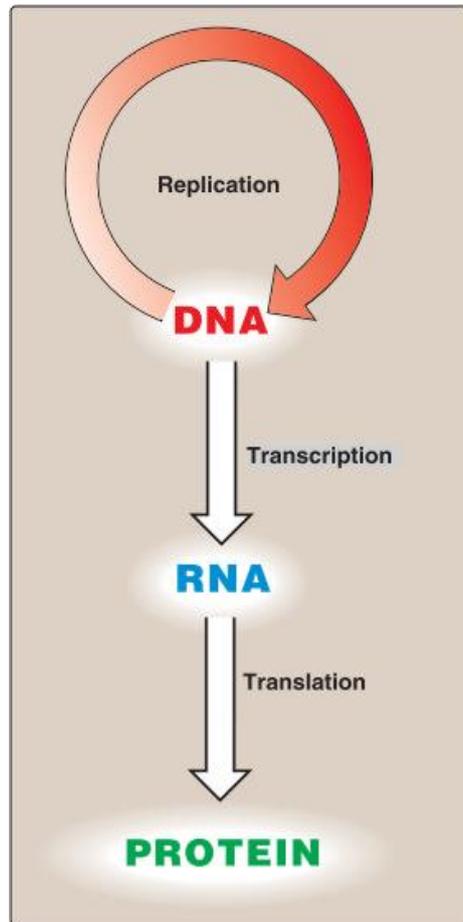
Figure 14: Central dogma of molecular biology. Adapted from (Harvey & Ferrier, 2011).

1.11 Statement of the problem

Diabetes mellitus (DM) is a key and worsening global and international health problem, presently affecting more than 570 million people and reducing their quality of life. Type 2 diabetes mellitus (T2DM) accounts for more than 90% of DM and the global epidemic of obesity, which largely explains the dramatic increase in the incidence and prevalence of T2DM in the past 20 years. Obesity is a major risk factor for DM which in turn is a key source of mortality and morbidity in diabetic individuals. The molecular and electro-mechanical function of the heart is often compromised in diabetic patients. The aim of this dissertation is to clarify the molecular basis of electro-mechanical dysfunction in obesity and diabesity. The electro-mechanical function of hearts will be explored in Zucker diabetic fatty (ZDF) and Zucker fatty (ZF) rats and compared to Zucker Lean (ZL) controls. The following sections will discuss diabetes and obesity in more detail.

1.12 Diabetes: Epidemiology and pathophysiology

DM is a major metabolic disorder in which patients have elevated blood glucose or hyperglycemia (Hg). DM is a major global health crisis. Statistics from the *International Diabetes Federation* (IDF) *in 2021* (International Diabetes Federation, 2021), reveal that 573 million adults between the ages of (20-79 years) worldwide had DM. The number of diabetic patients is expected to reach 643 million by the year 2030 and around 783 million by the year 2045. In 2021, there were an estimated 73 million people with diabetes in the Middle East and Northern Africa (MENA) region. Diabetes is divided into various types. Type 1 diabetes mellitus (T1DM) is characterized by almost total destruction of pancreatic cells, which usually leads to an absolute lack of insulin. T2DM is the most common form of diabetes and accounts for more than 90 percent of DM. In T2DM, in addition to progressive β-cell failure, there is also evidence of insulin resistance (IR) and insulin deficiency. The third type of DM affects pregnant women, known as gestational diabetes (GD), which is characterized by IR and insulin deficiency. Other forms of diabetes include types related to genetic defects of β-cell function, genetic defects in insulin action, endocrinopathies, drug or chemical-induced and diseases of the exocrine pancreas (Mayfield, 1998). When the disease is diagnosed late or untreated, it can cause a number of long-term complications, including DCM, which causes the patient's quality of life to be reduced. Cardiovascular diseases (CVDs) are the main cause of mortality and morbidity in diabetic patients (Low Wang et al., 2016). In young people with T1DM ages between (8-43 years), around 5 people out of 1,000 die from CVDs on a yearly basis, whereas among middle-aged people with T2DM living in high and middle income countries, up to 27 people out of 1,000 die from CVDs each year; a third of them die from stroke, and a quarter die from coronary artery disease (CAD) (International Diabetes Federation., 2017). Electro-mechanical heart dysfunction is common in diabetic patients (Demir et al., 2016). Atrial fibrillation (AF) and ventricular arrhythmias (VAs) are the most common forms of arrhythmias found in diabetic patients. Left ventricular diastolic dysfunction and prolonged QTc of the ECG are also frequently reported in the diabetic heart.

1.12.1 Metabolic alterations in type 1 diabetes mellitus

T1DM is an autoimmune disease characterized by autoreactive T cell-mediated destruction of insulin-producing β-cells which leads to insulin insufficiency and hyperglycemia. Changes occur in three major tissues: the liver, muscle and adipose tissues. In the liver, increased liver glucose production, combined with decreased peripheral utilization, leads to hyperglycemia. This is due to increased liver glucose metabolism and reduced glucose absorption by insulin-sensitive glucose transporter (GLUT-4) in fat tissue and muscles. To eliminate free fatty acids from fat tissue, the body develops ketosis which results from massive mobilization of fatty acids from adipose followed by hepatic ketogenesis with accelerated hepatic fatty acid β-oxidation and synthesis of 3-hydroxybutyrate and acetoacetate. However, not all fatty acids are converted to ketones in the liver, in fact some get converted into triacylglycerol which is packaged in very low-density lipoproteins (VLDL) and then secreted in the blood. On the other hand, some diabetic patients have a lack of enzymes that are responsible for the degradation of chylomicrons that are derived from food lipids by intestinal mucosal cells. For these patients, the degradation of lipoprotein lipase enzyme will be inhibited, resulting in the accumulation of chylomicrons in the blood, eventually the plasma chylomicron and VLDL levels are elevated, resulting in hypertriacylglycerolemia (Figure 15) (Harvey & Ferrier, 2011).
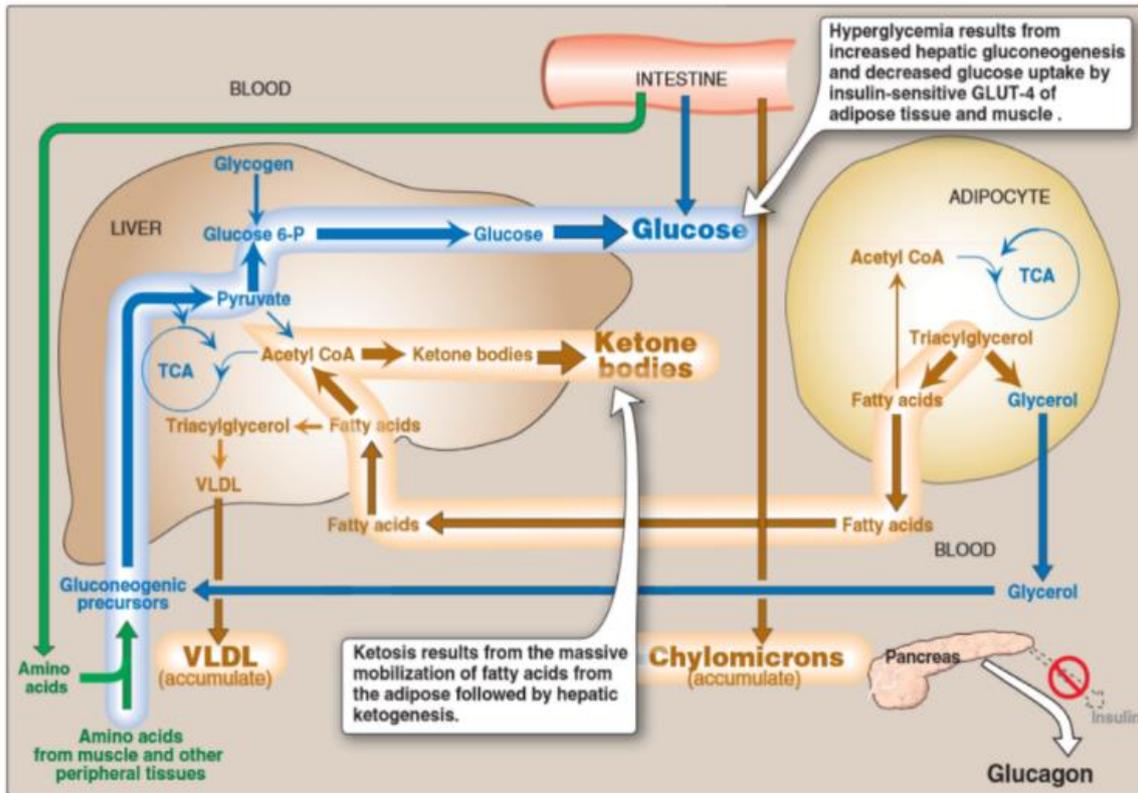
Figure 15: Metabolic alterations in type 1 diabetes mellitus. Adapted from (Harvey & Ferrier, 2011).

1.12.2 Metabolic alterations in type 2 diabetes mellitus

In 2021, it was estimated that the number of adults (aged 20-79 years) with diabetes was around 573 million and projected to reach 643 million by 2030, and 783 million by 2045. By 2021, about 6.7 million people will die of diabetes-related disease. About 319 million adults (6.7 percent of the global adult population) suffer from impaired fasting glucose (IFG). It is estimated that 441 million adults, or 6.9 percent of the global adult population, are expected to have IFG by 2045. (International Diabetes Federation, 2021). Patients with T2DM differ from those with T1DM because they do not have total destruction of the pancreatic cells, but instead, suffer from IR that affects three major tissues of the body: the liver, muscle and adipose tissues. In IR, there is minimum ketosis because insulin reduces liver ketogenesis. Dyslipidemias are similar to those with T1DM with increased plasma levels of VLDL and chylomicrons resulting in hypertriacylglycerolemia, although lower plasma high density lipoproteins (HDLs) may

also be present (Harvey & Ferrier, 2011). Figure 16 shows the metabolic changes which occur in the body of a patient with T2DM.
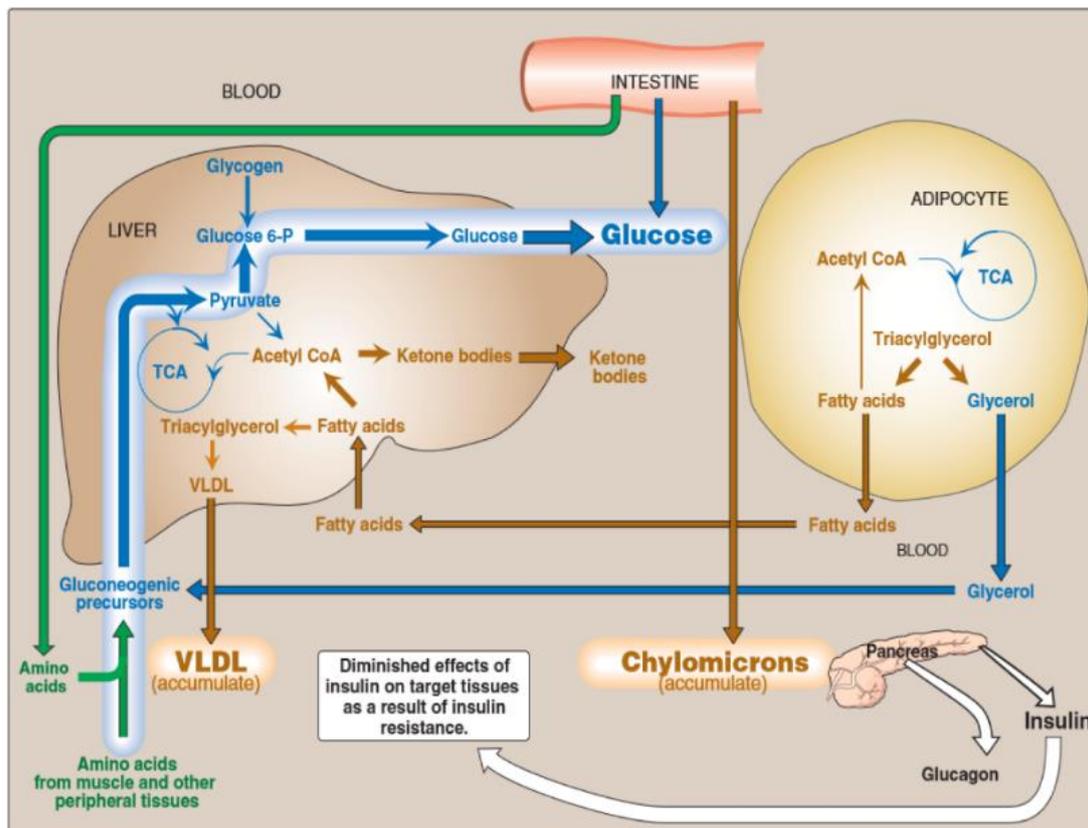
Figure 16: Metabolic alterations in type 2 diabetes mellitus. Adapted from (Harvey & Ferrier, 2011).

1.12.3 Complications of diabetes

Many cardiovascular risk factors are involved in diabetes, particularly T2DM. Some of the risk factors include diabetes, hypertension, diet, obesity, smoking, decreased exercise, genetics, and others that exacerbate cardiovascular symptoms of the disease (Martín-Timón et al., 2014).

It is known that DM can cause short- and long-term complications caused by damage to the blood vessels in various organs of the body. Some of these complications include macrovascular diseases such as hypertension, hyperlipidemia, heart attacks, coronary artery disease, strokes, cerebral vascular disease, and peripheral vascular disease

and some include microvascular diseases including retinopathy, nephropathy, and neuropathy (Khalil et al., 2018; Wu et al., 2014).

1.13 Obesity: Epidemiology and pathophysiology

Obesity is a serious global health problem and it is associated with metabolic syndrome which has been described as the combination of IR, hypertension, hyperlipidemia and obesity (Fellmann et al., 2013; Reaven, 1988). The *World Health Organization* (WHO) (World Health Organization, 2018) defines obesity as "an abnormal or excessive fat accumulation in adipose tissue, to the extent that health is impaired". The current gold standard classification of obesity is the Body Mass Index (BMI) which is calculated as a person's weight in kilograms divided by the square of height in meters (kg/m^2). For epidemiological reasons, a person is considered overweight if the BMI is greater than $25\ kg/m^2$ and obese if the BMI $\geq 30\ kg/m^2$ (World Health Organization, 2018). Excessive adiposity is a vital risk aspect in the pathophysiology of DM, IR, dyslipidemia, atherosclerosis, hypertension, stroke, psychological, CAD, liver disease, osteoarthritis, sleep apnea, some musculoskeletal conditions, gynecological complications, cancer including colon and breast cancer (NHLBI Obesity Education Initiative Expert Panel. National Institutes of Health. National Heart Lung and Blood Institute., 1998). Recently, a new method of assessing body weight has been developed, called the Body Shape Index (ABSI). It quantifies the risk associated with abdominal obesity. ABSI is based on waist circumference (WC) and is adjusted for height and weight.

ABSI Equation 1:

$$ABSI = WC / (BMI\ (2/3)\ x\ height\ (1/2))$$

ABSI might be considered to be a more valuable predictor of mortality than BMI (Krakauer & Krakauer, 2012). Obesity is considered a global health crisis, mainly because of its remarkable increase in prevalence in recent decades. In 2016, about 1.9 billion adults aged 18 and over worldwide were pre-obese or overweight, with estimates of more than 600 million adults being overweight. It is estimated that 13 percent of the world's adult population (11 per cent of men and 15 percent of women) are obese in 2016, meanwhile

39 percent of adults aged 18 years and above (38 percent of men and 40 percent of women) were overweight (World Health Organization, 2018). Between 1975 and 2016, global obesity rates tripled, accounting for 30 percent of the world's population. It is estimated that 340 million children and adolescents aged 5-19 were obese or overweight in 2016, an issue of extreme concern to governments around the world (World Health Organization, 2018). According to estimates from the latest Lancet Commission report, in 2015, obesity affected 2 billion people worldwide and the annual cost was about $2 trillion from losses in economic productivity and direct medical expenditure (Swinburn et al., 2019).

Obesity is a disorder resulting from a mixture of lifestyle, genetic and environmental factors and has a multi-factorial basis. A sedentary lifestyle, reduction in exercise or physical activity, reduced metabolic rate, thermal evolution and reduced energy expenditure will ultimately lead to an increase in energy storage and obesity. Causes of obesity include easy access to fast and addictive food, leptin resistance, junk foods, assertive marketing of food, sedentary lifestyle, certain medications as well as genetic factors. It is also worth noting that both overweight and obesity can be avoided. Figure 17 shows some of the environmental and genetic factors that may contribute to obesity and consequently, metabolic syndrome (Gurevich-Panigrahi et al., 2009).
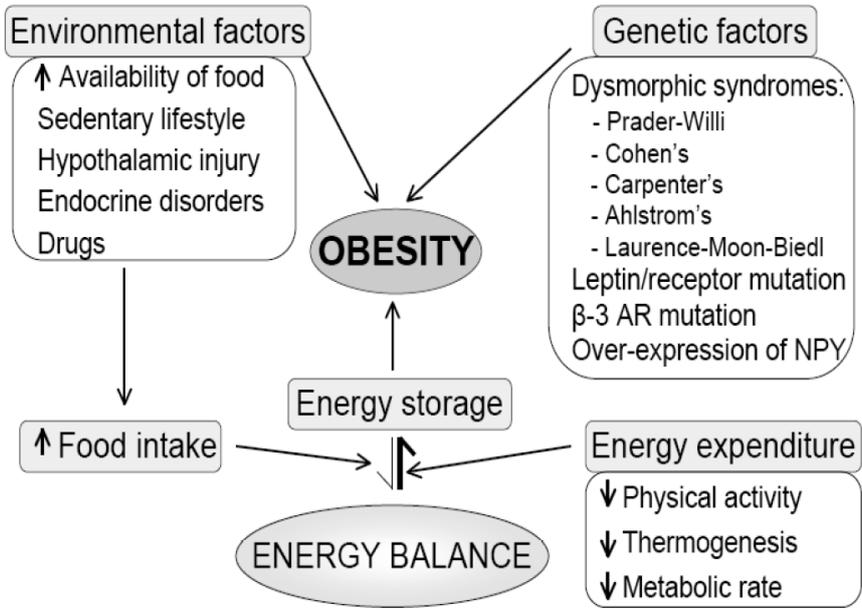
Figure 17: Flow diagram showing the energy balance and etiology of obesity. Adapted from (Gurevich-Panigrahi et al., 2009).

Obesity is characterized by excess fat in the body and contributes significantly to harmful metabolic effects. In addition, obesity is an important medical and socio-economic burden. According to a recent report, the global cost of obesity treatment has increased to a staggering 2 trillion USD (Dobbs & Swinburn, 2015; Swinburn et al., 2019).

Obesity is a consequence of an adverse increase in the mass of fat tissues resulting from an increase in the size (hypertrophy) or number (hyperplasia) of fat cells. (F. C. Howarth et al., 2017; Vasanji et al., 2004). These two events combine to orchestrate a series of co-morbidities that lead to obesity. It is important to identify potential factors regulating these processes of adipocyte biology in order to prevent and treat obesity.

Chronic energy imbalance leads to adipocyte hyperplasia and hypertrophy, stress of endoplasmic reticulum, and mitochondrial dysfunction. These processes induce an increase in intracellular and systemic release of adipokines, free fatty acids, and inflammatory mediators that cause adipocyte dysfunction and adverse effects in the pancreatic β-cells, liver, and skeletal muscles and more importantly, the heart itself, in addition to the vascular beds (De Ferranti & Mozaffarian, 2008).

1.13.1 Obesity and the heart

According to the Framingham study, both overweight and obesity are associated with an increased relative risk of developing cardiovascular risk factors and CVDs and people with T2DM are 2/3 times more likely to develop CVDs (International Diabetes Federation., 2017; Turpie et al., 2002).

The spread of APs depends on voltage-dependent ion channels, so it is helpful to discuss these channels in more detail, because their dysfunction can cause CVDs. The voltage-gated ion channels are important transmembrane proteins that control physiological activities such as contraction and relaxation of heart muscle cells. Obese Wistar rats fed a high fat diet demonstrate significant changes in gene expression of ion channels in the left ventricle, which may predispose to arrhythmias. The heart of these obese rats presents significant upregulation of various transport proteins including Cav1.2, Kir2.1, HCN4, NCX1, SERCA2a, RYR2 mRNA and downregulation of ERG mRNA. In

these obese rats, there was also a significant increase in HCN4 protein expression. (Ashrafi et al., 2016).

Axelsen et al. (2015) demonstrated that the hearts of fructose-fat fed Sprague-Dawley rats (FFFRs) displayed QRS prolongation *in-vivo*, along with decreased conduction velocity (CV) *ex-vivo*. Similarly, the hearts of FFFRs rats revealed numerous premature ventricular contractions (Axelsen et al., 2015) under relaxed conditions *in-vivo*. Likewise, the isolated hearts from FFFRs displayed an increase in susceptibility to ventricular fibrillation (VF) following cardiac ischemia-reperfusion. There were no changes in the coupling between the gap junctions, the density of K^+ or Na^+ current, and the differences in cell size or fibrosis. This indicates that the mechanism of conductance disturbances in the pre-diabetic heart varies from the disturbances seen in cardiac ischemia and heart failure (HF) (Axelsen et al., 2015). In another study, a high-energy (HE) diet consisting of 33% kcal as fat was fed to Sprague-Dawley rats to create an experimental model of obesity. These rats did not develop heart hypertrophy, whether at organ or cell level. In addition, the kinetics and density of the four main ionic membrane currents that control heart AP were similar in obese and control rats. These ionic currents included I_{CaL}, I_{NCX}, the transient outward potassium current and the delayed rectifier potassium current. Even though leptin receptor (LepR) expression was downregulated in the hearts of the HE obese group, no leptin modification was observed in the current densities except for the I_{NCX} densities in the control group which were fed standard chow (Ricci et al., 2006).

In another study, Huang et al. (2013) found evidence of decreased protein expression of voltage-gated K^+ channels in the obese heart, leading to long QT interval. Their experiments in diet induced obesity (DIO) C57BL/6J wild-type mice revealed that diminished protein and mRNA levels of the potassium channel Kv1.5 were triggered by a decline of the transcription factor cyclic-AMP response element binding protein (CREB) in heart. CREB knock-down by siRNA diminished Kv1.5. CREB is linked to the Kv1.5 promoter in the heart and increases transcription of human and mouse Kv1.5 promoters. The reduction in CREB proteins during lipotoxicity can be rescued by inhibiting protein kinase D (PKD) (H. Huang et al., 2013).

F. C. Howarth et al. (2012) previously reported age-dependent changes in myocyte contractility in the hearts of young and ageing ZDF rats. These changes in contraction are accompanied by changes in Ca^{2+} transport, including a decline in I_{CaL} and subtle changes in expression of a variety of genes including the Ca^{2+} channel, membrane transporters, SR Ca^{2+} and cardiac muscle proteins (F. C. Howarth, 2012). However, DIO causes a heart-upregulation of Ca^{2+} transport genes in SR. While obesity also causes an increase in the levels of SERCA2a, RyR and phospholamban (PLB) mRNA, it did not modify the mRNA levels of L-type Ca^{2+} channel (CACNA1C) and NCX in the hearts of Wistar rat (Lima-Leopoldo et al., 2008). There were no changes in the L-type Ca^{2+} channel protein levels and SERCA2a behavior (expression and activity) (Leopoldo et al., 2011). Surprisingly, a short period of high-fat diet (16 weeks) in *Psammomys obesus*, a polygenic model of rodents, developed for research into obesity, T2DM and CVDs (Chaudhary et al., 2018), led to severe changes in heart structure, activation of inflammatory and apoptotic mechanisms and modification of expression of calcium cycle elements. (Sahraoui et al., 2016). Aromolaran & Boutjdir et al. (2017) reviewed the literature for altered functional expression of ion channels in various animal models associated with obesity and the data are presented in Table 1.

Table 1: Altered functional expression of ion channels in animal models. Adapted from reference (Aromolaran & Boutjdir, 2017).

Current	Gene	mRNA	Protein	Current density	Obese model	Cardiac tissue	QT$_C$	Reference
I_{Na}	SCNA5	NR	NR	↔	Rat (SD)	Ventricle	↑	Axelsen et al., 2015
		↑	NR	↑ *	Rat (WR)	Ventricle	NR	Ashrafi et al., 2016
$I_{Ca,L}$	CACNA1c	NR	NR	↔	Rat (SDCD)	Ventricle	↑	Ricci et al., 2006
		↔	NR	NR	Rat (WR)	WH	NR	Lima-Leopoldo et al., 2008
		↑	NR	↓	Rat (ZDF)	Ventricle	NR	Howarth et al., 2012
		NR	↔	NR	Rat (WR)	Ventricle	NR	Leopoldo et al., 2011
		NR	↓	↓	Rat (OZR)	Ventricle	↑	Lin et al., 2012
		↓	NR	NR	Rat (WR)	WH	NR	Lima-Leopoldo et al., 2013
		↑	NR	↑ *	Rat (WR)	Ventricle	NR	Ashrafi et al., 2016
		↓	NR	NR	Gerbils	WH	NR	Sahraoui et al., 2016
		NR	NR	↓	Rabbit	Ventricle	NR	Luo et al., 2004
		NR	↓	↓	Mice (C57BL/6J/db/db)	Ventricle	NR	Pereira et al., 2006
I_{to}	K$_V$4.2/K$_V$4.3	NR	NR	↔	Rat (SDCD)	Ventricle	NR	Ricci et al., 2006
		NR	↑	NR	Mice (ICR)	Atria	NR	Ricci et al., 2006
		NR	↔	NR	Mice (C57BL/6J)	Ventricle	↑	Huang et al., 2013
		NR	NR	↔	Rat (SD)	Ventricle	↑	Axelsen et al., 2015
		↑	NR	↑ *	Rat (WR)	Ventricle	NR	Ashrafi et al., 2016
	K$_V$1.4	↑	NR	↑ *	Rat (WR)	Ventricle	NR	Ashrafi et al., 2016
I_{Kur}	K$_V$1.5	↓	↓	NR	Mice (C57BL/6J)	Ventricle	↑	Huang et al., 2013
		↑	NR	↑ *	Rat (WR)	Ventricle	NR	Ashrafi et al., 2016
		NR	↑	NR	Mice (ICR)	Atria	NR	Ricci et al., 2006
I_K	I_{Kr}:ERG	↓	NR	NR	Rat (WR)	Ventricle	NR	Ashrafi et al., 2016
	I_{Ks}:KCNQ1	↑	NR	NR	Rat (WR)	Ventricle	NR	Ashrafi et al., 2016
	I_K	NR	NR	↔	Rat (SDCD)	Ventricle	NR	Ricci et al., 2006
		NR	NR	↑	Guinea pig	Atria	NR	Aromolaran et al., 2016
I_{K1}	K$_{ir}$2.1	↑	NR	↑ *	Rat (WR)	Ventricle	NR	Ashrafi et al., 2016

↑, Increased; ↓, decreased; ↔, no change; *predicted from computer simulations; NR, not reported; SD, Sprague Dawley; WR, Wistar Rats; SDCD, Sprague Dawley Cesarean Derived; ZDF, Zucker Diabetic fatty rat; OZR, Obese Zucker Rat; ICR, imprinting control region; QT$_C$, QT interval corrected for heart rate; WH, whole heart.

1.13.2 Animal models of obesity and their relevance to the heart

In order to study the mechanisms of heart remodeling in the context of obesity, several animal models have been used over the years to study the function and dysfunction of the heart. These models resemble obesity in humans, as well as comorbidities such as IR, glucose tolerance failure, hypertension and diabetes. ZDF rats were isolated and

derived from the ZF rat and are extensively used for obesity and T2DM research and will be discussed in more detail later.

Storage of fat, especially in heart muscle, is associated with a reduction in the production of cardiac force, which has negative hemodynamic consequences and ultimately leads to HF. In addition, fats in the blood can be absorbed by heart muscle cells, where they can be used to generate energy that can be stored or used in mitochondria. Experiments in ZDF rats have shown that fat actually accumulates in the heart due to increased transport across different membranes. Current experiments also show that lipids accumulate in the heart despite normal mitochondrial content, morphology and oxidation of long-chain fatty acids (LCFA) (Holloway et al., 2011). In addition, increased transport rates of LCFA and LCFA protein result in a larger number of lipid drops stored in heart muscle (Holloway et al., 2011).

Obesity is associated with high blood pressure (BP), which increases the risk of CVDs. Simonds et al. (2014) observed that the increase in leptin levels observed in DIO promotes an increase in BP in rodents, an outcome that was not previously seen in leptin deficient or LepR deficient animals. Similarly, humans, with a loss in function of mutations in leptin and LepR, have reduced BP despite severe obesity. This fascinating observation indicates that leptin is linked with changes in body weight in both human and mammals leading to an alteration in BP. Thus, leptin and LepR effects are essential for diabesity and can be used to establish useful therapeutic targets for the prevention and treatment of obesity-associated hypertension and/or obesity-associated CVDs (Simonds et al., 2014).

In a study in ZL, ZF and Sprague-Dawley rats Lin et al. (2015) examined the SAN to test for the function of specific behaviors of leptin on heart rate (HR) and ventricular repolarization. They discovered that adipocytes and LepR were present in the myocardium and as a result, it was speculated that leptin could directly alter the electrical properties of the heart such as HR and QT intervals and that it can control cardiac electrical activity via the activation of the β-adrenergic receptor (β-AR). These findings suggested that leptin, at high doses (150–300 μg/kg), can stimulate a biphasic effect (decrease followed by an increase) in HR while at low doses (0.1–30 μg/kg), it can decrease resting HR. Resting

HR inhibition induced by leptin was abolished by the presence of a leptin antagonist. Leptin also corrected QTc interval time and increased HR. However, leptin antagonist did not change these two parameters. It was also reported that in isolated ventricular myocytes, leptin (0.03–0.3 µg/ml) increased the APD and the effects were reversible. Leptin has a direct effect on the reduction of HR and the increase of QT interval by its own receptor and independently of β-AR stimulation. Moreover, high concentrations of leptin in the myocardium can produce long QT intervals, deep bradycardia, and VA by inhibiting the activity of the β-AR (Lin et al., 2015). We will discuss our investigation of β-AR in chapter 7.

1.14 Relationship between obesity and type 2 diabetes mellitus

Obese people are more likely to develop T2DM and obesity is an independent and important metabolic marker of T2DM. T2DM, induced by obesity, is usually referred to as metabolic syndrome or IR, or pre-diabetes that leads to a high blood glucose level. In this condition, the body synthesizes and releases sufficient insulin in the blood, but the cells of the body have become resistant to the effects of insulin (Weyer et al., 2001).

In recent years, scientists have developed a new T2DM rat model, the ZDF rat (Yokoi et al., 2013). This model is naturally obese and develops T2DM and inflammation. As such, it is an ideal model to understand how obesity-induced T2DM can lead to DCM.

Due to the strong connection between obesity and diabetes, the term "diabesity" was created. Although the majority of T2DM patients are obese, only a relatively small proportion of obese people develop T2DM (Zimmet et al., 2001). The molecular mechanisms proposed to explain these complications are not yet well understood. Figure summarizes the three main hypotheses which have been developed in recent years to explain the molecular basis of diabesity (Chadt et al., 2000) and they include the following:

1. The "inflammation hypothesis" suggests that obesity represents a state of chronic inflammation where inflammatory molecules released by the infiltration of macrophages into adipose tissue cause pathological changes in β-cells and insulin-sensitive tissues such as the endocrine glands, the muscles, the endocrine pancreas, and the liver.

2. The "lipid overflow hypothesis" suggests that obesity may lead to an increase in ectopic lipid storage, as obese people have limited fat storage capacity in fat tissues. These potentially harmful lipid components and metabolites can be used to stimulate cytotoxicity of peripheral cells of the pancreas, muscles, and liver.

3. The "adipokine hypothesis" suggests that the main role of white fat cells is to function as an endocrine organ and secrete a range of hormones with autocrine and paracrine activity. Diabesity enlarging fat reserves can cause the dysfunctional secretion of these endocrine factors, thus resulting in metabolic impairment of insulin target tissues and ultimately failure of insulin producing β-cells. Moreover, these adipokines have direct effects on the muscles, the central nervous system (CNS) and the liver.
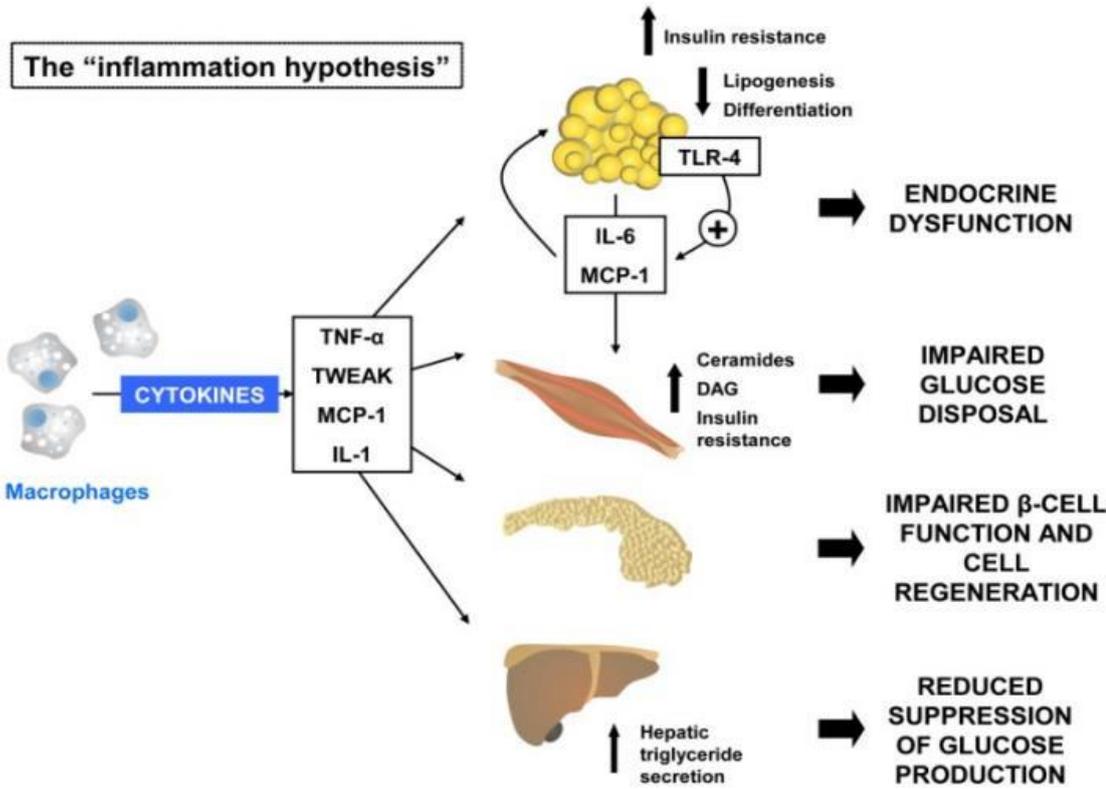
(A)

Figure 18: Three main hypotheses that link obesity and diabetes. (A) Inflammation. Adapted from (Chadt et al., 2000).
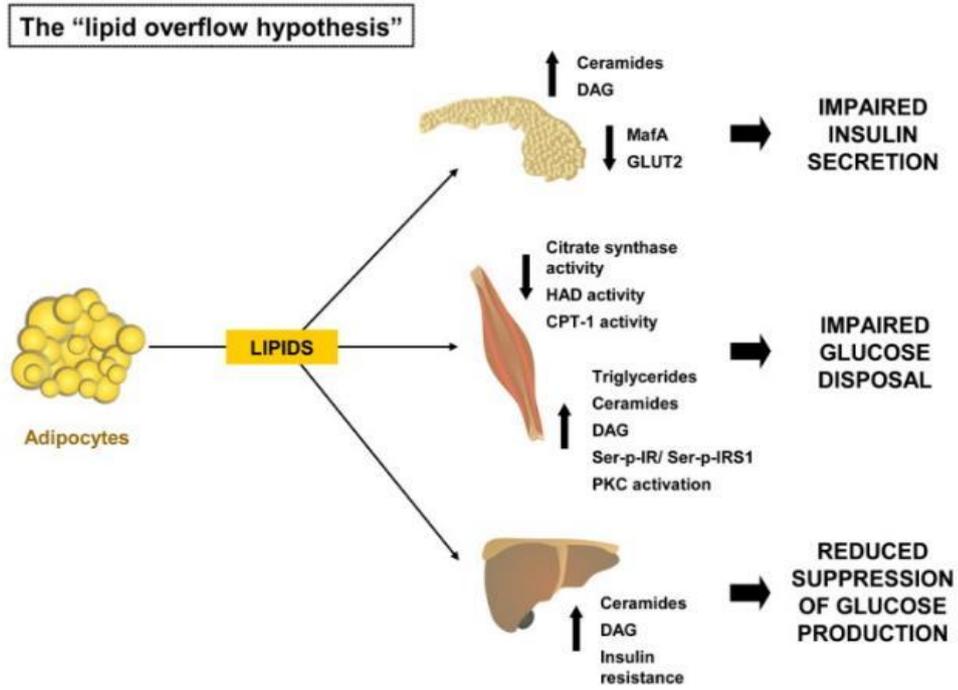
(B)
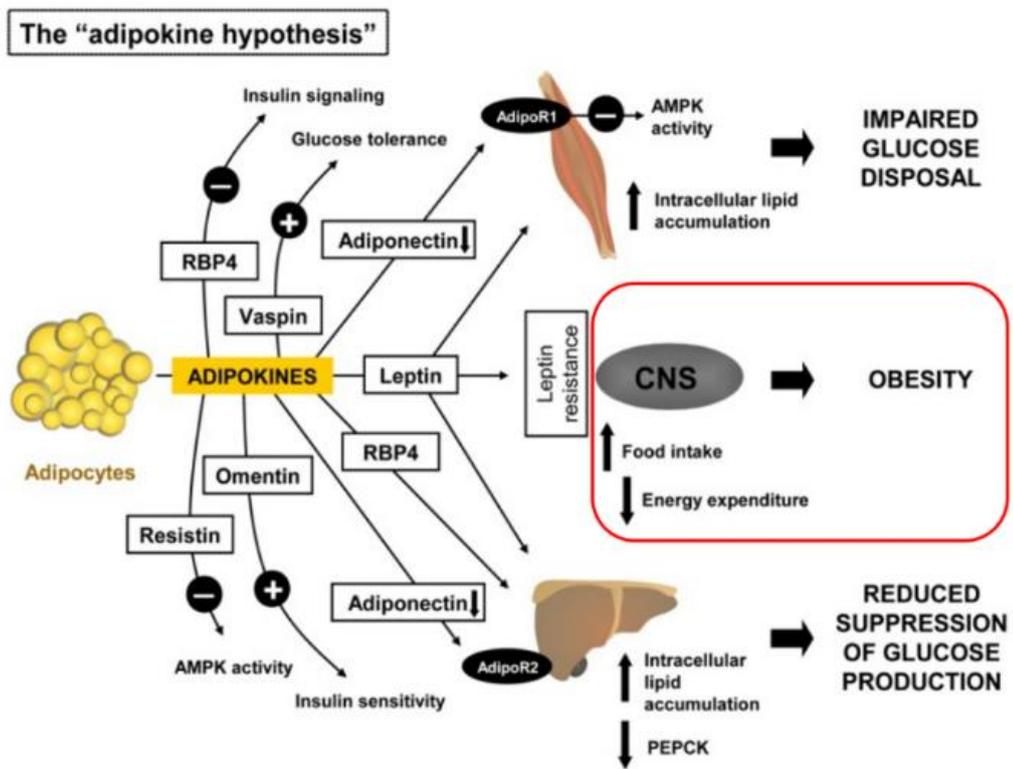
(C)

Figure 18: Three main hypotheses that link obesity and diabetes. (B) Lipid overflow and (C) adipokines. Adapted from (Chadt et al., 2000) (Continued).

Obesity is correlated with various disorders such as hypertension, sleep apnea syndrome, atherosclerosis, and CAD. Obesity also precedes changes in the structure and function of the heart and ultimately leads to HF. Obesity can cause changes in myocardial structure and increase the risk of ventricular fibrillation or HF, as well as sudden cardiac death (SCD) (Csige et al., 2018). That is why it is important to investigate the effects of obesity on the heart and its relationship to DCM.

1.15 Development of diabetic cardiomyopathy

More than 80% of obese patients die from DCM. As such, it is important to understand this disease, including several risk factors such as hyperlipidemia, high BP, diet, obesity, smoking, reduced physical activity and genetics as well as the development of DCM in T2DM (Mortuza & Chakrabarti, 2014; Schaffer, 1991). It is known that DM can cause both short- and long-term complications due to damage of blood vessels in various organs of the body. Some of these complications include macrovascular diseases such as high blood pressure, high cholesterol, heart attack, CAD, stroke, cerebral vascular disease and peripheral vascular disease. Other complications include microvascular diseases such as retinal, nephrological, and neurologic diseases. Macrovascular complications and, to a lesser extent, microvascular complications such as nephropathy can lead to DCM (Falcão-Pires & Leite-Moreira, 2012; Isfort et al., 2014; Murarka & Movahed, 2010). DCM is a major adverse complication of T2DM characterized by diastolic and systolic dysfunction. In T2DM, factors contributing to DCM include a defective regulation of Ca^{2+} cell homeostasis due to the dysregulation of calcium transport proteins in cells. First, there is a significant impairment in sarcolemmal NCX activity, limiting the ability of the diabetic heart to extrude Ca^{2+} leading to an elevation in diastolic $[Ca^{2+}]_i$. Second, there is a decrease in Na^+/K^+ ATPase activity, which is known to increase $[Ca^{2+}]_i$ secondary to a rise in $[Na^+]_i$. Third, Ca^{2+} influx via the Ca^{2+} channel is stimulated (Schaffer, 1991). Fourth, SERCA activity is reduced in diabetic hearts and fifth, the RyR becomes desynchronized leading to elevated diastolic calcium (H. Huang et al., 2017; Snyders, 1999). In addition, the dysfunction of vascular endothelial cells and cardiac endothelial cells can also contribute to the pathogenesis of DCM leading to oxidative stress, elevation in methylglyoxal (MG), fibrosis, hypertrophy and remodeling of the heart

(Matafome et al., 2017; Mortuza & Chakrabarti, 2014). Since DCM is a major hallmark of diabetes, including both T1DM and T2DM and since obesity also plays a role in the development of T2DM, then it is important to ascertain how obesity-induced DM, as in the model of ZDF rats, can induce DCM. Therefore, it is important to understand the development of the ZDF model and what is currently known about DCM in this model.

1.16 Aims and Objectives

[1] To explore the general characteristics of ZDF and ZF compared to ZL rats.

[2] To explore the effects of obesity and diabesity on the electrical conduction system of the heart using *in-vivo* biotelemetry techniques in ZDF and ZF compared to ZL rats.

[3] To explore the effects of obesity and diabesity on the electrical conduction system in the isolated perfused heart using an extracellular suction electrode in the ZDF and ZF compared to ZL rats.

[4] To explore the effects of obesity and diabesity on ventricular myocyte shortening using cell imaging in the ZDF and ZF compared to ZL rats.

[5] To explore the effects of obesity and diabesity on ventricular myocyte Ca^{2+} transport using fluorescence photometry techniques in the ZDF and ZF compared to ZL rats.

[6] To explore the effects of obesity and diabesity on ventricular myocyte Ca^{2+} transport using whole-cell patch clamp techniques in the ZDF and ZF compared to ZL rats.

[7] To explore the effects of Isoprenaline (ISO) on obesity and diabesity on ventricular myocyte shortening and Ca^{2+} transport using cell imaging and fluorescence photometry techniques in the ZDF and ZF compared to ZL rats.

[8] To explore the effects of obesity and diabesity on the expression of proteins and structure of ventricular muscle using Western blot and Transmission electron microscope (TEM) techniques in the ZDF and ZF compared to ZL rats.

Chapter 2: Investigating the general characteristics of ZDF and ZF compared to ZL rats

2.1 Introduction

The ZF rat inherits obesity as an autosomal Mendelian recessive trait. ZDF rats originated from ZF and are widely used in T2DM research. ZF rats have a mutation (fatty, fa) in the LepR gene which leads to excessive eating or hyperphagia and the development of obesity without DM. A missense mutation (conversion A to C in nucleotide position 806) was found in the extracellular domain of all isoforms in ZF rats (fa/fa), which resulted in an amino acid change from glycine (Gln) to proline (Pro) at +269. The obese mouse named the "ob/ob" mouse model was discovered in 1949 at the Jackson laboratories in Maine (Ingalls et al., 1950). It was later hypothesized by Jeffrey Friedman that the responsible gene was Leptin (as of the Greek term *Lepto* signifying thin) (Friedman, 2012, 2016; Neill, 2013). Leptin is a versatile 16 kDa peptide hormone which is secreted by fat cells with various actions, one of them is controlling hunger and satiety (Frühbeck, 2006). These (OB-R) leptin receptor isoform mRNAs are present in the brain from ZF (fa/fa) rats at similar amounts to those in their lean littermates (ZL) (Takaya et al., 1996). ZF rats are obese, hyper-insulinemic and hyperphagic, but blood glucose remains at normal levels. Hypertriglyceridemia in these animals is usually due to increased liver production of VLDL. Adipocytes increase in number and size and, in general, subcutaneous fat stores have the largest number of fat cells. The lipogenesis of glucose occurs abruptly in young animals but decreases with age. Enzymatic patterns of glycolysis and gluconeogenesis seem to reflect a changed internal environment, rather than specific defects. Endocrine changes in fatty rats include a reduction in glucagon levels, hyperinsulinemia, and hypothyroidism, and during their first introduction they had defective reproductive function (Bray, 1977).

From a ZF rat colony (Yokoi et al., 2013), a new strain of homozygous male rats fa/fa with reproductive capability was found by mating male fa/fa and heterozygous fa/+ female. This new fa/fa male rat strain showed DM-selective breeding and showed relatively high blood sugar levels at 10 weeks of age which resulted in the establishment of a diabetic strain that was designated: ZDF -Lepr fa. These fa/fa male heterogeneous

rats developed DM at the age of 10 weeks and all the rats had DM at the age of 21 weeks, while none of the male fa/+ rats developed DM. The phenotypical characteristics of this diabetic species differ from those of normal-glycemic ZF rats. Several studies have shown progressive functional and structural changes in the heart and kidneys from 16 weeks, without evidence that one pathology precedes or causes the other in ZDF rats (Baynes & Murray, 2009). The highly reproductive ZDF rats provide a useful animal model of T2DM (Yokoi et al., 2013).

2.2 Aims and objectives

- To investigate the characteristics of ZDF and ZF compared to ZL control rats in terms of their body weight, heart weight, non-fasting glucose and their plasma insulin levels.
- To investigate the differences in glucose tolerance in ZDF and ZF compared to ZL control rats.

2.3 Methods

Ethical consent for this research project was acquired from the UAE University Animal Research Ethics Committee and experiments were executed in agreement with institutional guidelines.

Four different batches (10 each) of Male Zucker rats (40 ZF, 40 ZDF, 40 ZL) were purchased from Charles River (USA) aged 28–34 days on the day of their arrival and housed in our animal facility. Rats were housed individually and received water and standard rat chow *ad libitum*. The temperature was maintained at (22–24°C) and rats were exposed to a 12/12-hour light/dark cycle. The following Table 2 provides the detailed composition of the standard chow animal feed.

Table 2: Standard Chow Animal feed.

Animal Feed		
Rats & Mice Feed (12 mm Pellets)		
(Diet-A feed pellets)		
Each Sack - 50 Kg		
Food Composition:		
C. Protein	24% min	
C. Fiber	5% Max	
C. Ash	8% Max	
Calcium	1% Min	
Phosphorus	0.75% Min	
From Vitamin Premix		
A	IU/Kg	14500
D	IU/Kg	4500
25-OH Vit D	µg/Kg	68.75
E	mg/Kg	111.67
K3	mg/Kg	3.3
Thiamine (B1)	mg/Kg	3.175
Riboflavin (B2)	mg/Kg	9.15
Pantothenic Acid	mg/Kg	18.12
Pyridoxine (B6)	mg/Kg	8.5
Biotin	µg/Kg	245
Niacin	mg/Kg	95.039
Folic Acid	mg/Kg	2.175
Cyanocobalamin	µg/Kg	25
Note:		
The animal feed was supplied by the Abu Dhabi Animal Flour and Feed Factory, Abu Dhabi		

Body weight and blood glucose (OneTouch Ultra 2, LifeScan) were measured periodically during the study. Glucose tolerance tests (GTTs) were administered just before the start of every experiment for each batch of animals. Blood was taken from the

rat tail vein of the non-anesthetized rats. Following an overnight fast the fasting blood glucose (FBG) was determined. Animals were then injected with glucose (2g kg^{-1} body weight, intraperitoneal) and blood glucose was measured at 30, 60, 120 and 180 minutes after glucose injection.

Insulin is the primary hormone responsible for the control of glucose metabolism. It is synthesized in the β-cells of the islets of Langerhans. Proinsulin which is the precursor to insulin is processed to form C-peptide and insulin which are then secreted into the portal circulation in equimolar amounts. The mature insulin consists of 51 amino acids that comprises two polypeptide chains, the A and B chains which are linked together by two inter-chain disulphide bridges. The A chain also has an intra-chain disulphide bridge. The main function of insulin is to control the uptake and utilization of glucose in peripheral tissues via the glucose transporter (Figure 19) (Harvey & Ferrier, 2011).
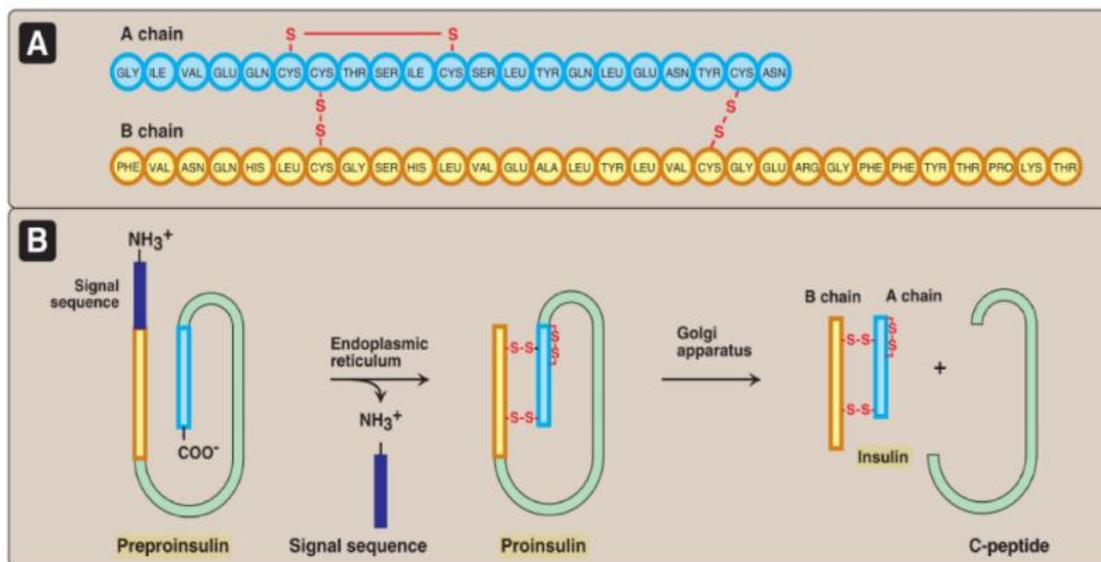
Figure 19: Insulin. (A) Structure of insulin and (B) formation of insulin. Adapted from (Harvey & Ferrier, 2011).

At the time of the experiments and during the sacrifice of the rats the blood was collected from the neck of the decapitated head in Ethylenediaminetetraacetic acid (EDTA) coated glass tubes which is an anticoagulant to prevent blood from clotting (Nguyen & Wahed, 2013), then it was centrifuged at 400 revolutions per minute (RPM)

(Centurion Scientific, C2 series) for 5 minutes and the supernatant blood plasma was removed then stored at -80ºC for insulin ELISA measurements. A commercially available rat insulin ELISA kit (10-1250-01, Mercodia AB, Sweden) was used. It is a solid phase two-site enzyme immunoassay based on the direct sandwich technique in which two monoclonal antibodies are directed against separate antigen determinants on insulin. During incubation insulin in the sample reacts with peroxidase-conjugated anti-insulin antibodies and anti-insulin antibodies bound to the microtiter well. During washing the unbound enzyme labeled antibody is removed. Then the bound conjugate is detected by reacting with 3,3',5,5'-tetramethylbenzidine. The reaction is stopped by adding acid to give a colorimetric endpoint that is read using a spectrophotometer.

2.4 Statistics

Results were presented as the mean ± standard error of mean (SEM) of n observations. Statistical comparisons were done by IBM SPSS and Origin 9.0 (OriginLab, Northampton, Massachusetts, USA) statistics software using either the independent samples t-test or one-way ANOVA and then by Bonferroni corrected t-tests for multiple comparisons, as appropriate. P values of 0.05 and less were considered statistically significant.

2.5 Results

The general characteristics of the ZL, ZF and ZDF rats are shown in Table 3. The ZF and ZDF groups exhibited significantly ($p < 0.05$) increased body weight and heart weight compared to ZL rats. Non-fasting blood glucose was significantly higher in ZDF (384.44±20.28 mg/dl) compared to ZF (140.00±4.58 mg/dl) and ZL (118.25±2.62 mg/dl) rats. Non-fasting blood glucose was not significantly ($p > 0.05$) different between ZF and ZL rats. Heart weight / body weight ratio was increased in ZF (3.27±0.09 g/mg) rats compared with (ZL 2.71±0.07 g/mg) and ZDF (2.79±0.05 g/mg). Insulin was measured by ELISA in blood plasma using a commercially available rat insulin ELISA kit (10-1250-01, Mercodia rat Insulin ELISA). ZF (12.70±1.15 µg/L) had significantly ($p < 0.05$) higher insulin levels compared to ZL (2.09±0.57 µg/L) and ZDF (2.14±0.29 µg/L) rats and these results are similar to a previously published study (Chohnan et al.,

2020).

Table 3: General characteristics of Zucker rats.

	ZL (n)	ZF (n)	ZDF (n)
Body weight (g)	439.82±6.46 (33)	695.85±14.30 (33)*	558.83±21.44 (36)*#
Heart weight (g)	1.66±0.05 (33)	2.15±0.05 (33)*	2.00±0.06 (36)*
Non-fasting blood Glucose (mg/dl)	118.25±2.62 (32)	140.00±4.58 (33)	384.44±20.28 (36)*#
Heart weight/ Body weight ratio (mg/g)	2.71±0.07 (33)	3.27±0.09 (33)*	2.79±0.05 (36)#
Plasma Insulin (µg/L)	2.09±0.57 (10)	12.70±1.15 (9)*	2.14±0.29 (8)#

Data are mean ± SEM, number of animals is in parenthesis. P values of 0.05 and less were considered statistically significant. * $p<0.05$ compared to ZL, # $p<0.05$ compared to ZF.

The glucose tolerance test was performed just before commencement of experiments (Figure 20). The fasting blood glucose was highest in ZDF (223.4±12.86 mg/dL, n=35), intermediate in ZF (133.53±2.99 mg/dL, n=34) and lowest in ZL (94.55±1.59 mg/dL, n=33) rats and these differences were significant ($p<0.05$). At 180 minutes following the glucose challenge, blood glucose remained significantly elevated ($p<0.05$) in ZDF (373.97±23.86 mg/dL, n=33) and ZF (212.29±14.43 mg/dL, n=34) in contrast to ZL (113.88±4.32 mg/dL, n=33-35) control rats.
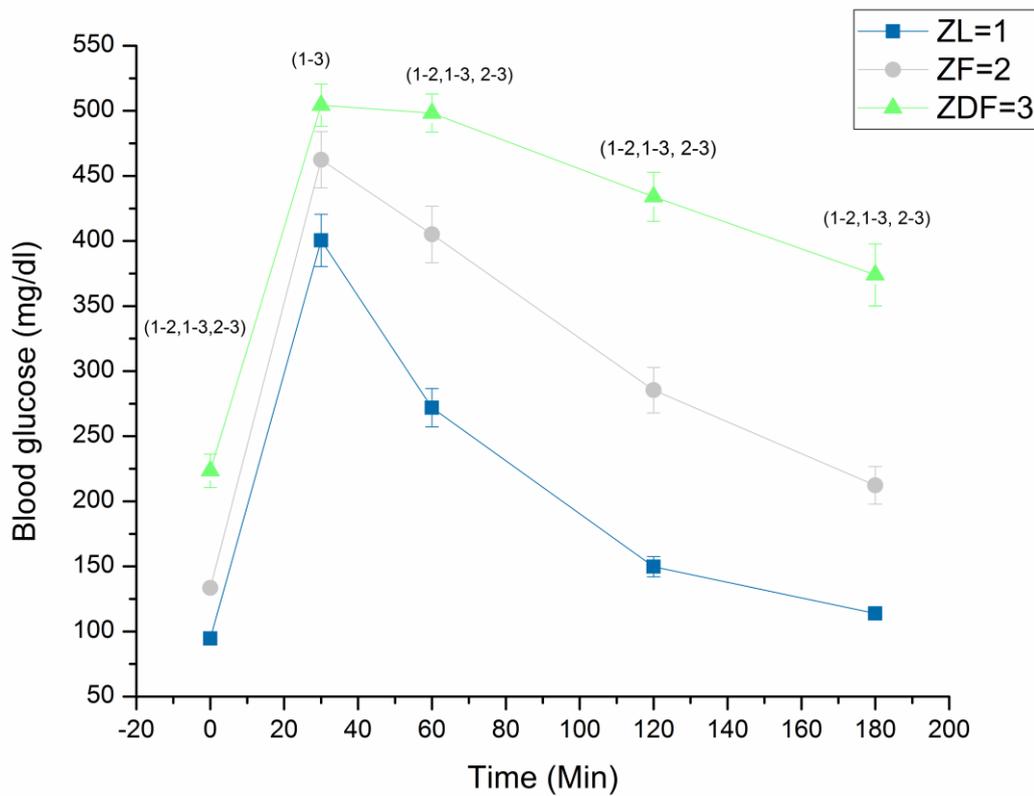
Figure 20: Glucose tolerance test. Data are mean ± SEM, n=33 ZL, 34 ZF and 33-35 ZDF rats. Numbers in parenthesis represent significant differences. P values of 0.05 and less were considered statistically significant.

2.6 Discussion

ZDF and ZF rats were characterized by increased body weight and heart weight compared to ZL rats and ZDF rats had elevated non-fasting blood glucose compared to ZF and ZL rats. Heart weight/body weight ratio was highest in ZF compared to ZL and ZDF rats. Fasting blood glucose was highest in ZDF, intermediate in ZF and lowest in ZL rats. At 180 minutes, following the glucose challenge, blood glucose was still significantly elevated in ZDF and in ZF compared to ZL rats. It was interesting to find that blood insulin was significantly raised in ZF rats but not in ZDF rats compared to ZL rats however, these findings are consistent with previous studies (Chohnan et al., 2020; Jonas et al., 2005). Another study reported raised fasting serum glucose, insulin, cholesterol and triglyceride and impaired glucose tolerance in ZDF rats (Sárközy et al.,

2013). These results might be explained by considering the mechanisms involved in insulin signaling and degradation. The ratio of the bound and unbound insulin to its receptors could be compromised in ZF rat. Insulin signaling starts with binding to a tyrosine kinase receptor called insulin receptor kinase (IRK). Following autophosphorylation, it is internalized into the endosomal system (ENS) where it is activated to tyrosine phosphorylate key cellular substrates which then recruit glucose transporters from intracellular stores in skeletal, cardiac muscle and adipose tissue which in turn activates various biological processes. Degradation of insulin is controlled by intra-endosomal acidification, in which "insulinase" promotes the dissociation of insulin from the IRK. This degradation may also be compromised in the ZF rat (Harvey & Ferrier, 2011; Posner, 2017). The observed increase in the body weight is consistent with the hyperphagia seen in ZDF and ZF rats. Previous studies have reported similar changes in FBG, GTT and RBG and serve to demonstrate the relationship between obesity and diabesity on glucose metabolism (Di Nardo et al., 2015; F. C. Howarth et al., 2011, 2012; López-Soldado et al., 2016).

2.7 Conclusions

- Non-fasting and fasting blood glucose was significantly elevated in ZDF compared to ZF and ZL rats.
- Heart weight / body weight ratio was increased in ZF rats compared with ZL and ZDF.
- ZF rats had significantly higher insulin levels compared to ZDF and ZL rats.

Chapter 3: Investigating the electrical conduction system using *in-vivo* biotelemetry techniques in the ZDF and ZF compared to ZL rats

3.1 Introduction

There is currently limited research on ECG measurement and assessment in ZDF rats. Early signs of diabetic autonomic neuropathy in the ECG include widening of QTc interval, elevated R wave amplitude (AMP) and decreased heart rate variability (HRV) which is a measure of the autonomic nervous system and discussed below. The severity of neuropathy is directly related to the risk of mortality. Aerobic exercise training (AET) is a common recommendation for postponing and possibly reversing cardiac dysfunction. A previous study demonstrated alterations in R wave AMP, HRV, QT and QTc intervals in ZDF rats. AET had beneficial effects and was able to correct the changes in the AMP of the R wave as well as ECG correlates of the left ventricle mass (VanHoose et al., 2010).

SAN from the right atria of male obese and ZL rats, male Sprague-Dawley, as well as the ventricles of male Sprague-Dawley rats have been used to investigate the direct actions of leptin on HR and ventricular repolarization. Since LepR and adipocytes are present in the myocardium, it has been proposed that Leptin modulates the electrical properties of the heart through activation of the β-AR and that it can directly regulate cardiac electrical properties such as HR and QT interval through its receptor. The results from the study showed that leptin, at low doses (0.1–30 μg/kg), decreased resting HR while at high doses (150–300 μg/kg), it produced a biphasic effect (decrease followed by an increase) on HR. The leptin-induced inhibition of resting HR was fully reversed by leptin antagonist. Leptin also increased HR and corrected QTc interval, however, leptin antagonist did not reverse these two parameters. In isolated ventricular myocytes, leptin (0.03–0.3 μg/ml) reversibly increased the APD. In summary, leptin can directly increase QT interval and decrease HR through its receptor independent of β-AR stimulation. During inhibition of β-ARs, higher concentrations of leptin in myocardial cells can cause deep bradycardia, delayed QT intervals and VAs (Lin et al., 2015).

3.2 Hypothesis

- Defects in electrical transmission partly underlie electro-mechanical dysfunction in the ZDF and ZF rat heart.

3.3 Aims and objectives

- The general aim was to explore the effects of obesity and diabesity on the electrical conduction system using *in-vivo* biotelemetry techniques in the ZF and ZDF compared to ZL control rats.

- The specific aims were to investigate the effects of obesity and diabesity on HR, physical activity, body temperature and ECG in the ZDF and ZF compared to ZL control rats.

3.4 Methods

Biotelemetry experiments in ZF, ZDF and ZL rats were performed according to previously described techniques (F. C. Howarth et al., 2008). Heart biopotential, body temperature and physical activity were monitored with a biotelemetry system (Data Sciences Int.). The biotelemetry system consisted of the transmitter devices (TA11CTA-F40, Data Sciences Int.), the receivers (RPC-1, Data Sciences Int.), a data exchange matrix (20CH, Data Sciences Int.) and a personal computer for system acquisition, control, configuration and data storage. The transmitter devices were implanted in 10 ZF, 10 ZDF and 10 ZL rats at 70–75 days of age, under general anesthesia (sodium pentobarbitone, 45–55 mg kg^{-1}, intraperitoneal). The transmitter devices were surgically implanted into the peritoneal cavity and electrodes from the transmitter were arranged in Einthoven bipolar lead II configuration (right foreleg and left hind leg) and recording was continued up to 195 days of age as shown in Figure 21.

Figure 21: Biotelemetry system. Top left panel: configuration of receivers. Top right panel: electrodes configuration (lead II). Bottom left panel: transmitter next to anesthetized animal. Bottom right panel: rats in separate cages on top of the receivers.

3.4.1 Biotelemetry data collection and analysis

ECG, body temperature, and physical activity data were collected for 5 minutes per hour per animal, 24 hours per day, and 7 days per week for the full duration of the 6.5-month study. From the collected ECG data, secondary physiological measurements were determined, including the average 5-minute PQ, QRS, QT, QTc, HR, average 24-hour HRV and HRV power spectral density (PSD). The PQ interval was identified as the time from the beginning of the P wave to the beginning of the QRS complex. The QRS duration was the time from the start to the end of the QRS complex. The QT was measured as the time from the onset of the QRS to the end of the T-wave. QTc is the HR adjusted QT interval. The average 5-minute PQ, QRS, QT, and QTc intervals were determined using the Physiostat ECG Analysis application (Data Sciences Int.). The PQ, QRS, and QT intervals were defined as the per-beat time between each of the ECG locations. The QTc was defined as corrected QT interval whereby the Bazett algorithm was implemented by dividing each QT interval by the square root of the associated R-R interval. The 5-minute

average HR was determined from the average normal-to-normal R-wave interval and then converted to beats per minute (BPM). The HRV was computed over 24 hours as the standard deviation of the average normal-to-normal HR, which is termed the SDANN (Task Force, 1996). To estimate the 24-hour HRV PSD, first the normal-to-normal R-wave intervals were computed for each 5-minute ECG. Then, each 5-minute strip was interpolated to 0.1 seconds equally spaced data with the average suppressed. Then the Burg Method was used to estimate the normalized PSD of each 5-minute strip, by determining the Fourier transform of the least squares, autoregressive model. Power normalization was implemented by dividing each spectral estimate by the sum total. Since the 5 minutes, beat-to-beat HRV signal had been interpolated to 0.1 seconds, the PSD frequencies ranged from 0 to 5 Hz, as per the Nyquist sampling criteria. Lastly, 24 consecutive PSD estimates were averaged to determine the 24-hour HRV PSD estimate per animal. From the 24-hour HRV PSD, the low frequency (LFq) and high frequency (HFq) ranges were set by inspection and computed as the magnitude total between 0.5-1.5 Hz and 2.5-3.5 Hz, respectively. The LFq/HFq ratio was also computed (F. C. Howarth et al., 2005). An example of our acquisition software (Data Sciences Int.) is shown in Figure 22.
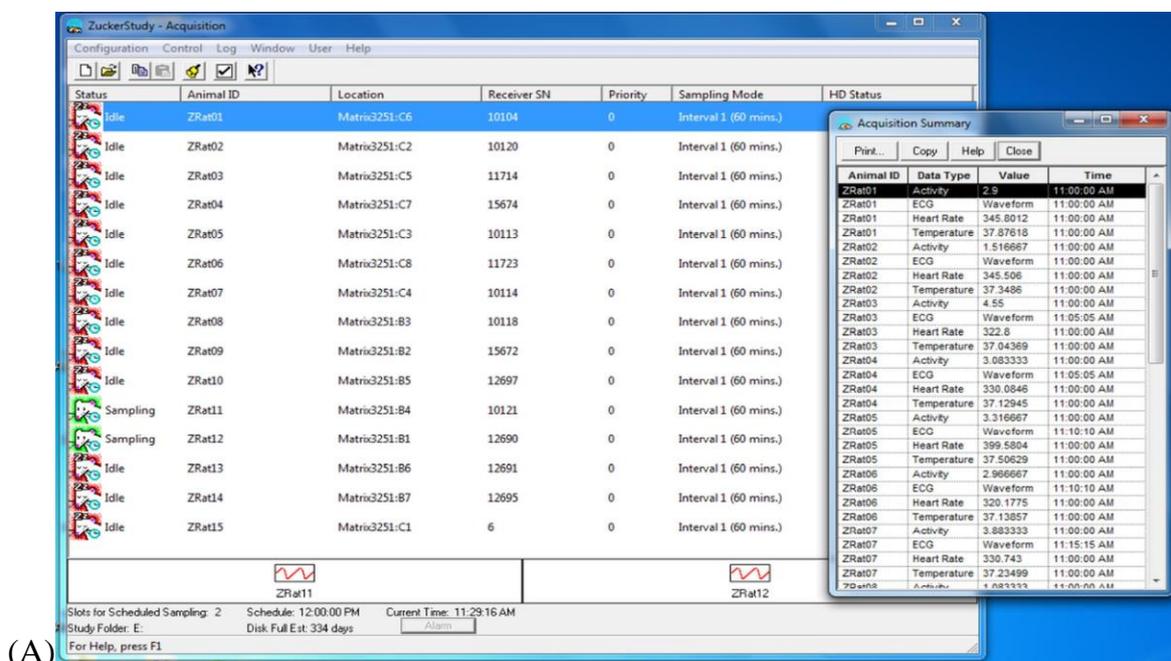
Figure 22: Acquisition software (Data Sciences Int.). (A) Sampling and acquisition summary.
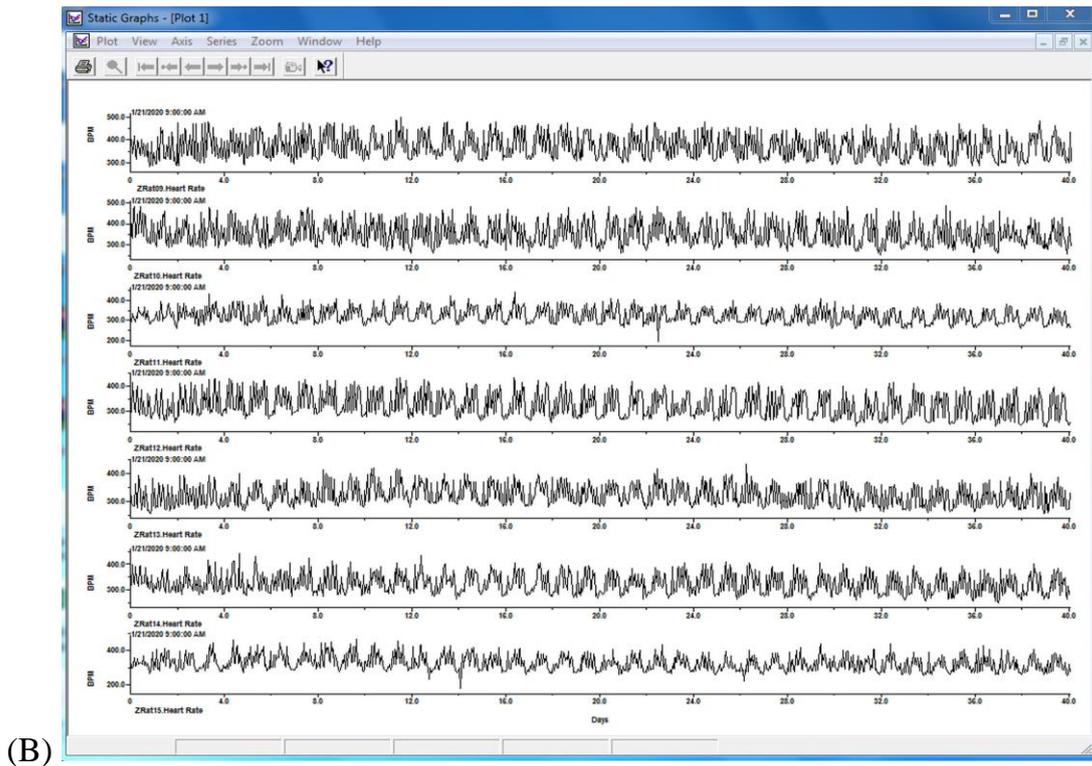
Figure 22: Acquisition software (Data Sciences Int.). (B) Typical ECG records (Continued).

3.5 Statistics

Two-way repeated measures ANOVA was used to investigate the effect of group (ZDF, ZF and ZL rats), age (105, 135, 165 and 195 days of age) and the interaction of group and age on HR, HRV and other physiological parameters. Repeated measures ANOVA was used because the same unit was observed at four different time points. The main assumptions of the repeated measure ANOVA were tested for each outcome. The normality assumption was tested using the Shapiro-Wilk test, and the sphericity assumption was tested using the Mauchly's test. Additionally, the Independent Samples t Test was used to further analyze the differences, in HR and other physiological parameters, between the groups at each age and the Paired Samples t Test was used to further analyze the differences, in HR and other physiological parameters, between the different ages for each group. P values of 0.05 and less were considered statistically significant.

3.6 Results

3.6.1 Bioteletry physical activity results

Physical activity was determined by measuring changes in the animal's transmitter signal strength. Specifically, the transmitter signal strength was sampled at 64 Hz and calibrated to counts per minute (CPM). When the animal changed position, the corresponding transmitter signal strength changed, which resulted in a change in CPM. Low counts indicate reduced physical activity in the animal. The continuous average physical activity in ZDF, ZF and ZL groups for the 4-month study is shown in Figure 23A. There were some significant ($p < 0.05$) differences in mean physical activity between the groups and ages of the rats as shown in Figure 23B. At 195 days, the physical activity was (1.41 ± 0.20 CPM, n=10 in ZL), (1.38 ± 0.15 CPM, n=10 in ZF) and (1.65 ± 0.11 CPM, n=10 in ZDF) rats; however, these differences in physical activity were not significant ($p > 0.05$) (Figure 23B).
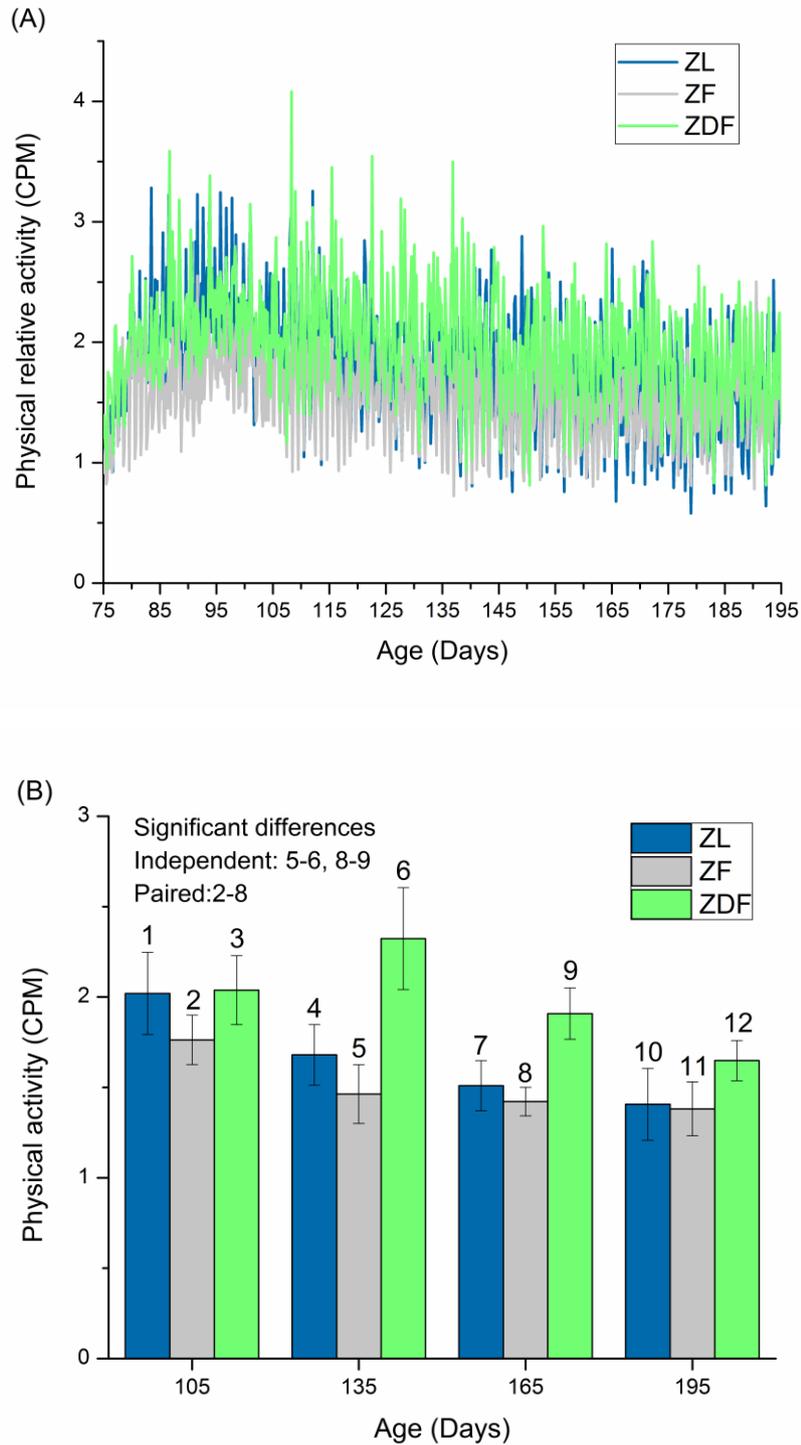
Figure 23: Physical activity. (A) Continuous mean physical activity recorded throughout the study and (B) mean physical activity at 105, 135, 165 and 195 days. Data are mean ± SEM, n=10 ZL, 10 ZF, and 10 ZDF rats. P values of 0.05 and less were considered statistically significant.

3.6.2 Biotelemetry body temperature results

The animal body temperatures were measured hourly. The continuous average body temperature in ZDF, ZF and ZL rats for the 4-month study are shown in Figure 24A. There were some significant ($p<0.05$) changes in mean body temperature between groups and ages of the rats as shown in Figure 24B. At 195 days the body temperature was ($37.24\pm0.12°C$, n=10 in ZL), ($37.18\pm0.11°C$, n=10 in ZF) and ($37.45\pm0.10°C$, n=10 in ZDF) rats and the differences were not significant ($p>0.05$) (Figure 24B).
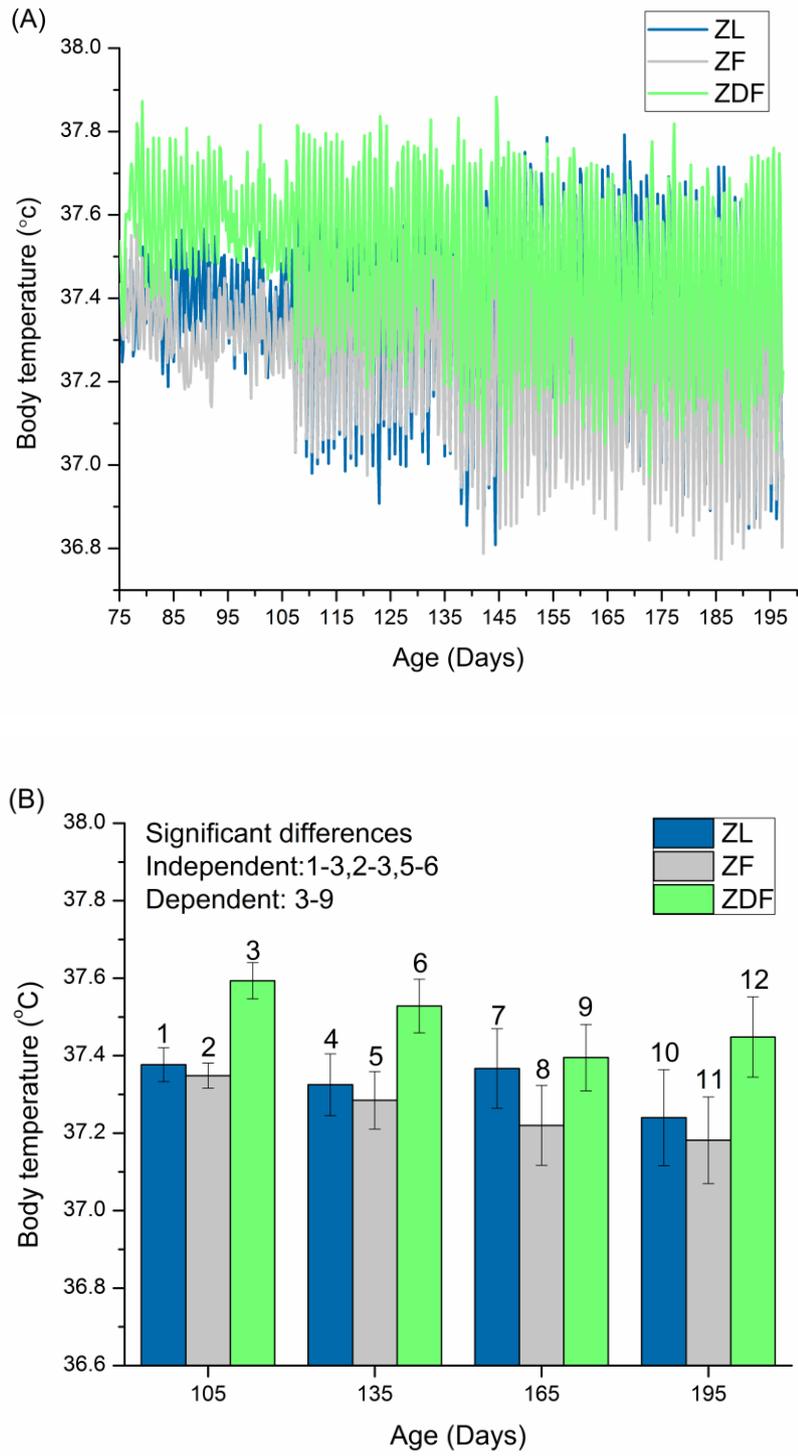
Figure 24: Body temperature. (A) Continuous mean body temperature recorded throughout the study and (B) mean body temperature at 105, 135, 165 and 195 days. Data are mean ± SEM, n=10 ZL, 10 ZF, and 10 ZDF rats. P values of 0.05 and less were considered statistically significant.

3.6.3 Biotelemetry heart rate

The HR was determined from the 5-minute average of all normal R-wave to R-wave intervals in the ECG. The continuous group average HR for ZDF, ZF and ZL rats over the 4-month study is shown in Figure 25A. There were some significant ($p < 0.05$) changes in mean HR between the groups and the ages of the rats as shown in Figure 25B. At 195 days, HR was significantly ($p < 0.05$) lower in ZDF (265 ± 8 BPM, n=10) compared to ZF (336 ± 9 BPM, n=10) and ZL (336 ± 10 BPM, n=10) rats. HR was 21% lower in ZDF compared to ZF and ZL rats (Figure 25B).
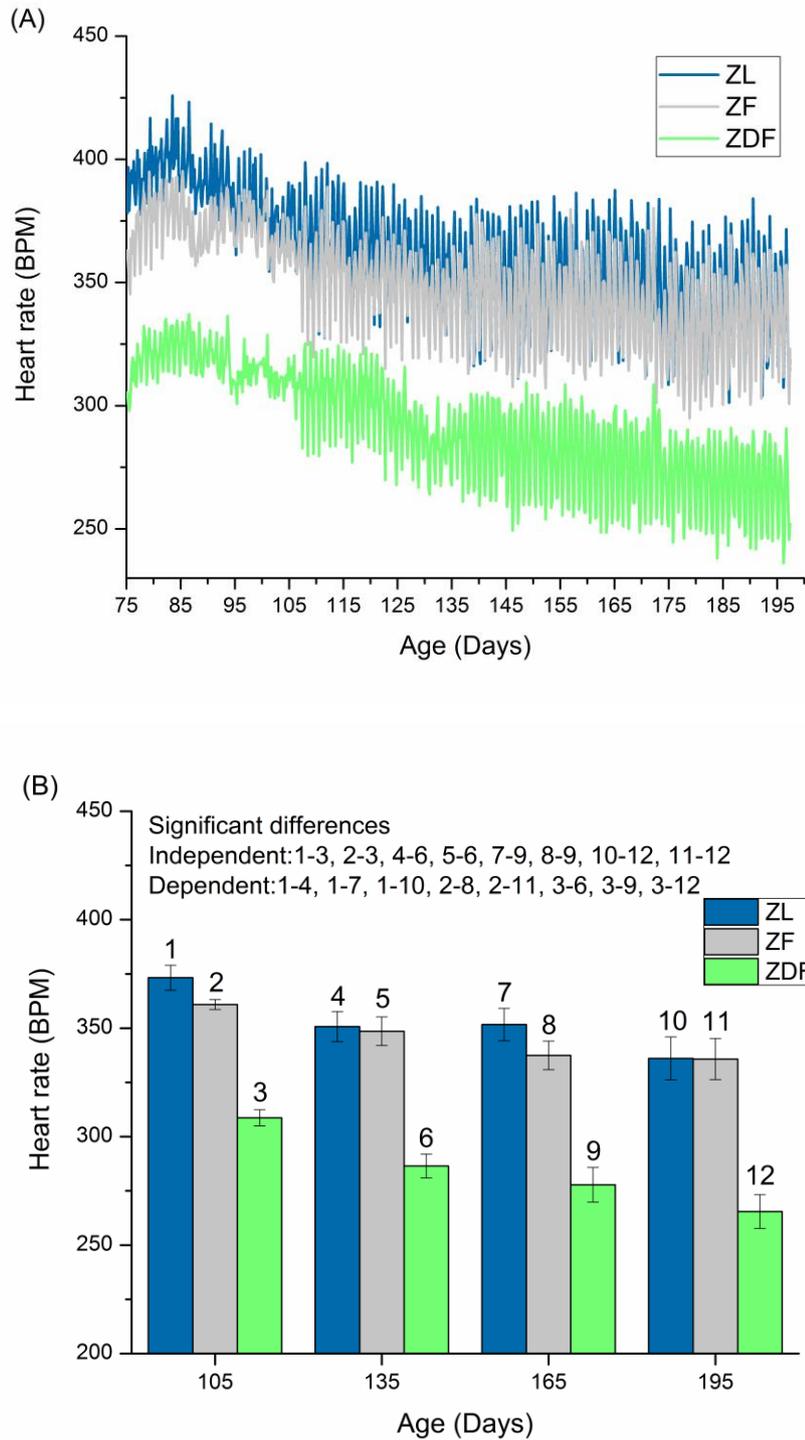
Figure 25: Heart rate. (A) Continuous mean heart rate recorded throughout the study and (B) mean heart rate at 105, 135, 165 and 195 days. Data are mean ± SEM, n=10 ZL, 10 ZF, and 10 ZDF rats. P values of 0.05 and less were considered statistically significant.

3.6.4 Biotelemetry heart rate variability

The HRV was computed over 24 hours as the SDANN. The continuous group average HRV for ZDF, ZF and ZL rats over the 4-month study is shown in Figure 26A. There were some significant ($p<0.05$) changes in mean HRV between the groups and the ages of the rats as shown in Figure 26B. At 195 days HRV was lowest in ZDF (22 ± 1 BPM, n=10), intermediate in ZF (27 ± 1 BPM, n=10) and highest in ZL (31 ± 1 BPM, n=10) rats. The differences were significant ($p<0.05$) (Figure 26B).
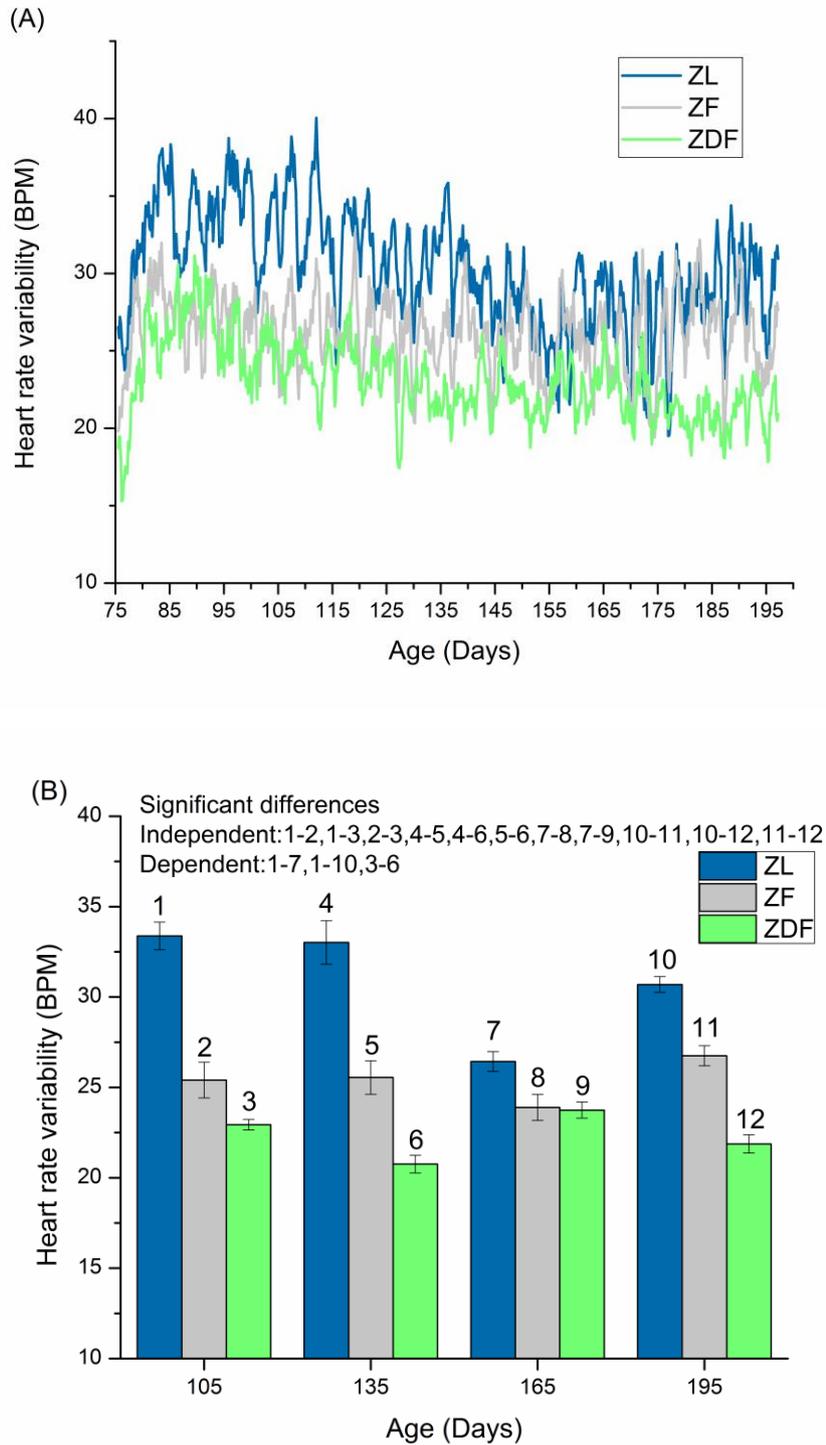
Figure 26: Heart rate variability. (A) Continuous mean heart rate variability recorded throughout the study and (B) mean heart rate variability at 105, 135, 165 and 195 days. Data are mean ± SEM, n=10 ZL, 10 ZF, and 10 ZDF rats. P values of 0.05 and less were considered statistically significant.

3.6.5 Electrocardiogram

3.6.5.1 PQ Interval

The continuous group average PQ interval for ZDF, ZF and ZL rats over the 4-month study is shown in Figure 27A. There were some significant ($p<0.05$) changes in mean PQ interval between the ages of rats as shown in Figure 27B. At 195 days, PQ interval was not significantly changed ($p>0.05$) in ZDF (46.25 ± 1.10 msec, n=10) compared to ZF (45.22 ± 0.88 msec, n=10) and compared to ZL (44.13 ± 1.09 msec, n=10) rats (Figure 27B).
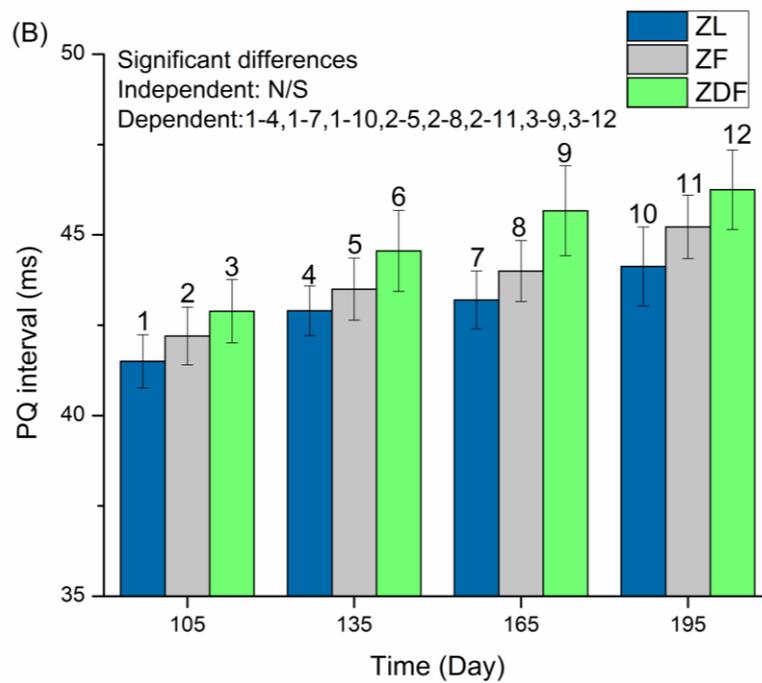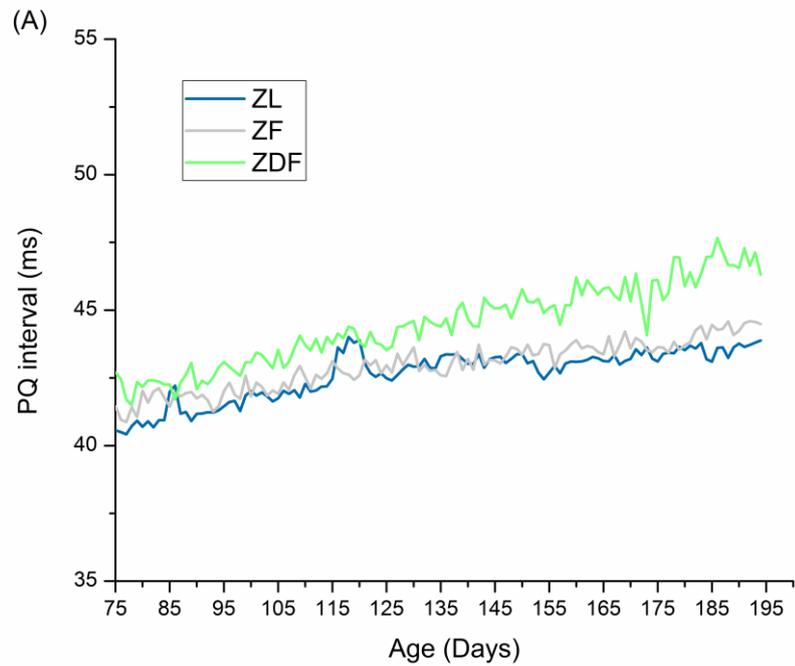
Figure 27: PQ interval. (A) Continuous PQ interval recorded throughout the study and (B) mean PQ interval data at 105, 135, 165 and 195 days. Data are mean ± SEM, n=10 ZL, 10 ZF, and 10 ZDF rats. P values of 0.05 and less were considered statistically significant.

3.6.5.2 QRS complex

The continuous group average QRS complex for ZDF, ZF and ZL rats over the 4-month study is shown in Figure 28A. There were some significant ($p<0.05$) differences in QRS interval between groups and the ages of the rats as shown in Figure 28B. At 195 days, the QRS complex was not significantly changed ($p>0.05$) in ZDF (19.13 ± 0.48 msec, n=10) compared to ZF (17.56 ± 0.24 msec, n=10) and compared to ZL (18.25 ± 0.59 msec, n=10) rats (Figure 28B).
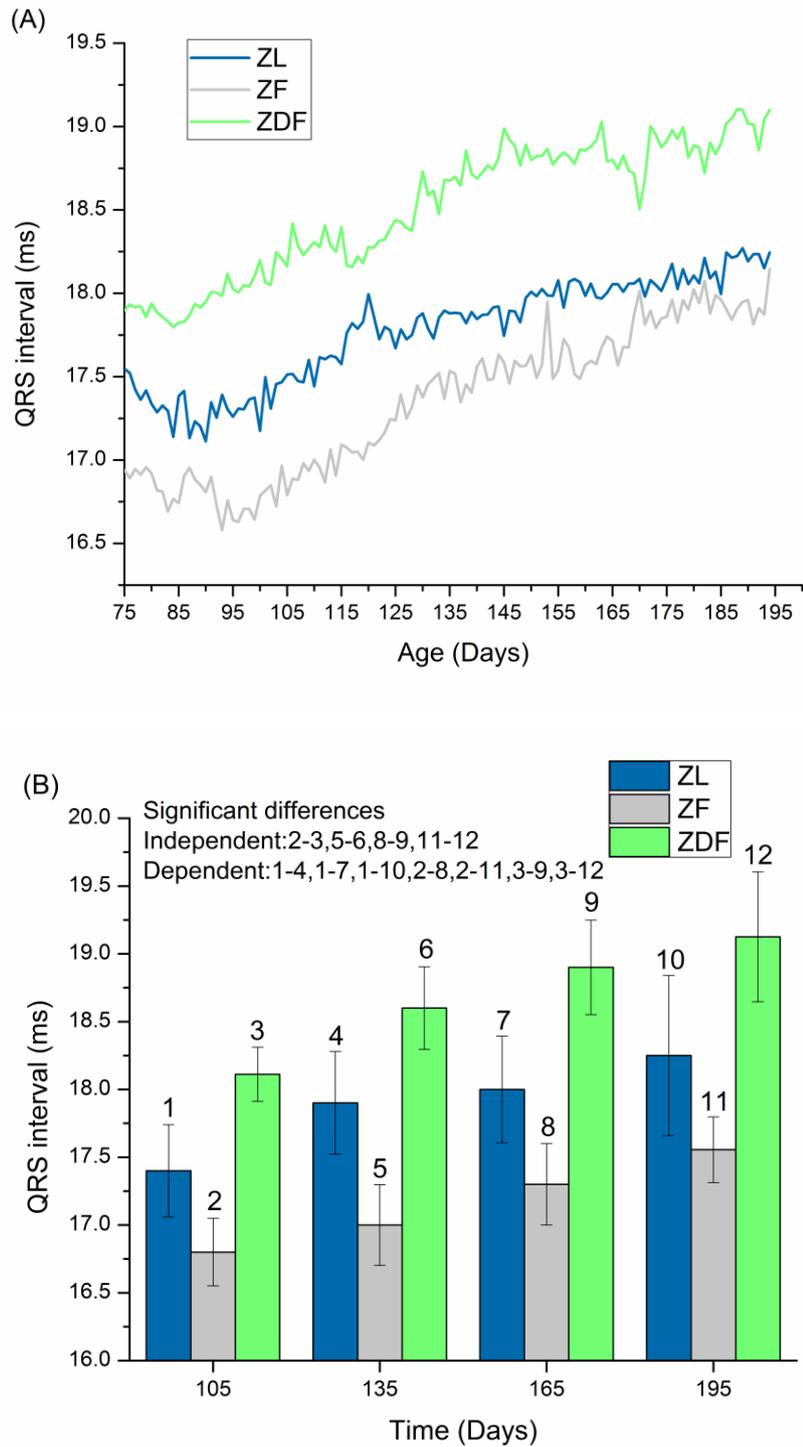
Figure 28: QRS interval. (A) Continuous QRS interval recorded throughout the study and (B) mean QRS interval data at 105, 135, 165 and 195 days. Data are mean ± SEM, n=10 ZL, 10 ZF, and 10 ZDF rats. P values of 0.05 and less were considered statistically significant.

3.6.5.3 QT and QTc interval

The continuous group average QT and QTc interval for ZDF, ZF and ZL rats over the 4-month study are shown in Figure 29A & Figure 30A. The group average QT and QTc for ZL, ZF and ZDF rats at selected time points are shown in Figure 29B & Figure 30B. There were some significant ($p < 0.05$) changes in QT and QTc intervals between groups and ages of rats as shown in Figures 29F and 30H. At 195 days, the QT interval was not significantly changed ($p > 0.05$) in ZDF (71.88 ± 3.97 msec, n=10) compared to ZF (74.11 ± 1.88 msec, n=10) and compared to ZL (67.88 ± 1.78 msec, n=10) rats (Figure 29B). After correction for HR rate the QTc interval at 195 days was significantly ($p < 0.05$) increased in ZF (171.78 ± 5.56 msec, n=10) compared to ZDF (148.75 ± 8.90 msec, n=10) rats (Figure 30B).
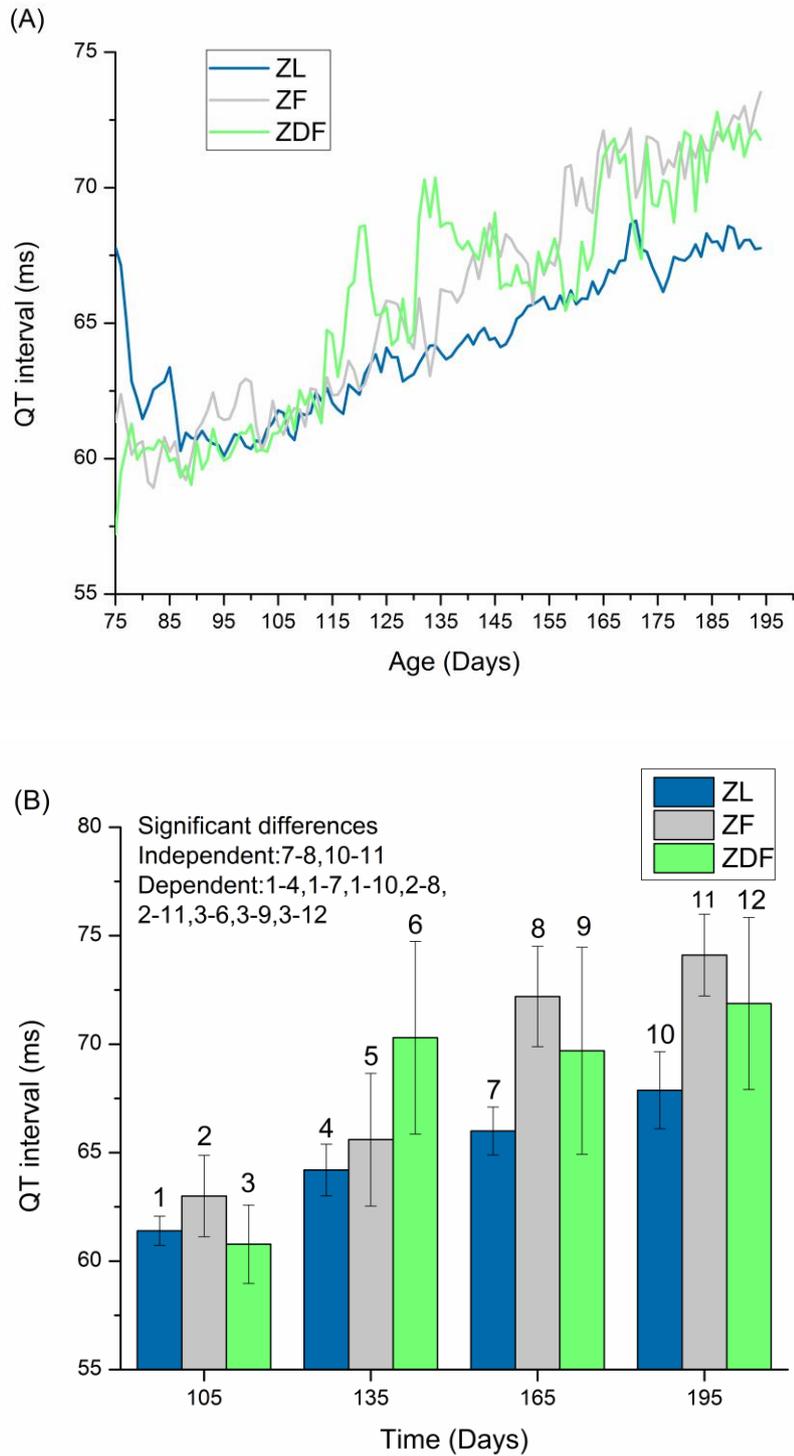
Figure 29: QT interval. (A) Continuous QT interval recorded throughout the study and (B) mean QT interval data at 105, 135, 165 and 195 days. Data are mean ± SEM, n=10 ZL, 10 ZF, and 10 ZDF rats. P values of 0.05 and less were considered statistically significant.
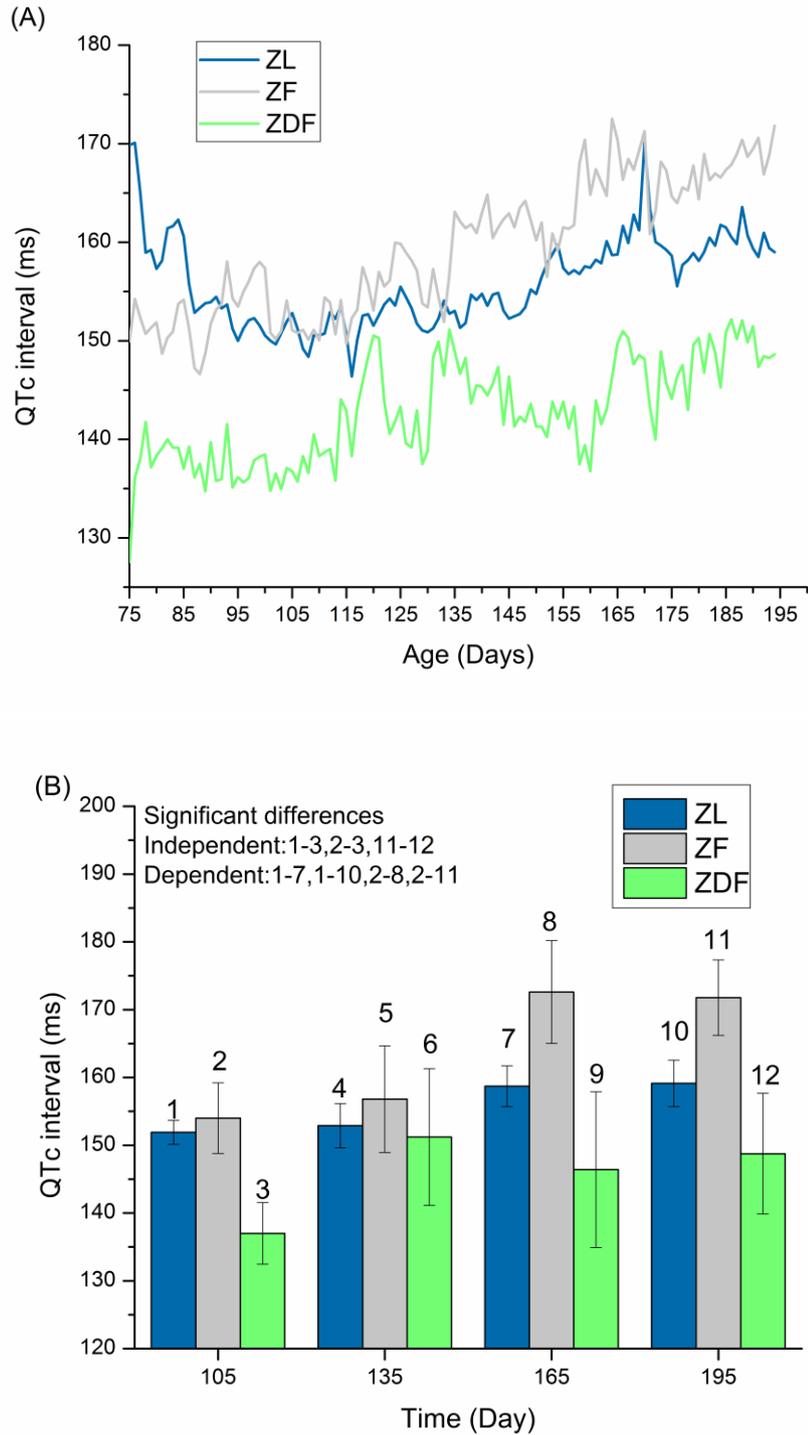
Figure 30: QTc interval. (A) Continuous QTc interval recorded throughout the study and (B) mean QTc interval data at 105, 135, 165 and 195 days. Data are mean ± SEM, n=10 ZL, 10 ZF, and 10 ZDF rats. P values of 0.05 and less were considered statistically significant.

3.6.6 Heart rate variability power spectral density

To further characterize the group differences on autonomic control of HR the group 24-hour HRV PSD was analyzed. Group HRV PSD at 105, 135, 165 and 195 days of age are shown in Figure 31A-D. At each of the time points, there was a small increase in normalized HRV PSD at LFs and a larger reduction in normalized HRV PSD at HFqs in ZDF compared to ZF and ZL rats (Figure 31A-D). There were some significant changes (p<0.05) in HRV at LFq, HFq and LFq/HFq between groups and age of rats as shown in Figure 31E, 31F and 31G. At 105, 135 and 165 days, there were significant (p<0.05) differences within groups. At 195 days of age, there were no significant changes (p>0.05) within groups in HRV at LFq (Figure 31E). At HFq there were significant (p<0.05) and progressive reductions in HRV in ZDF rats compared to ZF and ZL rats at 135, 165 and 195 days of age (Figure 31F). At 135, 165 and 195 days the LFq/HFq was significantly higher (p<0.05) in ZDF compared to ZF and ZL rats (Figure 31G).
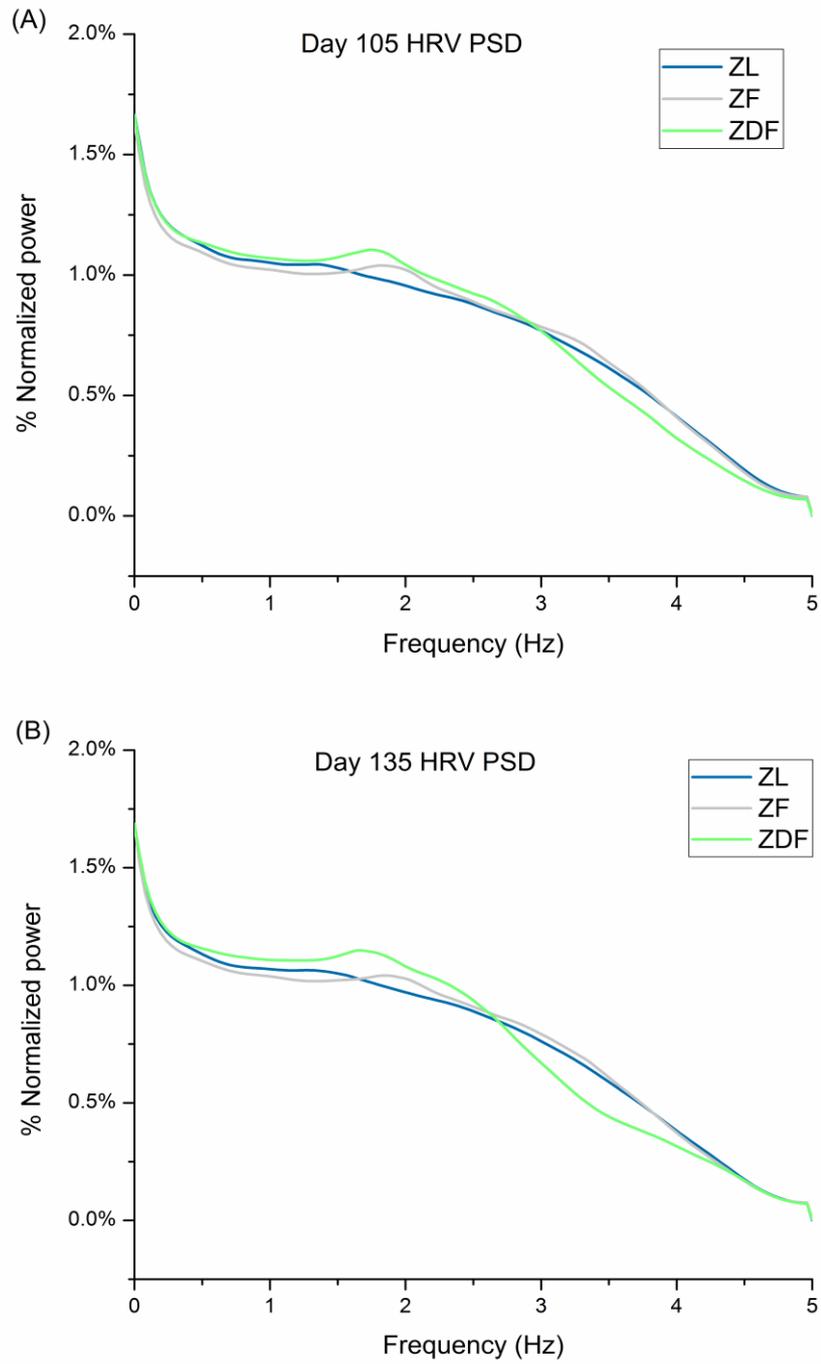
Figure 31: Spectral density analysis. Group heart rate variability, normalized power spectral density at (A) 105 and (B) 135.
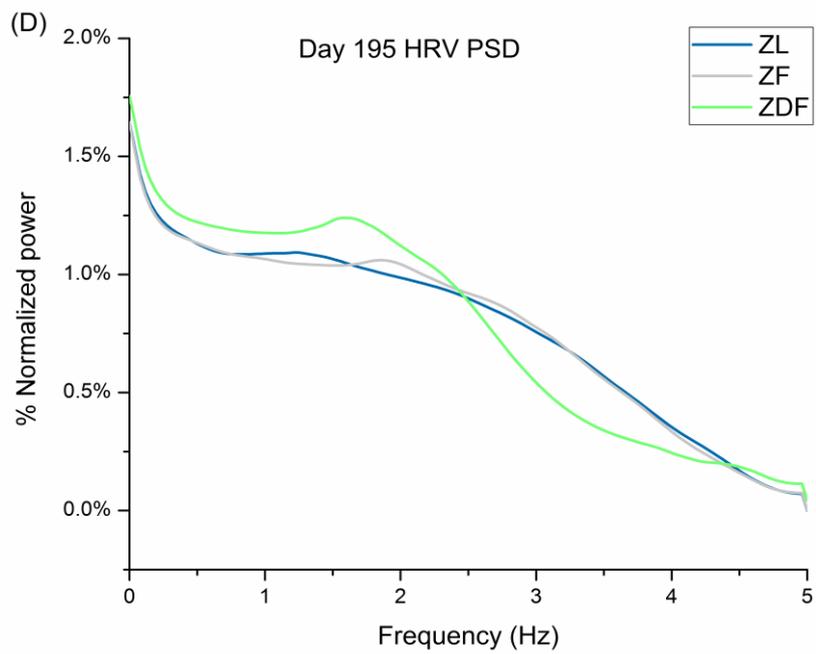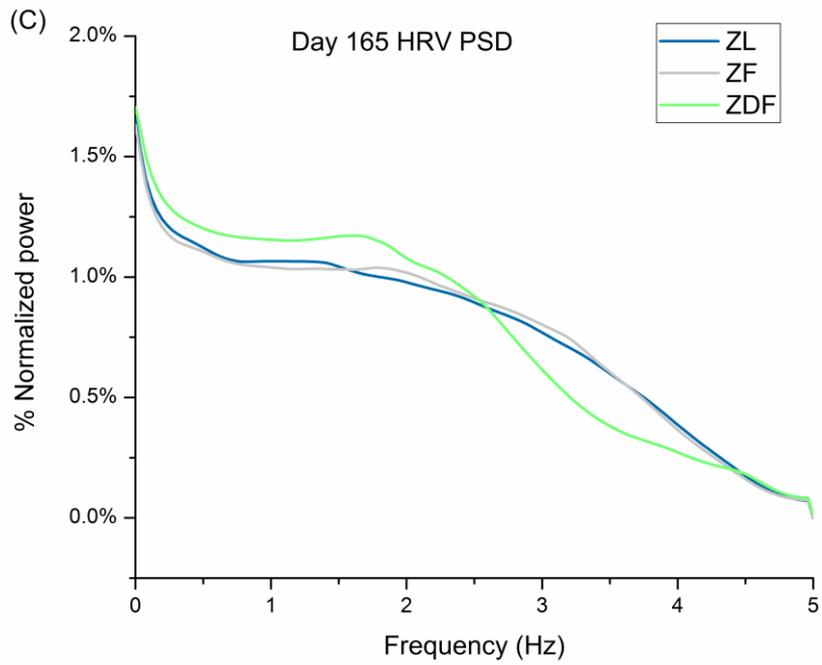
Figure 31: Spectral density analysis. Group heart rate variability, normalized power spectral density at (C) 165 and (D) 195 days (Continued).
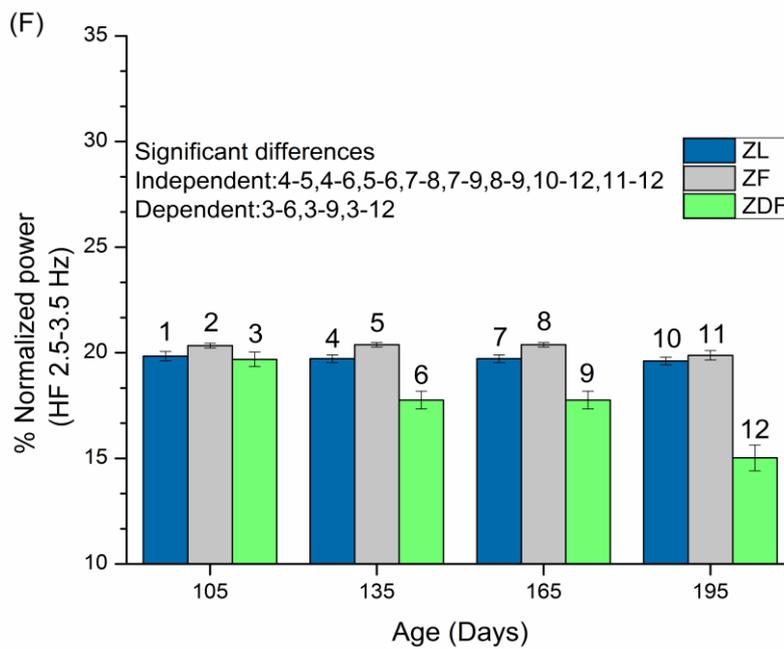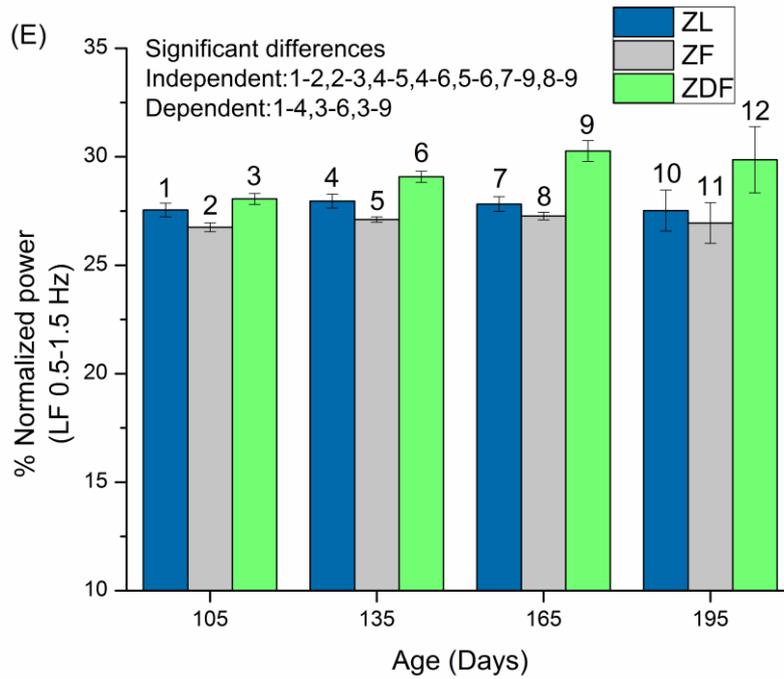
Figure 31: Spectral density analysis. (E) Mean group heart rate variability, normalized power spectral density, across the LFq range of 0.5– 1.5 Hz and (F) HFq range of 2.5– 3.5 Hz (Continued).
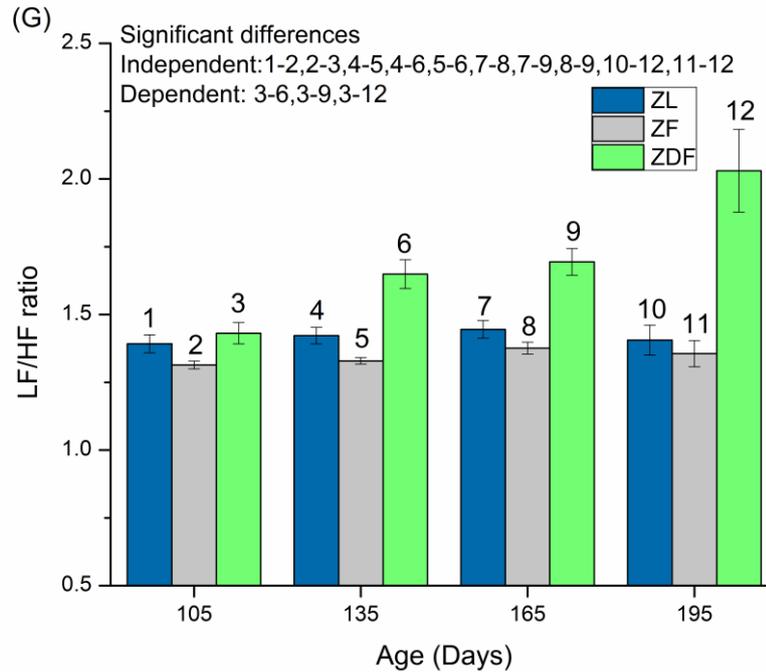
Figure 31: Spectral density analysis. (G) LFq/HFq ratio at 105, 135, 165 and 195 days. Data are mean ± SEM, n=10 ZL, 10 ZF, and 10 ZDF rats. P values of 0.05 and less were considered statistically significant (Continued).

3.7 Discussion

HR was gradually reduced with age in ZDF, ZF and ZL rats. At 195 (6.5 months) days of age HR was lowest in ZDF (265±8 BPM, n=10), compared to ZF (336±9 BPM, n=10) and ZL (336±10 BPM, n=10). HR was 21% lower in ZDF compared to ZF and ZL rats. Various factors may be responsible for the reduced HR in the ZDF rat including changing physical activity, body temperature, autonomic drive, distribution of autonomic receptors, circulating cardioactive factors and defects in the generation and propagation of electrical activity within the heart. Physical activity and body temperature remained relatively stable throughout the study so alterations in these parameters are unlikely to explain the reduction in HR in ZDF compared to ZF and ZL rats. Analysis of the ECG revealed a progressive age-dependent prolongation of PQ and QRS intervals. At 105, 135, 165 and 195 days (3.5, 5.5 and 6.5 months) of age the QRS interval was significantly prolonged in ZDF compared to ZF rats. Age-dependent prolongation of the PQ interval and QRS complex may suggest prolongation of atrial depolarization and/or electrical

conduction through the atrioventricular node and prolongation of ventricular depolarization, respectively. There was a progressive prolongation of QT and QTc interval with age and at 195 days of age QTc was significantly prolonged in ZF compared to ZDF rats. The QT interval reflects the total duration of ventricular depolarization and repolarization and the QTc is the QT interval corrected for HR. Prolongation of QRS interval, which reflects ventricular depolarization, might partly underlie the reduction in HR seen in ZDF compared to ZF and ZL rats. The significant reduction in HR coupled with prolongation of the PQ interval and QRS in ZDF rats compared to ZF and lean rats could also point to obesity- and diabesity-induced defects in the heart of diabetic and obese rats. Obesity and diabetes are risk factors for the development of major cardiovascular events including arrhythmia, myocardial infarction, cardiogenic shock and HF.

HRV provides a measure of sympathovagal modulation of the heart and alterations of HRV might be partly attributed to disturbed autonomic control of the heart (Fazan et al., 1997; Lo Giudice et al., 2002). HRV was lowest in ZDF, intermediate in ZF and highest in ZL rats. PSD analysis showed that HRV at LFq was generally increased in ZDF compared to ZF and ZL rats and HRV HFq was generally decreased in ZDF compared to ZF and ZL rats. The LFq and HFq ranges in rodents do not have standard definitions (Aubert et al., 1999; Cerutti et al., 1991; De Maria et al., 2019; Kuwahara et al., 1994; Rowan et al., 2007). The HFq component is commonly recognized as a marker of parasympathetic control (Aubert et al., 1999; Cerutti et al., 1991) and the LFq component seems to be a complex mix of sympathetic and vagal effects (Bootsma et al., 1994). In this study, the LFq and HFq ranges were set by inspection of the PSD and in agreement with previous studies (F. C. Howarth et al., 2005). HR increases during inhalation and decreases during exhalation, as defined by the respiratory sinus arrhythmia, which gives rise to a spectral peak in the HRV PSD (Al-Ani et al., 1996). As such, the very low spectral power and power associated with respiration were avoided in setting the LFq and HFq ranges. The power spectral LFq/HFq ratio, which is used to assess sympathovagal balance (Chiou & Zipes, 1998), was progressively increased with age in ZDF compared to ZF and ZL rats. In the clinical setting reductions in the power of HR fluctuations at all frequencies have been reported in diabetic patients as compared to controls indicating depression of both parasympathetic and sympathetic activity (Lishner et al., 1987). In the current experiments

there were progressive increases in LFq (sympathetic) between ZDF, ZF and ZL rats and progressive decreases in HFq (parasympathetic) in ZDF compared to ZF and ZL rats. These findings of increases in sympathetic, decreases in parasympathetic and increases in LFq/HFq ratio might be expected to increase HR. Previous studies have reported reduced expression of adrenoceptors in the ZDF heart (Haley et al., 2015; Thaung et al., 2015). Presynaptic alpha 2-adrenoceptors and muscarinic receptors that are linked to inhibition of norepinephrine (NE) release during nerve stimulation are impaired in the STZ-induced diabetic rat (Gando et al., 1993). Parasympathetic denervation and degeneration of sympathetic nerves have been reported in the alloxan-induced diabetic rat (Tomlinson & Yusof, 1983). In the Kob (spontaneously diabetic) rat there was a decreased HFq power, but not LFq/HFq ratio. The response of HFq power to atropine remained intact whilst the response of the LFq/HFq ratio to propranolol was diminished, indicating functionally inhomogeneous damage to the cardiac autonomic nerves (Sanyal et al., 2002). All of these physiological alterations of the functions of the heart may be due to DM and obesity-induced structural changes in the heart of ZDF and ZF rats compared to ZL rats, because it has been reported that more than a third of people with DM have CVD.

Circulating cardioactive factors may also be involved in changed HR in ZDF rats (Haley et al., 2015; Laughlin et al., 2008). Previous studies have reported age-dependent changes in insulin, modest reductions in thyroid hormone (Nam et al., 2013), increased NE (Marsh et al., 2007), reduced levels of glucagon and increases in serum leptin (Wang et al., 2014). Simonds et al. (2014) demonstrated the association of weight gain, leptin levels, HR and blood pressure in mice that were implanted with radiotelemetric blood pressure devices. Feeding the mice with a high fat diet (HFD) caused a progressive increase in body weight. After 4 weeks of HFD there was an increase in HR and after 12 weeks of HFD an increase in systolic and diastolic BP. At 20 weeks, mice were returned to normal chow and there was a progressive reduction in body weight which was followed by reductions in HR, diastolic and systolic BP (Simonds et al., 2014). In the current experiments HR was reduced in ZDF compared to ZF and ZL rats. Circulating leptin is taken up into the brain where it mainly acts to regulate food intake, appetitive behaviors, and energy expenditure. Although leptin levels are generally elevated in the ZDF rat, ZF and ZDF rats are LepR-deficient (Wang et al., 2014). In addition to its actions in the brain

leptin has been suggested to control cardiac electrical properties through β-AR activation. Lin et al. (2015) identified LepR in atrial, sinus node, and ventricular myocytes isolated from rat heart in which they showed that leptin at low doses (0.1-30 μg/kg) decreased resting HR whilst at high doses (150-300 μg/kg), leptin produced a biphasic effect (decrease followed by increase) in HR. In the presence of propranolol, high-dose leptin only decreased HR and occasionally caused sinus pauses and ventricular tachycardia. The leptin-induced inhibition of resting HR was completely reversed by leptin antagonist. Leptin additionally increased HR-corrected QT interval (QTc), while leptin antagonist did not. These results support the hypothesis that in addition to an indirect pathway through sympathetic tone, leptin can directly reduce HR and prolong QT interval through its receptor independent of β-AR stimulation (Lin et al., 2015).

Intrinsic defects in the electrical conduction system of the heart might also be involved in the changed HR in ZDF rats. Previous isolated perfused heart studies have demonstrated a reduction in basal HR in the ZDF rat (Cook et al., 2019; Haley et al., 2015; Thaung et al., 2015). Experiments in the authors laboratory have also demonstrated reduced HR in ZDF (100±5 BPM, n=16) and ZF (135±15 BPM, n=12) compared to ZL controls (176±11 BPM, n=11) in the isolated perfused spontaneously beating heart (unpublished data). Reductions in HR have also been previously reported in various experimental models of type 1 and type 2 diabetes (C. F. Howarth et al., 2007; F. C. Howarth et al., 2005, 2008, 2009, 2018; X. Huang et al., 2017; Kondo et al., 2019; Mabe & Hoover, 2011; Zhang et al., 2019).

Disturbances in the generation and propagation of SAN APs might underlie the reductions in HR in the ZDF and ZF rat hearts. Previous studies have reported lengthened sinoatrial conduction time, prolonged pacemaker cycle length and prolonged APD that was associated with a reduction in HCN proteins including expression of HCN2 and HCN4 in STZ-induced diabetic rat (C. F. Howarth et al., 2007; X. Huang et al., 2017). A reduction in SAN beating rate associated with a reduction in funny current density and capacitance and expression of various HCN proteins including HCN4 and gap junction proteins including Cx43 has also been reported in the STZ-induced diabetic rat (Zhang et al., 2019). In the AKITA mouse model of diabetes, the acetylcholine-activated K^+ current (IKACh) was reduced providing evidence for impaired parasympathetic regulation of HR and SAN

function (Krishnaswamy et al., 2015). In human studies autopsy nodal tissue from type 2 diabetic patients was characterized by diffuse interstitial fibrosis and chronic ischemic lesions with central areas of the SAN being worst affected (Hostiuc et al., 2013). In the STZ-induced mouse there was a reduction in HR associated with fibrosis, infiltration of macrophages, increased production of reactive oxygen species and depressed HCN4 in sinus node tissue (Kondo et al., 2019). Collectively, these studies suggest that structural and functional defects may partly underlie the reduced HR that has been widely reported in diabetic heart.

In short, the HR was reduced by normal aging and further reduced by diabesity in the absence of changes in body temperature and physical activity. Reductions in HRV linked with altered sympathovagal drive might partly underlie disturbed HR in the ZDF rat.

3.8 Conclusions

- HR was reduced by ageing and further reduced by diabesity in the absence of changes in body temperature and physical activity.
- Power spectral analysis showed no significant differences in HRV at low frequencies, reduced HRV at high frequencies and increased sympathovagal balance in ZDF compared to ZF and ZL rats.
- Reductions in HRV linked with altered sympathovagal drive might partly underlie disturbed HR in the ZDF rat.

Chapter 4: Investigating the electrical conduction system in isolated perfused heart in the ZDF and ZF compared to ZL rats

4.1 Introduction

Every cell in our body derives its electrical properties from the lipid bilayer cellular membrane which acts as a barrier. The cell membrane allows the movement of nonpolar hydrophobic molecules such as ions (K^+, Na^+, Ca^{2+}) between the intracellular and extracellular compartments through ion channels and transporters. The electrical difference between the exterior and interior is called the "transmembrane potential" or voltage and is measured in volts (V). In general, the value of the RMP is different between cell types. However, most cells maintain a negative RMP (i.e., the cell interior membrane is negative compared to the extracellular surface). The usual RMP is in the millivolt range (from -80 mV to -30 mV). Numerous cell types are described as excitable cells, such as nerve and muscle cells. These cells can depolarize spontaneously or depolarize in response to a stimuli which causes transient and rapid changes in their RMP, these changes are the APs. For their work on the giant squid axon Hodgkin and Huxley were awarded the Nobel Prize in Physiology or Medicine in 1963 (Hacker et al., 2009; Sherman-Gold et al., 2012).

Increased very low-density lipoprotein-triglyceride (VLDL-TG) secretion by the liver in the ZF rat model for dyslipidemia is mainly due to the relative hyperactivity of the sympathetic and/or hypo-activity of parasympathetic liver innervation (Bruinstroop et al., 2015). Experiments have been carried out to investigate the involvement of the autonomic nervous system through surgical denervation of sympathetic or parasympathetic liver nerves in ZF rats. Their results show that the cutting of the sympathetic liver nerve reduces the secretion of VLDL-TG in obese rats and reduces plasma TG concentrations after 6 weeks. On the other hand, parasympathetic denervation results in an increase in plasma cholesterol concentration. E Bruinstroop et al. (2015) also examined whether the effect of sympathetic or parasympathetic liver enlargement was independent of changes in humoral factors or changes in body weight or food intake. These studies demonstrated that sympathetic denervation improves the lipid profile of ZF rats, while parasympathetic denervation increases total cholesterol levels (Bruinstroop et al., 2015).

4.2 Hypothesis

- An intrinsic defect is responsible for changes in heart rhythm in the ZDF and ZF rats.

4.3 Aims and objectives

- To explore the effects of obesity and diabesity on the electrical conduction system in the isolated perfused heart in the ZDF and ZF compared to the ZL rat.
- The purpose of these experiments was to investigate whether alterations in electrical conduction could be observed after removing extrinsic influences including autonomic innervation and cardioactive substances circulating in the blood.

4.4 Methods

4.4.1 Measurement of action potential in isolated perfused heart

After completion of the biotelemetry experiments hearts were mounted in Langendorff mode and retrogradely perfused at a constant flow rate of 8 ml per g heart^{-1} min^{-1} at physiological temperature (36-37°C) with a normal Tyrode (NT) solution containing: 1.8 mM CaCl$_2$, 1 mM MgCl$_2$, 5 mM KCl, 140 mM NaCl, 10 mM glucose, 5 mM 4-(2-hydroxyethyl)-1-piperazineethanesulfonic acid (HEPES) and adjusted to pH 7.4 with NaOH and uninterruptedly gassed with oxygen. Cardiac metabolic activity will be altered when the heart is perfused using NT since there will no longer be cardiac protective substances and as a result an acute adaptation in metabolic activity will be different for different rats. A suction electrode was attached to the left ventricle of the heart as shown in Figure 32. The suction electrode was used to measure surface APs in the isolated perfused heart. The APs were recorded in spontaneously beating and paced (5 Hz, Grass medical SD5 stimulator) hearts. Signals were collected at 1000/sec, amplified (ADInstruments, ML136 Bioamp) and conveyed via a digitizer (ADInstruments, Powerlab 4/30) to a PC and displayed on a monitor. Data were analyzed with ADInstruments labchart 7 pro software v 7.3.8 (ADInstruments, Australia).
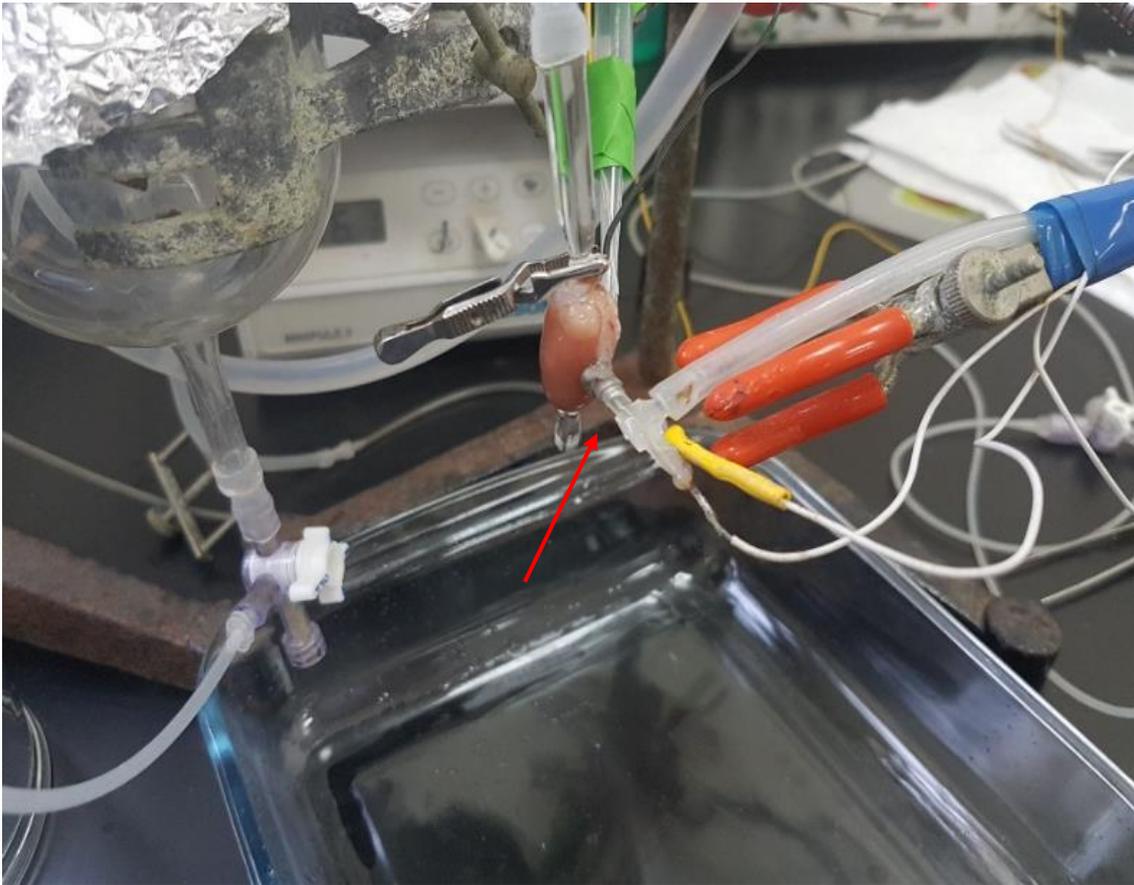
Figure 32: Suction electrode connected to the heart for action potential measurements. The arrow shows the location of the suction electrode.

4.4.2 Measurement of electrocardiogram in isolated perfused heart

After AP measurements had been recorded, the suction electrode was removed, and the ECG electrodes were connected and placed on the left ventricle and apex of the isolated heart (Figure 33).
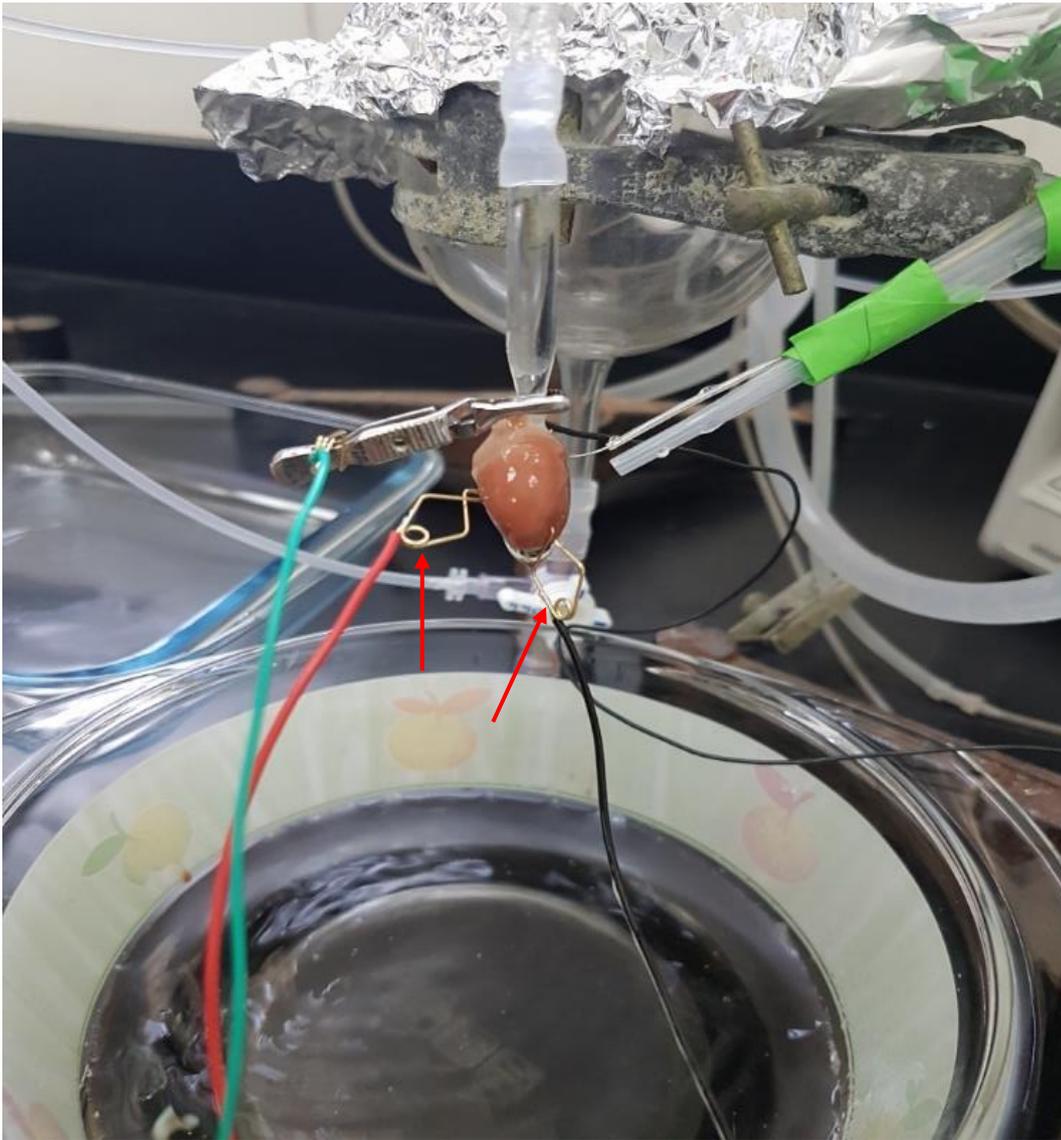
Figure 33: Electrodes placed on the left ventricle and apex of the heart for ECG measurements. The arrows show the location of the ECG electrodes.

4.5 Statistics

Results were reported as the mean ± SEM of 'n' observations. The statistical comparisons were done with IBM SPSS and Origin 9.0 (OriginLab, Northampton, Massachusetts, USA) statistics software using either the independent samples t-test or one-way ANOVA and then by Bonferroni corrected t-tests for multiple comparisons, as applicable. P values of 0.05 and less were considered statistically significant.

4.6 Results

4.6.1 Action potential in isolated perfused heart

Typical records of AP in isolated perfused heart from ZL, ZF and ZDF rats are shown in Figure 34A-C. The mean HR in spontaneously beating heart and paced (5 Hz) heart is shown in Figure 34D. ZDF rats had the slowest heartbeat compared to the ZF and ZL rats, however, the difference in HR was not statistically ($p>0.05$) significant (Figure 34D). Time to peak (TPK) AP was significantly higher in the ZF (9.68 ± 1.76 msec, n=12-13) compared to ZL (5.05 ± 0.67 msec, n=10) but not compared to ZDF (7.47 ± 0.67 msec, n=16) in the spontaneously beating heart (Figure 34E). The APD (50% recovery) (Figure 34F) and APD (70% recovery) (Figure 34G) showed no significant differences between groups. AMP of AP also showed no significant differences between groups (Figure 34H).
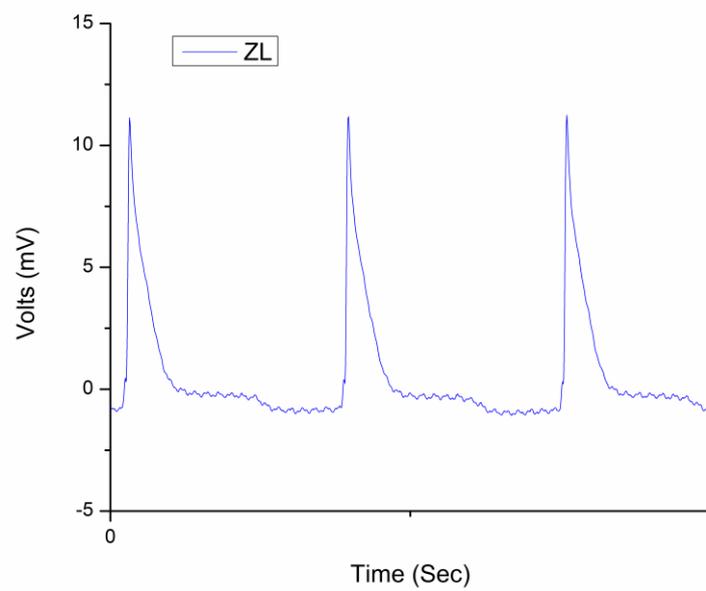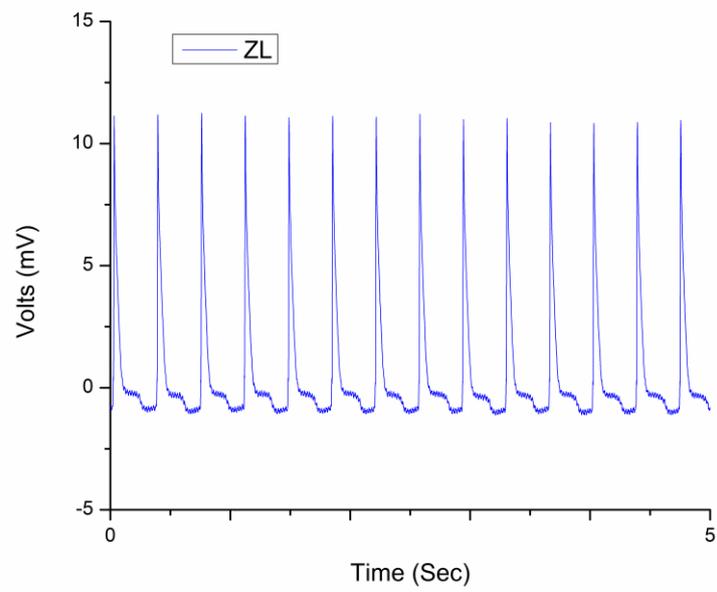
Figure 34: Ex-vivo action potential results. (A) Typical records of action potential from ZL rat 5 and 1 sec expanded scale.
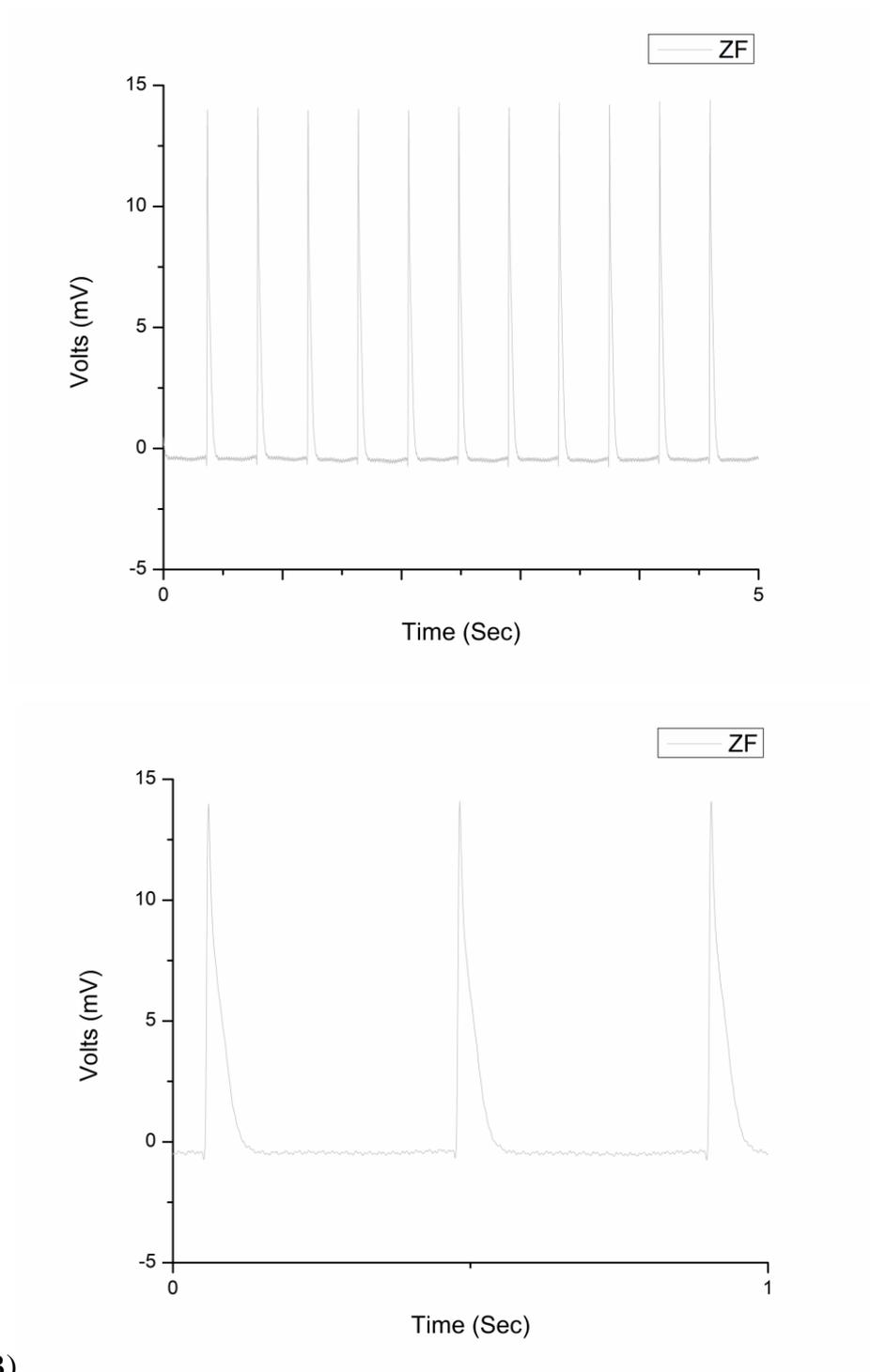
(B)

Figure 34: Ex-vivo action potential results. (B) Typical records of action potential from ZF rat at 5 and 1 sec expanded scale (Continued).

(C)
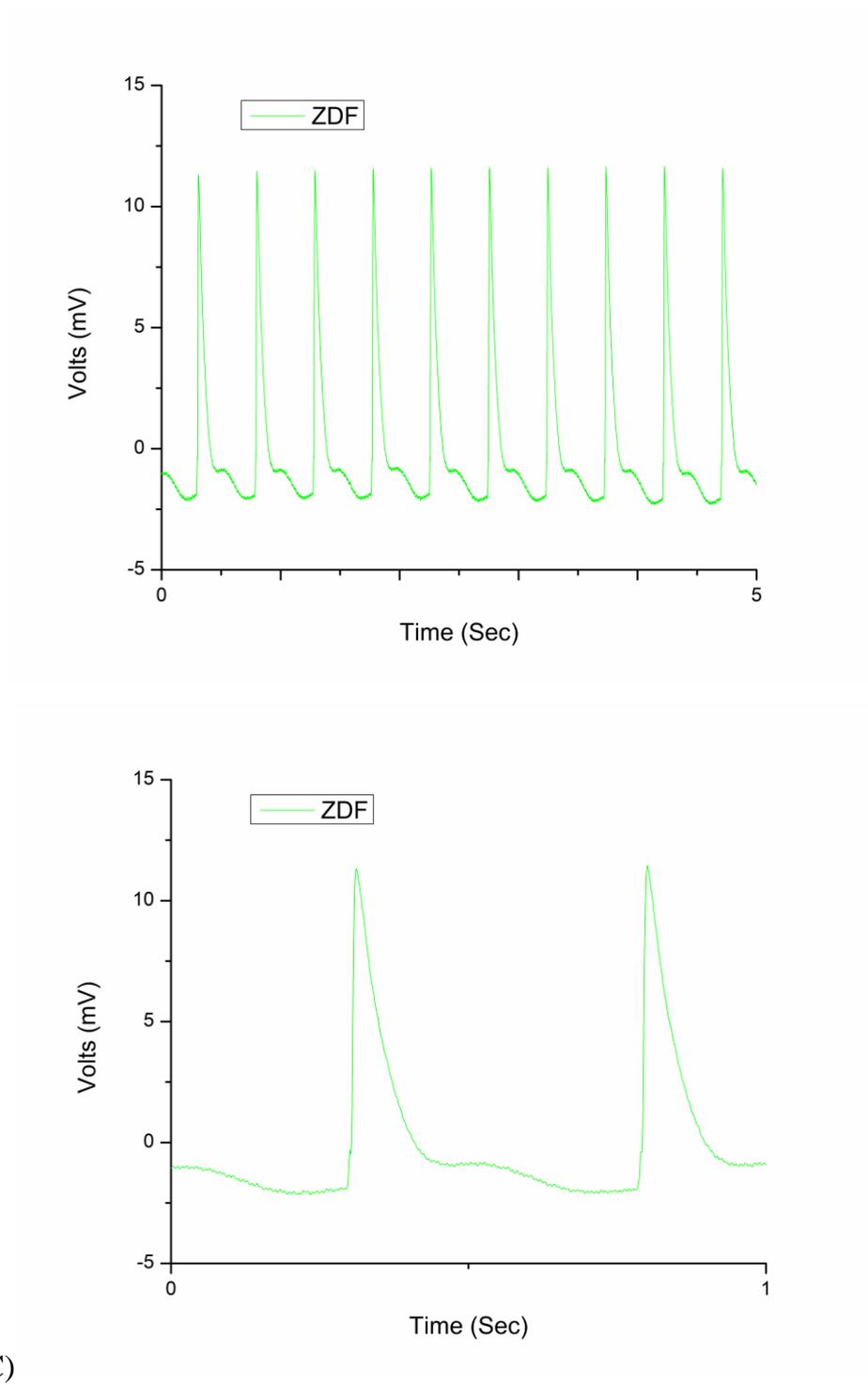
Figure 34: Ex-vivo action potential results. (C) Typical records of action potential from ZDF rat at 5 and 1 sec expanded scale (Continued).
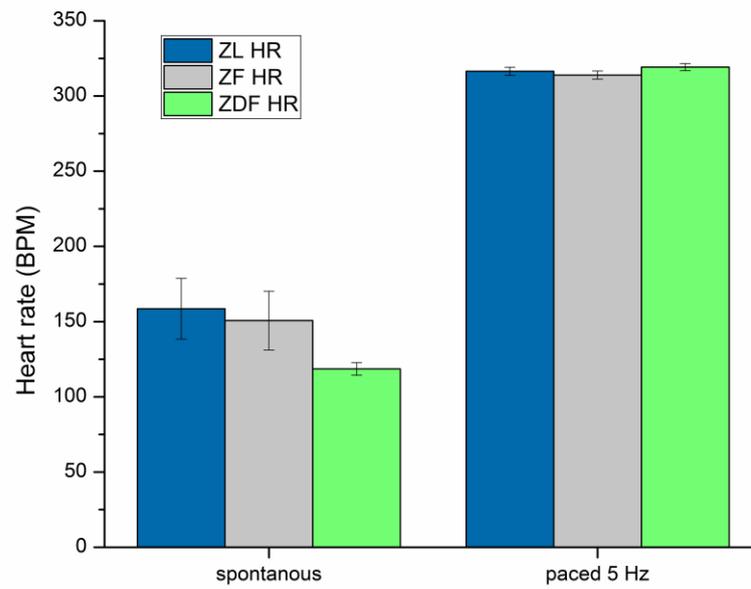
(D)
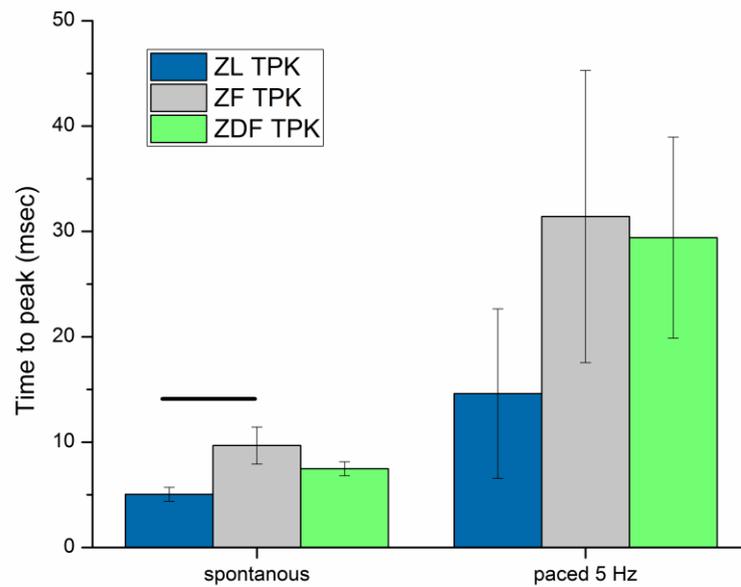
(E)

Figure 34: Ex-vivo action potential results. (D) Mean heart rate calculated from APDs and (E) time to peak of action potential (Continued).
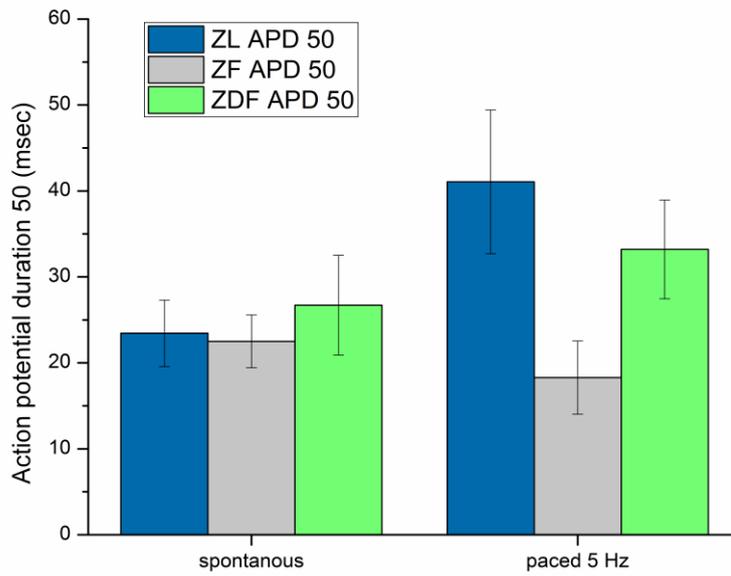
(F)
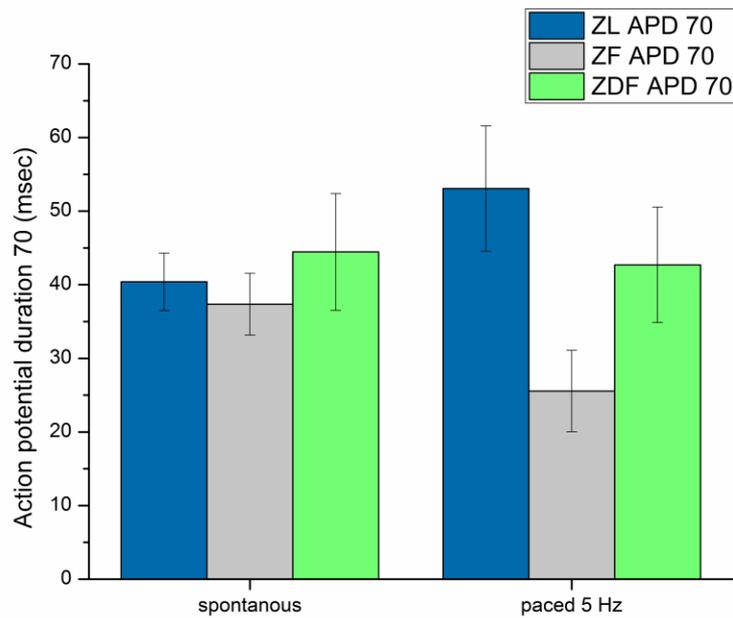
(G)

Figure 34: Ex-vivo action potential results. (F) Action potential duration (50% recovery) and (G) action potential duration (70% recovery) (Continued).

(H)
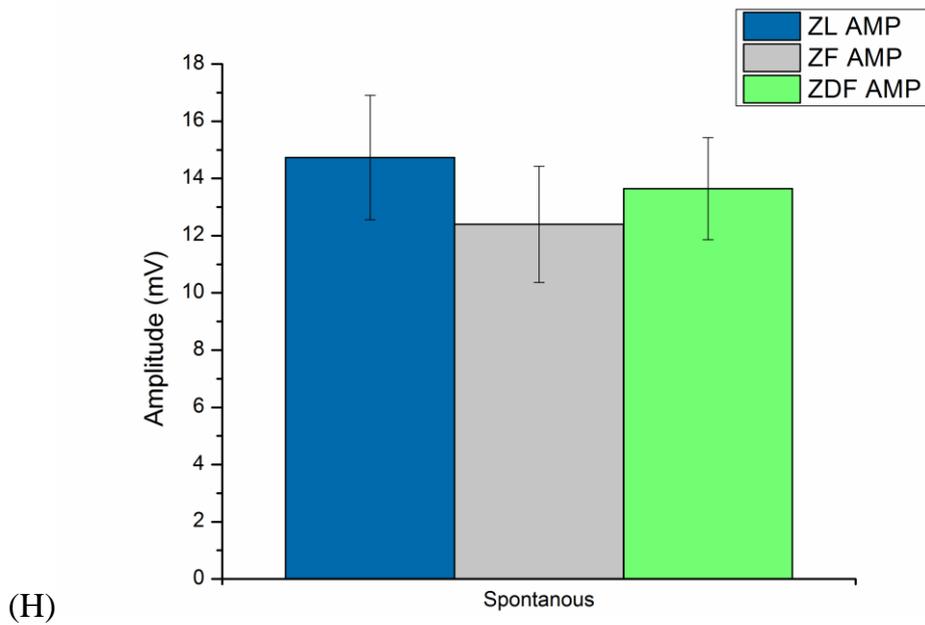
Figure 34: Ex-vivo action potential results. (H) Amplitude of action potential. Data are mean ± SEM. n=10 ZL, 12-13 ZF and 16 ZDF hearts. P values of 0.05 and less were considered statistically significant (Continued).

4.6.2 Electrocardiogram in isolated perfused heart

Typical records of ECG in isolated perfused heart from ZL, ZF and ZDF rats at 5 and 1 sec intervals are shown in Figure 35A-C. The mean spontaneous HRs were significantly (p<0.05) different. HR was lowest in the ZDF (99.55±5.39 BPM, n=16), intermediate in ZF (135.02±14.87 BPM, n=11-12) and highest in ZL (176.06±11.02 BPM, n=11) rats (Figure 35D). The QRS intervals on the other hand did not show any significant differences (p>0.05) between the groups (Figure 35E).
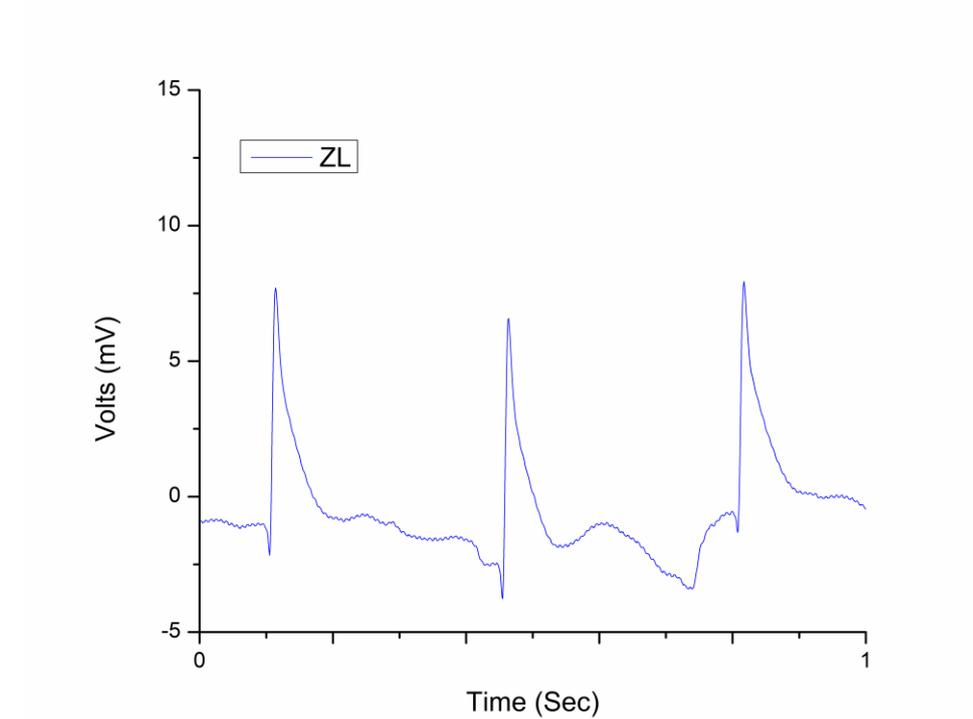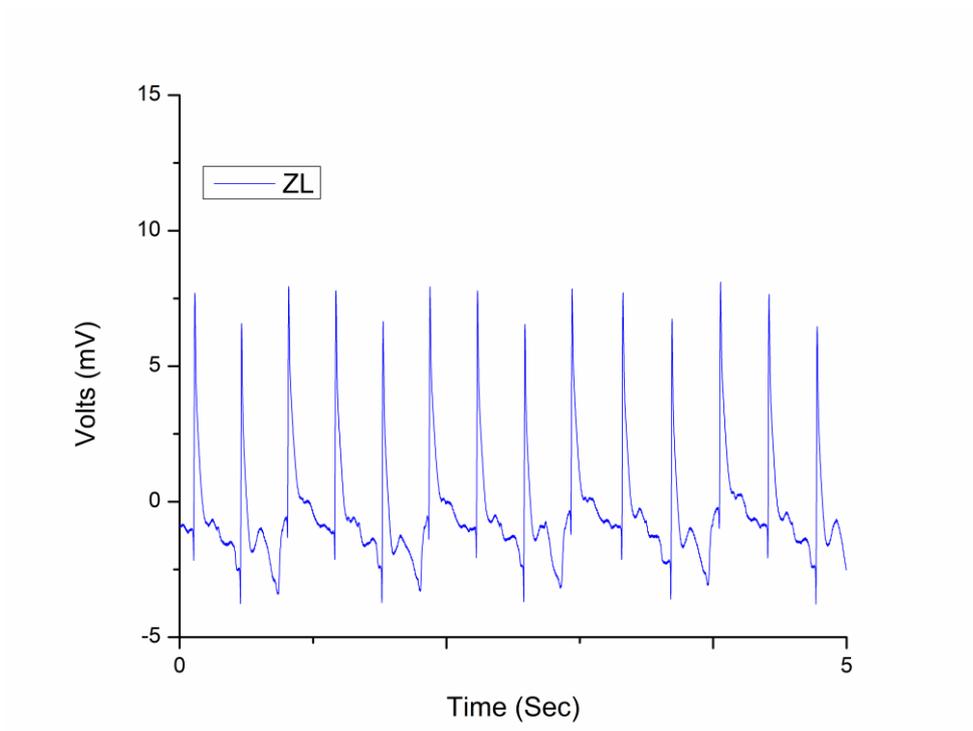
(A)

Figure 35: Ex-vivo ECG results. (A) Typical records of ECG from ZL rat 5 and 1 sec.
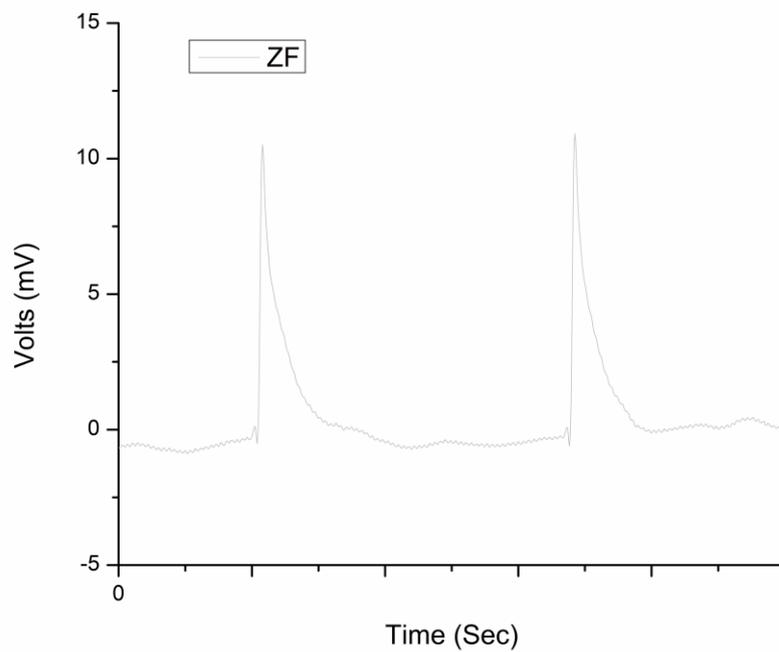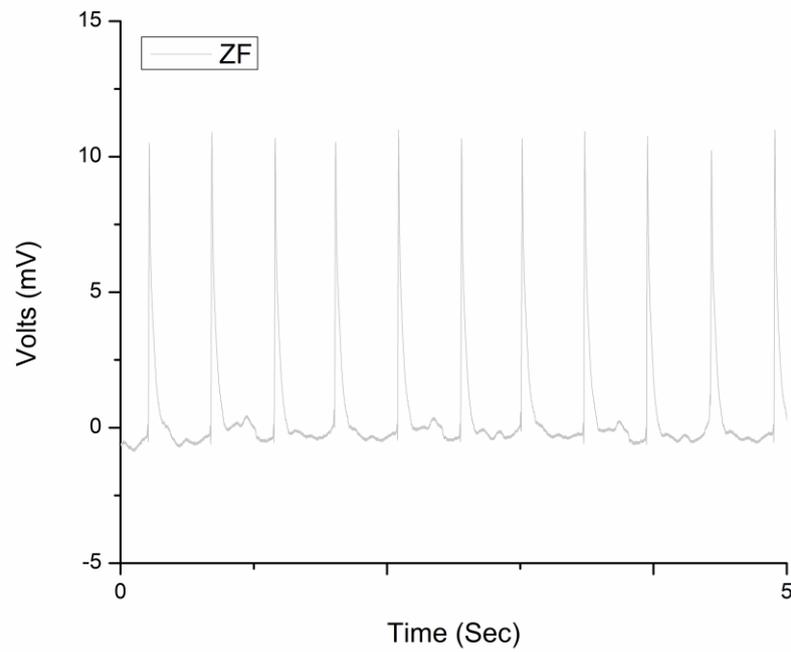
(B)

Figure 35: Ex-vivo ECG results. (B) Typical records of ECG from ZF rat 5 and 1 sec (Continued).
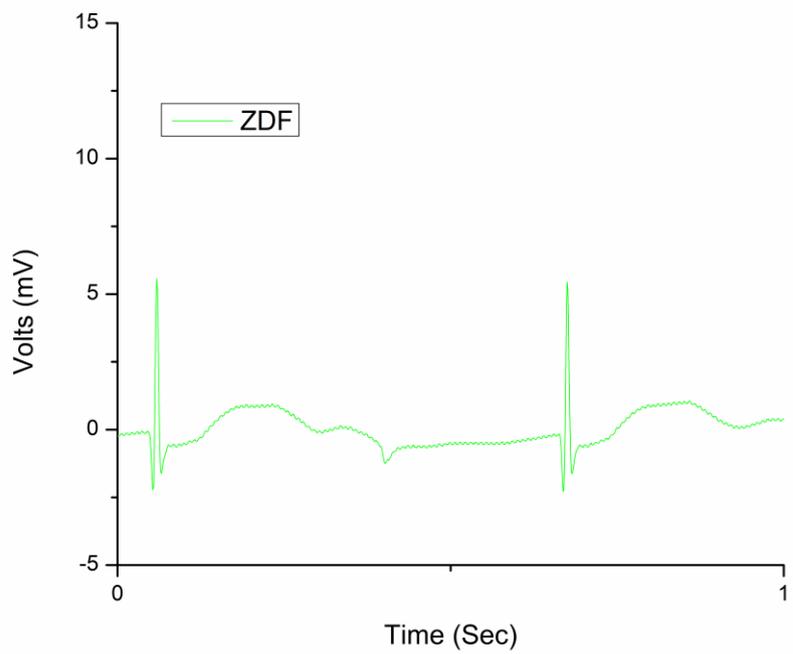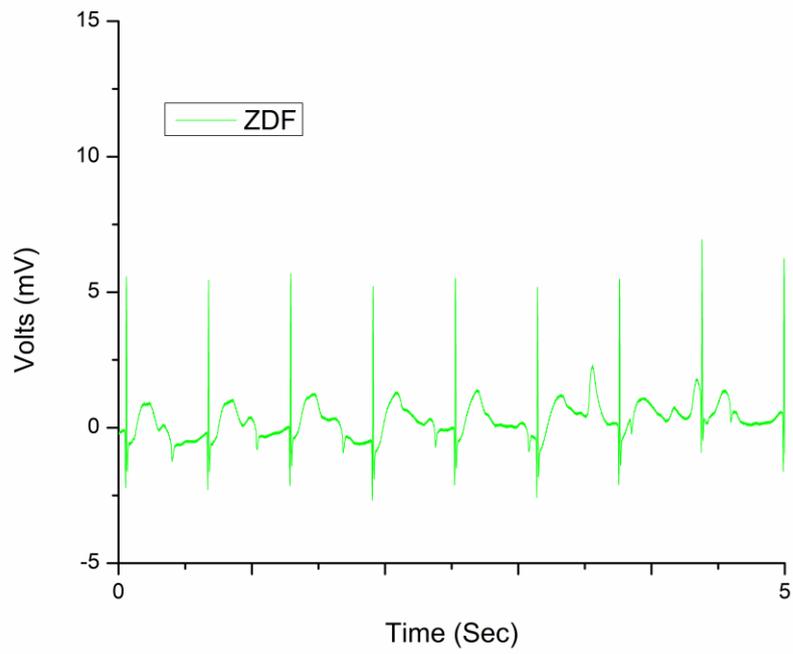
C

Figure 35: Ex-vivo ECG results. (C) Typical records of ECG from ZDF rat 5 and 1 sec (Continued).
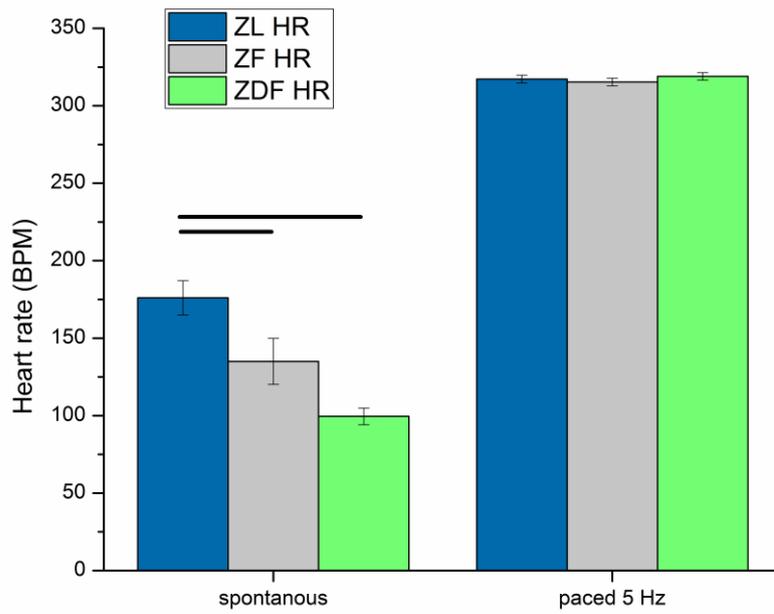
(D)
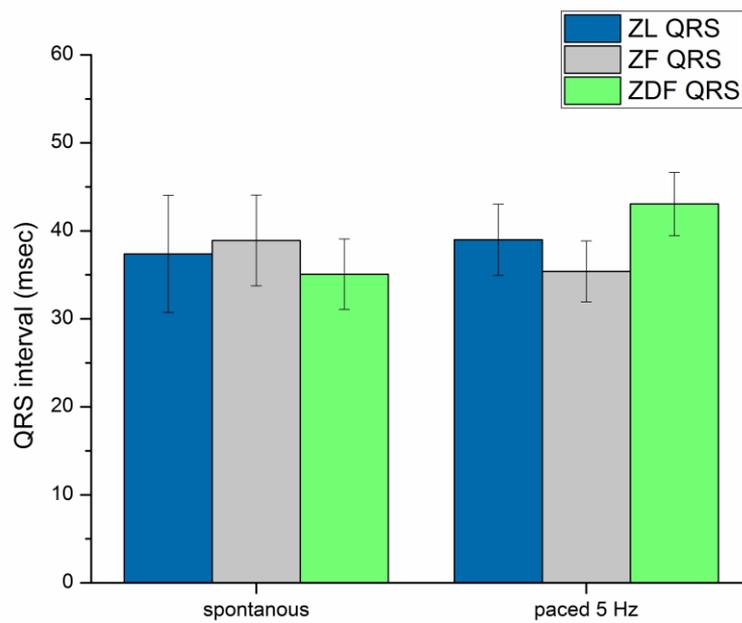
(E)

Figure 35: Ex-vivo ECG results. (D) Heart rate from ECG and (E) QRS interval. Data are mean ± SEM. n=11 ZL, 11-12 ZF and 16 ZDF hearts. P values of 0.05 and less were considered statistically significant (Continued).

4.7 Discussion

4.7.1 Action potential in isolated perfused heart

In the biotelemetry experiments, the heart was *in-vivo* hence, the heart was still regulated by the ANS and circulatory cardioactive substances. In the isolated perfused heart, the heart is not regulated by the ANS or circulatory cardioactive substances. The mean HR in spontaneously beating heart calculated from AP records revealed that the ZDF group had the slowest heartbeat compared to the other groups. TPK of AP was significantly prolonged in the ZF compared to ZL but not compared to ZDF in the spontaneously beating heart. In a previous study in single ventricular myocytes using voltage clamp, the maximal AP upstroke velocity and resting potential were similar in control and STZ diabetic rats (Nygren et al., 2007). Another study reported that monophasic APD at 90% repolarization of the left atrial myocardium in the aged (2 year old) group was shorter than in the adult (7-8 months old) and middle-aged (13-15 months old) groups suggesting age related changes (C. Huang et al., 2006). Both age and disease related changes may affect the AP measurements which was evident in this study.

4.7.2 Electrocardiogram in isolated perfused heart

Mean spontaneous HR in isolated perfused heart calculated from ECG records revealed marked reductions in the ZDF compared to ZF and ZL groups similar to that of the results from the biotelemetry study in section 3.6.3. The isolated heart QRS intervals on the other hand did not indicate significant differences between groups unlike that seen in the section 3.6.5.2 where the QRS complex showed some differences which has also been reported in a large cohort study indicating that QRS duration was in fact influenced by body mass index (Rao et al., 2021).

In the previous chapter, *in-vivo* experiments showed marked reductions in HR in the presence of ANS. Similarly in this chapter, when the heart was isolated and no longer regulated by ANS we also saw evidence of reduced HR from ECG readings. This suggests an intrinsic defect may be responsible for changes in heart rhythm observed in obesity and diabesity. Further studies will be required to investigate the changes happening within the

heart muscles that might explain these rhythm disturbances. The following chapters will investigate these changes.

4.8 Conclusions

- The mean HR in the spontaneously beating heart was slowest in ZDF rats, intermediate in ZF and fastest in ZL controls.
- TPK AP was significantly prolonged in the ZF compared to ZL but not compared to ZDF.
- Even in the absence of ANS control, ZDF heart rhythm was disturbed.

Chapter 5: Investigating ventricular myocyte shortening using cell imaging in the ZDF and ZF compared to ZL rats

5.1 Introduction

The effects of ventricular myocyte shortening has been widely investigated in various models of diabetes. In a previous study STZ-induced diabetic rats showed lower myocyte circumferential shortening compared to controls (Noda et al., 1993). One study showed that the AMP of shortening was smaller and the rates of contraction and relaxation were lower in myocytes from STZ compared to control rats (Choi et al., 2002). Another study showed that the time course of shortening was prolonged to comparable amounts in endocardial and epicardial regions of myocytes from STZ compared to control rats (Smail et al., 2016). The time course of shortening was also prolonged in epicardial myocytes from Goto-Kakizaki (GK) rats which are considered to be an experimental model of type 2 diabetes compared to epicardial controls (Smail et al., 2018). Furthermore, cell shortening in db/db mice was found to be slowed in diabetic myocytes compared to controls (Pereira et al., 2006).

5.2 Hypothesis

- Ventricular myocyte shortening is altered in ZDF and ZF rats.

5.3 Aims and objectives

- To investigate the effects of obesity and diabesity on the resting cell length (RCL), TPK shortening, time to half (THALF) relaxation of shortening and AMP of shortening in ventricular myocytes from ZDF, ZF compared to ZL rats.

5.4 Methods

Left ventricular myocytes were isolated from rat heart according to previously described techniques (F. C. Howarth et al., 2020). Hearts were mounted on a modified Langendorf perfusion system as shown in Figure 36.
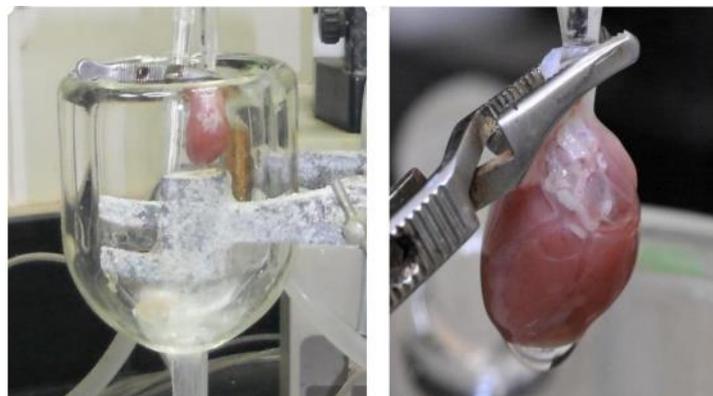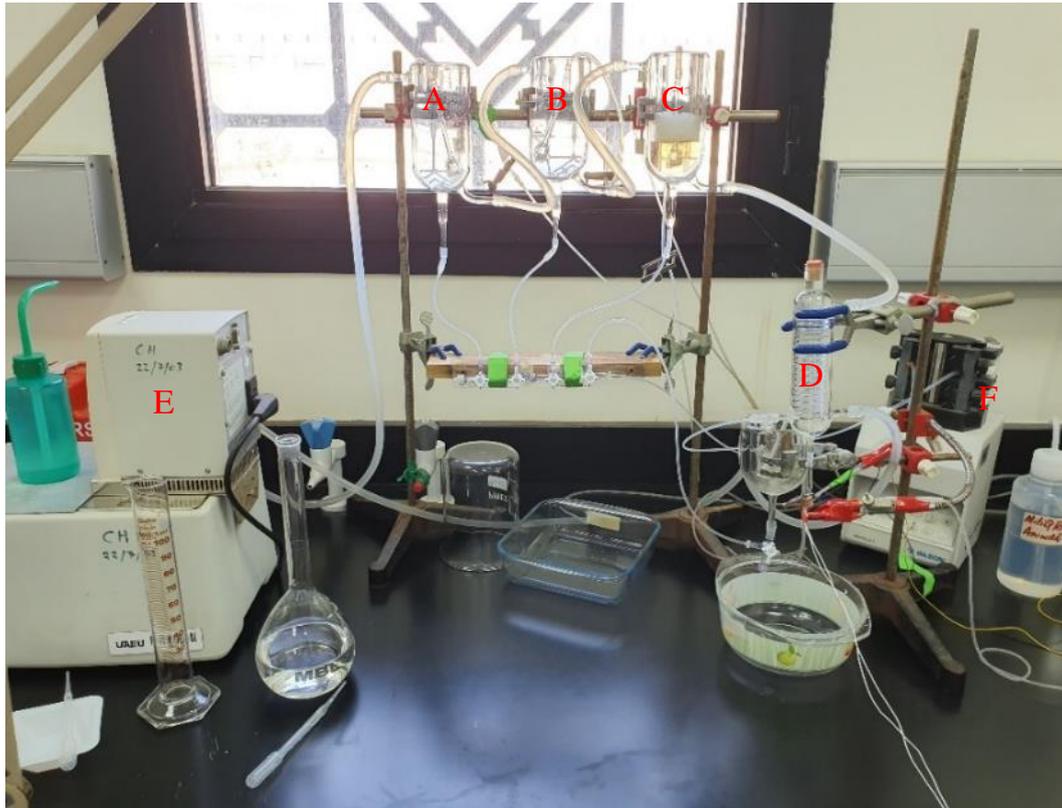
Figure 36: Cell isolation apparatus. The upper panel shows the cell isolation apparatus. The lower panel shows a close-up of the canulated heart. (A) The lettering in the photograph shows Ca^{2+}-containing isolation solution, (B) Ca^{2+}-free EGTA isolation solution, (C) protease/collagenase isolation solution, (D) Langendroff apparatus, (E) water bath and (F) peristaltic pump.

In short, the rats were euthanized utilizing a guillotine and hearts swiftly separated and mounted for retrograde perfusion corresponding to the Langendorff method. Initially,

hearts were perfused and maintained at a regular flow of 8 ml g heart^{-1} min^{-1} (36–37°C) with cell dissociation solution comprising in mmol/l: 1.4 MgCl$_2$, 5.4 KCl, 130 NaCl, 0.4 NaH$_2$PO$_4$, 0.75 CaCl$_2$, 10 glucose, 5.0 HEPES, 10 creatine, and 20 taurine (pH 7.3). Perfusion flow rate was modified to permit for variations in heart weight among animals. After heart stabilization perfusion was switched for 4 min to Ca^{2+}-free cell dissociation solution containing 0.1 mmol/l EGTA, and then for 6 min with Ca^{2+}-free cell dissociation solution containing 0.05 mmol/l Ca^{2+}, 0.075 mg/ml type XIV protease (Sigma, Taufkirchen, Germany) and 0.75 mg/ml type 1 collagenase (Worthington Biochemical Corp, NJ, USA). Left ventricle tissue was removed from the heart, shredded, and gently agitated in collagenase-containing dissociation solution complemented with 1% bovine serum albumin (BSA) for 4-5 min at 36-37°C. Cells were filtered using a 300 micron nylon mesh (Cadisch Precision Meshes LTD, London, England). Tissue remaining in the nylon mesh was then resuspended in more isolation solution supplemented with BSA. This process was repeated 4 times. Cell filtrates were centrifuged and resuspended in cell dissociation solution containing 0.75 mmol/l Ca^{2+}. An example of isolated myocytes is shown in Figure 37.
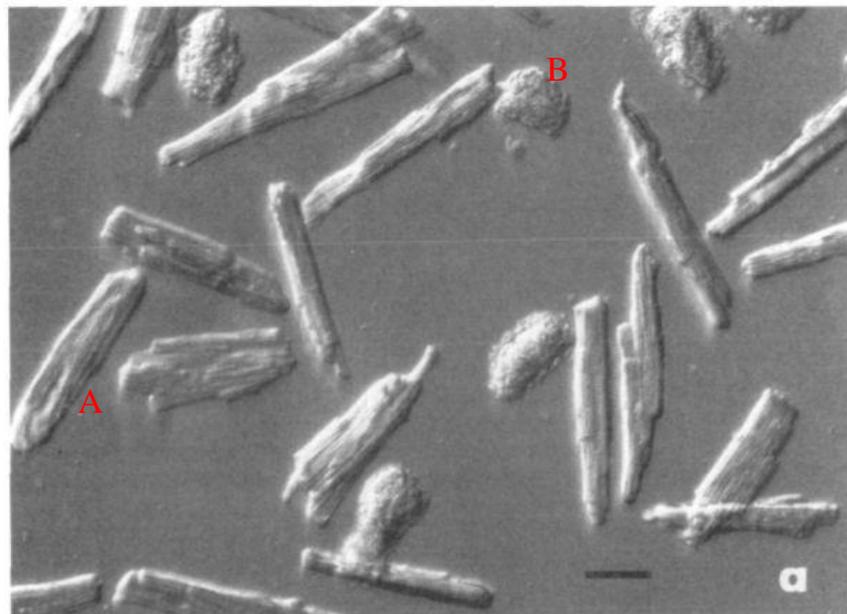
Figure 37: Rat myocytes original magnifications of 200X. (A) Rod shaped and (B) round shaped. Adapted from (Sheu et al., 1984).

After isolation, myocytes were allowed to settle by gravity on the bottom of a glass Perspex chamber on the stage of an inverted Axiovert 35 microscope (Zeiss, Göttingen, Germany). Ventricular myocyte shortening was measured according to previously described techniques (F. C. Howarth et al., 2020). Typical records of shortening are shown in Figure 38. Cells were perfused (3–5 ml/min) with NT comprising in mmol/l: 1.0 $MgCl_2$, 140 NaCl, 1.8 $CaCl_2$, 5 KCl, 5 HEPES, and 10 glucose (pH 7.4) at (35-36°C). Shortening was measured in electrically stimulated (1 Hz) ventricular myocytes recorded with an IonOptix MyoCam imaging system (IonOptix Corporation, Milton, MA, USA). RCL, TPK shortening, THALF relaxation and AMP of shortening were measured. Data were acquired and analyzed with IonWizard 6.6 version 10 software (IonOptix LLC, 396 University Ave. Westwood, MA 02090 USA).

Figure 38: Typical records of myocyte shortening and intracellular Ca^{2+}. Top panel shows shortening, second, third and fourth panels show measures of Fura-2. Second panel 340 nm, third panel 380 nm and fourth panel ratio of 340/380 nm. Fifth panel shows shortening image analysis cursors in place at the ends of the myocyte.

A typical IonWizard shortening analysis is seen in Figure 39.
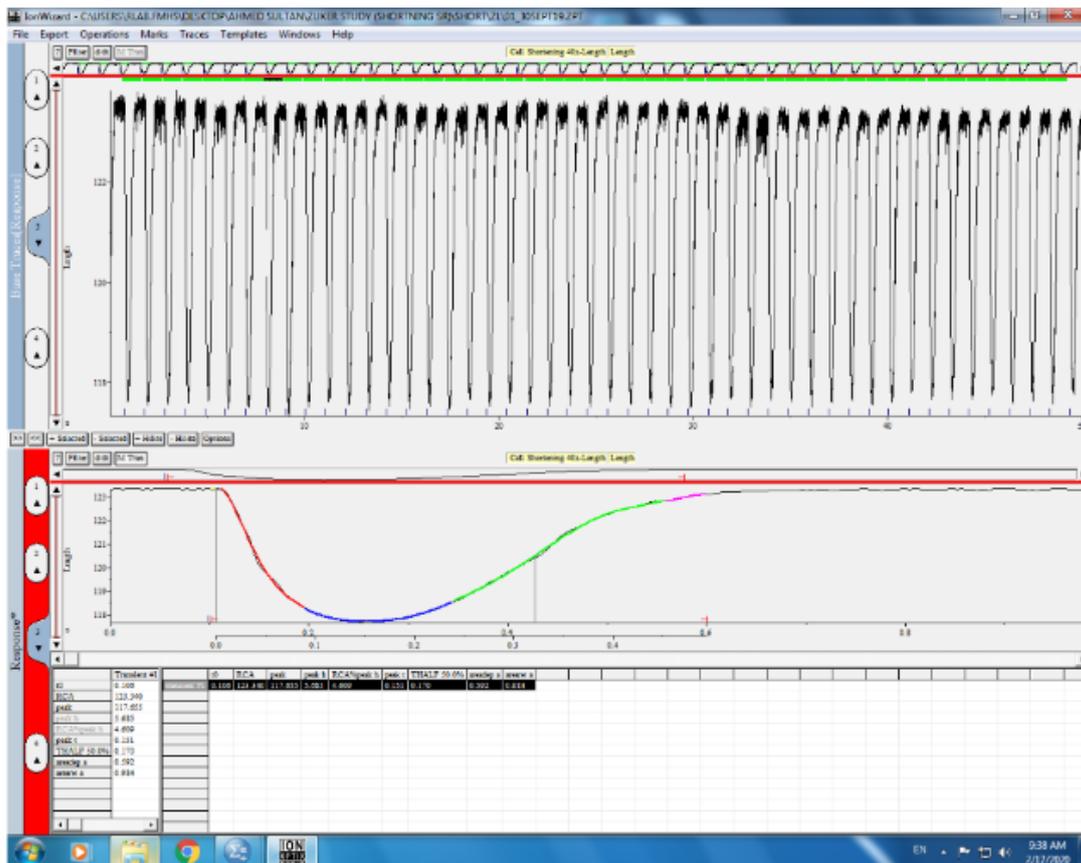
Figure 39: Typical IonWizard shortening analysis from ZL rat. Upper panel shows a train of shortening records. The middle panel shows the average of several records and the lower panel shows typical analysis output.

5.5 Statistics

Results were reported as the mean ± SEM of 'n' observations. The statistical comparisons were done by IBM SPSS and Origin 9.0 (OriginLab, Northampton, Massachusetts, USA) statistics software using either the independent samples t-test or one-way ANOVA and then by Bonferroni corrected t-tests for multiple comparisons, as applicable. P values of 0.05 and less were considered statistically significant.

5.6 Results

Typical records of myocyte shortening are shown in Figure 40A. The mean RCL was significantly longer (p<0.05) in ZDF (117.93±0.99 µm) compared to ZL (112.58±1.42 µm) myocytes (40B). The mean TPK shortening was significantly prolonged (p<0.05) in ZDF (158.59±3.05 msec) compared to ZF (130.33±2.57 msec) and ZL myocytes

(126.54±3.09 msec) (40C). THALF relaxation of shortening (40D) and AMP shortening (40E) were not significantly changed (p>0.05) in ZDF or ZF compared to ZL myocytes.

(A)

(B)
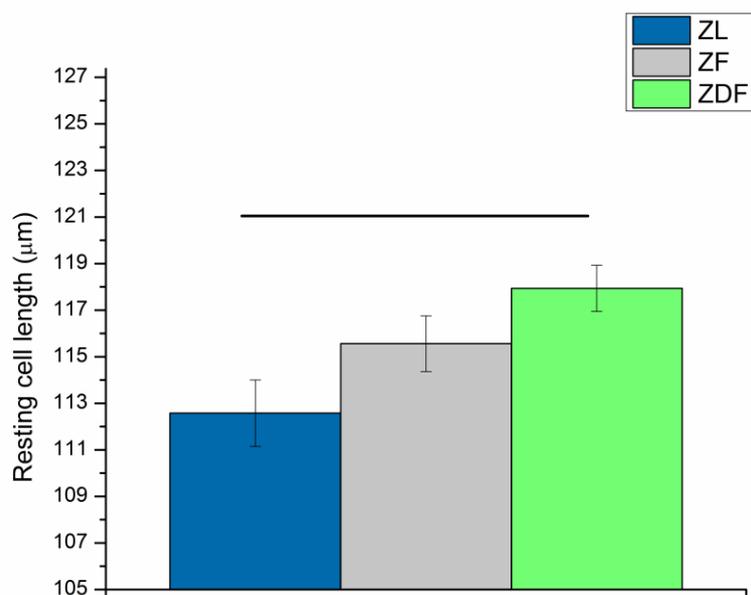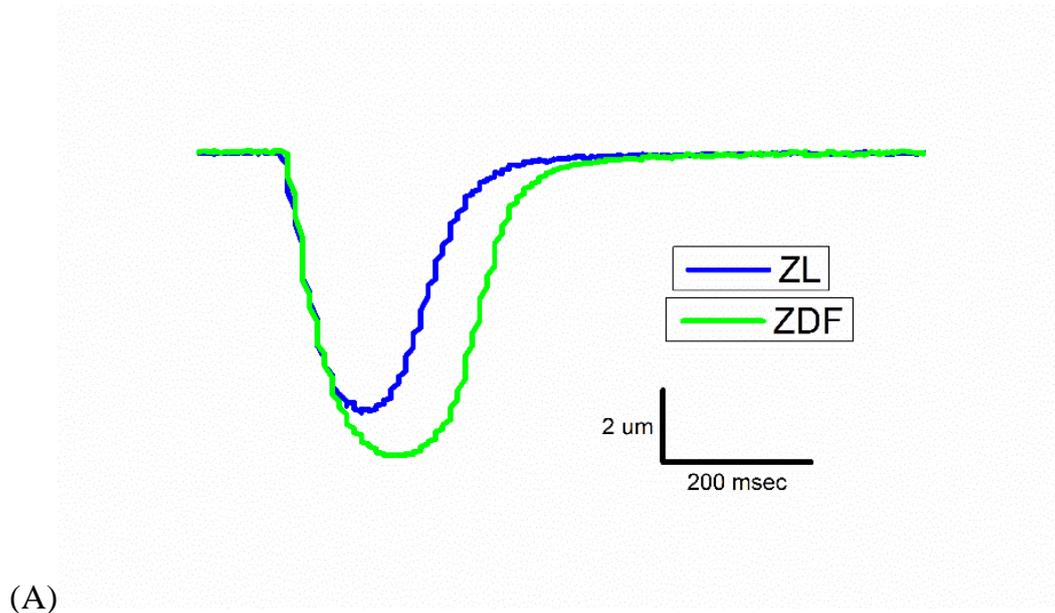
Figure 40: Electrically-evoked ventricular myocyte shortening. (A) Typical filtered records of ventricular myocyte shortening in an electrically-stimulated cell and (B) resting cell length.
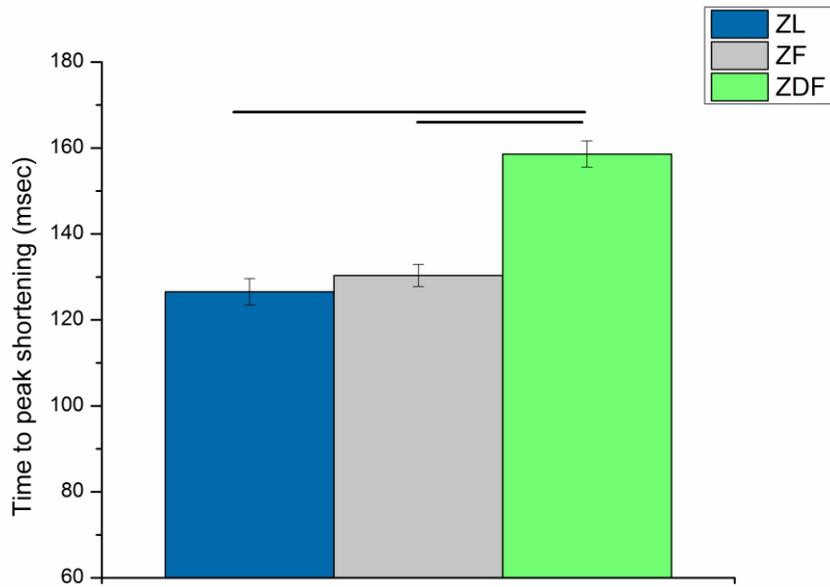
(C)
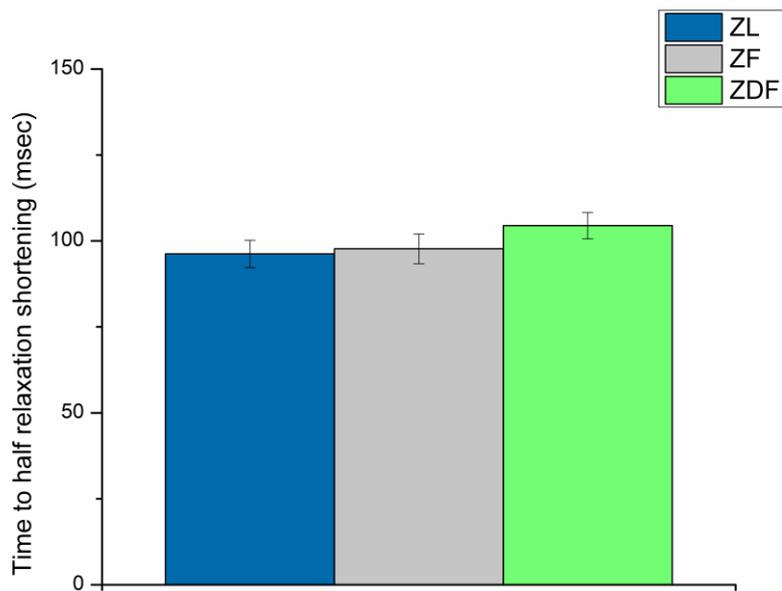
(D)

Figure 40: Electrically-evoked ventricular myocyte shortening. (C) Time to peak shortening and (D) time to half relaxation of shortening (Continued).
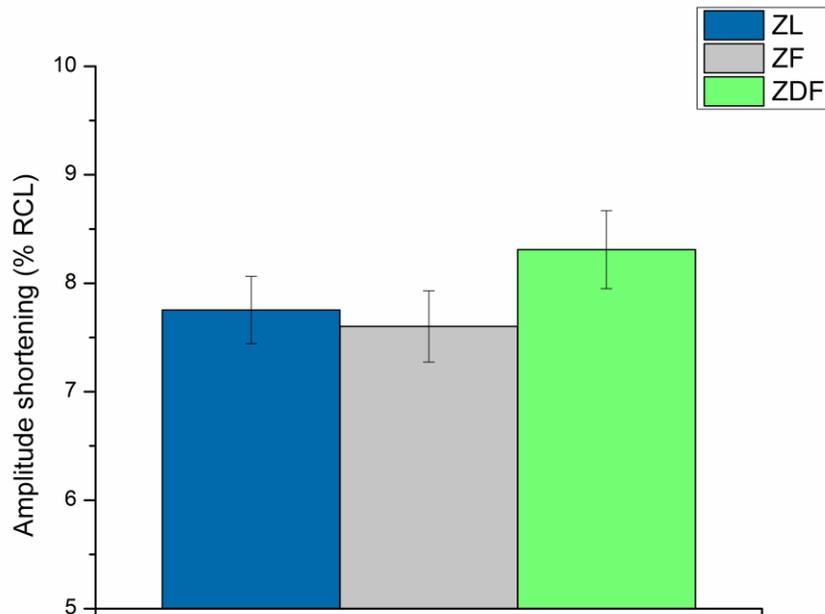
(E)

Figure 40: Electrically-evoked ventricular myocyte shortening. (E) Amplitude of shortening. Data are mean ± SEM. n=79 ZL, 92 ZF and 87 ZDF cells from 13 ZL, 16 ZF and 16 ZDF hearts. P values of 0.05 and less were considered statistically significant (Continued).

5.7 Discussion

RCL was longer in ZDF compared to ZF and ZL myocytes which may indicate hypertrophy in ZDF rat hearts. The force of contraction may be changed by either altering the amount of free intracellular Ca^{2+}, and/or by altering the sensitivity of the myofilaments to Ca^{2+}. Increasing the cell length of the myocyte increases the sensitivity of TnC (a cardiac regulatory protein) to Ca^{2+} which is called "length-dependent Ca^{2+} sensitivity" and it can also lead to enhanced intracellular Ca^{2+} (Pinnell et al., 2007). Evidence from the current study suggests that ZDF is not able to contract as efficiently as ZL and ZF, perhaps due to reduced forced of contraction and/or ventricular dilatation of myocytes (Obayashi et al., 2006; Pinnell et al., 2007). TPK shortening was prolonged in ZDF compared to ZF and ZL myocytes which might partly be attributed to the increased length of ZDF myocytes. It might also be attributed to alterations in Ca^{2+} transport as well as the velocity of contraction and relaxation (Mattiazzi et al., 1986).

Neither THALF relaxation nor AMP shortening were significantly altered in ZDF or ZF compared to ZL myocytes. Preserved THALF relaxation and AMP of shortening has been previously reported in ZDF myocytes compared to ZL myocytes from rats aged 30-34 weeks of age (F. C. Howarth et al., 2012). In another study, AMP of shortening at 6 and 22 weeks were unchanged and the time course of shortening at 6 weeks was also unaffected. However, the TPK shortening and THALF relaxation of shortening were prolonged in ZDF rats at 22 weeks (Fulop et al., 2007).

5.8 Conclusions

- Hypertrophy in the ZDF may be present as suggested by the mean RCL which was significantly longer in ZDF compared to ZL myocytes.

- The mean TPK shortening was significantly prolonged in ZDF compared to ZF and ZL myocytes.

- THALF relaxation of shortening and AMP shortening were well preserved in ZDF or ZF compared to ZL myocytes.

- Defects in the uptake and release of SR Ca^{2+} might partially underlie the altered time course of shortening in ventricular myocytes from ZDF rat.

Chapter 6: Investigating ventricular myocyte Ca^{2+} transport using fluorescence photometry techniques in the ZL, ZF and ZDF rats

6.1 Introduction

The effects of ventricular myocyte Ca^{2+} transport has been widely investigated in various models of diabetes. A previous study showed that intracellular Ca^{2+} signaling was defective in myocytes from STZ rats, and may contribute to cardiomyopathy, by showing that the AMP of caffeine induced Ca^{2+} transients was lower in STZ compared to control myocytes (Choi et al., 2002). The study also suggested defects in Ca^{2+} release from the SR by showing that the rate of rise of intracellular Ca^{2+} was decreased and the TPK of intracellular Ca^{2+} was prolonged in myocytes from STZ compared to control rats (Choi et al., 2002). Another study on db/db diabetic mice showed that intracellular Ca^{2+} transients were decreased in isolated myocytes compared to controls as well as decreased SR Ca^{2+} transients which were measured by caffeine application (Pereira et al., 2006). Furthermore, asymptomatic type 2 diabetic patients had slower SR Ca^{2+} release mainly due to decreased expression of RyR in atrial myocardium compared to non-diabetic patients (Reuter et al., 2008).

6.2 Hypothesis

- Alterations in Ca^{2+} signaling including SR Ca^{2+} transport might partly underlie defects in ventricular myocyte shortening in ZDF and ZF rats.

6.3 Aims and objectives

- To investigate the effects of obesity and diabesity on resting Fura-2 ratio, TPK Ca^{2+} transient, THALF decay of the Ca^{2+} transient, and the AMP of Ca^{2+} transients in ventricular myocytes from ZDF and ZF compared to ZL rats.
- To investigate the effects of obesity and diabesity on SR Ca^{2+} release and refilling in ventricular myocytes from ZDF and ZF compared to ZL rats.
- To investigate the effects of obesity and diabesity on myofilament sensitivity to Ca^{2+} in ventricular myocytes from ZDF and ZF compared to ZL rats.

6.4 Methods

6.4.1 Measurement of intracellular Ca^{2+} concentration

Intracellular Ca^{2+} concentration was assessed according to previously described techniques (F. C. Howarth et al., 2020). Myocytes were loaded with the fluorescent indicator Fura-2 AM (F-1221, Molecular Probes, OR, USA). In short, 6.25 µl of a 1.0 mmol/l stock solution of Fura-2 AM (dissolved in dimethylsulphoxide DMSO) was added to 2.5 ml of cell suspension to give a Fura-2 concentration of 2.5 µmol/l. Myocytes were gently shaken for 10 min at room temperature (24°C). Following loading, myocytes were centrifuged, rinsed with NT to remove extracellular Fura-2 and kept for 30 minutes to allow full hydrolysis of the intracellular Fura-2 ester. To determine intracellular Ca^{2+} concentration myocytes were interchangeably illuminated by 340 and 380 nm light utilizing a monochromator (Cairn Research, Faversham, UK) which switched the excitation light every 2 msec. The subsequent fluorescence emitted at 510 nm was collected by a photomultiplier tube and the ratio of the emitted fluorescence at the two excitation wavelengths (340/380 ratio) was analyzed to give an index of intracellular Ca^{2+} concentration. Resting Fura-2 ratio, TPK Ca^{2+} transient, THALF decay of the Ca^{2+} transient, and the AMP of Ca^{2+} transients were measured in electrically stimulated (1 Hz) ventricular myocytes maintained at 35–36°C. The system used to measure intracellular Ca^{2+} is shown in Figure 41. Typical records of 340 nm and 380 nm and 340/380 nm Fura-2 signals are shown in Figure 42.
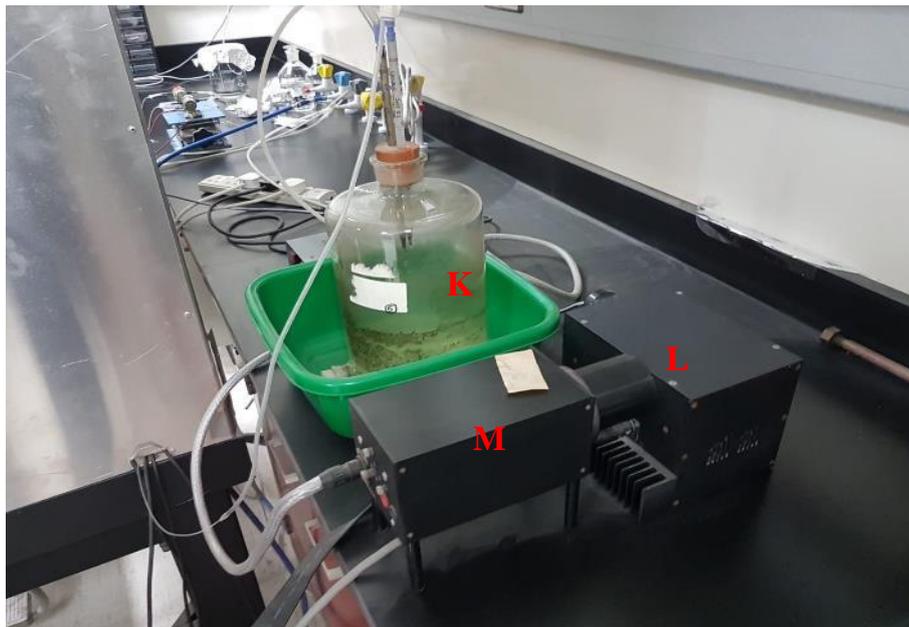
Figure 41: Fluorescence photometry system. (A) Personal Computer, (B) electric stimulator, (C) temperature controller, (D) Cairn fluorescence photometer control system, (E) Ionoptix power supply, (F) inverted light microscope, (G) antivibration table, (H) Ionoptix camera, (I) Faraday cage for noise insulation, (J) solution exchange power supply, (K) waste, (L) monochromator and (M) light source.

Data were acquired and analyzed with IonWizard 6.6 version 10 software (IonOptix LLC, 396 University Ave. Westwood, MA 02090 USA). A typical example of the analysis is shown in Figure 42.
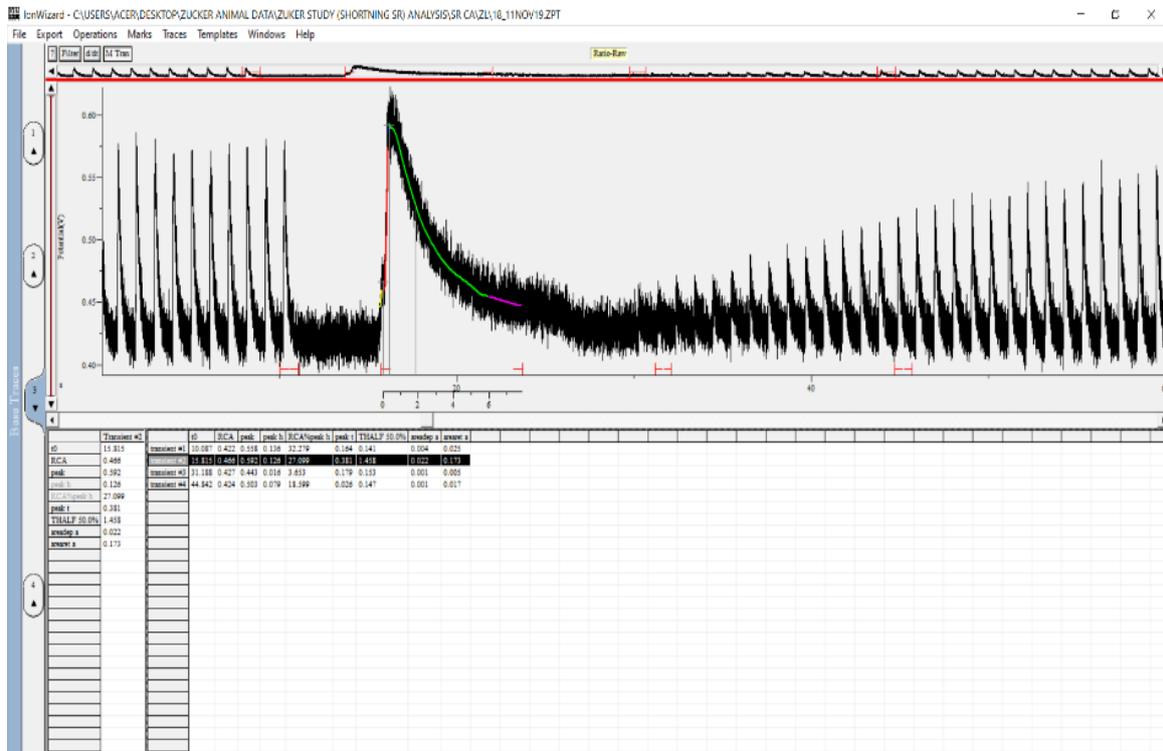
Figure 42: Typical IonWizard SR Ca^{2+} analysis from ZL rat. The top panel shows electrically-evoked and caffeine-evoked Ca^{2+} transients. The bottom panel shows typical analysis output.

6.4.2 Measurement of sarcoplasmic reticulum Ca^{2+} transport

SR Ca^{2+} release was evaluated using previously described techniques (F. C. Howarth et al., 2020). After achieving steady state Ca^{2+} transients in electrically stimulated (1 Hz) myocytes maintained at 35–36°C and loaded with Fura-2, stimulation was stopped for a period of 5 seconds. Caffeine (20 mM) was then applied for 10 seconds using a rapid solution changing device (Levi et al., 1996). Electrical stimulation was then continued and the Ca^{2+} transients were allowed to recover to steady state. Fractional release of SR Ca^{2+} was evaluated by comparing the AMP of the electrically-evoked steady state Ca^{2+} transients with that of the caffeine-evoked Ca^{2+} transient. Ca^{2+} refilling of SR was evaluated by measuring the rate of recovery of electrically evoked Ca^{2+} transients

following application of caffeine. Data were acquired and analyzed with IonWizard 6.6 version 10 software (IonOptix LLC, 396 University Ave. Westwood, MA 02090 USA).

6.4.3 Measurement of myofilament sensitivity to Ca^{2+}

Ventricular myocyte shortening and intracellular Ca^{2+} were simultaneously measured in Fura-2 AM loaded myocytes. Ventricular myocyte shortening and intracellular Ca^{2+} were measured according to previously described techniques and described on page 102 in the previous chapter (F. C. Howarth et al., 2020).

Myofilament sensitivity was measured according to previously described techniques (Smail et al., 2018) as shown in FigureA & B. The Fura-2 ratio was plotted against shortening. Myofilament sensitivity to Ca^{2+} was evaluated from the resulting phase–plane diagram by measuring the gradient of the Fura-2 cell length trajectory during late relaxation (500-800 msec) of the twitch contraction as previously described (F. C. Howarth et al., 2011, 2012). The position of the trajectory reflects the relative myofilament response to Ca^{2+} and therefore can be used as a measure of myofilament sensitivity to Ca^{2+} (Spurgeon et al., 1992).

6.5 Statistics

Results were reported as the mean ± SEM of 'n' observations. The statistical comparisons were done by IBM SPSS and Origin 9.0 (OriginLab, Northampton, Massachusetts, USA) statistics software using either the independent samples t-test or one-way ANOVA and then by Bonferroni corrected t-tests for multiple comparisons, as applicable. P values of 0.05 and less were considered statistically significant.

6.6 Results

6.6.1 Ventricular myocyte intracellular Ca^{2+} concentration and sarcoplasmic reticulum Ca^{2+} transport results

The experimental protocol to investigate intracellular Ca^{2+} is shown in Figure 43A. Typical records of electrically-evoked Ca^{2+} transients are shown in Figure 43B. The mean resting Fura-2 ratio (340/380 nm) was significantly increased (p<0.05) in ZF (0.47±0.007

RU) compared to ZL (0.44±0.006 RU) myocytes (Figure 43C). The mean TPK Ca^{2+} transient was significantly prolonged ($p<0.05$) in ZF (67.26±5.69 msec) compared to ZL (51.54±2.32 msec) myocytes (Figure 43D). THALF decay of the Ca^{2+} transient was significantly prolonged ($p<0.05$) in ZDF (155.35±2.92 msec) compared to ZF (131.11±3.26 msec) and ZL (129.17±3.12 msec) myocytes (Figure 43E). AMP of the Ca^{2+} transient was significantly increased ($p<0.05$) in ZF (0.118±0.007 RU) compared to ZDF (0.094±0.004 RU) myocytes (Figure 43F).

TPK of caffeine-evoked Ca^{2+} transients was significantly prolonged ($p<0.05$) in ZDF (575.46±30.96 msec) compared to ZF (468.81±29.73 msec) and in ZDF compared to ZL myocytes (377.82±29.41 msec) (Figure 43G). THALF decay of the caffeine-evoked Ca^{2+} transient was also significantly prolonged ($p<0.05$) in ZDF (2050.71±76.1 msec) compared to ZF (1638.03±75.2 msec) and in ZDF compared to ZL myocytes (1459.4±60.6 msec) (Figure 43H). AMP of the caffeine-evoked Ca^{2+} transient was not significantly changed ($p>0.05$) in ZDF or ZF compared to ZL myocytes (Figure 43I). Fractional release of Ca^{2+} (Figure 43J) and recovery of the Ca^{2+} transients (Figure 43K) were significantly lower in the ZDF compared to ZF myocytes.
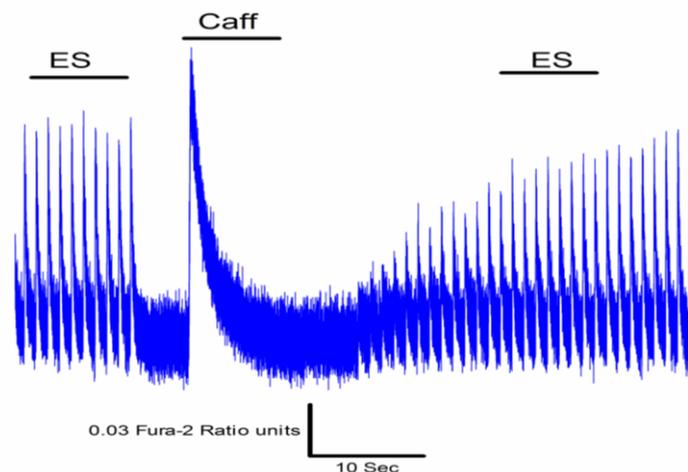
(A)

Figure 43: Electrically-evoked Ca^{2+} transients and caffeine-evoked Ca^{2+} transient. (A) Typical recording to illustrate the experimental protocol in a ventricular myocyte from a ZL rat.
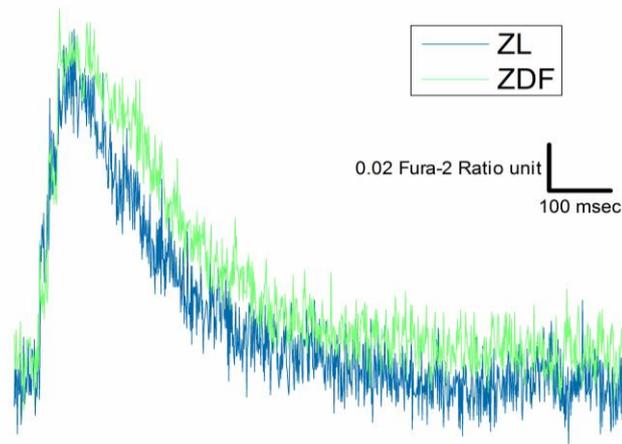
(B)
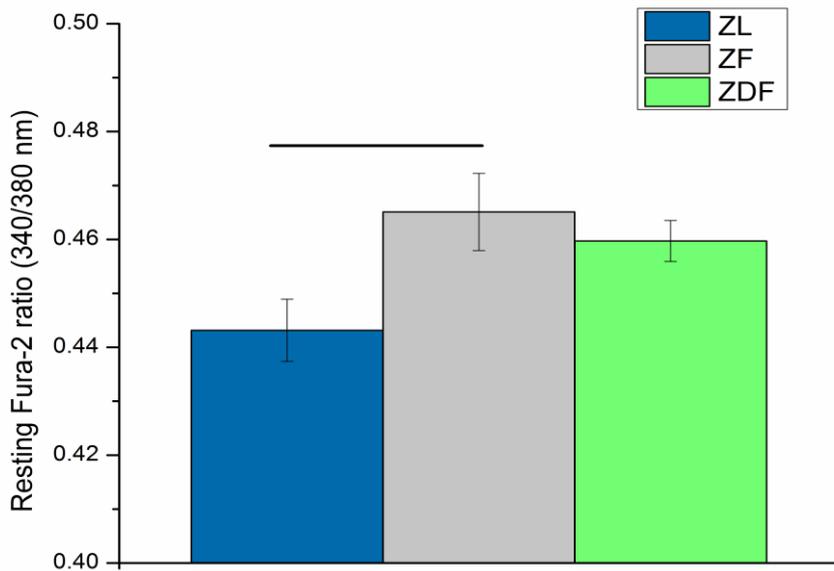
(C)

Figure 43: Electrically-evoked Ca^{2+} transients and caffeine-evoked Ca^{2+} transient. (B) Typical filtered records of electrically-evoked Ca^{2+} transients and (C) resting Fura-2 ratio (Continued).
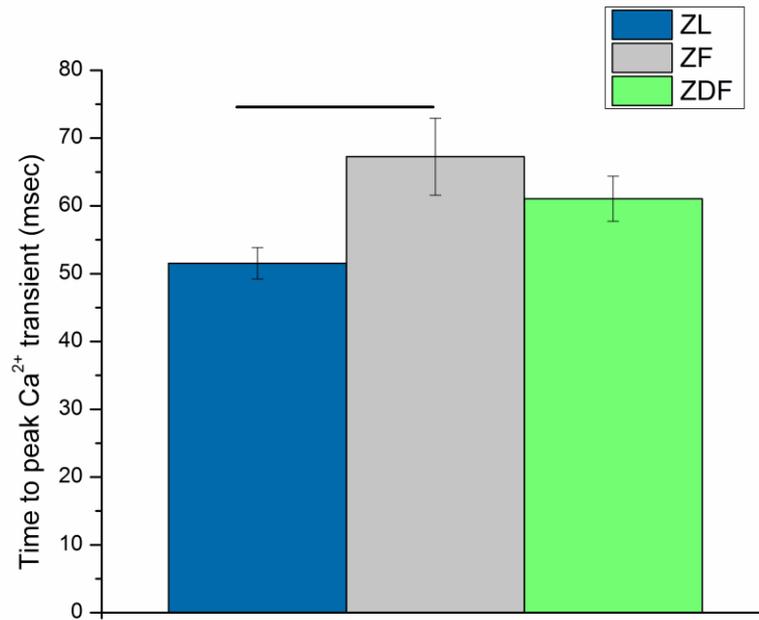
(D)
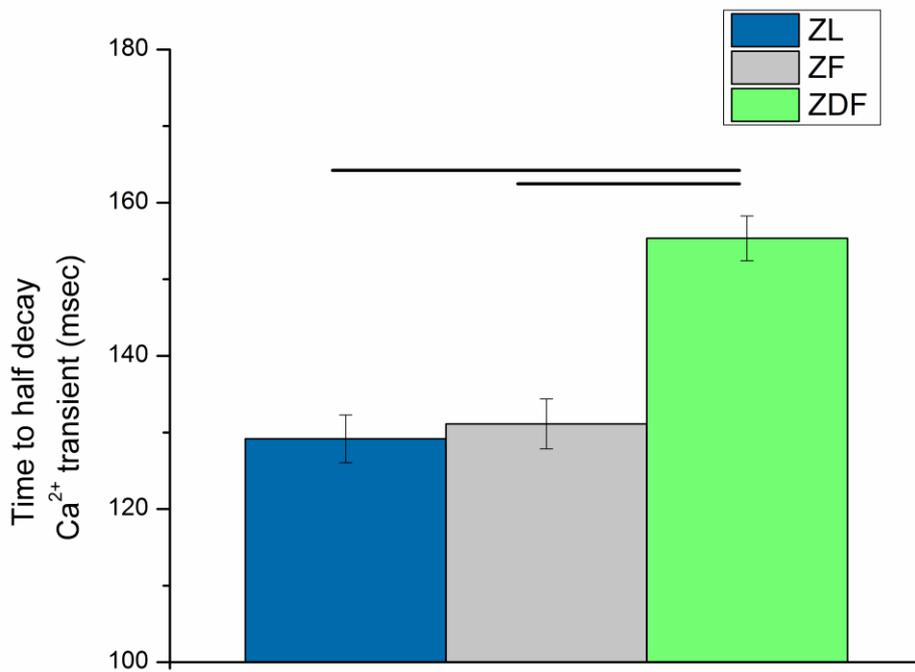
(E)

Figure 43: Electrically-evoked Ca^{2+} transients and caffeine-evoked Ca^{2+} transient. (D) Time to peak Ca^{2+} transient and (E) time to half decay Ca^{2+} transient (Continued).
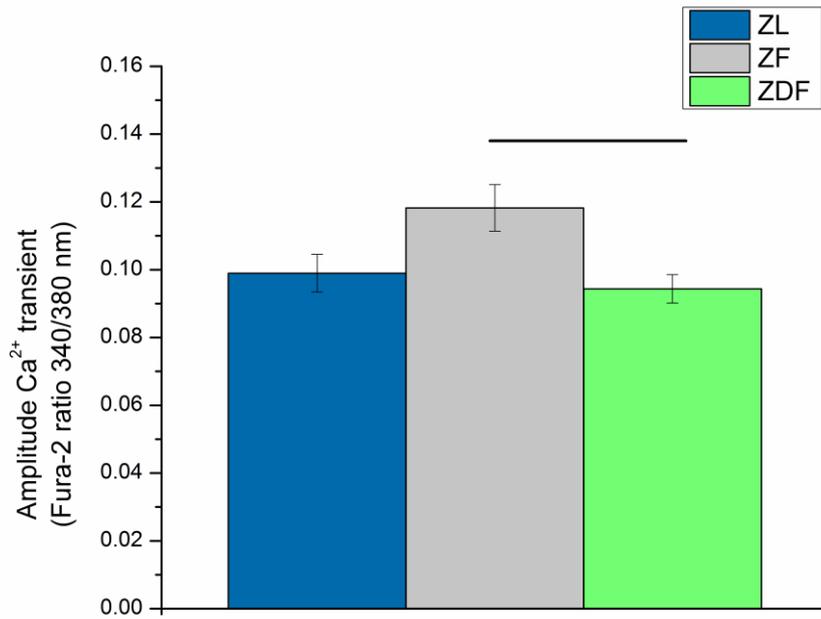
(F)
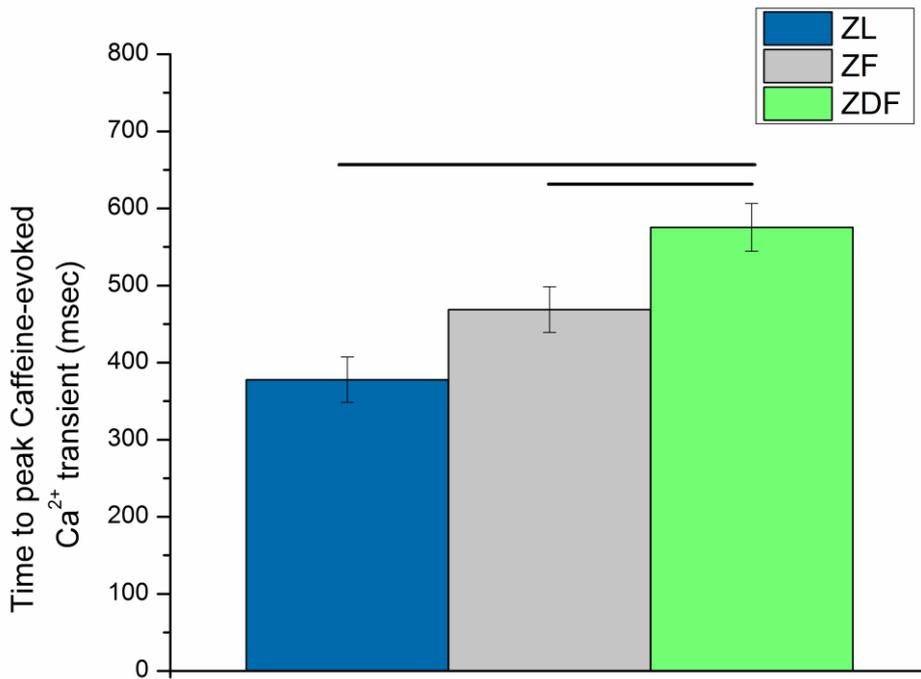
(G)

Figure 43: Electrically-evoked Ca^{2+} transients and caffeine-evoked Ca^{2+} transient. (F) Amplitude of the Ca^{2+} transient and (G) time to peak of caffeine-evoked Ca^{2+} transient (Continued).
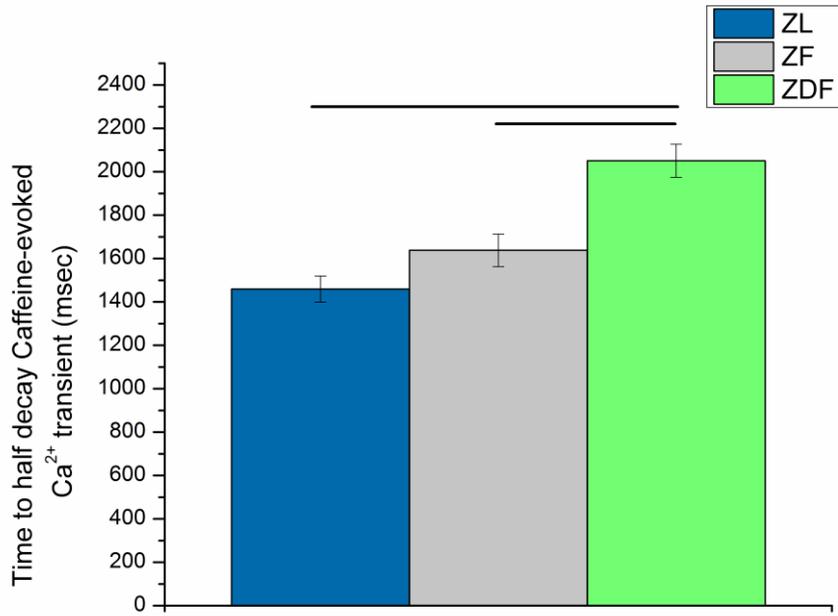
(H)
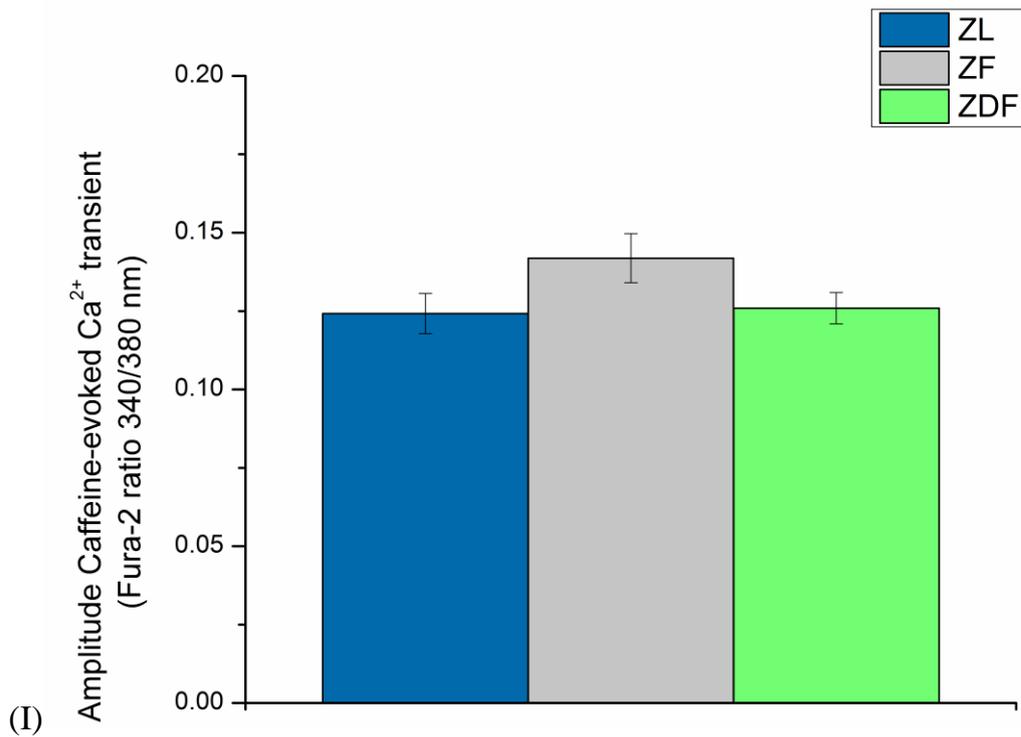
(I)

Figure 43: Electrically-evoked Ca^{2+} transients and caffeine-evoked Ca^{2+} transient. (H) Time to half decay of caffeine-evoked Ca^{2+} transients and (I) amplitude of caffeine-evoked Ca^{2+} transient (Continued).
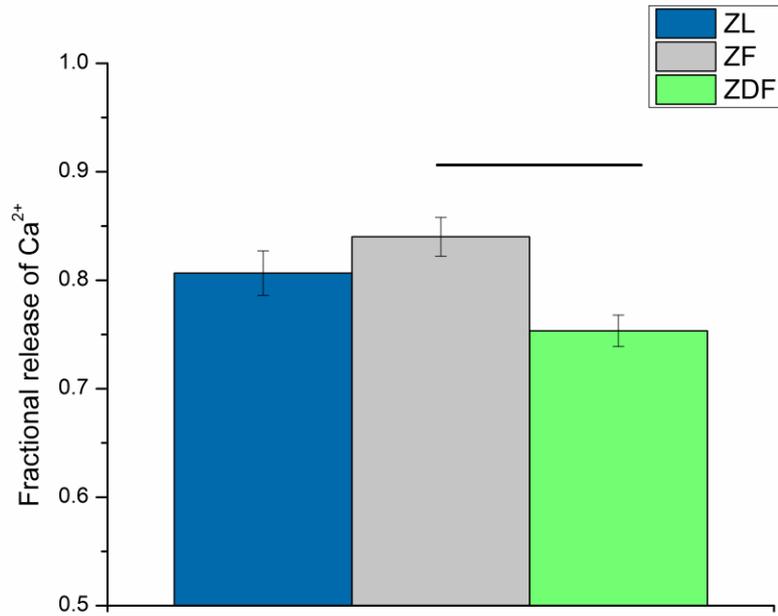
(J)
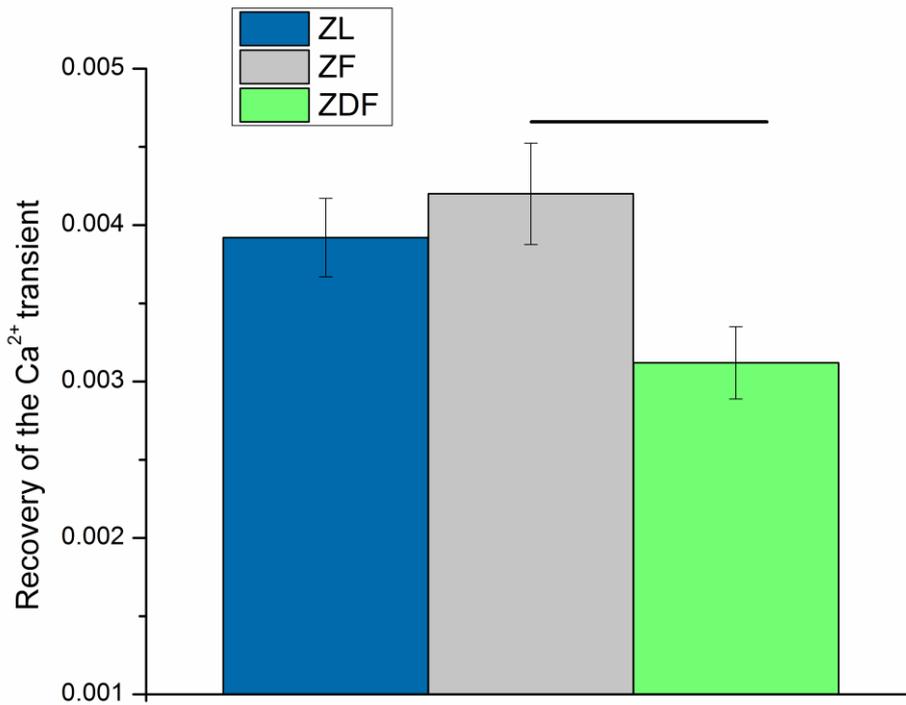
(K)

Figure 43: Electrically-evoked Ca^{2+} transients and caffeine-evoked Ca^{2+} transient. (J) Fractional release of Ca^{2+} and (K) recovery of Ca^{2+} transient. Data are mean ± SEM. n=72 ZL, 70 ZF, 82 ZDF cells from 13 ZL, 16 ZF and 16 ZDF hearts. P values of 0.05 and less were considered statistically significant. ES - Electrical stimulation, Caff - Caffeine stimulation (Continued).

6.6.2 Myofilament sensitivity to Ca²⁺ results

Typical records of electrically-evoked Fura-2 loaded myocyte shortening are shown in (Figure 44A, upper panel). The mean RCL was not significantly altered in ZDF (110.50±1.75 µm) or in ZF (107.04±1.96 µm) compared to ZL (107.33±1.66 µm) (Figure 44C). The mean TPK shortening was also not altered in ZDF (138.31±4.56 msec) or in ZF (138.77±3.33 msec) compared to ZL myocytes (144.84±4.13 msec) (Figure 44D). The THALF relaxation of shortening was also not altered (Figure 44E). However, the AMP shortening (Figure 44F) was significantly increased (p<0.05) in ZF (6.38±0.41% RCL) compared to ZL (5.13±0.35% RCL) but not compared to ZDF (5.60±3.33% RCL) myocytes.

Typical records of electrically-evoked Ca²⁺ transients are shown in (Figure 44A, lower panel). The mean resting Fura-2 ratio (340/380 nm) was significantly increased (p<0.05) in ZDF (0.35±0.008 RU) compared to ZL (0.31±0.007 RU) myocytes (Figure 44G). The mean TPK Ca²⁺ transient was not significantly different (p>0.05) between ZF (70.86±1.42 msec), ZDF (69.69±1.92 msec) and ZL (72.42±1.84 msec) myocytes (Figure 44H). THALF decay of the Ca²⁺ transient was significantly prolonged (p<0.05) in ZDF (123.23±2.68 msec) compared to ZL (112.54±3.46 msec) and shortened in ZF (106.08±2.30 msec) compared to ZL (112.54±3.46 msec) myocytes (Figure 44I). AMP of the Ca²⁺ transient was not significantly different (p>0.05) between ZF (0.034±0.0013 RU), ZDF (0.035±0.0017 RU) and ZL (0.037±0.0016 RU) myocytes (Figure 44J).

Electrically-evoked myocyte shortening and intracellular Ca²⁺ were recorded simultaneously and a typical record in a ZL control myocyte is shown in (Figure 44A). A typical phase-plane diagram of Fura-2 ratio versus cell length in a ZL control is shown in (Figure 44B). The mean gradients of the Fura-2 cell length trajectory measured during the late relaxation period of the twitch contraction (500–800 msec) are shown in (Figure 44K). Results were not significantly changed in ZDF and ZF compared to ZL myocytes.
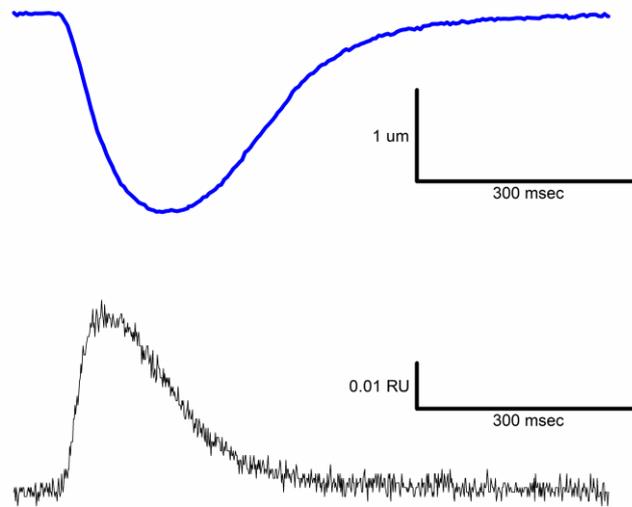
(A)
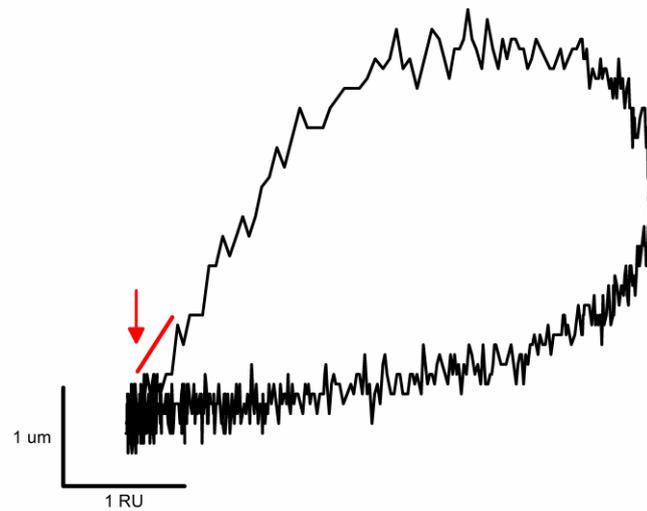
(B)

Figure 44: Simultaneous measurement of shortening and intracellular Ca^{2+} in electrically stimulated (1 Hz) ventricular myocytes. (A) Typical simultaneous recording of shortening and Ca^{2+} in a ventricular myocyte from a ZL rat and (B) typical phase plane diagram of Fura-2 ratio versus cell length and the arrow shows the area that the gradient was measured.
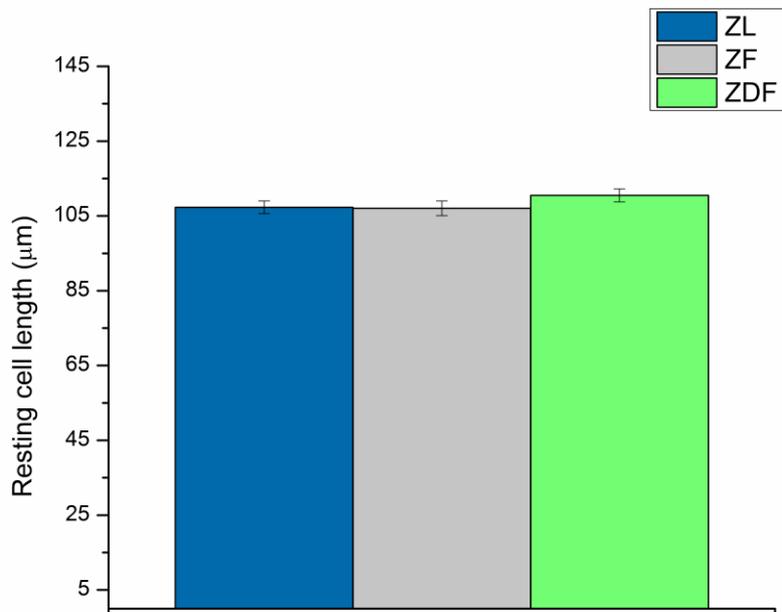
(C)
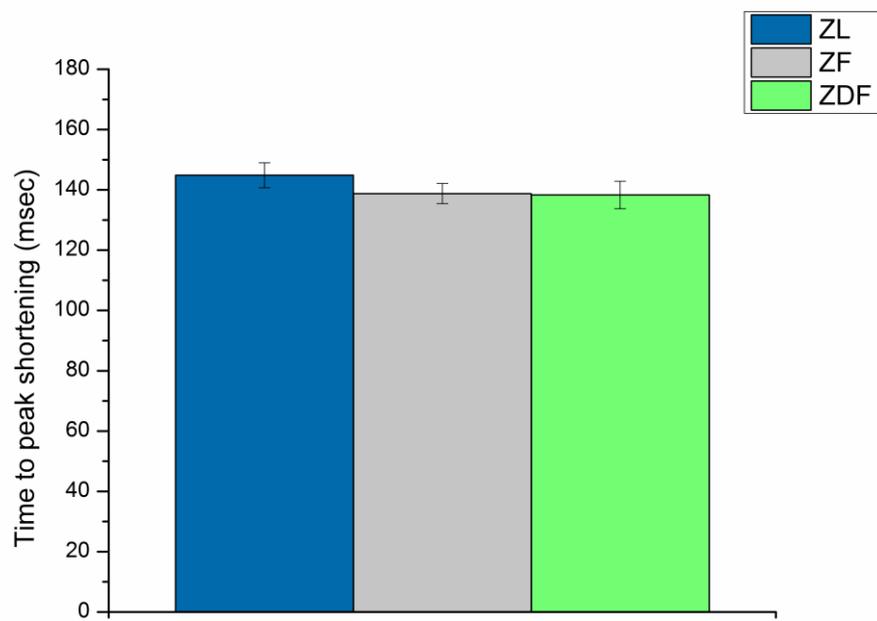
(D)

Figure 44: Simultaneous measurement of shortening and intracellular Ca^{2+} in electrically stimulated (1 Hz) ventricular myocytes. (C) Resting cell length and (D) time to peak shortening (Continued).
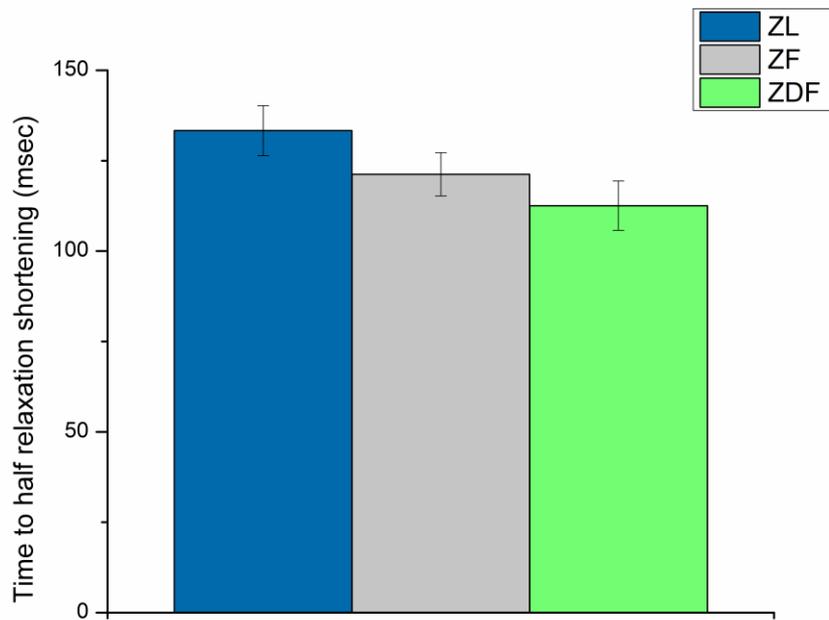
(E)
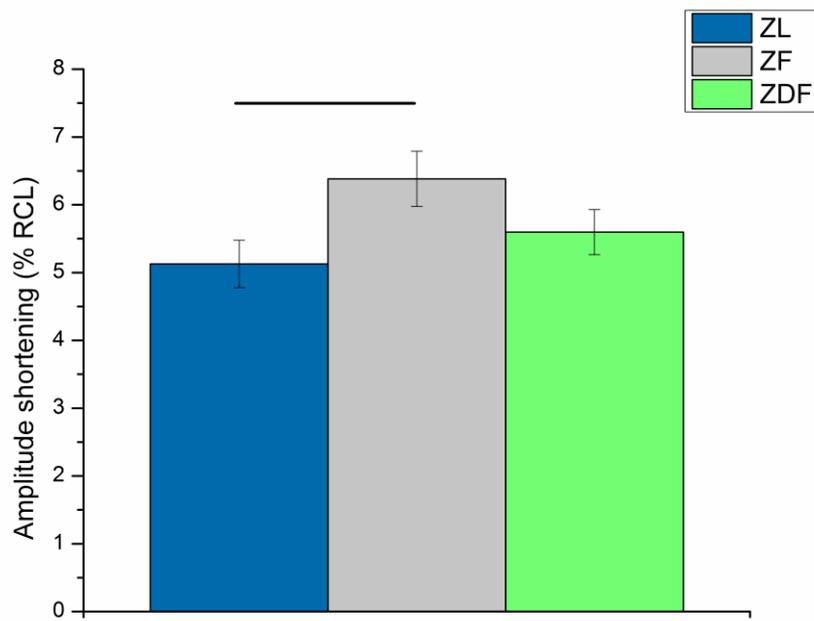
(F)

Figure 44: Simultaneous measurement of shortening and intracellular Ca^{2+} in electrically stimulated (1 Hz) ventricular myocytes. (E) Time to half relaxation of shortening and (F) amplitude shortening (Continued).
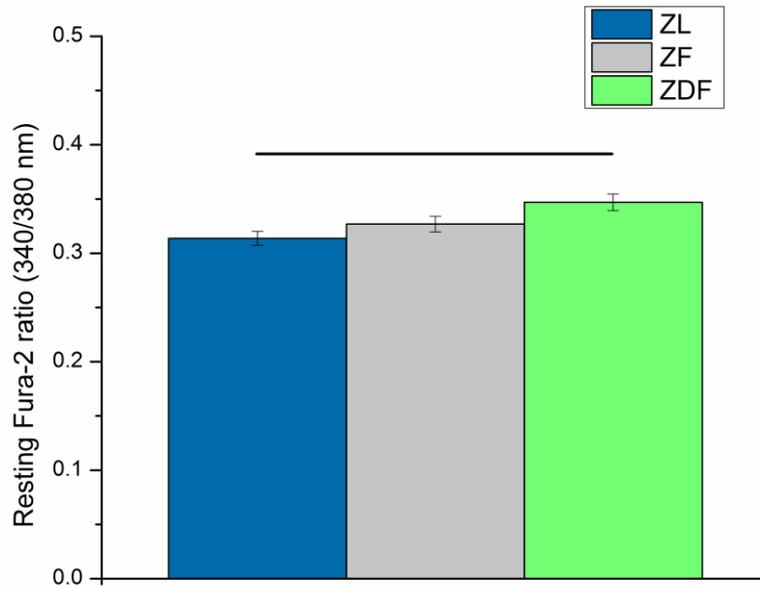
(G)
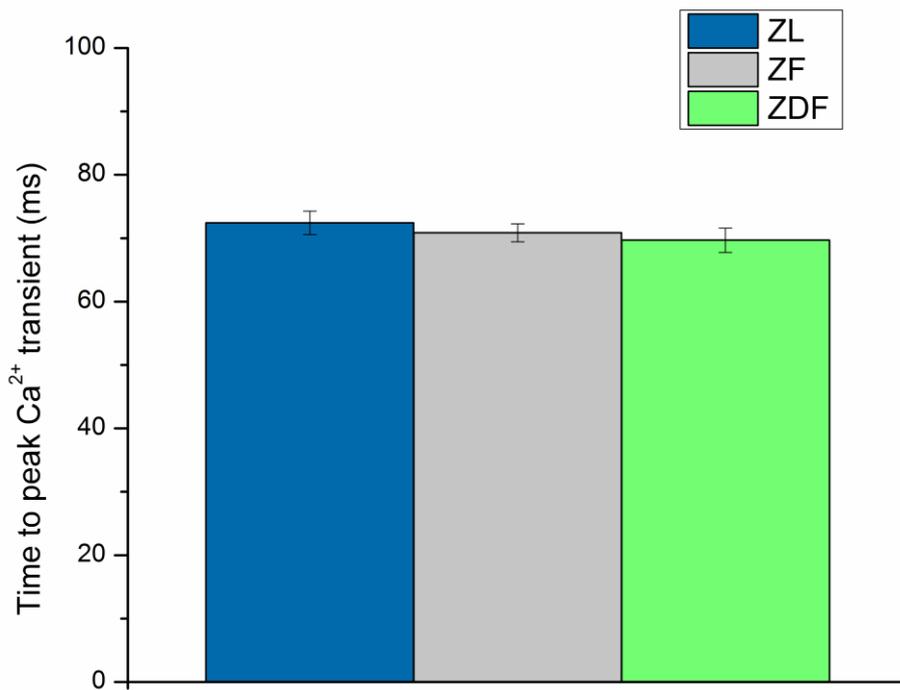
(H)

Figure 44: Simultaneous measurement of shortening and intracellular Ca^{2+} in electrically stimulated (1 Hz) ventricular myocytes. (G) Resting Fura-2 ratio and (H) time to peak of the Ca^{2+} transient (Continued).
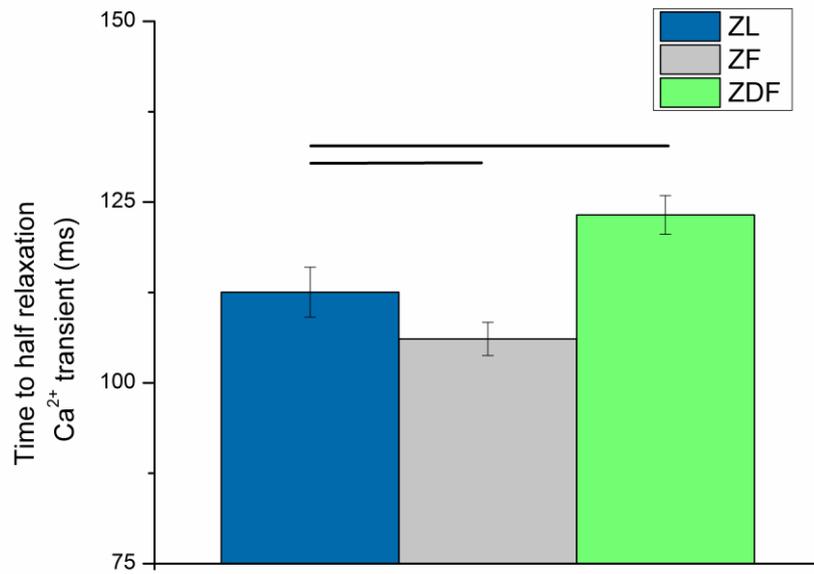
(I)
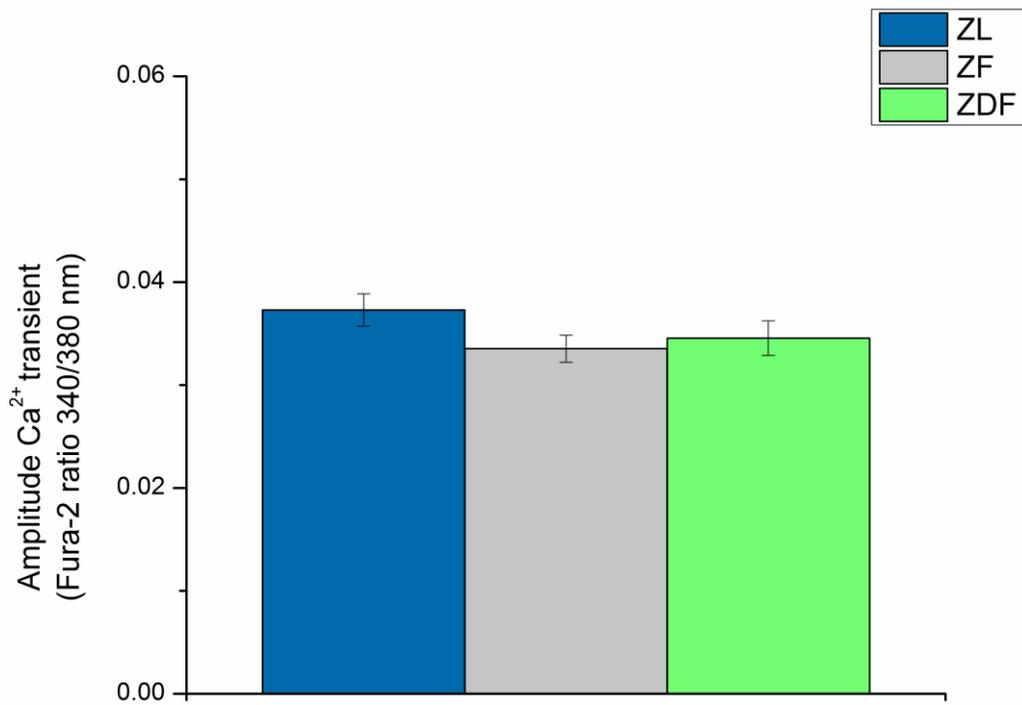
(J)

Figure 44: Simultaneous measurement of shortening and intracellular Ca^{2+} in electrically stimulated (1 Hz) ventricular myocytes. (I) Time to half decay of the Ca^{2+} transient and (J) amplitude of the Ca^{2+} transient (Continued).
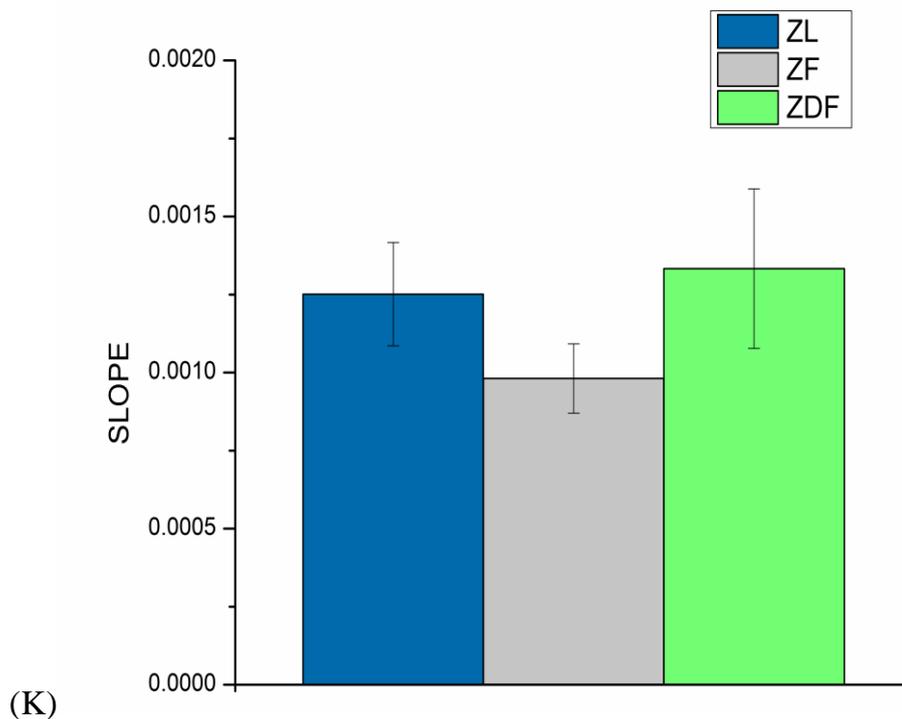
(K)

Figure 44: Simultaneous measurement of shortening and intracellular Ca^{2+} in electrically stimulated (1 Hz) ventricular myocytes. (K) Mean gradient of the Fura-2 trajectory during late relaxation of the twitch contraction during the period (500-800 msec). Data are mean ± SEM. Differences considered significant where $p<0.05$. n=57 ZL, 65 ZF and 52 ZDF cells from 5 ZL, 5 ZF and 5 ZDF rats (Continued).

6.7 Discussion

6.7.1 Ventricular myocyte intracellular Ca^{2+} concentration

To investigate SR Ca^{2+} transport Fura-2 loaded myocytes were electrically stimulated to generate Ca^{2+} transients and then, after a pause, were rapidly exposed to caffeine to release Ca^{2+} from the SR. The resting Fura-2 ratio was higher in ZF compared to ZL myocytes. Our study did not find any significant differences in cell capacitance between ZDF, ZF and ZL myocytes. Further investigation of the molecular structure (see chapter 9) specifically, the SR and the sarcomeres, which are important in ECC might clarify the cause of the elevated Fura-2 ratio in ZF myocytes (Bers & Despa, 2013; Craig et al., 2014; Lainé et al., 2018; Qadota & Benian, 2010; ter Keurs et al., 2008). The SR

consists of longitudinal tubules, which release Ca^{2+} ions, and the terminal cisternae, which are large regions in close proximity to the ends of the transverse tubules known as "T-tubules", that sequester and concentrate Ca^{2+}. Evidence suggests that loss of T-tubule integrity can profoundly affect ECC in myocytes (Ferrantini et al., 2014; Pavlović et al., 2010; Silverthorn et al., 2007). It is important to note that T-tubule density can be measured using whole-cell capacitance in voltage-clamped myocytes relative to cell area, previous results indicate that rat myocytes can be kept in quiescent culture for 24 hours with no detectable de-tubulation or loss of T-tubules (Pavlović et al., 2010). TPK Ca^{2+} transient was not changed in ZDF compared to ZL myocytes. However, TPK Ca^{2+} transient was prolonged in ZF compared to ZL myocytes. THALF decay of the Ca^{2+} transient was prolonged in ZDF compared to ZF and ZL myocytes. AMP of the Ca^{2+} transient was increased in ZF compared to ZDF myocytes. These disturbances in time course of the Ca^{2+} transient might be partly attributed to defective SR Ca^{2+} transport.

TPK and THALF decay of the caffeine-evoked Ca^{2+} transients were prolonged in ZDF compared to ZF and ZL myocytes as well as significantly lower fractional release of Ca^{2+} and recovery of Ca^{2+} transients in the ZDF compared to ZF myocytes. Collectively, these findings suggest delayed release and uptake of Ca^{2+} by the SR and this in turn might be caused by defective SR Ca^{2+} release channel RyR and/or SERCA pump activity (Currie & Smith, 1999; Fredersdorf et al., 2012; Obayashi et al., 2006; Yaras et al., 2005). Previous studies in different experimental models of diabetes have variously reported enhanced diastolic SR Ca^{2+} leakage, lower caffeine-evoked Ca^{2+} release and decreased rate of SERCA-mediated Ca^{2+} uptake in myocytes from db/db diabetic mice (Belke et al., 2004; Stølen et al., 2009), as well as lowered AMP of caffeine-releasable Ca^{2+}, SR store and rates of Ca^{2+} release and depressed re-sequestration into SR in myocytes from STZ-induced diabetic rats (Shao et al., 2007). Reduced release of Ca^{2+} may be linked to structural defects in the SR Ca^{2+} release channel, and lowered levels of expression of mRNA and protein for the Ca^{2+} release channel have been described in type 2 diabetic patients, db/db mice, STZ and alloxan-induced diabetic rats (Choi et al., 2002; Pereira et al., 2006; Reuter et al., 2008; Zhou et al., 2006).

6.7.2 Myofilament sensitivity to Ca^{2+}

The Fura-2 cell length trajectory during the late stages of relaxation of the twitch contraction was not significantly different in myocytes between groups, which indicates that myofilament sensitivity to Ca^{2+} is not altered. Myofilament activation is modulated by protein phosphorylation and myofilament proteins are substrates for PKC, PKA and Ca^{2+}/Calmodulin Dependent Protein Kinase II (CAMK) which in turn can induce changes in myofilament sensitivity to Ca^{2+} (Solaro & Rarick, 1998). We have investigated certain proteins that might affect myofilament sensitivity to Ca^{2+} and although no changes have been found in Fura-2 length trajectory, we have found changes in expression of proteins of TnC, Troponin I (TnI) and Troponin T (TnT) proteins between groups which may have a bearing on myofilament sensitivity to Ca^{2+}. Our previously published paper reported that, diabetic GK rat Fura-2 cell length trajectory was steeper in GK compared to control myocytes which suggested an increase in myofilament sensitivity to Ca^{2+} (F. C. Howarth & Qureshi, 2008).

It is important to note that when shortening was measured without Fura-2, the mean RCL was significantly longer in ZDF compared to ZL myocytes and the mean TPK shortening was significantly prolonged in ZDF compared to ZF and ZL myocytes. In the Fura-2 loaded cells in the myofilament study there was no significant changes in mean RCL and mean TPK but increased AMP of shortening in the ZF group. The mean resting Fura-2 ratio and mean TPK was higher in the ZF compared to ZL in the stand-alone study while in the myofilament sensitivity study mean resting Fura-2 ratio was increased in the ZDF compared to ZL and there was no significant difference in TPK Ca^{2+} transient. THALF decay Ca^{2+} transient in the stand-alone study was significantly prolonged in ZDF and ZF compared to ZL while in the myofilament sensitivity study it was prolonged in ZDF and shortened in ZF compared to ZL. AMP Ca^{2+} transient was increased in the ZF compared to ZDF in the stand-alone study while in the myofilament study there was no significant differences between groups. These differences in the results between the two sets of experiments could be due to experiments performed in cells from different batches of animals, different batches of enzymes used for cell isolation producing different levels of tissue digestion and different Fura-2 incubation times.

6.8 Conclusions

- Although the AMP of shortening was generally well preserved in ZF and ZDF myocytes, evidence of intracellular Ca^{2+} signaling defects were observed.

- Defects in the uptake and release of SR Ca^{2+} might partly underlie the altered time course of the Ca^{2+} transient and shortening in myocytes from ZF and ZDF rat.

- Myofilament sensitivity to Ca^{2+} was generally well preserved.

Chapter 7: Investigating the effects of Isoprenaline on ventricular myocyte shortening and Ca^{2+} transport using cell imaging and fluorescence photometry techniques in ZDF and ZF compared to ZL rats

7.1 Introduction

Isoprenaline (ISO) is a β-sympathomimetic that stimulates the heart through its actions on the β-ARs (National Center for Biotechnology Information, 2022). β-AR dysregulation and associated cardiac dysfunction have been reported in ZDF rat heart (Thaung et al., 2015). It was also reported that the $β_1$-adrenergic receptor was the main subtype of β-AR involved in cardiac dysfunction while $β_2$-adrenergic receptor had indirect effects (Cook et al., 2019). We have previously reported that there is increased sympathovagal balance in ZDF compared to ZF and ZL rats (Sultan et al., 2021). Changes in cardiac Ca^{2+} signaling vary across different experimental models of obesity and diabetes (Hamilton & Terentyev, 2018).

Impaired β-AR responsiveness causes cardiac abnormalities in patients with T2DM. β1 and β2 -AR responsiveness of HR, contraction and relaxation in the diabetic heart were investigated. In general, diabetic hearts showed lower basal HR (non-diabetic 216 ± 17 beats min^{-1} versus diabetic 151 ± 23 beats min^{-1}, $p<0.05$) and Western blots showed 41% higher phosphorylation levels of AMP-kinase (AMPK), a key regulator of cardiac energy metabolism in diabetic hearts since β2-AR activation in the heart has been linked to stimulation of metabolic kinases (Li et al., 2010). In summary, β1-adrenoceptors are the main subtype that regulates HR, contraction and relaxation which in turn regulates chronotropic, inotropic and lusitropic β-AR responses in the healthy heart and the T2DM heart. Moreover, the β2-AR subtype indirectly supports the β1-AR functional response in the diabetic heart (Cook et al., 2019).

7.2 Hypothesis

- Sympathetic stimulation of contractility in ventricular myocytes is impaired in ZDF and ZF rats.

7.3 Aims and objectives

- To investigate the effects of ISO on the RCL, TPK shortening, THALF relaxation of shortening and AMP of shortening in ventricular myocytes from ZDF and ZF compared to ZL rats.

- To investigate the effects of ISO on resting Fura-2, TPK, THALF and AMP of the Ca^{2+} transient in myocytes from ZDF and ZF compared to ZL rats.

- To investigate the effects of ISO on SR Ca^{2+} release and refilling in ventricular myocytes from ZDF and ZF compared to ZL rats.

7.4 Methods

In order to select an appropriate concentration for shortening experiments electrically-stimulated (1 Hz) ZL myocytes were exposed to different concentrations of ISO (10^{-6}, 10^{-7} and 10^{-8} M). Typical records of shortening in ISO 10^{-6} M are shown in (Figure 45A), 10^{-7} M (Figure 45B) and 10^{-8} M (Figure 45C). The upper panels of each graph show the effects of NT and NT+ISO on shortening and the lower panel shows an expanded scale showing the effects of NT+ISO on shortening. Our results showed that the best dose to use in the following experiments was 10^{-8} M since the other doses produced arrhythmic activity.
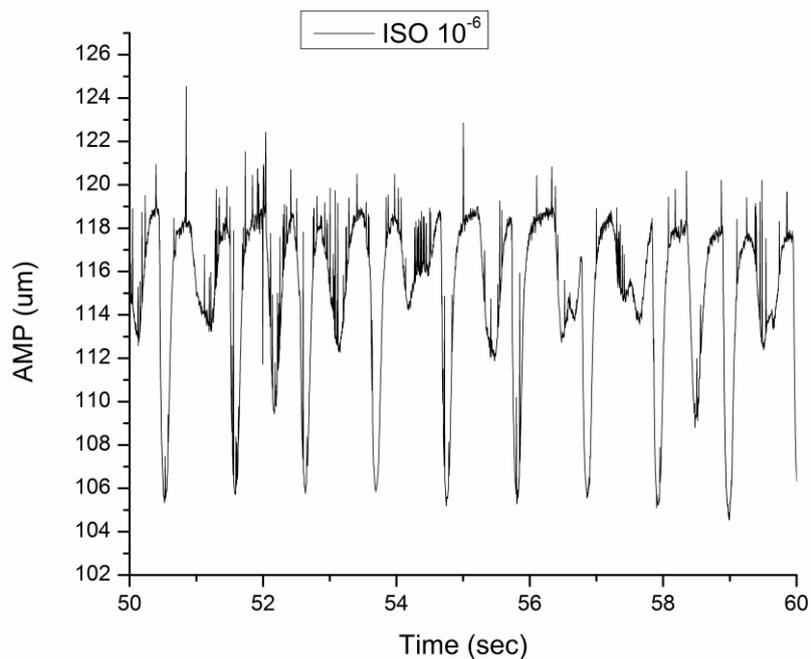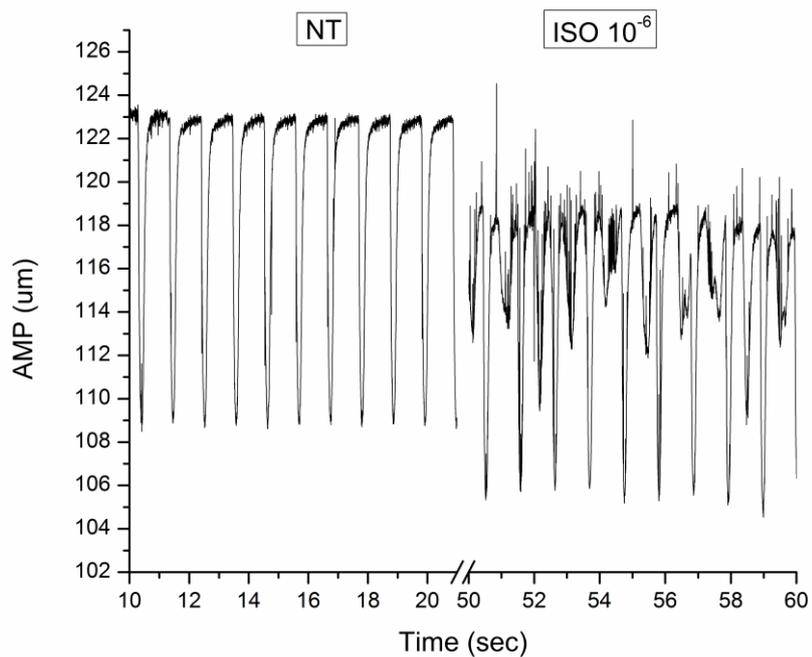
Figure 45: Typical records showing the effects of ISO (10^{-6}, 10^{-7} and 10^{-8} M) on electrically-evoked (1 Hz) shortening in ventricular myocytes from ZL rats. (A) Records of shortening in ISO 10^{-6} M. Upper panels show records of shortening in NT and NT+ISO and lower panels show expanded scales of shortening in NT+ISO.
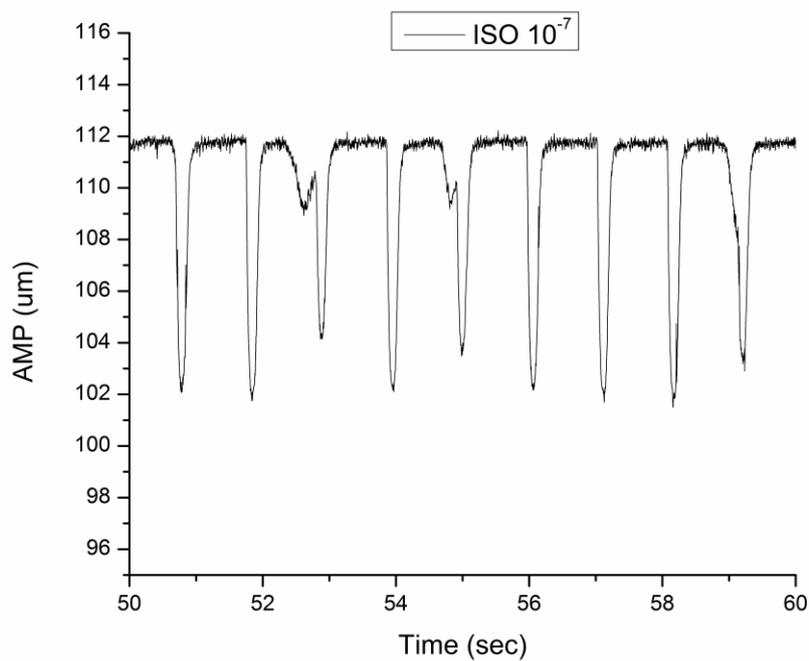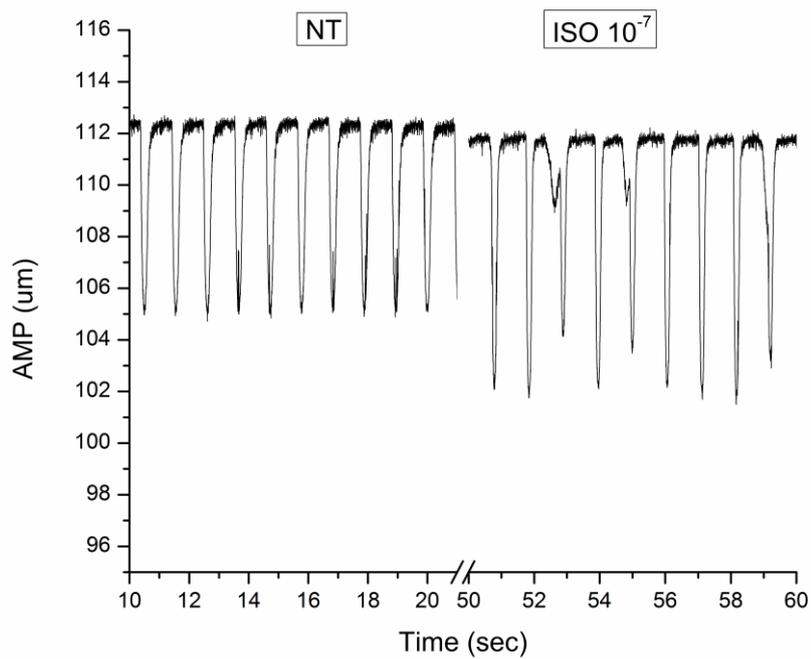
(B)

Figure 45: Typical records showing the effects of ISO (10^{-6}, 10^{-7} and 10^{-8} M) on electrically-evoked (1 Hz) shortening in ventricular myocytes from ZL rats. (B) 10^{-7} M. Upper panels show records of shortening in NT and NT+ISO and lower panels show expanded scales of shortening in NT+ISO (Continued).
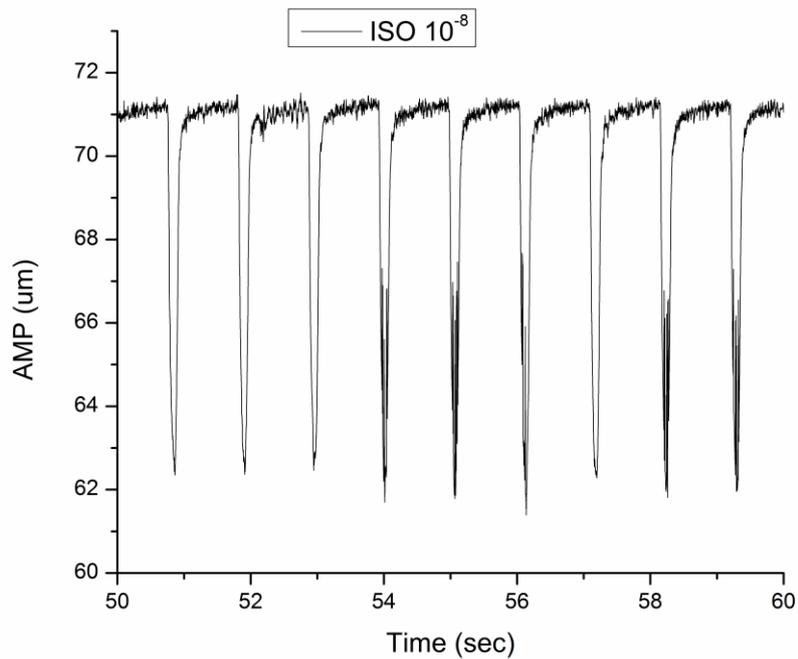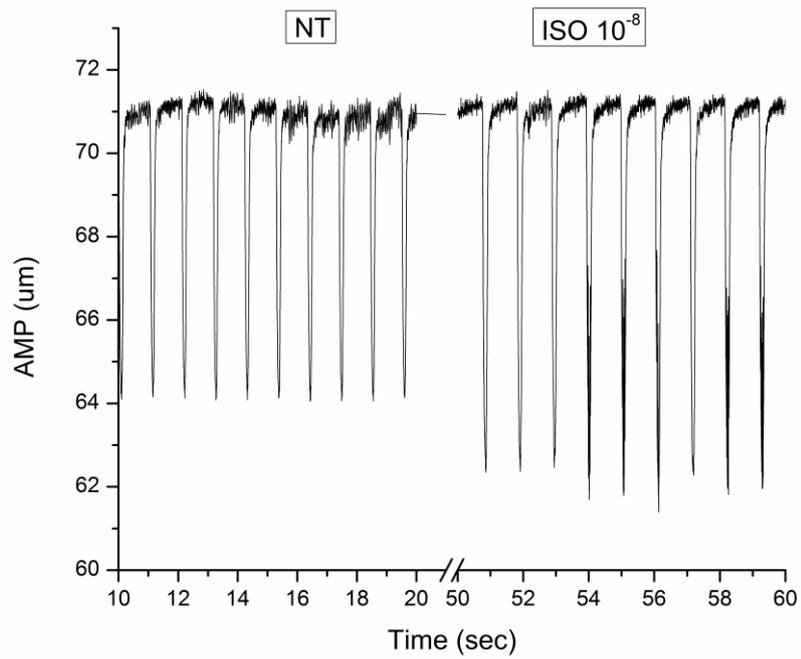
C

Figure 45: Typical records showing the effects of ISO (10^{-6}, 10^{-7} and 10^{-8} M) on electrically-evoked (1 Hz) shortening in ventricular myocytes from ZL rats. (C) 10^{-8} M. Upper panels show records of shortening in NT and NT+ISO and lower panels show expanded scales of shortening in NT+ISO (Continued).

The technique was previously described in chapter 5. The effects of ISO on electrically-evoked shortening in ventricular myocytes from ZL, ZF and ZDF rats. RCL, TPK shortening, THALF relaxation and AMP of shortening were measured in electrically stimulated (1 Hz) ventricular myocytes maintained at (35–36°C).

7.4.2 Measuring the effects of isoprenaline on ventricular myocyte intracellular Ca^{2+} results

The technique was described previously in chapter 6. The effects of ISO on electrically-evoked Ca^{2+} transients in ventricular myocytes from ZL, ZF and ZDF rats were also investigated. Resting Fura-2 ratio, TPK Ca^{2+} transient, THALF decay of the Ca^{2+} transient, and the AMP of Ca^{2+} transients were measured in electrically stimulated (1 Hz) ventricular myocytes loaded with Fura-2 AM and maintained at (35–36°C).

7.5 Statistics

Results were reported as the mean ± SEM of 'n' observations. The statistical comparisons were done by IBM SPSS and Origin 9.0 (OriginLab, Northampton, Massachusetts, USA) statistics software using either the independent samples t-test or one-way ANOVA and then by Bonferroni corrected t-tests for multiple comparisons, as applicable. P values of 0.05 and less were considered statistically significant.

7.6 Results

7.6.1 Effects of isoprenaline on ventricular myocyte shortening

The effects of ISO on electrically-evoked shortening in ventricular myocytes from ZDF and ZF compared to ZL control rats was investigated. Typical records of myocyte shortening are shown in (Figure 46A). The mean RCL was not significantly different between (p>0.05) ZDF, ZF and ZL myocytes (Figure 46B). Mean TPK shortening (Figure 46C) and THALF relaxation of shortening (Figure 46D) were also not significantly different (p<0.05) between groups. In ISO stimulated myocytes the AMP of shortening was significantly lower (p<0.05) in ZDF (8.75±0.57% RCL) and ZF (8.47±0.47% RCL)

compared to ZL (10.43±0.53% RCL) myocytes (Figure 46E). During NT washout the AMP of shortening returned to basal levels. Intracellular Ca^{2+} signaling is fundamental to the process of myocyte shortening so further experiments were performed to investigate if ISO induced changes in intracellular Ca^{2+} might partly underlie the changes in myocytes shortening in ZDF and ZF compared to ZL myocytes.
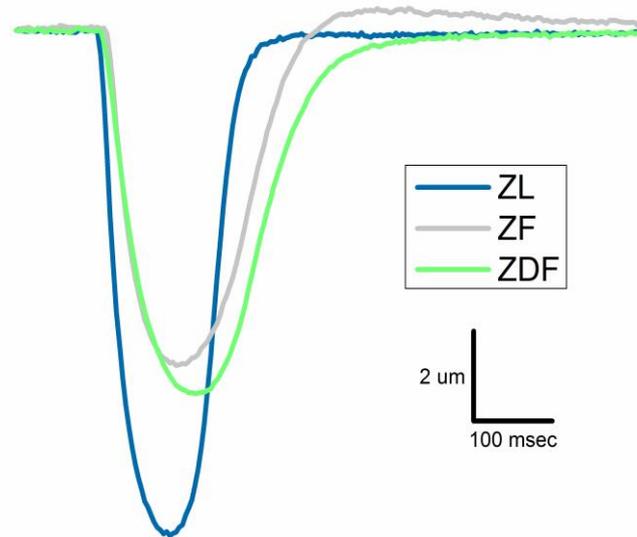
(A)

Figure 46: Effects of ISO on electrically-evoked shortening in ventricular myocytes from ZDF and ZF compared to ZL control rats. (A) Typical records.
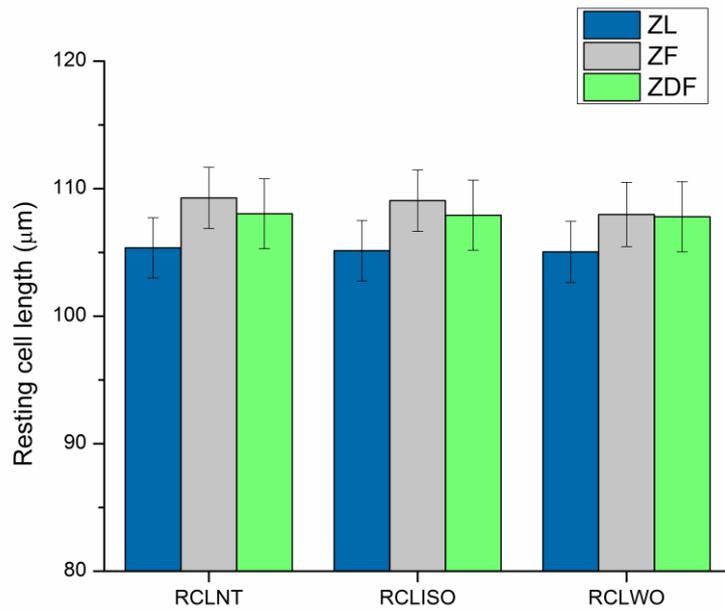
(B)
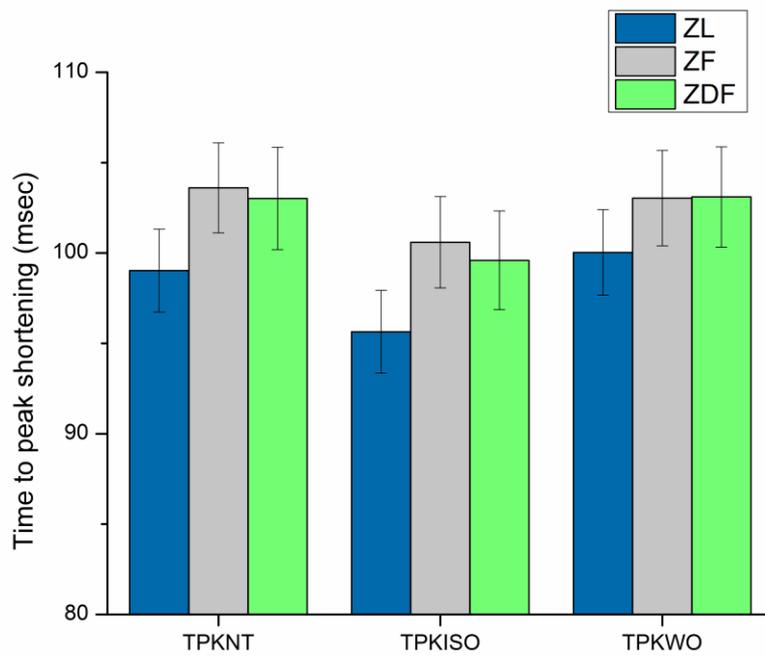
(C)

Figure 46: Effects of ISO on electrically-evoked shortening in ventricular myocytes from ZDF and ZF compared to ZL control rats. (B) Resting cell length and (C) time to peak shortening (Continued).
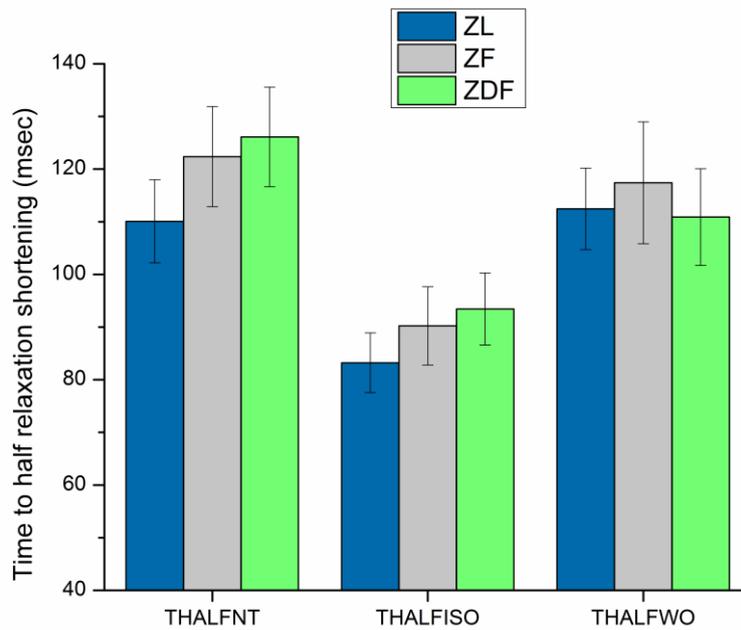
(D)
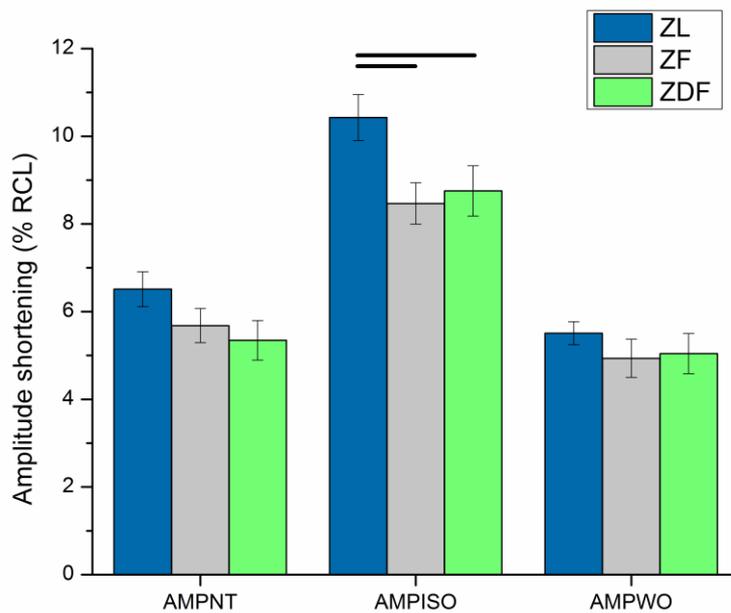
(E)

Figure 46: Effects of ISO on electrically-evoked shortening in ventricular myocytes from ZDF and ZF compared to ZL control rats. (D) Time to half relaxation of shortening and (E) amplitude of shortening. Data are mean ± SEM. n=33 ZL, 27 ZF and 28 ZDF cells from 7 ZL, 6 ZF and 8 ZDF rats. P values of 0.05 and less were considered statistically significant (Continued).

7.6.2 Effects of isoprenaline on ventricular myocyte intracellular Ca^{2+} results

The effects of ISO on electrically-evoked Ca^{2+} transients in ventricular myocytes from ZDF and ZF compared to ZL control rats was investigated. Typical records of the effects of ISO on electrically-evoked Ca^{2+} transient are shown in Figure 47A. The mean resting Fura-2 ratio (340/380 nm) was not significantly different ($p>0.05$) between groups (Figure 47B). The mean TPK Ca^{2+} transient was significantly shorter ($p<0.05$) in ZF (305.63±7.46 msec) compared to ZL (328.7±6.66 msec) myocytes. During ISO stimulation the TPK Ca^{2+} transient was also significantly shorter ($p<0.05$) in ZF (322.05±7.2 msec) compared to ZL (354.7±7.12 msec) myocytes (Figure 47C). During application of ISO the THALF decay of the Ca^{2+} transient was significantly prolonged ($p<0.05$) in ZDF (104.64±4.39 msec) compared to ZL (81.7±6.15 msec) myocytes (Figure 47D). During NT the AMP of the Ca^{2+} transient was significantly lower ($p<0.05$) in ZF (0.047±0.003 RU) compared to ZL (0.056±0.003 RU) myocytes. During ISO application, the AMP of the Ca^{2+} transient was also significantly lower in ZF (0.061±0.005 RU) compared to ZL (0.073±0.004 RU) myocytes (Figure 47E).
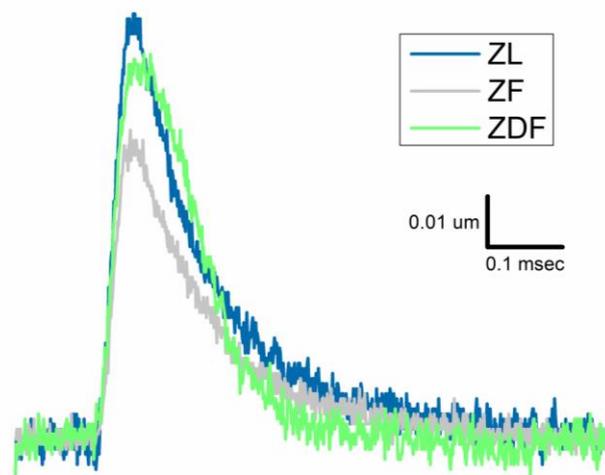
(A)

Figure 47: Effects of ISO on electrically-evoked Ca^{2+} transients in ventricular myocytes from ZDF and ZF compared to ZL control rats. (A) Typical records.
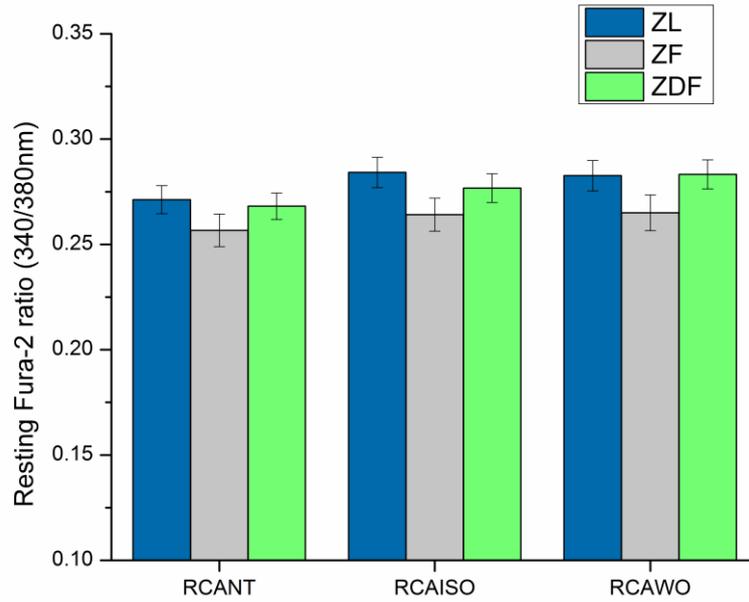
(B)
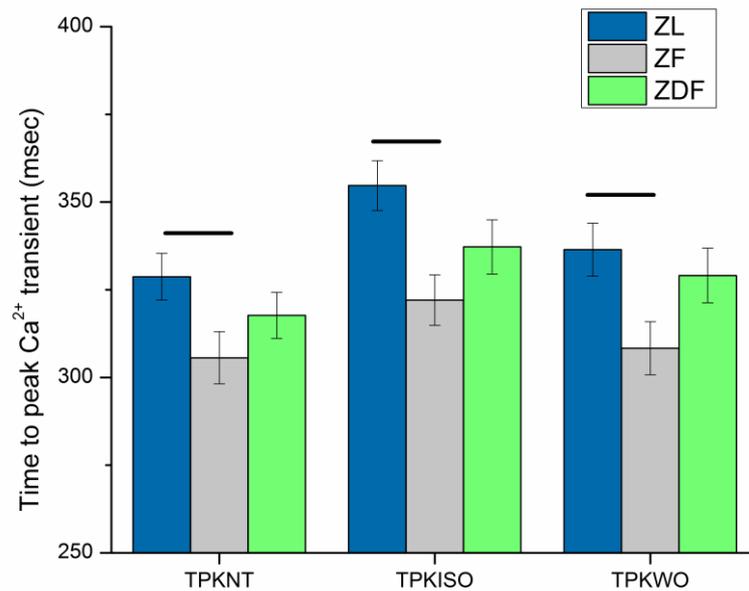
(C)

Figure 47: Effects of ISO on electrically-evoked Ca^{2+} transients in ventricular myocytes from ZDF and ZF compared to ZL control rats. (B) Resting Fura-2 ratio and (C) time to peak Ca^{2+} transient (Continued).
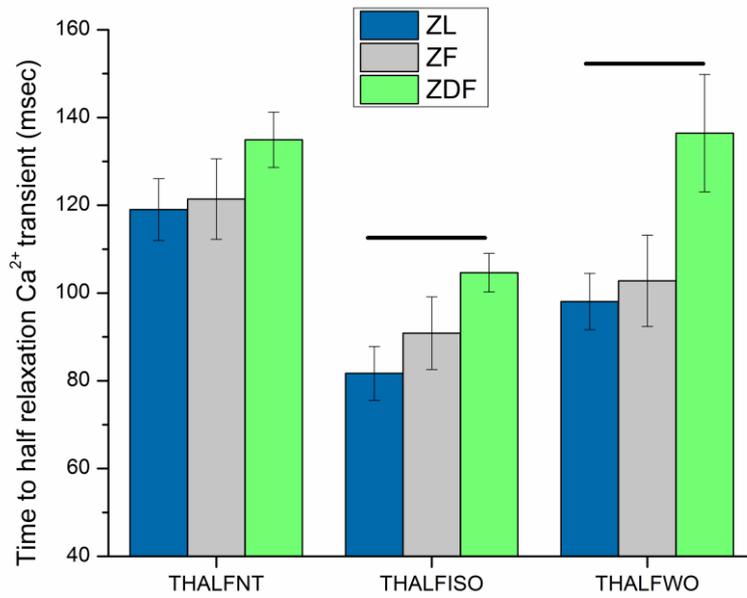
(D)
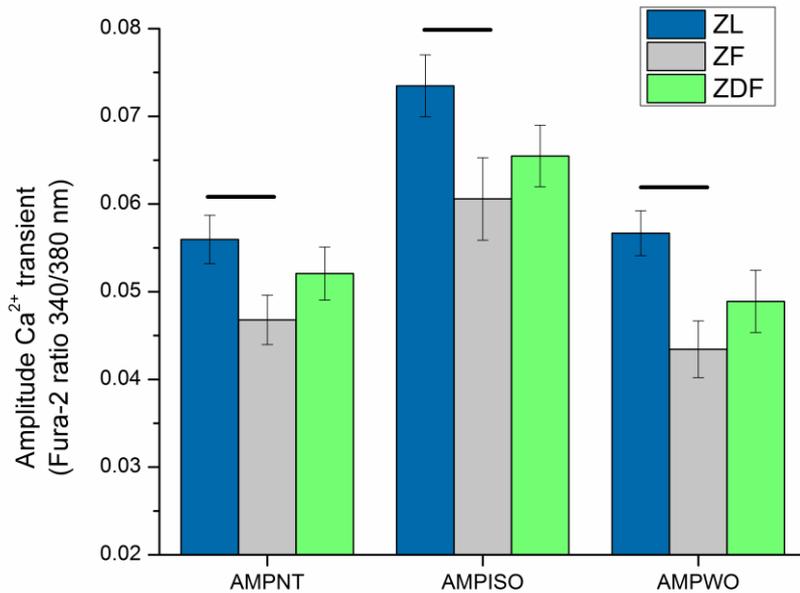
(E)

Figure 47: Effects of ISO on electrically-evoked Ca^{2+} transients in ventricular myocytes from ZDF and ZF compared to ZL control rats. (D) Time to half relaxation of the Ca^{2+} transient and (E) amplitude of the Ca^{2+} transient. Data are mean ± SEM.). n=23 ZL, 19 ZF, 25 ZDF cells from 7 ZL, 6 ZF and 8 ZDF rats. P values of 0.05 and less were considered statistically significant (Continued).

The effects of ISO on caffeine-evoked Ca^{2+} transients in ventricular myocytes from ZDF and ZF compared to ZL rats was also investigated. Typical records of the effects of ISO in electrically-evoked and caffeine-evoked Ca^{2+} transients in a ventricular myocyte from a ZL rat are shown in Figure 48A. Typical records of caffeine-evoked Ca^{2+} transient in a ventricular myocyte from a ZL rat are shown in an expanded scale in Figure 48B. TPK caffeine-evoked Ca^{2+} transients were significantly prolonged ($p<0.05$) in ZF (270.00 ± 36.07 msec) compared to ZL myocytes (185.3 ± 15.88 msec) and during ISO application in ZF (284.36 ± 3.78 msec) compared to ZL myocytes (188.81 ± 18.55 msec) (Figure 48C). THALF decay of the caffeine-evoked Ca^{2+} transient was not significantly different ($p>0.05$) between groups (Figure 48D). AMP of ISO-stimulated Ca^{2+} transient was significantly ($p<0.05$) decreased in ZF (0.05 ± 0.006 RU) and ZDF (0.046 ± 0.005 RU) compared to ZL (0.063 ± 0.005 RU) myocytes (Figure 48E). Fractional release of Ca^{2+} (Figure 48F) and recovery of the Ca^{2+} transients (Figure 48G) were not significantly different between ZDF, ZF and ZL myocytes in NT or NT+ISO.
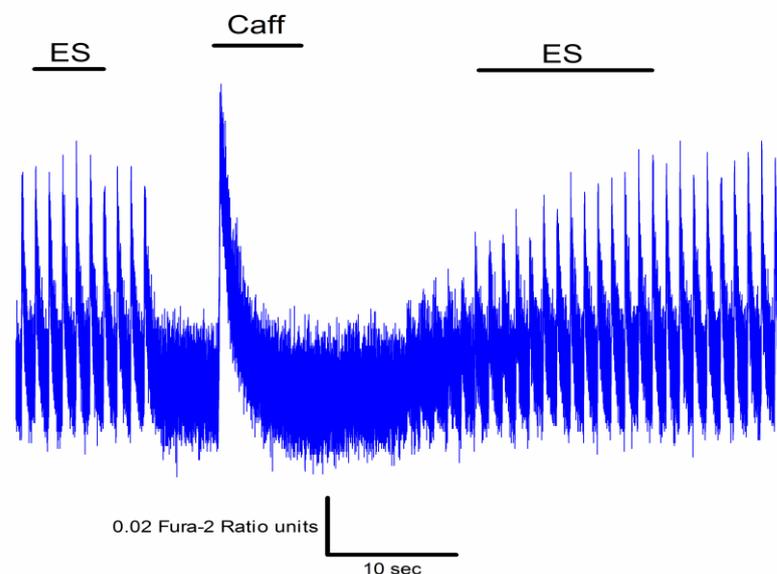
(A)

Figure 48: Effects of ISO on caffeine-evoked Ca^{2+} transients in ventricular myocytes from ZDF, ZF and ZL control rats. (A) Typical records showing electrically-evoked and caffeine-evoked Ca^{2+} transients in a ventricular myocyte from a ZL rat.
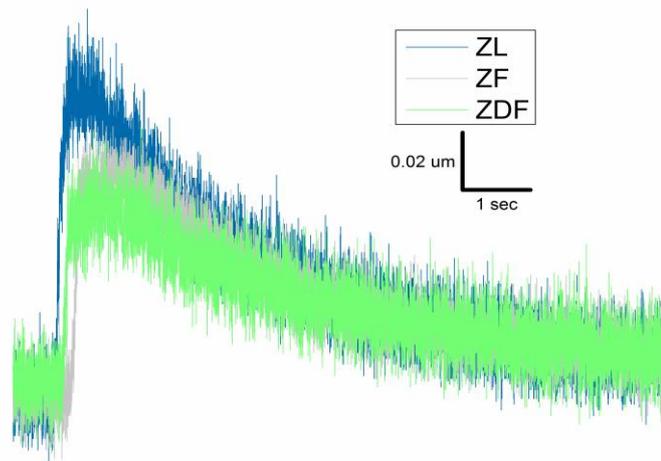
(B)
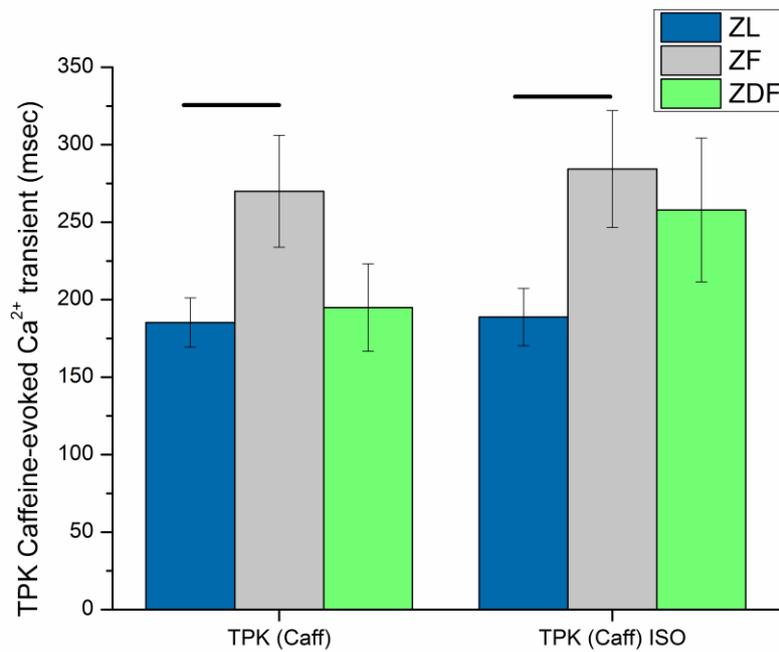
(C)

Figure 48: Effects of ISO on caffeine-evoked Ca^{2+} transients in ventricular myocytes from ZDF, ZF and ZL control rats. (B) Typical records showing caffeine-evoked Ca^{2+} transients in ventricular myocytes from ZDF, ZF and ZL rat and (C) time to peak caffeine-evoked Ca^{2+} transient (Continued).
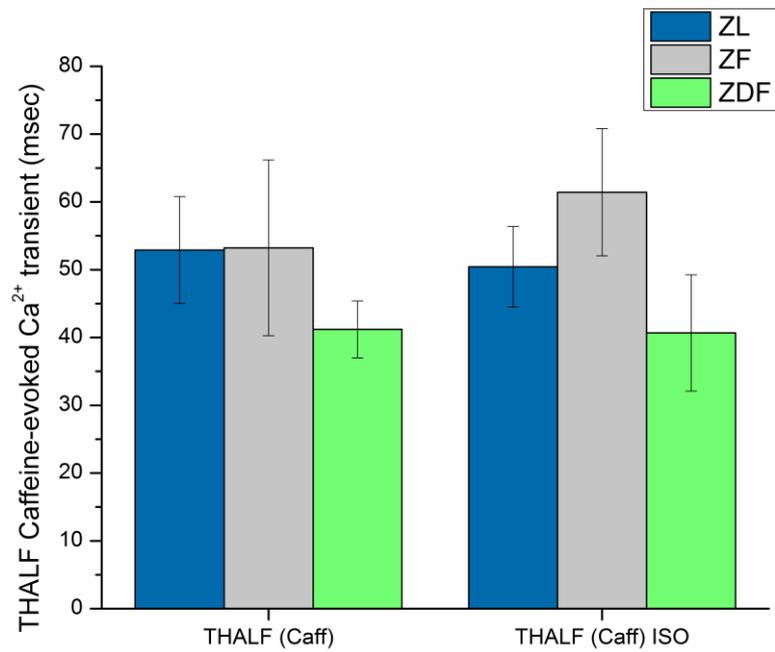
(D)
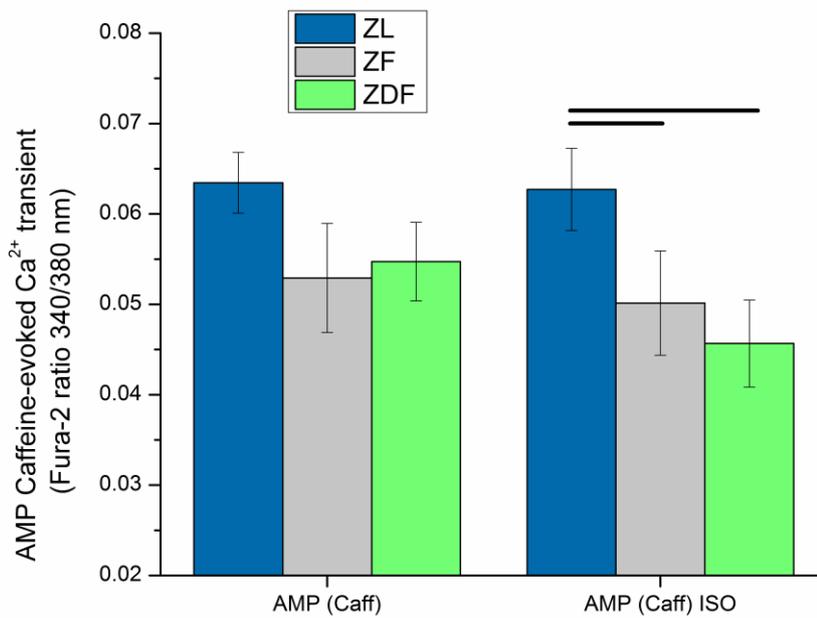
(E)

Figure 48: Effects of ISO on caffeine-evoked Ca^{2+} transients in ventricular myocytes from ZDF, ZF and ZL control rats. (D) Time to half relaxation caffeine-evoked Ca^{2+} transient and (E) amplitude of caffeine-evoked Ca^{2+} transients (Continued).
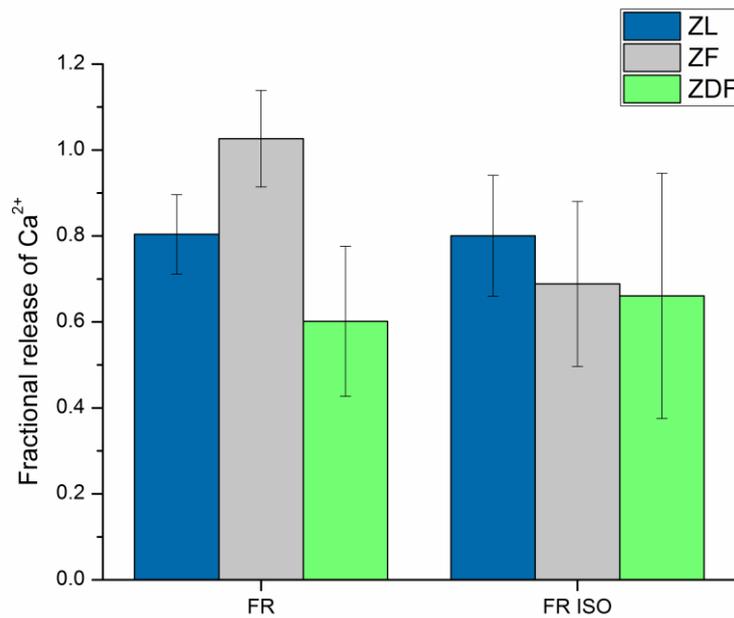
(F)
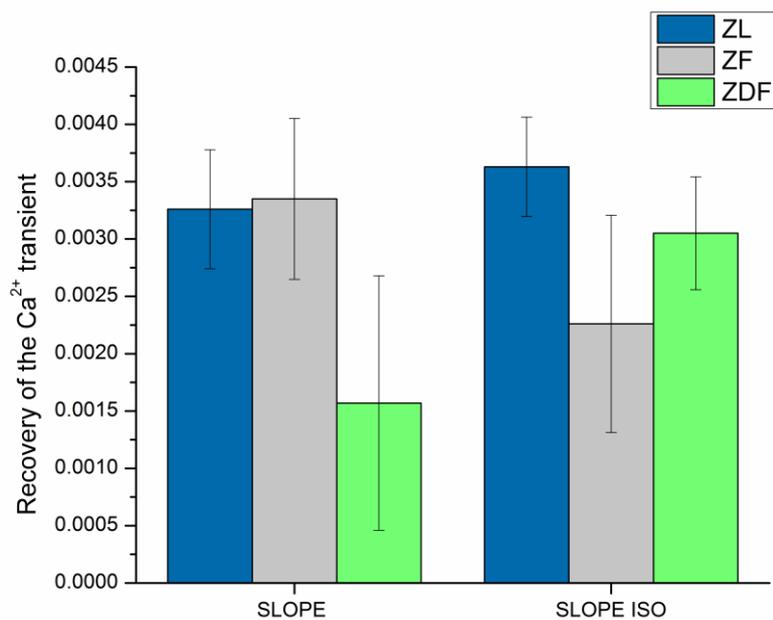
(G)

Figure 48: Effects of ISO on caffeine-evoked Ca^{2+} transients in ventricular myocytes from ZDF, ZF and ZL control rats. (F) Fractional release of Ca^{2+} and (G) recovery of Ca^{2+} transients. Data are mean ± SEM. n=20 ZL, 21 ZL ISO, 13 ZF, 14 ZF ISO, 15 ZDF, 15 ZDF ISO cells from 7 ZL, 6 ZF and 8 ZDF rats. P values of 0.05 and less were considered statistically significant. ES - Electrical stimulation, Caff - Caffeine stimulation (Continued).

7.7 Discussion

7.7.1 Effects of isoprenaline on ventricular myocyte shortening

The mean RCL was not substantially different between ZDF, ZF and ZL myocytes. Whilst the RCL data was not consistent with cardiac hypertrophy in ZF rat heart it must be appreciated that cardiac myocyte volume is a product of cell length, width and thickness. The mean TPK shortening as well as THALF relaxation of shortening were not significantly different between ZF, ZDF and ZL myocytes. Preserved THALF relaxation and AMP of shortening has been previously described in ZDF myocytes compared to ZL myocytes from rats aged 30-34 weeks of age (F. C. Howarth et al., 2012). In another study, AMP of shortening at 6 up to 22 weeks was unchanged and the time course of shortening at 6 weeks was also unaffected. However, the TPK shortening and THALF relaxation of shortening were increased in ZDF rats at 22 weeks (Fulop et al., 2007). ISO application increased the AMP of shortening to a lesser extent in ZDF and ZF compared to ZL myocytes suggesting that the β-adrenergic system and Ca^{2+} signaling may be altered in ZF and ZDF rats. It was reported previously that abnormalities in adrenal receptors in ZDF rat hearts were present at the molecular level where the expression level of $β_1$-adrenoceptors was downregulated whereas that of $β_2$-adrenoceptors was upregulated (Thaung et al., 2015).

7.7.2 Effects of isoprenaline on ventricular myocyte intracellular Ca^{2+}

The mean resting Fura-2 ratio (340/380 nm) was not significantly different between groups. The mean TPK Ca^{2+} transient was significantly lower in ZF compared to ZL myocytes during NT or NT+ISO. Application of ISO prolonged THALF decay of the Ca^{2+} transient in ZDF compared to ZL myocytes and continued even after washout. The AMP of the Ca^{2+} transient was significantly lower in ZF compared to ZL myocytes during NT and NT+ISO application and washout. The disturbances in time course of the Ca^{2+} transient might be partly due to defective SR Ca^{2+} transport. To investigate SR Ca^{2+} transport Fura-2 loaded myocytes were electrically stimulated to generate Ca^{2+} transients and then, after a pause, were rapidly exposed to caffeine to release Ca^{2+} from the SR. TPK of caffeine-evoked Ca^{2+} transients was significantly prolonged in ZF compared to ZL myocytes during NT and NT+ISO application. On the other hand, THALF decay of

the caffeine-evoked Ca^{2+} transient was not significantly different between ZF, ZDF and ZL myocytes. During application of ISO the AMP of the caffeine-evoked Ca^{2+} transient was smaller in ZDF and ZF compared to ZL myocytes. Reduction of caffeine-evoked SR Ca^{2+} release might partly underlie the decreased effectiveness of ISO on myocyte shortening in ZDF and ZF myocytes compared to ZL. Fractional release of Ca^{2+} during NT or NT+ISO was not significantly altered in ZDF compared to ZF and ZL myocytes suggesting that the fraction of SR Ca^{2+} mobilized during each stimulation was less in ZDF compared to ZF and ZL myocytes. The rate of recovery of the Ca^{2+} transient following NT or NT+ISO were not significantly different in ZDF and ZF compared to ZL myocytes suggesting that the refilling of the SR after stimulation was similar in the three groups. Collectively, these findings suggest delayed release of Ca^{2+} by the SR which in turn may be ascribed to defects in the SR Ca^{2+} release channel (Belke et al., 2004; Cagalinec et al., 2019; Maier et al., 2005). Previous studies in various experimental models of diabetes have reported enhanced diastolic SR Ca^{2+} leakage, lower caffeine-evoked Ca^{2+} release and decreased rate of SR Ca^{2+}-ATPase-mediated Ca^{2+} uptake in myocytes from db/db diabetic mice (Belke et al., 2004; Stølen et al., 2009), as well as lowered AMP of caffeine-releasable Ca^{2+}, SR store and rates of Ca^{2+} release and depressed re-sequestration into SR in myocytes from STZ-induced diabetic rats (Shao et al., 2007). Furthermore, ISO application was less effective in increasing the AMP of shortening in ZDF and ZF compared to ZL suggesting a defect in the β-adrenergic system as well as signs of either hypertrophy or dilatation in these groups (Cook et al., 2019; Thaung et al., 2015). Another reason for lower AMP in these rats could be lower release of SR Ca^{2+} which may be linked to structural defects in the SR Ca^{2+} release channel, and lower levels of expression of mRNA and Ca^{2+} release channel protein which have been previously reported in type 2 diabetic patients, db/db mice, STZ and alloxan-induced diabetic rats (Choi et al., 2002; Pereira et al., 2006; Reuter et al., 2008; Zhou et al., 2006).

7.8 Conclusions

- ISO was less effective at generating an increase in AMP of shortening in ZDF and ZF compared to ZL myocytes.

- Defects in Ca^{2+} signaling in the ZDF and ZF were present suggesting that defective SR Ca^{2+} transport might partly underlie these abnormalities.

Chapter 8: Investigating L-type Ca^{2+} current and Na$^+$/Ca^{2+} exchange current in ventricular myocytes from ZDF and ZF compared to ZL rats

8.1 Introduction

During the process of excitation-contraction coupling the arrival of an AP depolarizes the cardiac myocyte membrane, leading to the opening of L-type Ca^{2+} channels. There is a small entry of Ca^{2+} which triggers a large release of Ca^{2+} from the SR. The rise of intracellular Ca^{2+} initiates and regulates the process of contraction (S. P. Alexander, Mathie, et al., 2021; Catterall, 2011). Defects in I$_{Cal}$ might alter SR Ca^{2+} release and the generation of the Ca^{2+} transient.

Recovery of intracellular Ca^{2+} to resting levels is mainly driven by uptake of Ca^{2+} into the SR and extrusion of Ca^{2+} from the cell via the NCX, operating in forward mode. Defects in NCX might contribute to alterations in the decay of the Ca^{2+} transient (Armoundas et al., 2003; Ashrafi et al., 2016; Hamilton & Terentyev, 2018; Hattori et al., 2000).

8.2 Hypothesis

- Alterations in L-type Ca^{2+} and NCX current may partly underlie defective contraction in ZDF and ZF rats.

8.3 Aims and objectives

- To investigate the effects of obesity and diabesity on L-type Ca^{2+} current and NCX current in ventricular myocytes from ZDF and ZF compared to ZL rats.

8.4 Methods

The patch-clamp technique allows the researcher to measure the potential (voltage) differences in biological systems usually in millivolts (mV). It also allows the researcher to measure the current (I) measured in (Amperes), which is the flow of ions or electrical charge passing a point per unit of time. The usual current range is from Picoamperes (pA)

to Microamperes (μA) in biological systems. The ease of flow of current between two points is called conductance (G), and it is measured in Siemens (S). Current (I) can flow through conductors and resistors. Conductivity is an ion channel property, and it is usually measured in the Picosiemens (pS) range in biological systems while resistance (R) measured in Ohms (Ω) is the inverse of conductance (G). The total electrical conductivity of a membrane is the sum of all ion channel single conductivities in parallel. This provides one of the most important laws in electricity called "Ohms Law" (Hacker et al., 2009; Sherman-Gold et al., 2012).

Ohms Law Equation 2:

$$G = I/R \text{ or } G = I/(V_m - E_s) \text{ or } \Delta V = IR$$

G = Conductance (S)

I = Current (A)

R = Resistance (Ω)

V = Voltage or potential (V)

V_m = membrane potential or command potential or test potential

E_s = equilibrium potential or reverse potential

The second important equation in ion channel investigation informs us about the equilibrium potential (E_s) and it is also known as the "reversal potential". It is the cell membrane potential at which there is no net flow of ions through the membrane. Equilibrium reflects the fact that the net ion flow, for the specific ion, at the given voltage is zero (Hacker et al., 2009; Sherman-Gold et al., 2012).

Nernst Equation 3:

$$E_s = (RT/Z_sF) \ln ([S]_o/[S]_i)$$

R = the universal gas constant

T = the temperature in Kelvin

F = the Faraday constant

S = the particular ion type with charge Z_s

$[S]_o$ = the ion concentration outside the cell membrane

$[S]_i$ = the intracellular ion concentration

A picture of the patch-clamp electrophysiology rig used in the experiments is shown in Figure 49.

Figure 49: Patch-clamp electrophysiology rig. (A) Personal Computer, (B) power supply for microscope light, (C) amplifier, (D) digitizer, (E) chamber monitor, (F) manipulator controls, (G) inverted light microscope, (H) Faraday cage for noise insulation, (I) antivibration table, (J) waste line, (K) headstage, (L) micromanipulator, (M) reference electrode, (N) waste line and (O) pipette holder.

8.4.1 Measurement of L-type Ca^{2+} current

I_{CaL} was measured according to previously described techniques (F. C. Howarth et al., 2020). I_{CaL} was recorded with an Axopatch 200B amplifier (Molecular Devices, Sunnyvale, CA, USA). The analog signal was filtered using a four-pole Bessel filter with

a bandwidth of 2 kHz and digitized at a sampling rate of 10 kHz by software control (pClamp 10.6.2.2, Molecular Devices, CA, USA). Patch pipettes were fabricated from filamented TW150F-4 4 IN thin-wall borosilicate glass 1.5 OD/1.2 ID (World Precision Instruments, FL, USA). The pipettes were made using a flaming/brown horizontal micropipette puller (Sutter instruments CO., Model P-97) and then further air-heat polished using a List Medical L/M CPZ 101 Fire coating polisher. The whole cell bath solution comprised in mmol/l: 4 NaCl, 2 CaCl$_2$, 1 MgCl$_2$, 110 TEA-Cl, 4 CsCl, 10 HEPES and 10 glucose (pH 7.4 with CsOH). The pipette solution comprised in mmol/l: 2 MgCl$_2$, 2 MgATP, 10 TEA-Cl, 140 CsCl, 10 HEPES and 10 EGTA (pH 7.25 with CsOH). Electrode resistances were 1-3 MΩ, and seal resistances were 1-5 GΩ. Experiments were performed at room temperature (25-26°C). The current-voltage relationship was obtained by applying 1000 msec long pulses to different voltages between -60 and +50 mV from a holding potential of -50 mV. The inactivation was measured as the relationship of peak current at a test pulse of 0 mV and the AMP of peak current during the 1000 msec long pre-pulses. Recovery from inactivation was measured using a two-pulse protocol, in which one 1000 msec pulse was compared with 50 msec depolarizing pulses from -50 to 0 mV that were separated by inter-pulse intervals of different durations. The peak Ca^{2+} current AMP measured during the second pulse was normalized to the current measured by the first pulse and their ratio was plotted against the inter-pulse interval. Data were acquired and analyzed with pClamp software v 10.6.2.2 (Molecular Devices, CA, USA).

One important aspect of voltage gated ion channels is their "open probability" which is essentially the random opening and closing of the channel also referred to as "gating". The channels usually transition between three different conformational changes which are active or open, inactive and closed or resting (Figure 50). The transition from the open to the inactive is referred to as "inactivation" while the transition from the inactive to the closed is referred to as "recovery from inactivation" (Hacker et al., 2009; Kornreich, 2007). In our study we have recorded the recovery from inactivation of the L-type Ca^{2+} channels.
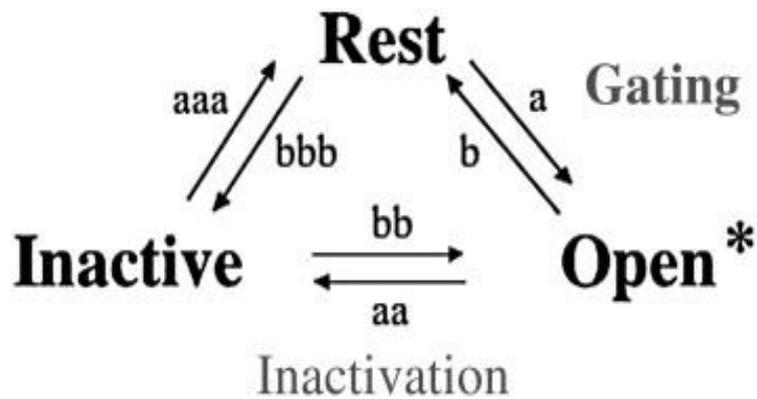
Figure 50: Markov model demonstrating the transition of an ion channel between its opened, closed, and inactivated configurations. The asterisk represents a state that passes current. Adapted from (Kornreich, 2007).

8.4.2 Measurement of Na^+/Ca^{2+} exchange current

I_{NCX} was measured according to previously described techniques (F. C. Howarth et al., 2014). I_{NCX} was recorded using a descending voltage ramp from $+100$ mV to -100 mV from a holding potential of -40 mV for 2 s duration. I_{NCX} was measured as the current sensitive to nickel (Ni^{2+}), hence, Ni^{2+}-insensitive components were subtracted from total currents to isolate I_{NCX}. Membrane current was recorded with an Axopatch 200B amplifier (Molecular Devices, Sunnyvale, CA, USA). The analog signal was filtered using a four-pole Bessel filter with a bandwidth of 2 kHz and digitized at a sampling rate of 10 kHz under software control (pClamp 10.6.2.2, Molecular Devices, CA, USA). Patch pipettes were fabricated from filamented 4 inch thin-wall borosilicate glass 1.5 OD/1.2 ID (TW150F-4, World Precision Instruments, Inc., FL, USA). The pipettes were made using a flaming/brown horizontal micropipette puller (Sutter Instruments Co., Model P-97) and then further air-heat polished using a List Medical L/M CPZ 101 fire coating polisher. The whole cell bath solution contained the following in mmol/l: 2 $MgCl_2$, 2 $CaCl_2$, 150 NaCl, 5 CsCl, 10 glucose and 10 HEPES (pH=7.4). Nifedipine (10 µM), Oubain (100 µM), and Niflumic acid (30 µM) were used to block Ca^{2+}, Na^+- K^+-ATPase, and Cl^- currents, respectively. 10 mM nickel chloride solution was used to block I_{NCX}. K^+ currents were minimized by Cs^+ substitution for K^+ in both pipette and external solutions. The pipette solution contained in mmol/l: 2 $MgCl_2$, 20 $NaCl_2$, 120 CsCl, 1 MgATP, 10 tetraethylammonium chloride (TEACl), 1 $CaCl_2$, 10 HEPES and 10 1,2-bis (o-

aminophenoxy) ethane-N,N,N',N'-tetraacetic acid (BAPTA) (pH=7.2) with CsOH. Electrode resistances were 1-3 MΩ, and seal resistances were 1-5 GΩ. Experiments were performed at room temperature (25-26°C).

8.5 Statistics

Results were reported as the mean ± SEM of 'n' observations. Statistical comparisons were done with IBM SPSS and Origin 9.0 (OriginLab, Northampton, Massachusetts, USA) statistics software using either the independent samples t-test or one-way ANOVA then by Bonferroni corrected t-tests for multiple comparisons, as appropriate. P values of 0.05 and less were considered statistically significant.

8.6 Results

8.6.1 L-type Ca^{2+} current

Typical records of I_{CaL} activation and inactivation are shown in Figure 51A & B. The current/voltage relationship (I-V curve) is shown in Figure 51C. There were no significant differences (p>0.05) in the AMP of I_{CaL} at test potentials in the range -60 to +50 mV. L-type Ca^{2+} activation and inactivation currents are shown in Figure 51D. The results indicate that the activation, inactivation and window current were not significantly altered (p>0.05) in ZDF and ZF compared to ZL myocytes. The mean membrane capacitance was not significantly different (p>0.05) between ZL (279.53±19.49 pF), ZF (291.24±25.46 pF) and ZDF (263.29±13.45 pF) myocytes.

Typical records of I_{CaL} after recovery from inactivation in a ventricular myocyte from a ZL rat is shown in Figure 51E. Mean recovery from inactivation at various inter-pulse intervals is shown in Figure 51F. There were no significant differences (p>0.05) between ZDF, ZF and ZL myocytes. The results are surprising considering the significant changes in Ca^{2+} signaling and signs of hypertrophy. Under these circumstances changes in current densities as well as changes in window current might be expected.
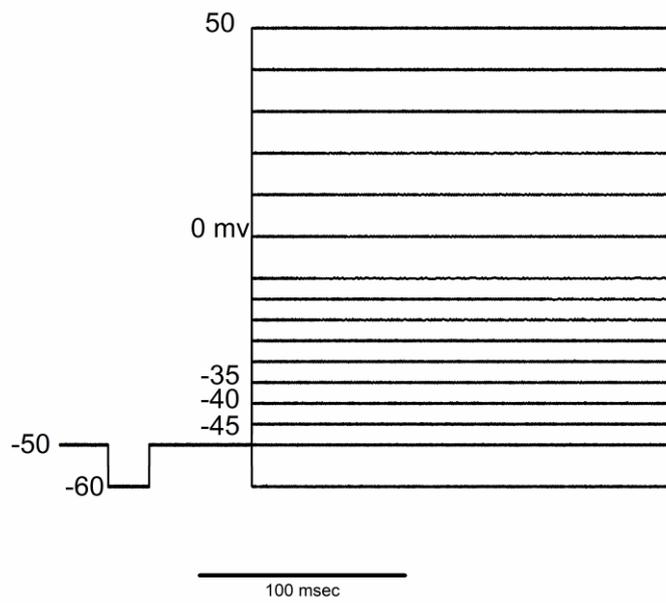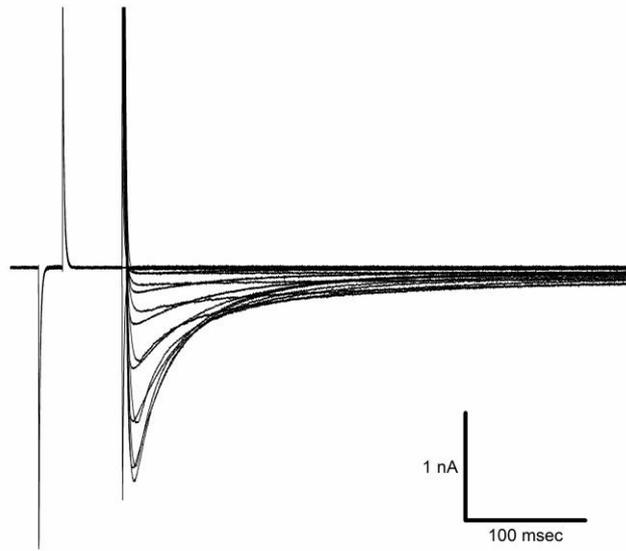
Figure 51: L-type Ca^{2+} current. (A) Typical records of I$_{CaL}$ activation (upper panel) together with voltage protocol (lower panel) in a ventricular myocyte from a ZL rat.
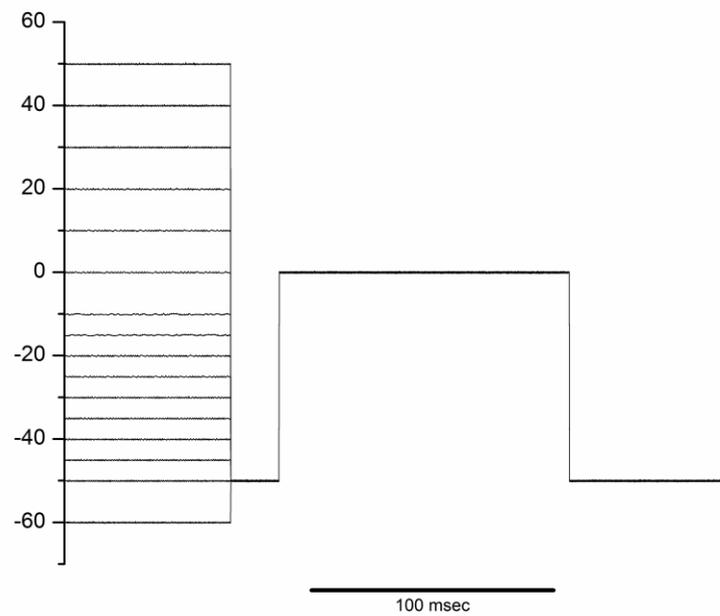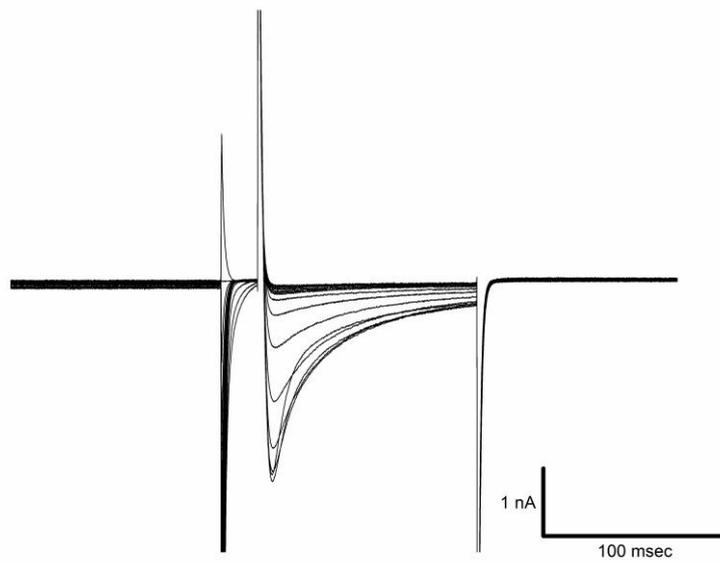
(B)

Figure 51: L-type Ca^{2+} current. (B) Typical records of I_{CaL} inactivation (upper panel) and voltage protocol (lower panel) in a ventricular myocyte from a ZL rat (Continued).
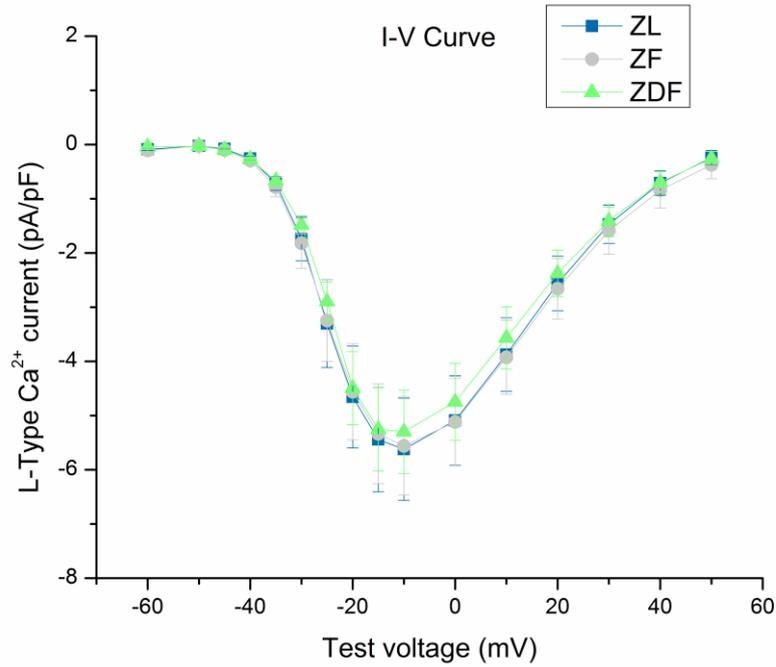
(C)

(D)
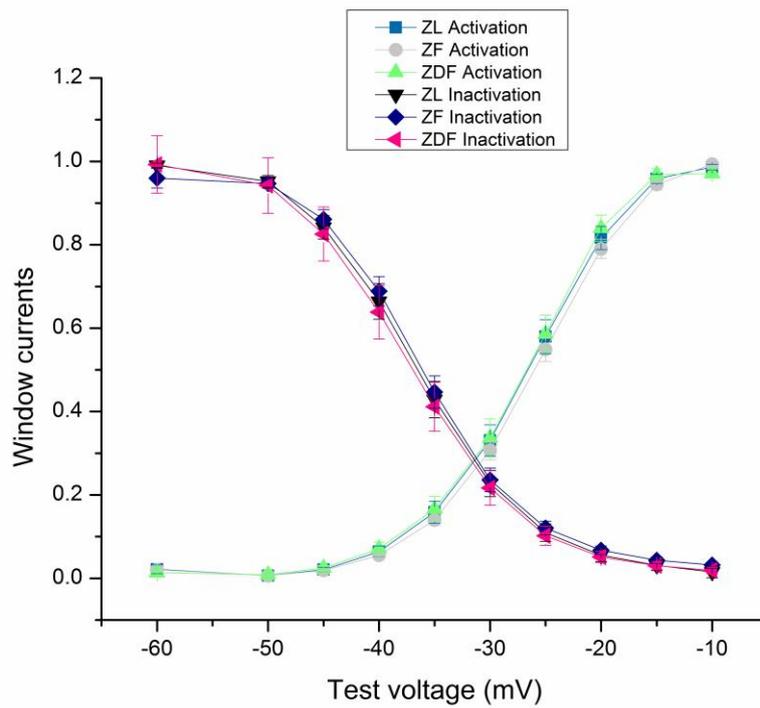
Figure 51: L-type Ca^{2+} current. (C) Graphs showing current-voltage relationship and (D) activation, inactivation, and window current. Data are means ± SEM. n=17 ZL, 17 ZF and 14 ZDF cells from 3 ZL, 3 ZF and 3 ZDF rats (Continued).

0.1 nA

700 msec

0 mV

-50 mV

-60 mV

10 mV

700 msec
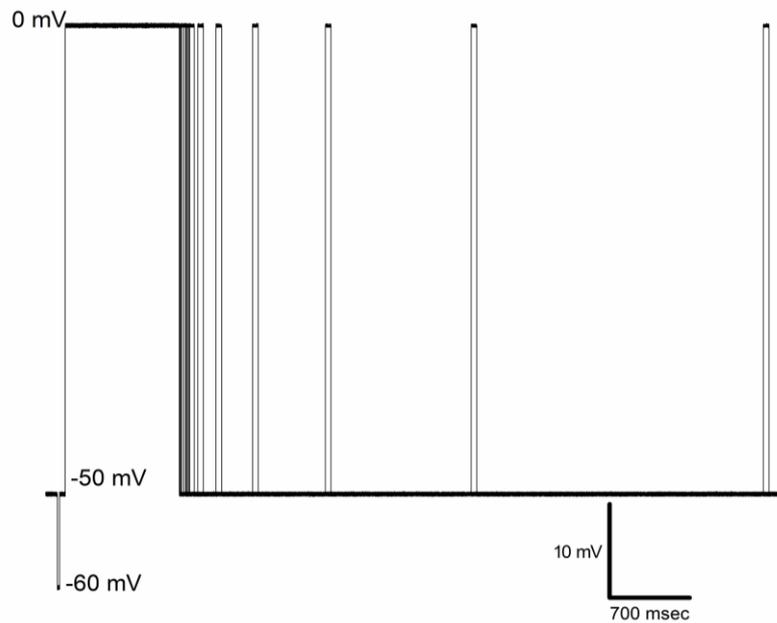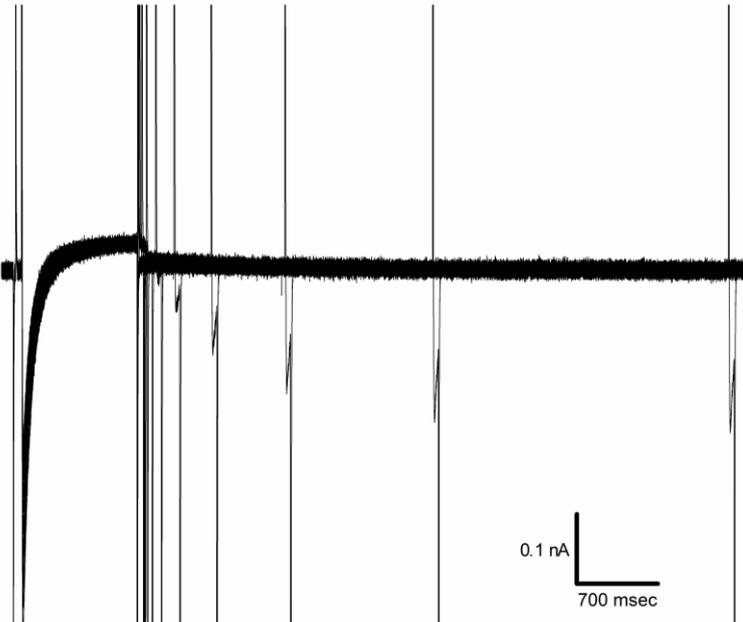
(E)

Figure 51: L-type Ca^{2+} current. (E) Typical records of recovery from inactivation at various inter-pulse intervals (upper panel) and voltage protocol (lower panel) in a ventricular myocyte from a ZL rat (Continued).
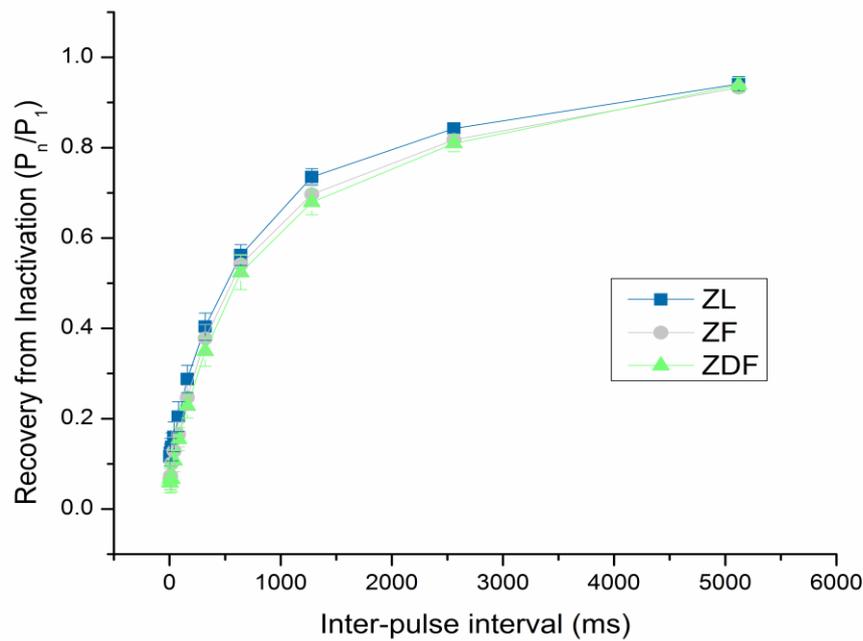
(F)

Figure 51: L-type Ca^{2+} current. (F) Graph showing recovery from inactivation at various inter-pulse intervals with variable duration. Data are means ± SEM. n=16 ZL, 17 ZF and 13 ZDF cells from 3 ZL, 3 ZF and 3 ZDF hearts. P values of 0.05 and less were considered statistically significant (Continued).

8.6.2 Na^+/Ca^{2+} exchange current results

The NCX is the main route by which Ca^{2+} is extruded from the cell facilitating recovery of intracellular Ca^{2+} to basal levels (S. P. Alexander, Kelly, et al., 2021) therefore experiments were performed to investigate I_{NCX}. Records of current in the absence (upper panel) and presence of 10 mM Ni^{2+} (middle panel) in a myocyte from a ZL rat together with the voltage protocol (lower panel) are shown in Figure 52A. Mean I_{NCX} density is shown in Figure 52B. Mean current density at selected voltages is shown in Figure 52C. There was no significant difference (p>0.05) in mean current density between ZDF, ZF and ZL rats at test potentials of 40, 60 and 80 mV. The mean membrane capacitance was not significantly (p>0.05) different between ZL (179.60±14.87 pF), ZF (213.50±15.87 pF) and ZDF (167.92±18.01 pF) myocytes. I_{NCX} was not significantly altered (p>0.05) in ZDF and ZF compared to ZL myocytes.
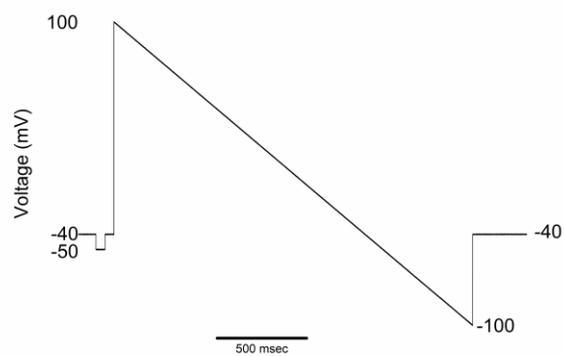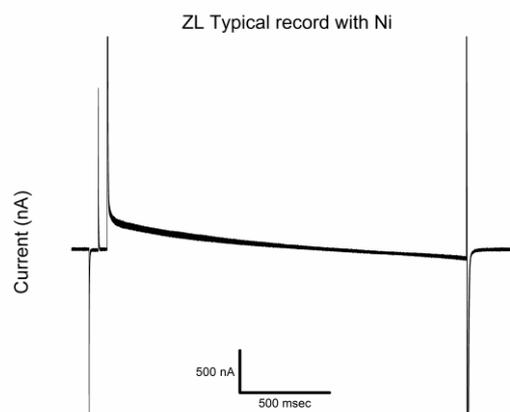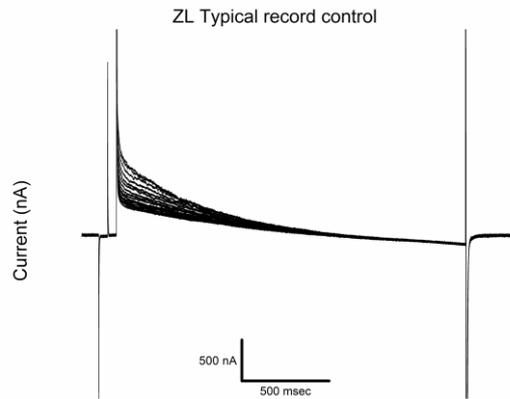
Figure 52: Na⁺/Ca²⁺ exchange current. (A) Typical records of I_{NCX} in the absence of Ni (upper panel), in the presence of Ni (middle panel) and voltage protocol (lower panel) in a ventricular myocyte from a ZL rat (Continued).
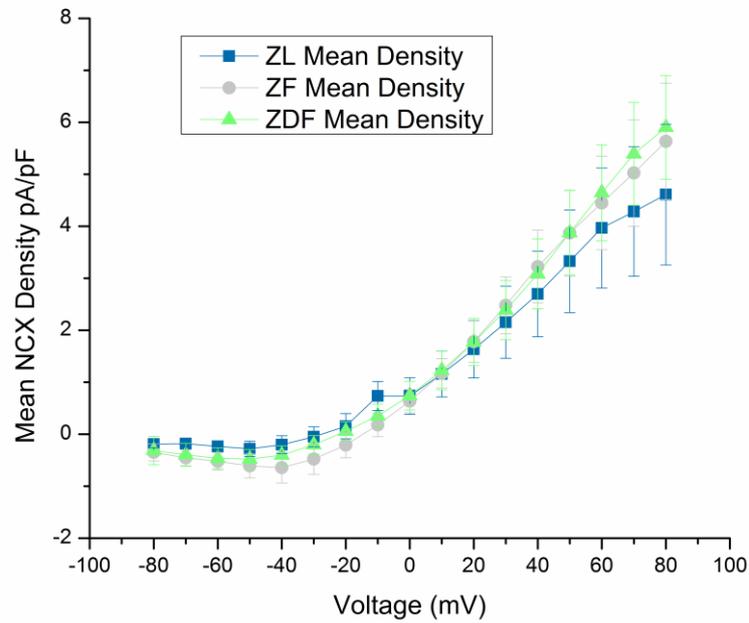
(B)
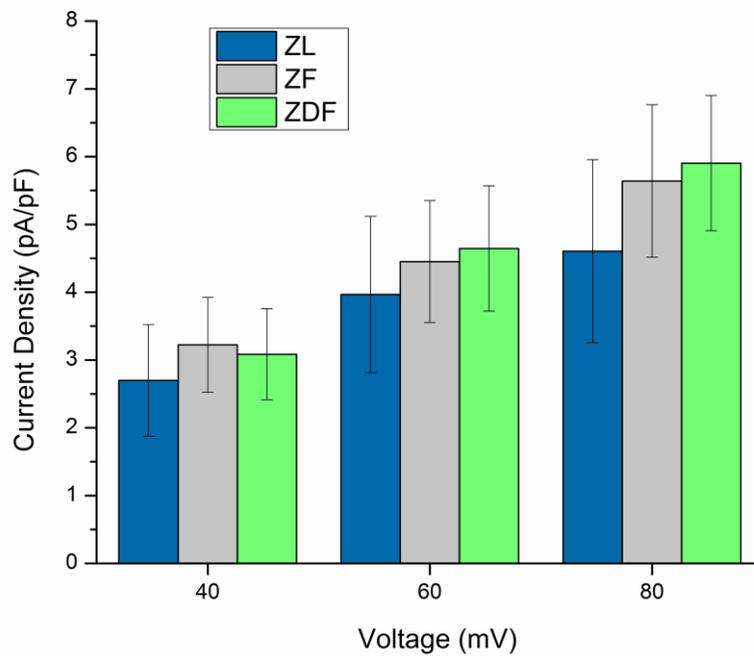
(C)

Figure 52: Na$^+$/Ca^{2+} exchange current. (B) Mean I_{NCX} density and (C) mean current density at selective voltages. Data are means $\pm$ SEM. n=10 ZL, 12 ZF and 13 ZDF cells from 7 ZL, 6 ZF and 8 ZDF hearts. P values of 0.05 and less were considered statistically significant (Continued).

8.7 Discussion

8.7.1 L-type Ca^{2+} current

Myocyte contraction is regulated by influx of Ca^{2+} via the L-type Ca^{2+} channels which provides the trigger for SR Ca^{2+} release. Disturbances of I_{CaL} would have implications for the release of SR Ca^{2+}. I_{CaL} was not significantly changed in ZDF or ZF compared to ZL myocytes over a wide range of test voltages. However, previous studies performed in Zucker rats aged 9-13 and 30-34 weeks have demonstrated reduction in I_{CaL} over a range of test potentials in ZDF myocytes (F. C. Howarth et al., 2011, 2012). Another study in ZF rats aged 16-17 weeks demonstrated a reduction in I_{CaL} and defective Ca^{2+} inactivation (Lin et al., 2012). I_{CaL} activation, inactivation, and recovery from inactivation were not significantly altered in myocytes from epicardial and endocardial regions in STZ treated rats or Wistar controls (Smail et al., 2016) which was also evident in the current Zucker study.

8.7.2 Na^+/Ca^{2+} exchange current

Recovery of intracellular Ca^{2+} to resting levels is mainly driven by uptake of Ca^{2+} into the SR and extrusion of Ca^{2+} from the cell via the NCX, operating in forward mode. Defects in NCX might contribute to alterations in the decay of the Ca^{2+} transient (Armoundas et al., 2003; Ashrafi et al., 2016; Hamilton & Terentyev, 2018; Hattori et al., 2000). In our study, I_{NCX} was not significantly changed in ZDF or ZF compared to ZL myocytes suggesting that the prolonged decay of the Ca^{2+} transient could not be attributed to defective I_{NCX}. Nevertheless, TPK and THALF decay of the caffeine-evoked Ca^{2+} transients were prolonged in ZDF suggesting there may be defects in SR Ca^{2+} release/uptake or NCX transport in ZDF myocytes (Armoundas et al., 2003; Ashrafi et al., 2016; Hamilton & Terentyev, 2018; Hattori et al., 2000). These results are consistent with a previous study by *Lima-Leopoldo et al* that showed no upregulation of NCX genes in high-fat diet (obese) Wistar rats (Lima-Leopoldo et al., 2008). However, *Hattori et al* (2000) showed that STZ-induced diabetic rats had diminished I_{NCX} density compared to control and reduced NCX channel expression and function due to reduced NCX protein and mRNA downregulation (Hattori et al., 2000).

8.8 Conclusions

- Mean I_{CaL} was not significantly altered in ZDF and ZF compared to ZL myocytes.

- Activation, inactivation and recovery of inactivation were not significantly altered in ZDF and ZF compared to ZL myocytes.

- Mean I_{NCX} was also not significantly altered in ZDF and ZF compared to ZL myocytes.

Chapter 9: Investigating the expression of proteins and structure of ventricular muscle using Western blot and transmission electron microscope techniques in the ZDF and ZF compared to ZL rats

9.1 Introduction

In T1DM, marked systolic dysfunction was linked with severe nitro-oxidative stress, fibrosis, and apoptosis. These pathological characteristics were less notable or absent, while hypertrophy of cardiomyocytes was comparable in T2DM, which was associated with an unchanged systolic function and an increase in diastolic stiffness. In addition to the pro-apoptotic caspase-12, the expression of mRNA of the hypertrophy markers c-fos, c-jun, and β-MHC was increased in T1DM, but remained or was only slightly increased in T2DM. Nonetheless, the expression of profibrotic TGF-β1 was enhanced in T1DM and showed a reduction in T2DM (Radovits et al., 2015).

In ZDF ventricular myocytes, alterations in the time course of contraction and Ca^{2+} transients could be due to changing expression of genes encoding myosin heavy chain and L-type Ca^{2+} channel proteins (F. C. Howarth et al., 2011). At the early stages of DM, changes in the pattern of genes encoding cardiac muscle regulatory proteins, can offer biomarkers that indicate the onset of heart muscle pathophysiology and chances for restorative interventions in the heart of T2DM (F. C. Howarth et al., 2011).

The impact of ageing on cardiomyocyte function and development of T2DM in ZDF rats has been investigated by (Fulop et al., 2007). They reported that an increase in O-linked N-acetylglucosamine (O-GlcNAc) on specific proteins may contribute to impaired cardiomyocyte function in diabetes and the elevated level of O-GlcNAc on different proteins seems to be regulated differently depending on age and diabetes (Fulop et al., 2007).

Recently, a new mediator of cardiac contractility has been reported (Daniels et al., 2018), myocardial isoform of Ca^{2+}/calmodulin-dependent protein kinase II-delta (CaMKIIδ). It is a multifunctional serine/threonine protein kinase that regulates proteins linked with cardiac Ca^{2+} flux, including RYR and L-type Ca^{2+} channels as well as proteins essential to sarcomere cross bridge cycling and structure. CaMKIIδ plays an important

role in cardiac contraction and relaxation. Constant activation of CaMKIIδ is associated with some cardiac pathologies, including maladaptive hypertrophy, apoptosis, and arrhythmias. It was found that CaMKIIδ activity is enhanced during hyperglycemia and can alter intracellular Ca^{2+} management in cardiovascular cells, which ultimately leads to reduced heart performance (Daniels et al., 2018). Daniels et al. (2018) investigated the effects of CaMKIIδ on cardiac contractility in ZDF rats. Their results showed that CaMKIIδ has an important role in modulating the performance of the diabetic heart, suggesting a potential therapeutic role for CaMKII inhibitors in improving myocardial function during T2DM (Daniels et al., 2018).

In isolated hearts of ZDF rats, the effect of modified substrate utilization on heart function was studied to determine whether changes in cardiac metabolism in T2DM are associated with contractile dysfunction or impaired response to ischemia. Hearts from ZDF and ZL control rats were isolated and perfused with glucose, lactate, pyruvate, and palmitate. The experiments indicated that the transition from carbohydrates to fatty acids for oxidative energy production did not increase myocardial oxygen consumption and was not linked with impaired response to ischemia and reperfusion (Wang et al., 2004).

The storage of fat in heart muscle was associated with a decrease in the production of force, which has consequences for the heart to pump blood effectively and because the accumulation of lipids in the heart muscle has been associated with HF. Fats in the blood can be transferred to heart muscle cells, where they can be stored or used to generate energy within the mitochondria, and with the help of transport proteins, ultimately pump blood through the rest of the body. Experiments in ZDF rats have shown that fat is increasingly accumulated in the heart as a result of increased fat transport across the heart cell membranes not due to reductions in mitochondrial number or function, indicating that lipids accumulate in the heart despite normal mitochondrial content, long-chain fatty acid (LCFA) oxidation and morphology (Holloway et al., 2011). Increased sarcolemma LCFA transport proteins and rates of LCFA transport result in a greater number of lipid droplets within cardiac muscle (Holloway et al., 2011).

Several studies have reported that metabolic changes in the heart of ZDF rats were higher compared to healthy controls (Baynes & Murray, 2009; Raza et al., 2012).

Increased ROS production and lipid peroxidation, increased cytochrome activity (CYP4502E1), accompanied by increased protein expression, oxidative protein carbonylation and increased expression of other oxidative stress marker proteins including inhaled nitric oxide (iNO) and heme oxygenase-1 (HO-1). Similarly, glutathione (GSH) concentration and activities of GSH-dependent enzymes, GSH reductase and glutathione S-transferase were, also significantly increased in ZDF rat heart tissues suggestive of a compensatory defense mechanism (Raza et al., 2012). The activities of complex I and IV mitochondrial respiratory enzymes were significantly reduced in the ventricle of ZDF rats compared to ZL rats. Other studies have suggested a reduction in the expression of IκB-α and phosphorylated-JNK in diabetic heart tissue. It was also reported that mitochondrial dysfunction and increased oxidative stress in ZDF rats could be associated, at least in part, with changes in the signaling of redox cells dependent on NF-κB/JNK (Raza et al., 2012).

In another study, the contractility of ventricular myocytes was well maintained, regardless of the altered Ca^{2+} transport mechanisms and a change in mRNA pattern in the older ZDF heart. The expression of genes that encode heart muscle proteins, cell membrane ion transport, membrane Ca^{2+} channels and intracellular Ca^{2+} transport proteins were altered in various ways. Atp2a1, Cacna1g, Cacna1h, and Myl2 were upregulated meanwhile Atp2a2, Cacna2d3, Tnnt2, Slc9a1, and Myh6 were downregulated in ZDF ventricle compared to ZL controls. Moreover, well-preserved shortening of ventricular myocytes was associated with a modified pattern of genes that encode different Ca^{2+} signals and cardiac muscle proteins in old ZDF rats (F. C. Howarth, 2012; F. C. Howarth et al., 2011).

Another study found increased mechanical rigidity, modified extracellular matrix, and pro-fibrotic gene expression profiles in the aorta of the insulin-resistant ZF/Fa rat. Mechanical experiments of the ZF fa/fa aorta showed increased vascular rigidity in longitudinal and circumferential directions compared to the ZL controls. The results also showed unequal elevations in developed strain, which favored the longitudinal direction, resulting in a loss of anisotropy. In ZF fa/fa aorta, an increase in the expression of fibronectin and collagen IV3 has been reported. Similarly, the expression of mRNA of the transforming growth factor and numerous Smad proteins were increased in vessels of insulin-resistant animals implicating a role for hyperinsulinemia in vascular stiffness.

These data provide structural, mechanical, and molecular evidence for arteriosclerosis in the ZF rat, all of which are hallmarks of DCM (Sista et al., 2005).

Previous studies have shown that T2DM, which is related to the progression of CVD in female and male ZDF rats, is mechanistically and structurally different (Lum-Naihe et al., 2017). Male rats show heart fibrosis and significant inhibition of intracardiac antifibrotic and anti-inflammatory cytokines. On the other hand, the heart of female rats is protected against the loss of antifibrotic cytokines and does not develop fibrosis. However, they still exhibit hypertrophy of the heart and cardiomyocyte, as shown by an increase in the phosphorylation of Ser2448 residues of mTOR. Moreover, a reduction in capillary density was common in male and female rats. It is possible that capillary rarefaction, cardiac hypertrophy, and a female-specific loss of cardio-reparative angiotensin II receptor 2 (AGTR2) in the setting of a very high expression of pro-hypertrophic miR-208a (a biomarker that promotes cardiac hypertrophy) could have contributed to increased structural damage in myocardial cells in the form of loss and scarring of cardiomyocytes. This study highlights the need for new heart assessments, such as non-invasive imaging in diabetic women, to detect myocardial deformation, heart hypertrophy, and capillary density (Lum-Naihe et al., 2017).

9.2 Hypothesis

- Expression of important cardiac muscle proteins and changes in muscle structure may underlie defects in muscle contraction in ZDF and ZF rat.

9.3 Aims and objectives

- To explore the effects of obesity and diabesity on the expression of proteins and structure of ventricular muscle in the ZDF and ZF compared to ZL rats.

9.4 Methods

9.4.1 Protein assessment

Commonly referred to as "protein immunoblot" is the gold standard in identifying and separating a specific protein in a pool of extracts from tissue lysate. The protein is extracted based on molecular weight through gel electrophoresis, which is then transferred to protein binding membrane (i.e. polyvinylidene fluoride (PVDF)), this membrane is then incubated with specific labeled antibodies (primary and secondary) that detect the protein of interest which can later be viewed using a developed film by means of fluorescent methods (Mahmood & Yang, 2012; Meftahi et al., 2021). Following protein extraction, the protein concentration in the extracts is measured and quantified by Bradford's assay which utilizes a spectrophotometer that measures the mass of the protein being loaded into each well and to compare them on equivalent bases (Kielkopf et al., 2020). This step is followed by electrophoresis by a porous acrylamide gel matrix, which separates proteins with excellent resolution based on molecular mass. Gel electrophoresis utilizes the use of sodium dodecyl sulfate polyacrylamide gels (SDS-PAGE) that denature the component proteins with an anionic detergent which binds them. This causes all the proteins to have a negative charge which is proportional to their molecular mass. The proteins then move across the pores of the matrix towards the positive electrode when voltage is applied (Mahmood & Yang, 2012; Nowakowski et al., 2014). A diagram showing the workflow is seen in Figure 53.
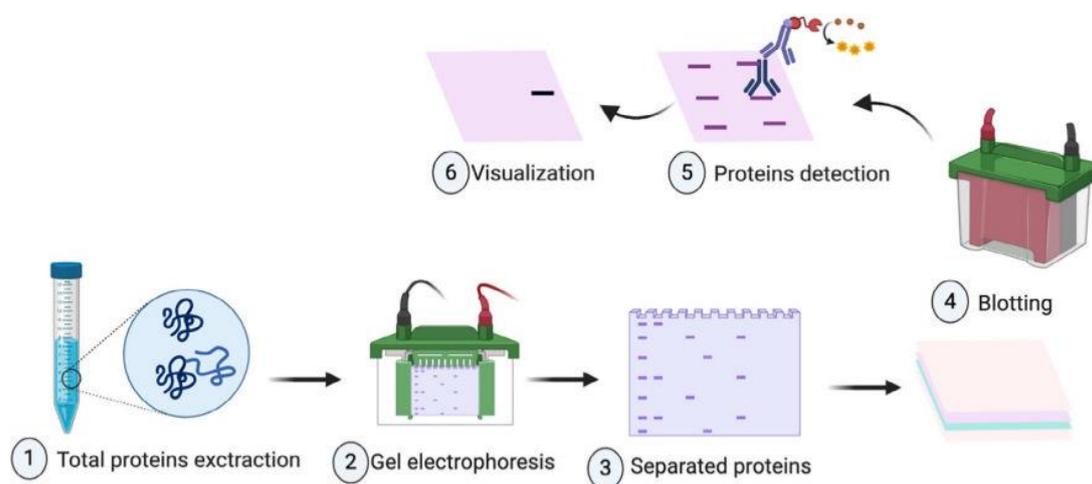
Figure 53: Western blot workflow. Adapted from (Meftahi et al., 2021).

Heart left ventricles were obtained from the rats after sacrifice. Then, tissue samples were snap-frozen in liquid nitrogen and stored in the freezer at -80°C for later use. After thawing, tissue extracts were prepared by homogenization on ice with radioimmunoprecipitation (RIPA) lysis buffer (1× phosphate-buffered saline (PBS), 50 mM NaF, 0.5% Na deoxycholate (w/v), 0.1% sodium dodecyl sulfate (SDS), 1% octylphenoxypolyethoxyethanol (IGEPAL), 1.5 mM Na_3VO_4, 1mM phenylmethylsulfonyl fluoride (PMSF) and 1× Halt) protease/phosphatase inhibitor cocktail, followed by centrifuging for 10 minutes at 3000-4000 RPM at 4ºC. The supernatant was collected and quantitated with Bradford's assay using BSA (10 mg/ml stock) as standard. Western blot analysis was performed with 20-50 µg of nuclear, cytoplasmic, or total cellular protein extracts which was loaded in 4-12% Tris-HCl SDS-PAGE gels (Bio-Rad) using MOPS running buffer which contains (Tris, Mops Sah, SDS, EDTA) and was transferred using a transfer buffer (Trizma Base, Glycine) onto a PVDF membrane. Blocking was performed for 2 hours at room temperature with 5% non-fat skimmed milk powder dissolved in TBST containing (Tween 20, NaCl, Trizma Base) for 1-3 hours. Extracts were then incubated with primary and secondary antibodies. The following primary antibodies were used: glyceraldehyde-3-phosphate dehydrogenase (GAPDH) (ab8245, Abcam), Myosin (ab50967, Abcam), Ryanodine (ab2868, Abcam), SERCA2 (MA3-919, ThermoFisher Scientific), Tm (ab7785, Abcam), TnC (ab137130, Abcam), TnI (ab47003, Abcam), TnT (ab8295, Abcam), Connexin (Cx45) (ab135474, Abcam). The following secondary antibodies were used: Anti-rabbit IgG HRP-linked antibody (7074S, Cell Signaling Technology) and Anti-mouse IgG HRP-linked antibody (7076S, Cell Signaling Technology). The loading marker used was Kaleidoscope (#1610375, Bio-Rad). Stripping of the membrane was done with a stripping buffer which contained (Tris, SDS) followed by β-Mercaptoethanol incubation in a water bath at 60ºC for 30 min followed by washing with TBST, then blocking and re-probing. Gel images were scanned, and the signal intensity was quantified using ImageJ software (NIH) (Schneider et al., 2012).

9.4.2 Ultrastructural assessment

The transmission electron microscope (TEM) (Figure 54) is an extremely important tool in microbiology. The main concept is that a beam of electrons accelerated though

condenser lenses at high voltage with wavelengths shorter than visible light by a factor of 10^5, are transmitted into a very thin (up to 20 nm) section of sample. The thin sample must be dry and capable of scattering electrons in a vacuum in order to pass through the sample and hit a fluorescent screen below the microscope and produce a detailed image which can be visualized, stored and analyzed. The image quality is limited by the biological samples which require specific processing techniques such as fixation and the use of electron-scattering heavy metal stains to produce adequate contrast for imaging. This allows the investigation of molecular structures of biological samples at greater depth (Burghardt & Droleskey, 2006; Malatesta, 2021; Pennycook et al., 2006).
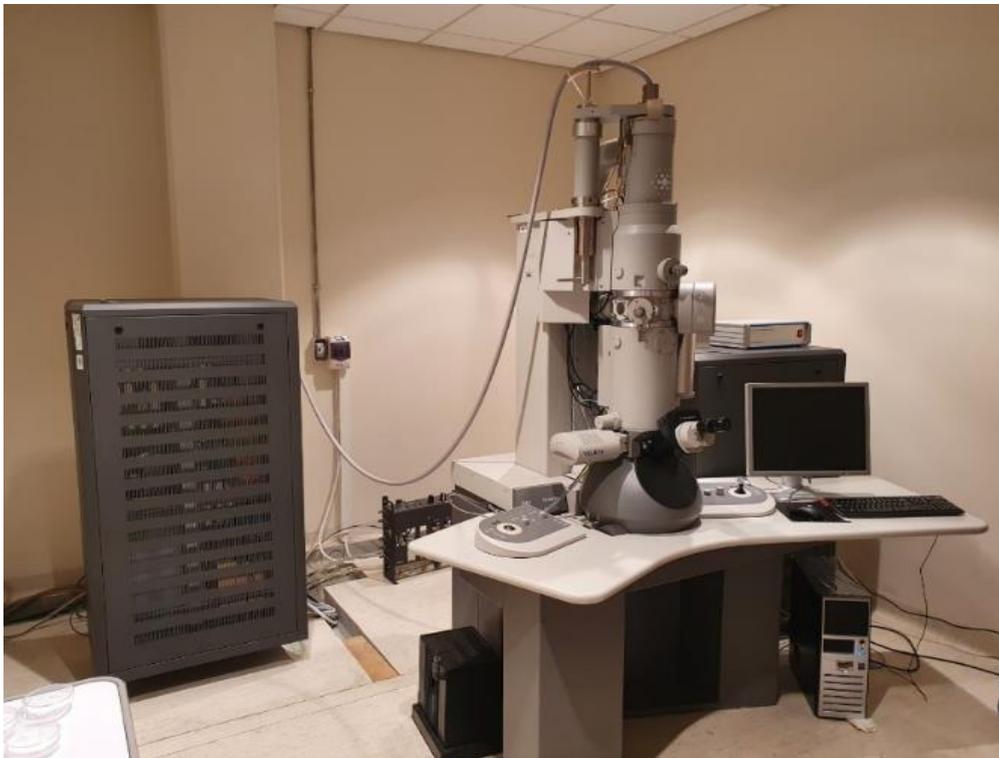
Figure 54: Transmission electron microscope

TEM was performed according to previously described techniques (Fahim et al., 2013). After sacrifice hearts were removed and left ventricle tissue samples were dissected from the same morphological area, free from other accessory tissues, cut into small pieces and washed with 0.1M phosphate buffer and then immersed in a modified McDowell and Trump (1976) fixative for 3 hours at room temperature. After rinsing with phosphate buffer, the tissues were postfixed with 1% osmium tetroxide for 1 hour. The tissue samples

were later washed with distilled water, dehydrated in a series of graded ethanol and propylene oxide and then infiltrated and embedded in Agar100 epoxy resin and polymerized at 65ºC for 24 hours. Blocks were trimmed to semithin and then ultrathin sections were cut with an ultramicrotome (Leica EM UC7 Ultracuts Vienna, Austria). Semithin sections (1.5 µm thickness) were stained with 1% aqueous toluidine blue on glass slides. Ultrathin sections (95 nm) with gold color were collected on 200 mesh copper grids and then were compared with uranyl acetate followed by lead citrate. The grids were examined and photographed with a TEM (Tecnai Biotwin Spirit G2, FEI company Eindhoven, Netherlands). Typical EM images in ventricular muscle from 5 ZL, 3 ZF and 5 ZDF groups of Zucker rat were analyzed per field at 6000x and 11500x magnification. Images were also analyzed and quantified using ImageJ software (NIH).

9.5 Statistics

Results were reported as the mean ± SEM of 'n' observations. Statistical comparisons were done by IBM SPSS and Origin 9.0 (OriginLab, Northampton, Massachusetts, USA) statistics software using either the paired samples t test, independent samples t test or one-way ANOVA then by Bonferroni corrected t tests for multiple comparisons, as appropriate. P values of 0.05 and less were considered statistically significant.

9.6 Results

9.6.1 Protein assessment results

Typical examples of Western blot gels are shown in Figure 55A. The mean fold changes in protein expression are shown in Figure 55B. GAPDH was used as the loading control. Myosin expression was significantly lower ($p<0.05$) in ZDF (0.53 ± 0.07) compared to ZF (1.45 ± 0.02) but not compared to ZL (1.06 ± 0.2) ventricle tissue. Ryanodine expression was modestly elevated in ZDF and ZF compared to ZL ventricle tissue. SERCA2 expression was significantly lower in ZDF (1.01 ± 0.1) and ZF (0.85 ± 0.04) compared to ZL (1.45 ± 0.11) ventricle tissue. Tm expression was significantly higher in the ZF (0.51 ± 0.05) group compared to ZDF (0.09 ± 0.02) and ZL (0.16 ± 0.03) controls. TnC

expression was significantly lower in ZDF (0.16±0.08) and in ZF (0.28±0.05) compared to ZL (0.64±0.05) ventricle tissue. Expression of TnI was significantly reduced in ZDF and ZF and TnT was reduced in ZDF compared to ZL ventricle tissue. Cx45 was reduced in ZDF and ZF compared to ZL ventricle tissue.
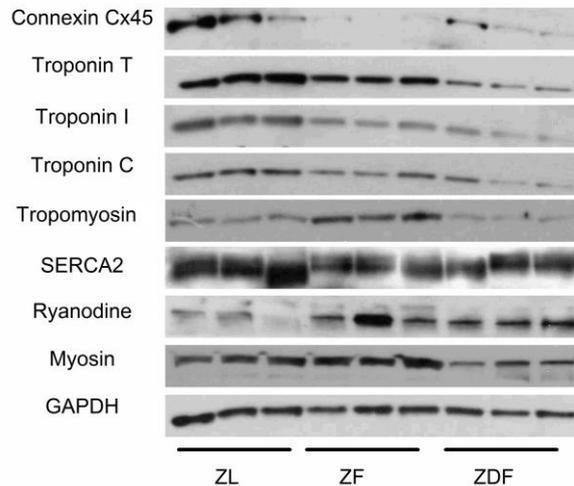
(A)
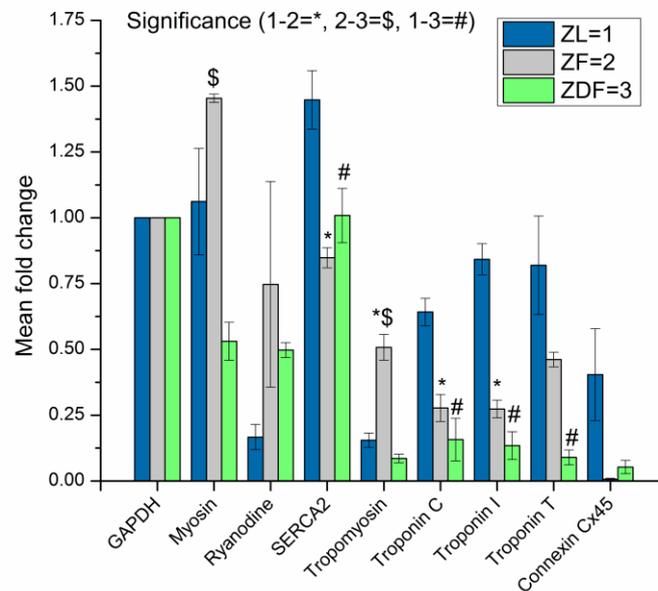
(B)

Figure 55: Assessment of proteins in ventricular muscle. (A) Original Western blot gels and (B) mean fold changes. Error bars represent mean ± SEM. GAPDH was used as the loading control (n=3-6 hearts). P values of 0.05 and less were considered statistically significant.

9.6.2 Ultrastructural assessment results

Morphometric analysis is shown in (Figure 56). Typical TEM images in ventricular muscle from a ZL rat at 6000x magnification are shown in Figure 56A, and 11,500x magnification in Figure 56B. Typical TEM images in ventricular muscle from a ZF rat at 6000x magnification are shown in Figure 56C, and 11,500x magnification in Figure 56D. Typical TEM images in ventricular muscle from a ZDF rat at 6000x magnification are shown in Figure 56E, and 11,500x magnification in Figure 56F. Mean sarcomere length is shown in Figure 56G and mean mitochondria count in Figure 56H. Sarcomere length was significantly ($p < 0.05$) shorter in ZF (1.21 ± 0.02 µm) compared to ZDF (1.61 ± 0.03 µm) and ZL (1.71 ± 0.01 µm) myocytes (Figure 56G). Mitochondria count was significantly ($p < 0.05$) lower in ZF (68.23 ± 7.26) compared to ZDF (100.81 ± 10.50) and ZL (122.15 ± 4.45) myocytes (Figure 56H).

Image analysis showed that ZL sarcomeres are well oriented with structured dark bands and intercalated disks that are clearly visible, and the mitochondria have normal shape. In ZF heart the sarcomeres are disorganized, dislocated, widened with spaces in between, mitochondria are clogged, deformed and small, lipid droplets are present. Furthermore, ZDF heart sarcomeres are not as well organized as in ZL, but better than in ZF heart. Spaces are present in ZDF heart but not as much as ZF, lipid droplets are present, and mitochondria are damaged as well as deformed.
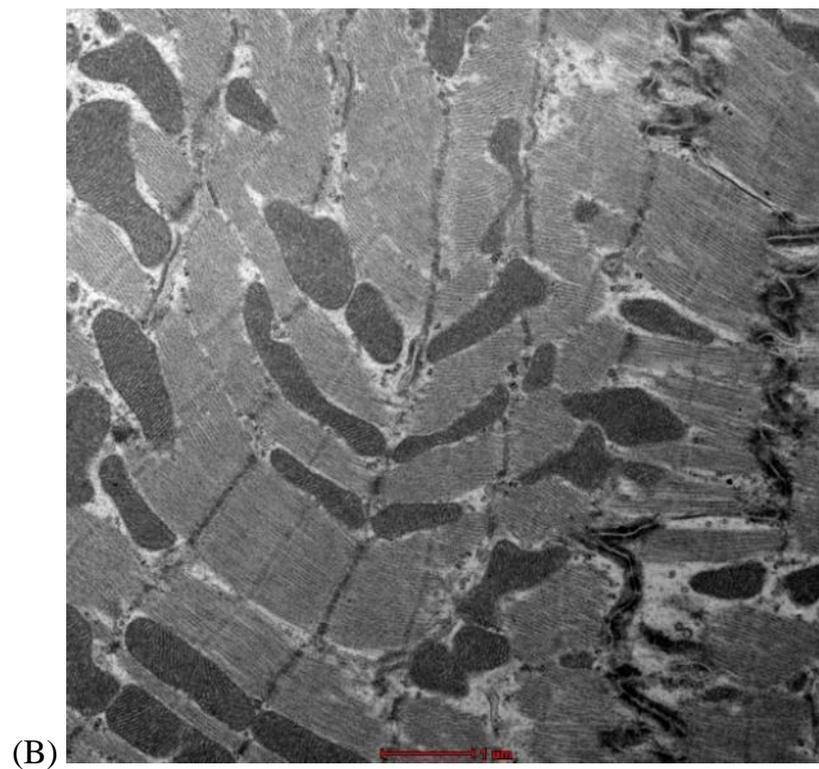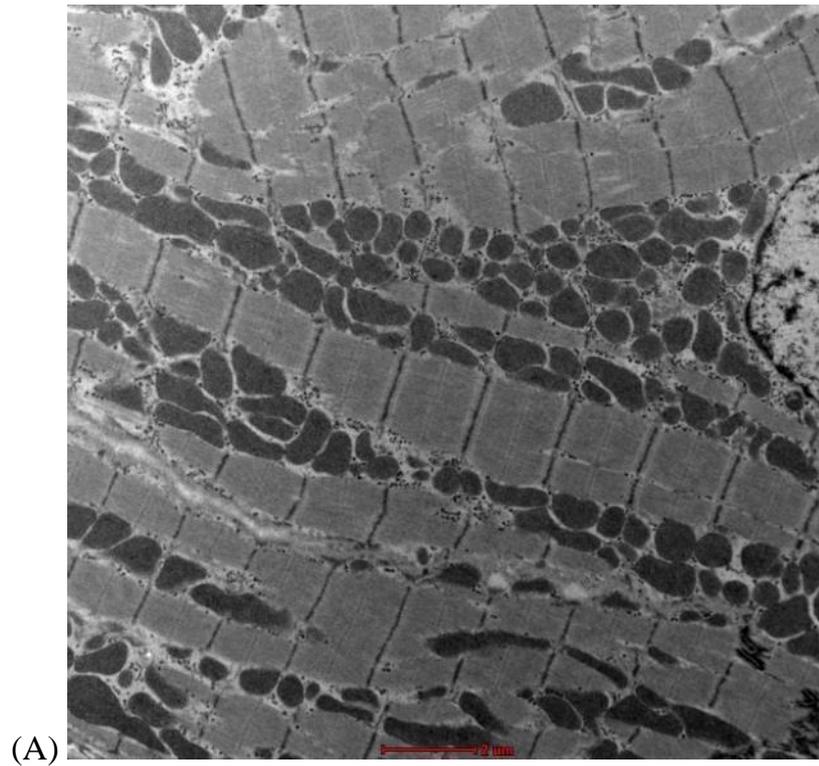
Figure 56: Assessment of structure in ventricular muscle. ZL: Sarcomeres are well oriented, structured the dark bands which are clearly visible, intercalated disks is connected and long, mitochondria are normal shaped. (A) Typical transmission electron microscope images from a ZL rat per field at 6000x magnification and (B) 11,500x magnification.
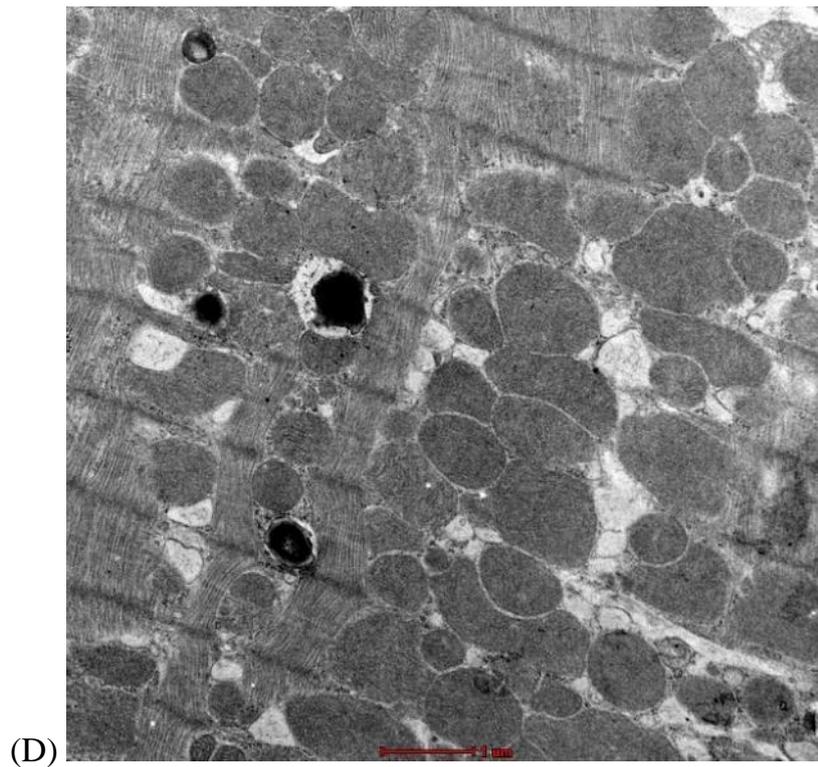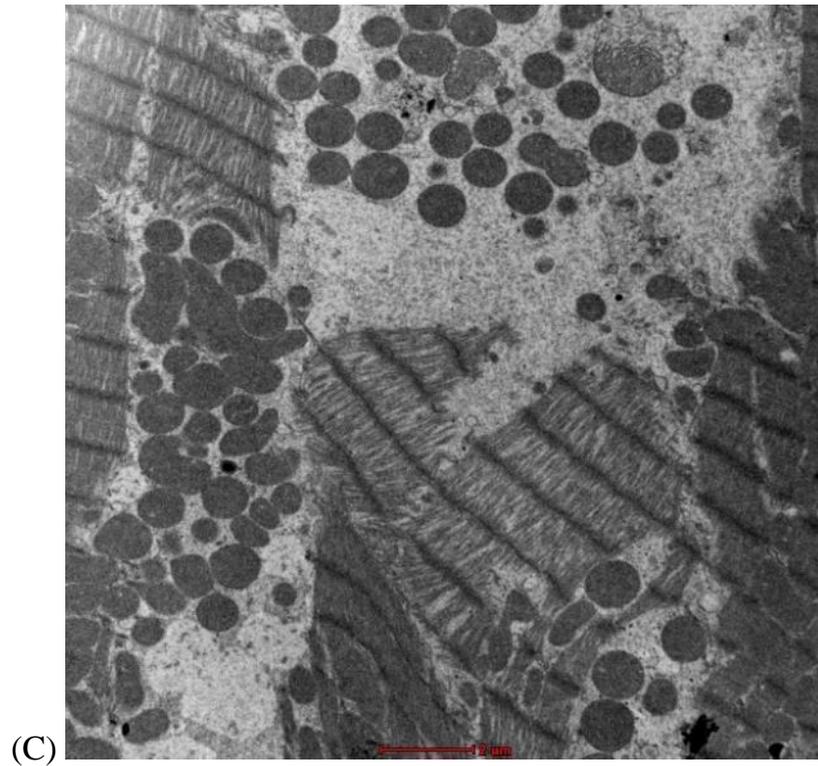
Figure 56: Assessment of structure in ventricular muscle. ZF: Sarcomeres are disorganized, dislocated, widened with spaces in between, mitochondria are clogged, deformed and small, lipid droplets are present. (C) Typical TEM images from a ZF rat per field at 6000x magnification and (D) 11,500x magnification (Continued).

(E)

(F)
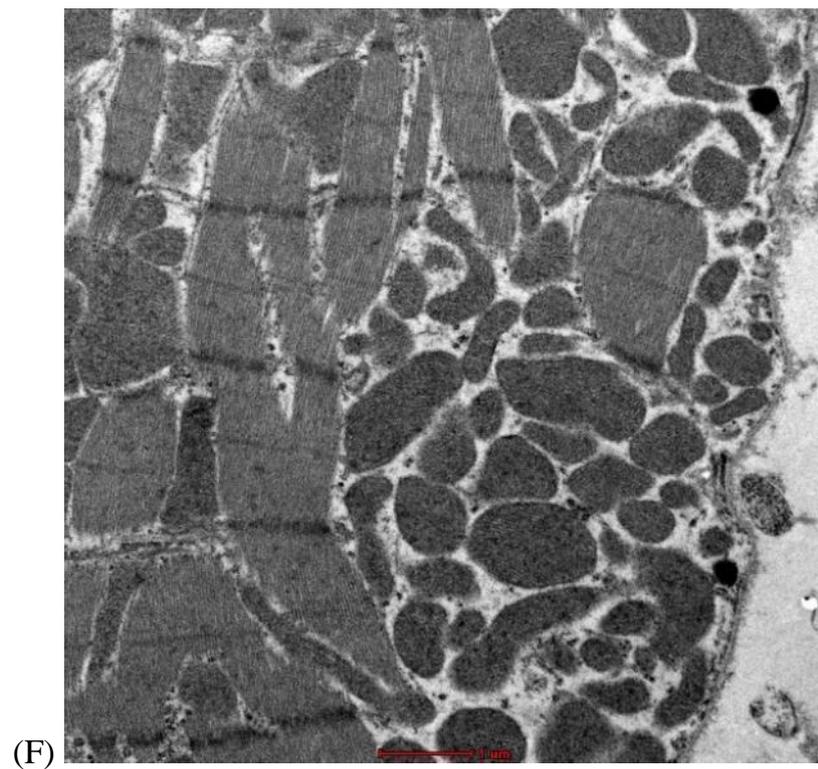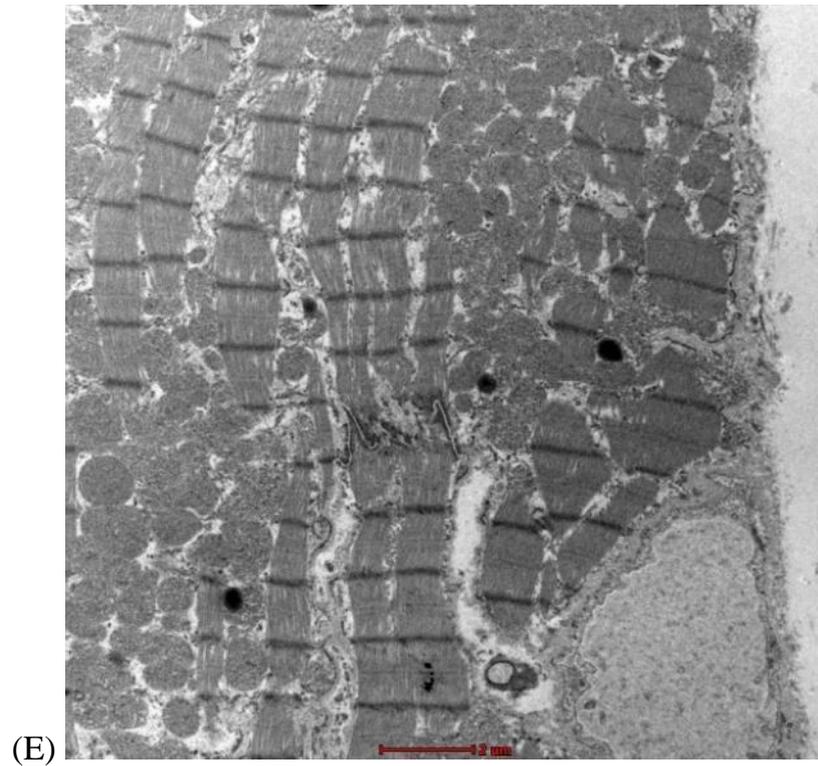
Figure 56: Assessment of structure in ventricular muscle. ZDF: Sarcomeres are not as well organized as in ZL but better oriented than ZF, spaces are present but not as much as ZF, lipid droplets are present, mitochondria are damaged and deformed. (E) Typical TEM images from a ZDF rat at 6000x magnification and (F) 11,500x magnification (Continued).
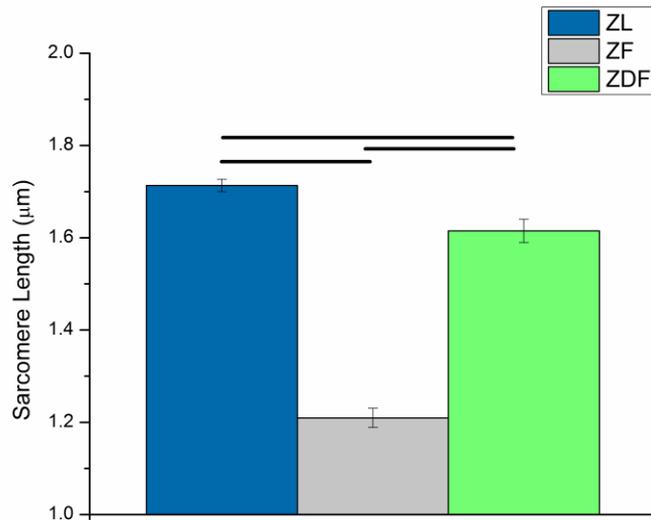
(G)
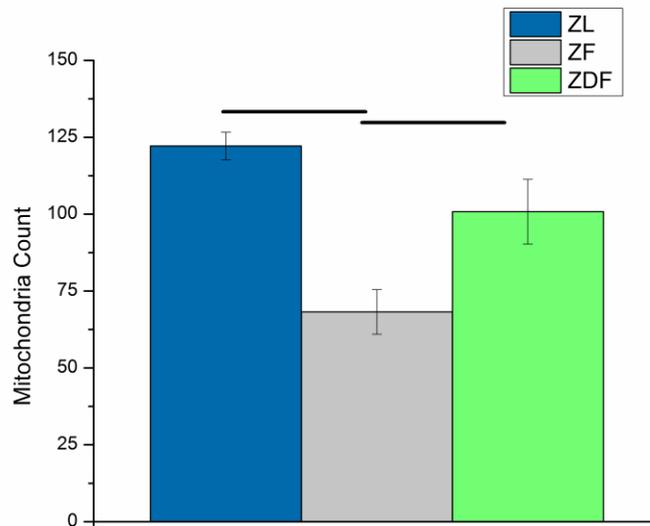
(H)

Figure 56: Assessment of structure in ventricular muscle. (G) Mean Sarcomere length and (H) mean mitochondria count. Data are means ± SEM. n=78 ZL, 33 ZF and 39 ZDF sections for Sarcomere length and n=26 ZL, 13 ZF and 16 ZDF for mitochondrial count all from 5 ZL, 3 ZF and 5 ZDF rats. P values of 0.05 and less were considered statistically significant (Continued).

9.7 Discussion

9.7.1 Protein assessment

Ventricular muscle protein was assessed with Western blot. Myosin expression was modestly lower in ZDF compared to ZF ventricle tissue which is consistent with a previous study (Dillmann, 1980). Myosin was significantly higher in ZF compared to ZL ventricular tissue. Ryanodine expression was modestly increased in ZDF and ZF compared to ZL ventricle tissue although both ZL and ZDF were significantly lower compared to GAPDH which was similarly reported previously compared to β-actin (Bidasee, Nallani, Henry, et al., 2003; Bidasee, Nallani, Yu, et al., 2003). SERCA2 expression was significantly lower in ZDF and ZF compared to ZL ventricle tissue. Expression of SERCA protein has been variously reported in different studies (Leopoldo et al., 2011; Lima-Leopoldo et al., 2008; Relling et al., 2006). As previously mentioned SERCA2 is important for SR Ca^{2+} handling and a reduction in SERCA protein maybe associated with a reduction in SERCA pump activity and lower uptake of Ca^{2+} into SR. Tm expression was higher in ZF compared to ZDF and ZL ventricle tissue. Tm has been previously linked to hypertrophic cardiomyopathy (Bottinelli et al., 1998; Sequeira et al., 2013). In this experiment we found evidence of structural defects in ZF rat heart that can be interpreted as signs of cardiac hypertrophy. TnC, TnI and TnT are very important in Ca^{2+} signaling and ECC coupling (Solaro & Rarick, 1998) and they also show the same trend with minor differences. Expression of TnI was reduced in ZDF and ZF and TnT was reduced in ZDF compared to ZL ventricle tissue. TnT was reduced in ZDF compared to ZL ventricle tissue. These myofilament proteins have been reported to be linked to dilated cardiomyopathy (Mirza et al., 2005) and diabetes is also associated with dilated cardiomyopathy (Sakakibara et al., 2011). In this study however, low expression indicates that contraction and relaxation may be effected possibly due to a lack of force or dilatation in the muscle which can be observed in the TEM sections in the ZF and ZDF groups. Finally, gap junction protein Cx45 is important for electrical signal conduction between cardiac myocytes (Teunissen & Bierhuizen, 2004). In this experiment the expression of Cx45 was reduced in ZDF and ZF compared to ZL ventricle tissue which may have implications for disturbances in heart rhythm which has been reported in a previous study (Sultan et al., 2021). Surprisingly, it

has been reported that mRNA expression levels for Gja7 (Cx45) was significantly increased in SAN from diabetic heart compared to controls (F. C. Howarth et al., 2007).

9.7.2 Ultrastructural assessment

Morphometric analysis of the sections indicated that sarcomeres are longest in ZL, intermediate in ZDF and shortest in ZF myocytes. Similarly, the mitochondrial count is highest in ZL, intermediate in ZDF and lowest in ZF myocytes. The differences in mitochondrial count may reflect differences in size or metabolic activity between the groups. Our research demonstrates that morphological changes in mitochondria and signs of injury in the ZDF are consistent with previous diabetic studies (Okruhlicova et al., 2005; Sakakibara et al., 2011) which indicates that cardiomyopathy is a common feature of obesity and diabetes. Additionally, reduced energy utilization is associated with diabetes (Taegtmeyer et al., 2002) and reductions in mitochondria could be a sign of altered energy utilization and might be attributed to a more sedentary lifestyle in ZF as well as ZDF rats and their increased body weights. Furthermore, diabetes has been associated with HF and metabolic abnormalities have been reported previously (Amaral & Okonko, 2015; From et al., 2010). Also, mitochondrial ROS are a major source of chronic oxidative stress in HF. They are also responsible for causing electrical instability that leads to SCD (Dey et al., 2018). Transplantation of mitochondria is a valuable method of therapeutic cardio-protection in conjunction with other therapies (Masuzawa et al., 2013).

9.8 Conclusions

- Evidence of molecular and structural defects in the ZF and ZDF rat heart were present.
- Reductions in mitochondrial count may suggest disturbances in energy metabolism in ZF and to a lesser extent in ZDF rat heart.
- Changed expression of Ca^{2+} transport and muscle proteins might partly underlie the defects in electro-mechanical function observed in ZDF and ZF rat heart.

Chapter 10: General discussion, conclusions, translational limitations and future directions

In general, both obesity and diabetes contribute to the disturbances in cardiac performance in the ZF and ZDF rat. In this study, we have found evidence of structural and molecular changes in the hearts of the animals which leads to disturbances in heart rhythm, defects in the uptake and release of SR Ca^{2+}, energy utilization and defects in molecular muscle proteins responsible for contraction and relaxation indicating poor cardiac functioning which leads to electro-mechanical dysfunction and eventually SCD.

Mortality and morbidity following an AMI in patients with T2DM may be caused by an increase in sensitivity to ischemia reperfusion damage or alteration in the activation of endogenous cardiovascular protection pathways modified by T2DM or ischemic preconditioning (IPC). Results from a previous study (Jensen et al., 2018) indicated that IPC reduced infarct size in all groups regardless of the presence of T2DM and its duration. Compared to prediabetic onset rats, myocardial glucose oxidation rates were reduced during stabilization and early reperfusion at onset of T2DM, but these animals retained the ability to increase oxidation rate in late reperfusion. However, late onset diabetic rats had low glucose oxidation rates throughout reperfusion and stabilization. Irrespective of intrinsic differences in sensitivity to ischemia reperfusion injury, the cardioprotective effect of IPC was conserved in pre, early and late stage T2DM and coupled with adaptations to myocardial glucose oxidation capacity (Jensen et al., 2018).

As mentioned earlier, CaMKIIδ plays an important role in cardiac contraction and relaxation. Since it plays an important part in altering intracellular Ca^{2+} handling in cardiomyocytes ultimately leading to reduced cardiac performance. It is important to consider it as one of the mechanisms underlying electromechanical dysfunction in the ZDF heart (Daniels et al., 2018). An example of such dysfunction is AF which is associated with high morbidity and mortality. Both structural and electrical remodeling contribute to AF. Recently (Onal et al., 2017), a role for CaMKII in the regulation of persistent "late" Na^+ current (I_{NaL}) has been identified. A computational approach was used to test the hypothesis that increased CaMKII-activated I_{NaL} in atrial myocytes interrupts Ca^{2+} homeostasis, potentiating arrhythmogenic after-depolarizations. Dynamic CaMKII

activity and regulation of multiple downstream targets [PLB, I_{CaL}, and the RyR] were entered to an existing well-validated computational model of the human atrial AP. Model simulations showed that constitutive CaMKII-dependent phosphorylation of $Na_{V1.5}$ and the subsequent increase in I_{NaL} successfully upset intracellular atrial myocyte CaMKII signaling and ion homeostasis. I_{NaL} stimulates intracellular Ca^{2+} overload via forward mode NCX activity, which increases the RyR open probability above that observed for the CaMKII-dependent phosphorylation of RyR alone. Increased I_{NaL} improved atrial myocyte repolarization defects (afterdepolarizations and alternans) in the setting of acute β-adrenergic stimulation. The model was created to help identify new mechanisms for controlling atrial $Na_{V1.5}$ regulation (Onal et al., 2017).

At 11 weeks of age, experiments in isolated perfused ZDF hearts demonstrated a preserved endothelium-dependent dilatation of coronary microvasculature regardless of depressed cardiac mechanical function, coronary flow and increased oxidative stress (Mourmoura et al., 2013). Another study examined whether arteriolar vasoconstrictor dysfunction of skeletal muscle occurs first or occurs simultaneously with the onset of diabetes and hypertension. Male ZDF rats aged 7, 13, and 20 months were used to represent pre-diabetic, short-term, and long-term diabetes (Laughlin et al., 2008). Vasoconstrictor responses, passive mechanical properties of isolated skeletal muscle arterioles along with conscious mean arterial pressure (MAP), fasted plasma insulin and glucose were measured. The study concluded that changes in vascular function resulting from T2DM at selected times differ in the progression of the disease. Also, in skeletal muscle arteriole, increased vasoconstrictor responses to NE and endothelin-1 (ET-1) in pre-diabetes are arbitrated by a decrement in the counterinfluence of the NOS (nitric oxide synthase) signaling mechanism. The results of the study by *Laughlin et al* (Laughlin et al., 2008) proposed that an early increase in ET-1 and adrenergic-mediated vasoconstriction impact the synchronized emergence of diabetes and hypertension. Additionally, it also suggests that interventions aimed at increasing nitric oxide (NO) bioavailability during the pre-diabetic state can help to combat hypertension associated with the onset of T2DM (Laughlin et al., 2008).

Cardiac NE overflow has also been investigated in ZDF rats. The results showed that cardiac NE overflow is inhibited in failing hearts from ZDF rats which can result from

inhibition of functional changes in the presynaptic alpha 2-adrenoceptor and can contribute to heart autonomic neuropathy (Burgdorf et al., 2006).

The relationship between cardiomyocyte rich perivascular tissues (PVT) and coronary arteries has been investigated in ZDF in T2DM. Specifically, the vasoactive effects of the PVT in the arteries of the ZDF rat were compared with other T2DM animal models. Vasocontractile and vasorelaxant functions of coronary septal arteries with and without PVT were studied with wire morphography. The experiments confirmed that the anti-contractual influences of PVTs are weakened in the coronary arteries of ZDF rats, but not affected in the arteries of STZ treated rats. Endothelial dysfunction was reported in the coronary septal arteries, with and without PVT, of ZDF rats, but not treated with STZ. Different signaling between cardiomyocyte-rich PVT and coronary arteries may contribute to cardiovascular complications in T2DM (Bonde et al., 2017).

In T2DM, impaired endothelium-dependent relaxation is due to a lack of endothelium derived hyperpolarization (EDH) that is controlled by a decrease in ion channel function in ZDF compared to ZL rats. It is proposed that the compensatory effect of NO and EDH-associated, endothelium-dependent relaxation is reduced in ZDF rats. Specific blockade of IK_{Ca} with TRAM-34 reduced NO and EDH-type relaxation in diabetic rats, indicating an elevated contribution of IK_{Ca} in diabetic small mesenteric artery (SMA) relaxation. This result was associated with increased IK_{Ca} mRNA and protein expression which suggests an important role for IK_{Ca} in diabetic SMA as a target for innovative treatment strategies (Schach et al., 2014).

Decreased CV, which is determined by cardiac structure, internal electrical resistance and excitability, is an independent risk factor for re-entry arrhythmias. The internal electrical resistance can be viewed as two resistors in series: first, the resistance of the cell cytoplasm, which is determined by the cellular composition, e.g. the number of intracellular organelles and non-conducting material like lipid droplets and second, the resistance at the cell-cell junctions (Kléber & Rudy, 2004). CV has been found to be reduced in ZDF rats. The CV dysfunction can be explained in part by the increased lateralization of Cx43. Moreover, lipotoxicity may play a role in the development of conduction disturbances and arrhythmias in T2DM (Ploug et al., 2013).

A recent method to detect cardiac dysfunction in rat models of T1DM (STZ) and T2DM (ZDF) has been investigated. It was found that contraction and active relaxation deteriorated more in T1DM than in T2DM by comparing speckle-tracking echocardiography (STE)-derived parameters to the indices of left ventricular pressure volume (LVPV) analysis. Among diastolic STE parameters, peak strain rate values isovolumic relaxation (SrIVR) was more decreased in T1DM, however, peak strain rate values in early diastole (SrE) were more reduced in T2DM. In contrast, diastolic stiffness was impaired in T2DM. Similarly, STE described more severe systolic dysfunction in T1DM. Also, in T1DM, peak strain rate values in systole (SrS) correlated with contractility, SrIVR with active relaxation, while in T2DM SrE was related to cardiac stiffness, cardiomyocyte diameter and fibrosis. In summary, strain and strain rate parameters can be both valuable and feasible physiological measures to describe the dynamic changes in contractility, active relaxation and LV stiffness in animal models of T1DM and T2DM (Benke et al., 2018). Figure 57 summarizes the time course of pathological changes that are taking place in the ZDF rat heart and that may lead to SCD.
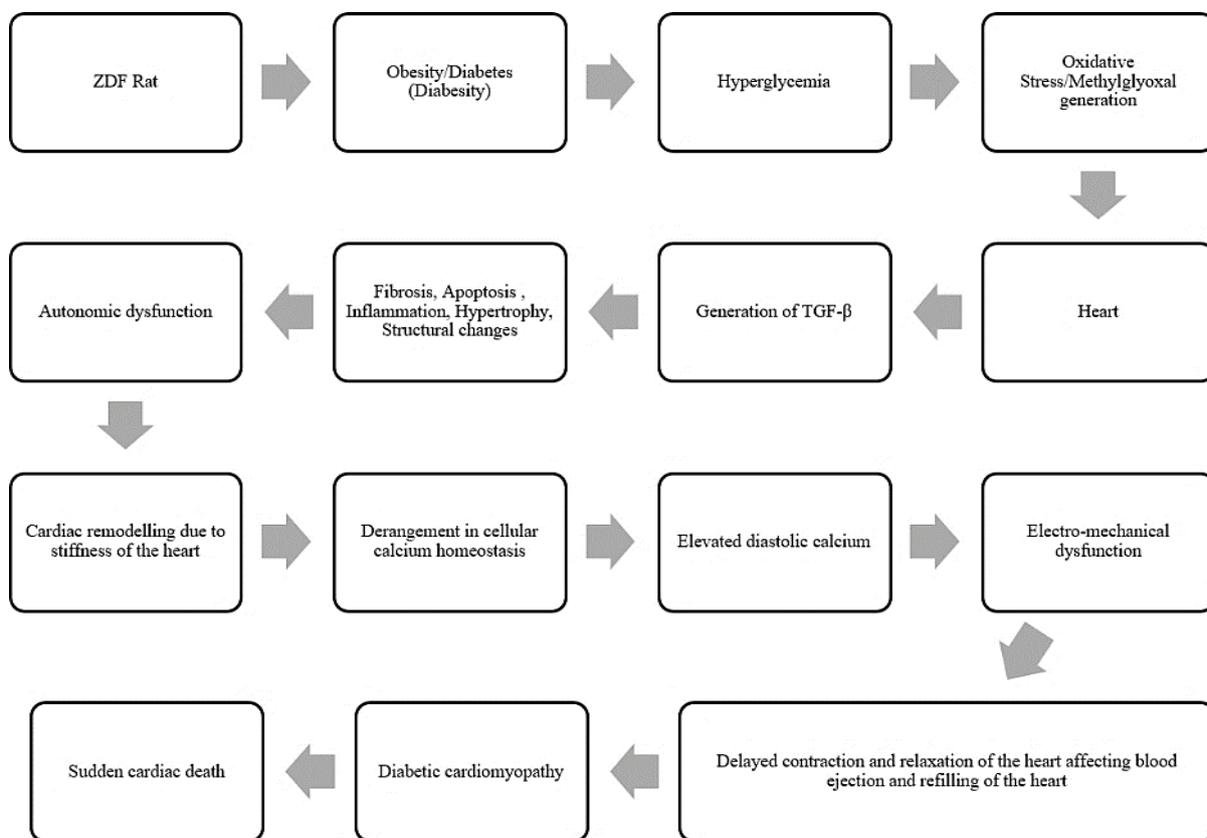
Figure 57: Pathological changes in the ZDF heart leading to sudden cardiac death.

10.1 Conclusions

The underlying mechanisms reveal disturbances in heart rhythm in ZDF and ZF rats are likely to be multifactorial. HR was reduced by ageing and by diabesity in the absence of changes in body temperature and physical activity. Reductions in HRV linked with altered sympathovagal drive could partially underlie the disturbed HR in the ZDF rat even in the absence of ANS control in the isolated perfused heart.

AMP of shortening is generally well preserved in ZDF myocytes. Defects in the uptake and release of SR Ca^{2+} might partly underlie the altered time course of the Ca^{2+} transient and shortening in ventricular myocytes from ZDF rat.

Our results also indicate that ISO was less effective at generating an increase in the AMP of shortening in ZDF and ZF compared to ZL myocytes and that defects in Ca^{2+} signaling, and in particular SR Ca^{2+} transport, might partly underlie these abnormalities.

We have found evidence of molecular and structural defects in the ZF and ZDF rat heart. Our evidence suggests that SR Ca^{2+} handling as well as energy utilization are compromised in ZDF and ZF myocytes. Myocyte contraction and relaxation may also be affected in the ZDF and ZF rat due to muscle protein structural defects which may lead to heart rhythm disturbance and poor cardiac function.

10.2 Translational implications

DCM is a complex disease with many factors influencing the disease progression and outcome. Our research demonstrates that ageing and prolonged exposure to diabetic risk factors would lead to worsened scenarios. It is important to target and implement strategies that will prevent disease progression such as exercise training and therapeutic interventions. Potential therapeutic interventions involving Ca^{2+}/ calmodulin-dependent kinase II (CaMKII) inhibitors might help improve myocardial function during T2DM as well as Leptin therapeutic interventions which might also prove effectiveness against obesity and T2DM.

10.3 Future directions

The results of this study provide a strong foundation on which to develop functional and structural studies to further understand the effects of obesity and diabesity on heart dysfunction in the Zucker rat. Future experiments might include electrophysiological investigation of different ion channels such as Na^+ and K^+ that are participating in the generation and propagation of electrical activity in the heart, as well as AP experiments in isolated ventricular myocytes. Further experiments could also investigate the AP of SAN and the electrophysiology of the atria. Experiments directed towards oxidative stress and measuring oxidative stress markers could also be performed. Experiments looking into fibrosis and the pathways leading to fibrosis might also be of interest. Imaging techniques including CT, MRI and echocardiography could be used to further understand the hemodynamic changes associated with obesity and diabesity.

10.4 Limitations

The *in-vivo* biotelemetry data presented in this study document the changes in electrophysiological and other physiological parameters in ZDF, ZF compared to ZL control rats 24 hours a day, 7 days a week from the age of 2 to 6 months. The mechanisms that underlie the disturbances in heart rhythm are likely to be multifactorial. The results of this study provide a firm basis on which to develop functional and structural studies to further understand the effects of obesity and diabesity on heart rhythm.

The number of rats was limited by the availability of grant funding, and experiments were conducted at a single time point. It would have been interesting to carry out experiments at different time points to evaluate the progression of electro-mechanical dysfunction in obesity and diabesity. Limitations include the time of start of the recording of the *in-vivo* biotelemetry which was commenced at 75 days of age where the animals were big enough for us to surgically implant the transmitters since the transmitters were relatively large. It would have been interesting to investigate the changes happening before that period.

References

Al-Ani, M., Forkins, A. S., Townend, J. N., & Coote, J. H. (1996). Respiratory sinus arrhythmia and central respiratory drive in humans. *Clinical Science (London, England : 1979)*, *90*(3), 235–241. https://doi.org/10.1042/CS0900235

Alexander, S. P., Kelly, E., Mathie, A., Peters, J. A., Veale, E. L., Armstrong, J. F., Faccenda, E., Harding, S. D., Pawson, A. J., Southan, C., Davies, J. A., Amarosi, L., Anderson, C. M. H., Beart, P. M., Broer, S., Dawson, P. A., Hagenbuch, B., Hammond, J. R., Inui, K., … Verri, T. (2021). The Concise Guide to Pharmacology 2021/22: Transporters. *British Journal of Pharmacology*, *178*(S1), S412–S513. https://doi.org/10.1111/BPH.15543

Alexander, S. P., Mathie, A., Peters, J. A., Veale, E. L., Striessnig, J., Kelly, E., Armstrong, J. F., Faccenda, E., Harding, S. D., Pawson, A. J., Southan, C., Davies, J. A., Aldrich, R. W., Attali, B., Baggetta, A. M., Becirovic, E., Biel, M., Bill, R. M., Catterall, W. A., … Zhu, M. (2021). The Concise Guide to Pharmacology 2021/22: Ion channels. *British Journal of Pharmacology*, *178*(S1), S157–S245. https://doi.org/10.1111/BPH.15539

Alexander, S., Sharman, J. L., Spedding, M., Peters, J. A., & Harmar, A. J. (2013). the Concise Guide To Pharmacology 2013 / 14 : GPCRs. *British Journal of Pharmacology*, 1706–1796. https://doi.org/10.1111/bph.12444/full

Amaral, N., & Okonko, D. O. (2015). Metabolic abnormalities of the heart in type II diabetes. *Diabetes and Vascular Disease Research*, *12*(4), 239–248. https://doi.org/10.1177/1479164115580936

Armoundas, A. A., Hobai, I. A., Tomaselli, G. F., Winslow, R. L., & O'Rourke, B. (2003). Role of sodium-calcium exchanger in modulating the action potential of ventricular myocytes from normal and failing hearts. *Circulation Research*, *93*(1), 46–53. https://doi.org/10.1161/01.RES.0000080932.98903.D8

Aromolaran, A. S., & Boutjdir, M. (2017). Cardiac Ion Channel Regulation in Obesity and the Metabolic Syndrome: Relevance to Long QT Syndrome and Atrial Fibrillation. *Frontiers in Physiology*, *8*, 431–448. https://doi.org/10.3389/fphys.2017.00431

Ashrafi, R., Yon, M., Pickavance, L., Yanni Gerges, J., Davis, G., Wilding, J., Jian, K., Zhang, H., Hart, G., & Boyett, M. (2016). Altered Left Ventricular Ion Channel Transcriptome in a High-Fat-Fed Rat Model of Obesity: Insight into Obesity-Induced Arrhythmogenesis. *Journal of Obesity*, *2016*, 1–12. https://doi.org/10.1155/2016/7127898

Aubert, A. E., Ramaekers, D., Beckers, F., Breem, R., Denef, C., Van De Werf, F., & Ector, H. (1999). The analysis of heart rate variability in unrestrained rats. Validation of method and results. *Computer Methods and Programs in Biomedicine*, *60*(3), 197–213. https://doi.org/10.1016/S0169-2607(99)00017-6

Axelsen, L. N., Calloe, K., Braunstein, T. H., Riemann, M., Hofgaard, J. P., Liang, B., Jensen, C. F., Olsen, K. B., Bartels, E. D., Baandrup, U., Jespersen, T., Nielsen, L. B., Holstein-Rathlou, N. H., & Nielsen, M. S. (2015). Diet-induced pre-diabetes slows cardiac conductance and promotes arrhythmogenesis. *Cardiovascular Diabetology*, *14*(1), 87–101. https://doi.org/10.1186/s12933-015-0246-8

Bartos, D. C., Grandi, E., & Ripplinger, C. M. (2015). Ion channels in the heart. *Comprehensive Physiology*, *5*(3), 1423–1464. https://doi.org/10.1002/cphy.c140069

Baynes, J. W., & Murray, D. B. (2009). The Metal Chelators, Trientine and Citrate, Inhibit the Development of Cardiac Pathology in the Zucker Diabetic Rat. *Experimental Diabetes Research*, *2009*, 696378–696384. https://doi.org/10.1155/2009/696378

Belke, D. D., Swanson, E. A., & Dillmann, W. H. (2004). Decreased sarcoplasmic reticulum activity and contractility in diabetic db/db mouse heart. *Diabetes*, *53*(12), 3201–3208. https://doi.org/10.2337/diabetes.53.12.3201

Benke, K., Braun, S., Mátyás, C., Barta, B. A., Merkely, B., Ruppert, M., Lakatos, B. K., Kovács, A., Németh, B. T., Oláh, A., Radovits, T., & Tokodi, M. (2018). Comparison of speckle-tracking echocardiography with invasive hemodynamics for the detection of characteristic cardiac dysfunction in type-1 and type-2 diabetic rat models. *Cardiovascular Diabetology*, *17*(1), 13–26. https://doi.org/10.1186/s12933-017-0645-0

Bers, D. M., & Despa, S. (2013). Cardiac Excitation-Contraction Coupling. *Encyclopedia of Biological Chemistry: Second Edition*, *415*(6868), 379–383. https://doi.org/10.1016/B978-0-12-378630-2.00221-8

Bidasee, K. R., Nallani, K., Henry, B., Dincer, U. D., & Besch, H. R. (2003). Chronic diabetes alters function and expression of ryanodine receptor calcium-release channels in rat hearts. *Molecular and Cellular Biochemistry*, *249*(1–2), 113–123. https://doi.org/10.1023/A:1024738706470

Bidasee, K. R., Nallani, K., Yu, Y., Cocklin, R. R., Zhang, Y., Wang, M., Dincer, U. D., & Besch, H. R. (2003). Chronic diabetes increases advanced glycation end products on cardiac ryanodine receptors/calcium-release channels. *Diabetes*, *52*(7), 1825–1836. https://doi.org/10.2337/DIABETES.52.7.1825

Bonde, L., Shokouh, P., Jeppesen, P. B., & Boedtkjer, E. (2017). Crosstalk between cardiomyocyte-rich perivascular tissue and coronary arteries is reduced in the Zucker Diabetic Fatty rat model of type 2 diabetes mellitus. *Acta Physiologica*, *219*(1), 227–238. https://doi.org/10.1111/apha.12685

Bootsma, M., Swenne, C. A., Van Bolhuis, H. H., Chang, P. C., Cats, V. M., & Bruschke, A. V. G. (1994). Heart rate and heart rate variability as indexes of sympathovagal balance. *The American Journal of Physiology*, *266*(4 Pt 2), H1565-H1571. https://doi.org/10.1152/AJPHEART.1994.266.4.H1565

Bottinelli, R., Coviello, D. A., Redwood, C. S., Pellegrino, M. A., Maron, B. J., Spirito, P., Watkins, H., & Reggiani, C. (1998). A mutant tropomyosin that causes hypertrophic cardiomyopathy is expressed in vivo and associated with an increased calcium sensitivity. *Circulation Research*, *82*(1), 106–115. https://doi.org/10.1161/01.RES.82.1.106

Boyett, M. R. (2009). "And the beat goes on" the cardiac conduction system: The wiring system of the heart. *Experimental Physiology*, *94*(10), 1035–1049. https://doi.org/10.1113/expphysiol.2009.046920

Bray, G. A. (1977). The Zucker-fatty rat: a review. *Federation Proceedings*, *36*(2), 148–153. http://www.ncbi.nlm.nih.gov/pubmed/320051

Bruinstroop, E., Eliveld, J., Foppen, E., Busker, S., Ackermans, M. T., Fliers, E., & Kalsbeek, A. (2015). Hepatic denervation and dyslipidemia in obese Zucker (fa/fa) rats. *International Journal of Obesity*, *39*(11), 1655–1658. https://doi.org/10.1038/ijo.2015.122

Burgdorf, C., Richardt, G., Schütte, F., Dendorfer, A., & Kurz, T. (2006). Impairment of presynaptic α2-adrenoceptor-regulated norepinephrine overflow in failing hearts from Zucker diabetic fatty rats. *Journal of Cardiovascular Pharmacology*, *47*(2), 256–262. https://doi.org/10.1097/01.fjc.0000202560.61667.3e

Burghardt, R. C., & Droleskey, R. (2006). Transmission electron microscopy. *Current Protocols in Microbiology*, *3(1)*, 2B.1.1-2B.1.39. https://doi.org/10.1002/9780471729259.MC02B01S03

Cagalinec, M., Zahradníková, A., Zahradníková, A., Kováčová, D., Paulis, L., Kureková, S., Hot'ka, M., Pavelková, J., Plaas, M., Novotová, M., & Zahradník, I. (2019). Calcium signaling and contractility in cardiac myocyte of wolframin deficient rats. *Frontiers in Physiology*, *10*. https://doi.org/10.3389/fphys.2019.00172

Catterall, W. A. (2000). From ionic currents to molecular mechanisms: The structure and function of voltage-gated sodium channels. *Neuron*, *26*(1), 13–25. https://doi.org/10.1016/S0896-6273(00)81133-2

Catterall, W. A. (2005). International Union of Pharmacology. XLVIII. Nomenclature and Structure-Function Relationships of Voltage-Gated Calcium Channels. *Pharmacological Reviews*, *57*(4), 411–425. https://doi.org/10.1124/pr.57.4.5

Catterall, W. A. (2011). Voltage-gated calcium channels. *Cold Spring Harbor Perspectives in Biology*, *3*(8), 1–23. https://doi.org/10.1101/CSHPERSPECT.A003947

Cerutti, C., Gustin, M. P., Paultre, C. Z., Lo, M., Julien, C., Vincent, M., & Sassard, J. (1991). Autonomic nervous system and cardiovascular variability in rats: a spectral analysis approach. *The American Journal of Physiology*, *261*(4 Pt 2). https://doi.org/10.1152/AJPHEART.1991.261.4.H1292

Chadt, A., Scherneck, S., Joost, H.-G., & Al-Hasani, H. (2000). Molecular links between Obesity and Diabetes: "Diabesity". [ebook]. In Endotext. MDText.com, Inc. Retrieved from http://www.ncbi.nlm.nih.gov/pubmed/25905279. Accessed on November 26, 2020

Chaudhary, R., Walder, K. R., Hagemeyer, C. E., & Kanwar, J. R. (2018). Psammomys obesus: a Natural Diet-Controlled Model for Diabetes and Cardiovascular Diseases. *Current Atherosclerosis Reports*, *20*(9), 46–56. https://doi.org/10.1007/s11883-018-0746-6

Chen, J. Q., Huang, Y. Y., Gusdon, A. M., & Qu, S. (2015). Irisin: A new molecular marker and target in metabolic disorder. *Lipids in Health and Disease*, *14*(1), 1–6. https://doi.org/10.1186/1476-511X-14-2

Chiou, C. W., & Zipes, D. P. (1998). Selective vagal denervation of the atria eliminates heart rate variability and baroreflex sensitivity while preserving ventricular innervation. *Circulation*, *98*(4), 360–368. https://doi.org/10.1161/01.CIR.98.4.360

Chohnan, S., Matsuno, S., Shimizu, K., Tokutake, Y., Kohari, D., & Toyoda, A. (2020). Coenzyme A and Its Thioester Pools in Obese Zucker and Zucker Diabetic Fatty Rats. *Nutrients*, *12*(2), 417. https://doi.org/10.3390/nu12020417

Choi, K. M., Zhong, Y., Hoit, B. D., Grupp, I. L., Hahn, H., Dilly, K. W., Guatimosim, S., Jonathan Lederer, W., & Matlib, M. A. (2002). Defective intracellular Ca2+ signaling contributes to cardiomyopathy in type 1 diabetic rats. *American Journal of Physiology - Heart and Circulatory Physiology*, *283*(4 52-4), H1398–H1408. https://doi.org/10.1152/ajpheart.00313.2002

Cook, R. F., Bussey, C. T., Fomison-Nurse, I. C., Hughes, G., Bahn, A., Cragg, P. A., & Lamberts, R. R. (2019). β2-Adrenoceptors indirectly support impaired β1-adrenoceptor responsiveness in the isolated type 2 diabetic rat heart. *Experimental Physiology*, *104*(6), 808–818. https://doi.org/10.1113/EP087437

Craig, R., Lee, K. H., Mun, J. Y., Torre, I., & Luther, P. K. (2014). Structure, sarcomeric organization, and thin filament binding of cardiac myosin-binding protein-C. *Pflügers Archiv - European Journal of Physiology*, *466*(3), 425–431. https://doi.org/10.1007/s00424-013-1426-6

Crawford, M., DiMarco, J., & Paulus, W. (2009). Cardiology. [ebook]. In Elsevier health sciences. https://www.elsevier.com/books/cardiology/crawford/978-0-7234-3485-6.

Csige, I., Ujvárosy, D., Szabó, Z., Lőrincz, I., Paragh, G., Harangi, M., & Somodi, S. (2018). The Impact of Obesity on the Cardiovascular System. *Journal of Diabetes Research*, *2018*, 1–12. https://doi.org/10.1155/2018/3407306

Currie, S., & Smith, G. L. (1999). Enhanced phosphorylation of phospholamban and downregulation of sarco/endoplasmic reticulum Ca2+ ATpase type 2 (SERCA 2) in cardiac sarcoplasmic reticulum from rabbits with heart failure. *Cardiovascular Research*, *41*(1), 135–146. https://doi.org/10.1016/S0008-6363(98)00241-7

Czick, M. E., Shapter, C. L., & Silverman, D. I. (2016). Atrial Fibrillation: The Science behind Its Defiance. *Aging and Disease*, *7*(5), 635–656. https://doi.org/10.14336/AD.2016.0211

Dal-Bianco, J. P., & Levine, R. A. (2013). Anatomy of the Mitral Valve Apparatus. *Cardiology Clinics*, *31*(2), 151–164. https://doi.org/10.1016/j.ccl.2013.03.001

Daniels, L. J., Wallace, R. S., Nicholson, O. M., Wilson, G. A., McDonald, F. J., Jones, P. P., Baldi, J. C., Lamberts, R. R., & Erickson, J. R. (2018). Inhibition of calcium/calmodulin-dependent kinase II restores contraction and relaxation in isolated cardiac muscle from type 2 diabetic rats. *Cardiovascular Diabetology*, *17*(1), 89–104. https://doi.org/10.1186/s12933-018-0732-x

De Ferranti, S., & Mozaffarian, D. (2008). The perfect storm: obesity, adipocyte dysfunction, and metabolic consequences. *Clinical Chemistry*, *54*(6), 945–955. https://doi.org/10.1373/clinchem.2007.100156

De Maria, B., Bari, V., Sgoifo, A., Carnevali, L., Cairo, B., Vaini, E., Catai, A. M., de Medeiros Takahashi, A. C., Dalla Vecchia, L. A., & Porta, A. (2019). Concomitant Evaluation of Heart Period and QT Interval Variability Spectral Markers to Typify Cardiac Control in Humans and Rats. *Frontiers in Physiology*, *10,* 1478. https://doi.org/10.3389/FPHYS.2019.01478

Demir, K., Avci, A., Kaya, Z., Marakoglu, K., Ceylan, E., Yilmaz, A., Ersecgin, A., Armutlukuyu, M., & Altunkeser, B. B. (2016). Assessment of atrial electromechanical delay and P-wave dispersion in patients with type 2 diabetes mellitus. *Journal of Cardiology*, *67*(4), 378–383. https://doi.org/10.1016/j.jjcc.2015.06.003

Dey, S., DeMazumder, D., Sidor, A., Brian Foster, D., & O'Rourke, B. (2018). Mitochondrial ROS drive sudden cardiac death and chronic proteome remodeling in heart failure. *Circulation Research*, *123*(3), 356–371. https://doi.org/10.1161/CIRCRESAHA.118.312708

Di Nardo, F., Cogo, C. E., Faelli, E., Morettini, M., Burattini, L., & Ruggeri, P. (2015). C-Peptide-based assessment of insulin secretion in the Zucker Fatty rat: a modelistic study. *PloS One*, *10*(5), e0125252. https://doi.org/10.1371/JOURNAL.PONE.0125252

Dillmann, W. H. (1980). Diabetes Mellitus Induces Changes in Cardiac Myosin of the Rat. *Diabetes*, *29*(7), 579–582. https://doi.org/10.2337/diab.29.7.579

Dobbs, R., & Swinburn, B. (2015). The global obesity threat. In Mckinsey.com, McKinsey & Company. Retrieved from https://www.mckinsey.com/mgi/overview/in-the-news/the-global-obesity-threat. Accessed on June 6, 2019

Fahim, M. A., Tariq, S., & Adeghate, E. (2013). Vitamin E modifies the ultrastructure of testis and epididymis in mice exposed to lead intoxication. *Annals of Anatomy - Anatomischer Anzeiger*, *195*(3), 272–277. https://doi.org/10.1016/J.AANAT.2012.11.001

Falcão-Pires, I., & Leite-Moreira, A. F. (2012). Diabetic cardiomyopathy: Understanding the molecular and cellular basis to progress in diagnosis and treatment. *Heart Failure Reviews*, *17*(3), 325–344. https://doi.org/10.1007/s10741-011-9257-z

Fazan, R. J., Ballejo, G., Salgado, M. C. O., Moraes, M. F. D., & Salgado, H. C. (1997). Heart rate variability and baroreceptor function in chronic diabetic rats. *Hypertension (Dallas, Tex. : 1979)*, *30*(3 Pt 2), 632–635. https://doi.org/10.1161/01.HYP.30.3.632

Fellmann, L., Nascimento, A. R., Tibiriça, E., & Bousquet, P. (2013). Murine models for pharmacological studies of the metabolic syndrome. *Pharmacology & Therapeutics*, *137*(3), 331–340. https://doi.org/10.1016/j.pharmthera.2012.11.004

Ferrantini, C., Coppini, R., Sacconi, L., Tosi, B., Zhang, M. L., Wang, G. L., Vries, E. De, Hoppenbrouwers, E., Pavone, F., Cerbai, E., Tesi, C., Poggesi, C., & Ter Keurs, H. E. D. J. (2014). Impact of detubulation on force and kinetics of cardiac muscle contraction. *The Journal of General Physiology*, *143*(6), 783–797. https://doi.org/10.1085/JGP.201311125

Fredersdorf, S., Thumann, C., Zimmermann, W. H., Vetter, R., Graf, T., Luchner, A., Riegger, G. A. J., Schunkert, H., Eschenhagen, T., & Weil, J. (2012). Increased myocardial SERCA expression in early type 2 diabetes mellitus is insulin dependent: In vivo and in vitro data. *Cardiovascular Diabetology*, *11(1), 57*. https://doi.org/10.1186/1475-2840-11-57

Friedman, J. (2012). Leading the charge in leptin research: An interview with Jeffrey Friedman. *DMM Disease Models and Mechanisms*, *5*(5), 576–579. https://doi.org/10.1242/dmm.010629

Friedman, J. (2016). The long road to leptin. *Journal of Clinical Investigation*, *126*(12), 4727–4734. https://doi.org/10.1172/JCI91578

From, A. M., Scott, C. G., & Chen, H. H. (2010). The Development of Heart Failure in Patients With Diabetes Mellitus and Pre-Clinical Diastolic Dysfunction. A Population-Based Study. *Journal of the American College of Cardiology*, *55*(4), 300–305. https://doi.org/10.1016/j.jacc.2009.12.003

Frühbeck, G. (2006). Intracellular signalling pathways activated by leptin. *The Biochemical Journal*, *393*(1), 7–20. https://doi.org/10.1042/BJ20051578

Fulop, N., Mason, M. M., Dutta, K., Wang, P., Davidoff, A. J., Marchase, R. B., Chatham, J. C., Fülöp, N., Mason, M. M., Dutta, K., Wang, P., Davidoff, A. J., Marchase, R. B., & Chatham, J. C. (2007). Impact of Type 2 diabetes and aging on cardiomyocyte function and O-linked N-acetylglucosamine levels in the heart. *American Journal of Physiology - Cell Physiology*, *292*(4), C1370–C1378. https://doi.org/10.1152/ajpcell.00422.2006

Gando, S., Hattori, Y., & Kanno, M. (1993). Altered cardiac adrenergic neurotransmission in streptozotocin-induced diabetic rats. *British Journal of Pharmacology*, *109*(4), 1276–1281. https://doi.org/10.1111/J.1476-5381.1993.TB13761.X

George, A. L. (2013). Molecular and genetic basis of sudden cardiac death. *Journal of Clinical Investigation*, 123(1), 75–83. https://doi.org/10.1172/JCI62928

Golob, M., Moss, R. L., & Chesler, N. C. (2014). Cardiac Tissue Structure, Properties, and Performance: A Materials Science Perspective. *Annals of Biomedical Engineering*, *42*(10), 2003–2013. https://doi.org/10.1007/s10439-014-1071-z

Gurevich-Panigrahi, T., Panigrahi, S., Wiechec, E., & Los, M. (2009). Obesity: Pathophysiology and Clinical Management. *Current Medicinal Chemistry*, *16*(4), 506–521. https://doi.org/10.2174/092986709787315568

Gutman, G. A. (2005). International Union of Pharmacology. LIII. Nomenclature and Molecular Relationships of Voltage-Gated Potassium Channels. *Pharmacological Reviews*, *57*(4), 473–508. https://doi.org/10.1124/pr.57.4.10

Hacker, M., II, W. S. M., & Bachmann, K. A. (2009). *Pharmacology: Principles and Practice*. Academic Press.

Hafeez, Y., & Grossman, S. A. (2022). Junctional Rhythm. [ebook]. In StatPearls. StatPearls publishing. http://www.ncbi.nlm.nih.gov/pubmed/29939537

Haley, J. M., Thackeray, J. T., Thorn, S. L., & DaSilva, J. N. (2015). Cardiac β-adrenoceptor expression is reduced in Zucker diabetic fatty rats as type-2 diabetes progresses. *PLoS ONE*, *10*(5), 1–13. https://doi.org/10.1371/journal.pone.0127581

Hamilton, S., & Terentyev, D. (2018). Proarrhythmic remodeling of calcium homeostasis in cardiac disease; Implications for diabetes and obesity. *Frontiers in Physiology*, *9*, 1517. https://doi.org/10.3389/fphys.2018.01517

Harvey, R. A., & Ferrier, D. (2011). Lippincott's Illustrated Reviews: Biochemistry. In R. A. Harvey & D. Ferrier (Eds.), *Lippincott Williams & Wilkins* (5th ed). 307–356. Wolters Kluwer Health, Lippincott Williams & Wilkins.

Hattori, Y., Matsuda, N., Kimura, J., Ishitani, T., Tamada, A., Gando, S., Kemmotsu, O., & Kanno, M. (2000). Diminished function and expression of the cardiac Na+-Ca2+ exchanger in diabetic rats: Implication in Ca2+ overload. *Journal of Physiology*, *527*(1), 85–94. https://doi.org/10.1111/j.1469-7793.2000.00085.x

Hille, B. (1978). Ionic channels in excitable membranes. Current problems and biophysical approaches. *Biophysical Journal*, *22*(2), 283–294. https://doi.org/10.1016/S0006-3495(78)85489-7

Holloway, G. P., Snook, L. A., Harris, R. J., Glatz, J. F. C. C., Luiken, J. J. F. P. F. P., & Bonen, A. (2011). In obese Zucker rats, lipids accumulate in the heart despite normal mitochondrial content, morphology and long-chain fatty acid oxidation. *The Journal of Physiology*, *589*(Pt 1), 169–180. https://doi.org/10.1113/jphysiol.2010.198663

Hong, T., & Shaw, R. M. (2017). Cardiac T-Tubule Microanatomy and Function. *Physiological Reviews*, *97*(1), 227–252. https://doi.org/10.1152/physrev.00037.2015

Hostiuc, S., Popescu, A., Guţu, E. D., Rusu, M. C., & Pop, F. (2013). Electrical conduction system apoptosis in type II diabetes mellitus. *Romanian Journal of Morphology and Embryology = Revue Roumaine de Morphologie et Embryologie*, *54*(4), 953–959. https://pubmed.ncbi.nlm.nih.gov/24398990/

Howarth, C. F., Al-Sharhan, R., Al-Hammadi, A., & Qureshi, M. A. (2007). Effects of streptozotocin-induced diabetes on action potentials in the sinoatrial node compared with other regions of the rat heart. *Molecular and Cellular Biochemistry*, *300*(1–2), 39–46. https://doi.org/10.1007/s11010-006-9366-5

Howarth, F. C. (2012). Ventricular myocyte contraction, intracellular calcium and expression of genes encoding cardiac muscle proteins in young and aging Zucker diabetic fatty rat heart reviewed. *Hamdan Medical Journal*, *5*(2), 165–172. https://doi.org/10.7707/hmj.v5i2.140

Howarth, F. C., Galadari, S., Rajesh, M., Thayyullathil, F. T., Oz, M., Shuba, Y. M., Yang, K.-H. S., Kury, L. T. Al, & Ali, R. M. (2014). Effects of endogenous cannabinoid anandamide on cardiac Na+/Ca2+ exchanger. *Cell Calcium*, *55*(5), 231–237. https://doi.org/10.1016/j.ceca.2014.02.017

Howarth, F. C., Jacobson, M., Qureshi, M. A., Shafiullah, M., Hameed, R. S., Zilahi, E., Al Haj, A., Nowotny, N., & Adeghate, E. (2009). Altered gene expression may underlie prolonged duration of the QT interval and ventricular action potential in streptozotocin-induced diabetic rat heart. *Molecular and Cellular Biochemistry*, *328*(1–2), 57–65. https://doi.org/10.1007/s11010-009-0074-9

Howarth, F. C., Jacobson, M., Shafiullah, M., & Adeghate, E. (2005). Long-term effects of streptozotocin-induced diabetes on the electrocardiogram, physical activity and body temperature in rats. *Experimental Physiology*, *90*(6), 827–835. https://doi.org/10.1113/expphysiol.2005.031252

Howarth, F. C., Jacobson, M., Shafiullah, M., & Adeghate, E. (2008). Long-term effects of type 2 diabetes mellitus on heart rhythm in the Goto-Kakizaki rat. *Experimental Physiology*, *93*(3), 362–369. https://doi.org/10.1113/expphysiol.2007.040055

Howarth, F. C., Norstedt, G., Boldyriev, O. I., Qureshi, M. A., Mohamed, O., Parekh, K., Venkataraman, B., Subramanya, S., Shmygol, A., & Al Kury, L. T. (2020). Effects of prolactin on ventricular myocyte shortening and calcium transport in the streptozotocin-induced diabetic rat. *Heliyon*, *6*(4), e03797. https://doi.org/10.1016/j.heliyon.2020.e03797. Heliyon

Howarth, F. C., Nowotny, N., Zilahi, E., El Haj, M. A., & Lei, M. (2007). Altered expression of gap junction connexin proteins may partly underlie heart rhythm disturbances in the streptozotocin-induced diabetic rat heart. *Molecular and Cellular Biochemistry*, *305*(1–2), 145–151. https://doi.org/10.1007/S11010-007-9537-Z

Howarth, F. C., Parekh, K., Jayaprakash, P., Inbaraj, E. S., Oz, M., Dobrzynski, H., & Adrian, T. E. (2017). Altered profile of mRNA expression in atrioventricular node of streptozotocin-induced diabetic rats. *Molecular Medicine Reports*, *16*(4), 3720–3730. https://doi.org/10.3892/mmr.2017.7038

Howarth, F. C., & Qureshi, M. A. (2008). Myofilament sensitivity to Ca2+ in ventricular myocytes from the Goto-Kakizaki diabetic rat. *Molecular and Cellular Biochemistry*, *315*(1–2), 69–74. https://doi.org/10.1007/s11010-008-9790-9

Howarth, F. C., Qureshi, M. A., Hassan, Z., Al Kury, L. T., Isaev, D., Parekh, K., Yammahi, S. R. K. D. K. D., Oz, M., Adrian, T. E., & Adeghate, E. (2011). Changing pattern of gene expression is associated with ventricular myocyte dysfunction and altered mechanisms of Ca2+signalling in young type 2 Zucker diabetic fatty rat heart. *Experimental Physiology*, *96*(3), 325–337. https://doi.org/10.1113/expphysiol.2010.055574

Howarth, F. C., Qureshi, M. A., Hassan, Z., Isaev, D., Parekh, K., John, A., Oz, M., Raza, H., Adeghate, E., & Adrian, T. E. (2012). Contractility of ventricular myocytes is well preserved despite altered mechanisms of Ca2+ transport and a changing pattern of mRNA in aged type 2 Zucker diabetic fatty rat heart. *Molecular and Cellular Biochemistry*, *361*(1–2), 267–280. https://doi.org/10.1007/s11010-011-1112-y

Howarth, F. C., Qureshi, M. A., Jayaprakash, P., Parekh, K., Oz, M., Dobrzynski, H., & Adrian, T. E. (2018). The Pattern of mRNA Expression Is Changed in Sinoatrial Node from Goto-Kakizaki Type 2 Diabetic Rat Heart. *Journal of Diabetes Research*, *2018*, 8454078–8454090. https://doi.org/10.1155/2018/8454078

Huang, C., Ding, W., Li, L., & Zhao, D. (2006). Differences in the aging-associated trends of the monophasic action potential duration and effective refractory period of the right and left atria of the rat. *Circulation Journal : Official Journal of the Japanese Circulation Society*, *70*(3), 352–357. https://doi.org/10.1253/CIRCJ.70.352

Huang, H., Amin, V., Gurin, M., Wan, E., Thorp, E., Homma, S., & Morrow, J. P. (2013). Diet-induced obesity causes long QT and reduces transcription of voltage-gated potassium channels. *Journal of Molecular and Cellular Cardiology*, *59*, 151–158. https://doi.org/10.1016/j.yjmcc.2013.03.007

Huang, H., Pugsley, M. K., Fermini, B., Curtis, M. J., Koerner, J., Accardi, M., & Authier, S. (2017). Cardiac voltage-gated ion channels in safety pharmacology: Review of the landscape leading to the CiPA initiative. *Journal of Pharmacological and Toxicological Methods*, *87*, 11–23. https://doi.org/10.1016/j.vascn.2017.04.002

Huang, X., Zhong, N., Zhang, H., Ma, A., Yuan, Z., & Guo, N. (2017). Reduced expression of HCN channels in the sinoatrial node of streptozotocin-induced diabetic rats. *Canadian Journal of Physiology and Pharmacology*, *95*(5), 586–594. https://doi.org/10.1139/CJPP-2016-0418

Ingalls, A. M., Dickie, M. M., & Snell, G. D. (1950). Obese, a new mutation in the house mouse*. *Journal of Heredity*, *41*(12), 317–318. https://doi.org/10.1093/oxfordjournals.jhered.a106073

International Diabetes Federation. (2017). IDF Diabetes Atlas, 8th edn. In *International Diabetes Federation*. Retrieved from http://www.diabetesatlas.org. Accessed on October 12, 2018

International Diabetes Federation. (2021). IDF Diabetes Atlas, 10th edn. In *International Diabetes Federation.* Retrived from https://diabetesatlas.org/atlas. Accessed on February 14, 2022

Isfort, M., Stevens, S. C. W., Schaffer, S., Jong, J. C., & Wold, L. E. (2014). Metabolic dysfunction in diabetic cardiomyopathy. *Heart Failure Reviews*, *19*(1), 35–48. https://doi.org/10.1007/s10741-013-9377-8

Jensen, R. V., Jespersen, N. R., Støttrup, N. B., Povlsen, J. A., Hjortbak, M. V., Bøtker, H. E., Laursen, M. R., Hjort, J., & Løfgren, B. (2018). Influence of diabetes mellitus duration on the efficacy of ischemic preconditioning in a Zucker diabetic fatty rat model. *Plos One*, *13*(2), e0192981–e0192997. https://doi.org/10.1371/journal.pone.0192981

Jonas, M., Edelman, E. R., Groothuis, A., Baker, A. B., Seifert, P., & Rogers, C. (2005). Vascular neointimal formation and signaling pathway activation in response to stent injury in insulin-resistant and diabetic animals. *Circulation Research*, *97*(7), 725–733. https://doi.org/10.1161/01.RES.0000183730.52908.C6

Kashou, A. H., Basit, H., & Chhabra, L. (2022). Physiology, Sinoatrial Node. [ebook]. In StatPearls. StatPearls publishing. https://pubmed.ncbi.nlm.nih.gov/29083608/

Khalil, C. A., Al Suwaidi, J., Refaat, M., & Mohammedi, K. (2018). Cardiac complications of diabetes. *BioMed Research International*, *2018*, 8578394. https://doi.org/10.1155/2018/8578394

Kielkopf, C. L., Bauer, W., & Urbatsch, I. L. (2020). Bradford Assay for Determining Protein Concentration. *Cold Spring Harbor Protocols*, *2020*(4), 136–138. https://doi.org/10.1101/PDB.PROT102269

Kléber, A. G., & Rudy, Y. (2004). Basic mechanisms of cardiac impulse propagation and associated arrhythmias. *Physiological Reviews*, *84*(2), 431–488. https://doi.org/10.1152/physrev.00025.2003

Kondo, H., Kira, S., Oniki, T., Gotoh, K., Fukui, A., Abe, I., Ikebe, Y., Kawano, K., Saito, S., Aoki, K., Okada, N., Nagano, Y., Akioka, H., Shinohara, T., Akiyoshi, K., Masaki, T., Teshima, Y., Yufu, K., Nakagawa, M., & Takahashi, N. (2019). Interleukin-10 treatment attenuates sinus node dysfunction caused by streptozotocin-induced hyperglycaemia in mice. *Cardiovascular Research*, *115*(1), 57–70. https://doi.org/10.1093/CVR/CVY162

Kornreich, B. G. (2007). The patch clamp technique: principles and technical considerations. *Journal of Veterinary Cardiology : The Official Journal of the European Society of Veterinary Cardiology*, *9*(1), 25–37. https://doi.org/10.1016/J.JVC.2007.02.001

Krakauer, N. Y., & Krakauer, J. C. (2012). A new body shape index predicts mortality hazard independently of body mass index. *PLoS ONE*, *7*(7), 1–10. https://doi.org/10.1371/journal.pone.0039504

Krishnaswamy, P. S., Egom, E. E., Moghtadaei, M., Jansen, H. J., Azer, J., Bogachev, O., Mackasey, M., Robbins, C., & Rose, R. A. (2015). Altered parasympathetic nervous system regulation of the sinoatrial node in Akita diabetic mice. *Journal of Molecular and Cellular Cardiology*, *82*, 125–135. https://doi.org/10.1016/J.YJMCC.2015.02.024

Kuwahara, M., Yayou, K. ichi, Ishii, K., Hashimoto, S. ichi, Tsubone, H., & Sugano, S. (1994). Power spectral analysis of heart rate variability as a new method for assessing autonomic activity in the rat. *Journal of Electrocardiology*, *27*(4), 333–337. https://doi.org/10.1016/S0022-0736(05)80272-9

Lainé, J., Skoglund, G., Fournier, E., & Tabti, N. (2018). Development of the excitation-contraction coupling machinery and its relation to myofibrillogenesis in human iPSC-derived skeletal myocytes. *Skeletal Muscle*, *8*(1), 1-13. https://doi.org/10.1186/s13395-017-0147-5

Landstrom, A. P., Dobrev, D., & Wehrens, X. H. T. (2017). Calcium Signaling and Cardiac Arrhythmias. In *Circulation Research*. 120(12), 1969–1993. https://doi.org/10.1161/CIRCRESAHA.117.310083

Laughlin, M. H., Woodman, C. R., Ray, C. A., Behnke, B. J., Lesniewski, L. A., Donato, A. J., & Delp, M. D. (2008). Decreased NO signaling leads to enhanced vasoconstrictor responsiveness in skeletal muscle arterioles of the ZDF rat prior to overt diabetes and hypertension. *American Journal of Physiology-Heart and Circulatory Physiology*, *294*(4), H1840–H1850. https://doi.org/10.1152/ajpheart.00692.2007

Leopoldo, A. S., Lima-Leopoldo, A. P., Sugizaki, M. M., do Nascimento, A. F., de Campos, D. H. S., de Azevedo Melo Luvizotto, R., Castardeli, E., Alves, C. A. B., Brum, P. C., & Cicogna, A. C. (2011). Involvement of L-type calcium channel and serca2a in myocardial dysfunction induced by obesity. *Journal of Cellular Physiology*, *226*(11), 2934–2942. https://doi.org/10.1002/jcp.22643

Levi, A. J., Hancox, J. C., Howarth, F. C., Croker, J., & Vinnicombe, J. (1996). A method for making rapid changes of superfusate whilst maintaining temperature at 37°C. *Pflugers Archiv European Journal of Physiology*, *432*(5), 930–937. https://doi.org/10.1007/s004240050217

Li, J., Yan, B., Huo, Z., Liu, Y., Xu, J., Sun, Y., Liu, Y., Liang, D., Peng, L., Zhang, Y., Zhou, Z.-N., Shi, J., Cui, J., & Chen, Y. H. (2010). β 2 - but not β 1 -adrenoceptor activation modulates intracellular oxygen availability. *The Journal of Physiology*, *588*(16), 2987–2998. https://doi.org/10.1113/jphysiol.2010.190900

Lima-Leopoldo, A. P., Sugizaki, M. M., Leopoldo, A. S., Carvalho, R. F., Nogueira, C. R., Nascimento, A. F., Martinez, P. F., Luvizotto, R. A. M., Padovani, C. R., & Cicogna, A. C. (2008). Obesity induces upregulation of genes involved in myocardial Ca2+ handling. *Brazilian Journal of Medical and Biological Research*, *41*(7), 615–620. https://doi.org/10.1590/S0100-879X2008000700011

Lin, Y.C. C., Hull, R., Huang, J., Martin, K. H., Davis, M., Hileman, S., Yu, H.-G. G., Martin, K. H., Hull, R., Davis, M., & Yu, H. G. G. (2015). Leptin decreases heart rate associated with increased ventricular repolarization via its receptor. *American Journal of Physiology-Heart and Circulatory Physiology*, *309*(10), H1731–H1739. https://doi.org/10.1152/ajpheart.00623.2015

Lin, Y. C., Huang, J., Kan, H., Castranova, V., Frisbee, J. C., & Yu, H. G. (2012). Defective calcium inactivation causes long QT in obese insulin-resistant rat. *American Journal of Physiology - Heart and Circulatory Physiology*, *302*(4), 1013–1022. https://doi.org/10.1152/ajpheart.00837.2011

Lishner, M., Akselrod, S., Mor Avi, V., Oz, O., Divon, M., & Ravid, M. (1987). Spectral analysis of heart rate fluctuations. A non-invasive, sensitive method for the early diagnosis of autonomic neuropathy in diabetes mellitus. *Journal of the Autonomic Nervous System*, *19*(2), 119–125. https://doi.org/10.1016/0165-1838(87)90005-1

Lo Giudice, P., Careddu, A., Magni, G., Quagliata, T., Pacifici, L., & Carminati, P. (2002). Autonomic neuropathy in streptozotocin diabetic rats: effect of acetyl-L-carnitine. *Diabetes Research and Clinical Practice*, *56*(3), 173–180. https://doi.org/10.1016/S0168-8227(01)00375-8

Lockhart, M. M., Phelps, A. L., van den Hoff, M. J. B., & Wessels, A. (2014). The epicardium and the development of the atrioventricular junction in the murine heart. *Journal of Developmental Biology*, *2*(1), 1–17. https://doi.org/10.3390/jdb2010001

López-Soldado, I., Niisuke, K., Veiga, C., Adrover, A., Manzano, A., Martínez-Redondo, V., Camps, M., Bartrons, R., Zorzano, A., & Gumà, A. (2016). Neuregulin improves response to glucose tolerance test in control and diabetic rats. *American Journal of Physiology. Endocrinology and Metabolism*, *310*(6), E440–E451. https://doi.org/10.1152/AJPENDO.00226.2015

Low Wang, C. C., Hess, C. N., Hiatt, W. R., & Goldfine, A. B. (2016). Clinical update: Cardiovascular disease in diabetes mellitus. *Circulation*, *133*(24), 2459–2502. https://doi.org/10.1161/CIRCULATIONAHA.116.022194

Lum-Naihe, K., Toedebusch, R., Mahmood, A., Bajwa, J., Carmack, T., Kumar, S. A., Ardhanari, S., Demarco, V. G., Emter, C. A., & Pulakat, L. (2017). Cardiovascular disease progression in female Zucker Diabetic Fatty rats occurs via unique mechanisms compared to males. *Scientific Reports*, *7*(1), 17823–17839. https://doi.org/10.1038/s41598-017-18003-8

Mabe, A. M., & Hoover, D. B. (2011). Remodeling of cardiac cholinergic innervation and control of heart rate in mice with streptozotocin-induced diabetes. *Autonomic Neuroscience : Basic & Clinical*, *162*(1–2), 24–31. https://doi.org/10.1016/J.AUTNEU.2011.01.008

Mahadevan, V. (2012). Anatomy of the heart. *Surgery (Oxford)*, *30*(1), 5–8. https://doi.org/10.1016/j.mpsur.2011.10.011

Mahmood, T., & Yang, P. C. (2012). Western Blot: Technique, Theory, and Trouble Shooting. *North American Journal of Medical Sciences*, *4*(9), 429. https://doi.org/10.4103/1947-2714.100998

Maier, L. S., Wahl-Schott, C., Horn, W., Weichert, S., Pagel, C., Wagner, S., Dybkova, N., Müller, O. J., Näbauer, M., Franz, W. M., & Pieske, B. (2005). Increased SR Ca2+ cycling contributes to improved contractile performance in SERCA2a-overexpressing transgenic rats. *Cardiovascular Research*, *67*(4), 636–646. https://doi.org/10.1016/j.cardiores.2005.05.006

Malatesta, M. (2021). Transmission Electron Microscopy as a Powerful Tool to Investigate the Interaction of Nanoparticles with Subcellular Structures. *International Journal of Molecular Sciences*, *22*(23), 12789. https://doi.org/10.3390/IJMS222312789

Marks, A. R. (2019). Cardiac and circulatory function. In *Goldman-Cecil Medicine* (26th ed)., Vol. 1, 241.e1-245.e3. Elsevier Inc.

Marsh, S. A., Powell, P. C., Agarwal, A., Dell'Italia, L. J., & Chatham, J. C. (2007). Cardiovascular dysfunction in Zucker obese and Zucker diabetic fatty rats: Role of hydronephrosis. *American Journal of Physiology - Heart and Circulatory Physiology*, *293*(1), H292-H298. https://doi.org/10.1152/ajpheart.01362.2006

Martín-Timón, I., Martin-Timon, I., Sevillano-Collantes, C., Segura-Galindo, A., & Del Canizo-Gomez, F. J. (2014). Type 2 diabetes and cardiovascular disease: Have all risk factors the same strength? *World Journal of Diabetes*, *5*(4), 444–471. https://doi.org/10.1080/15421400701220361

Martín, F. J. F., Martínez, A. L., Llopis, M. V., Rodriguez, J. C. C., Viejo, C. B., & Vershinin, Y. A. (2015). An ECG lab project for teaching signal conditioning systems in a master's degree in mechatronic engineering. *Advances in Engineering Education*, *4*(3), 29–37. https://doi.org/10.1152/advan.00105.2016

Masuzawa, A., Black, K. M., Pacak, C. A., Ericsson, M., Barnett, R. J., Drumm, C., Seth, P., Bloch, D. B., Levitsky, S., Cowan, D. B., & McCully, J. D. (2013). Transplantation of autologously derived mitochondria protects the heart from ischemia-reperfusion injury. *American Journal of Physiology - Heart and Circulatory Physiology*, *304*(7), H966–H982. https://doi.org/10.1152/ajpheart.00883.2012

Matafome, P., Rodrigues, T., Sena, C., & Seiça, R. (2017). Methylglyoxal in Metabolic Disorders: Facts, Myths, and Promises. *Medicinal Research Reviews*, *37*(2), 368–403. https://doi.org/10.1002/med.21410

Mattiazzi, A., Garay, A., & Cingolani, H. E. (1986). Critical evaluation of isometric indexes of relaxation in rat and cat papillary muscles and toad ventricular strips. *Journal of Molecular and Cellular Cardiology*, *18*(7), 749–758. https://doi.org/10.1016/S0022-2828(86)80946-4

Mayfield, J. (1998). Diagnosis and Classification of Diabetes Mellitus: New Criteria. *American Family Physician*, *58*(6), 1355–1362. https://doi.org/10.2337/dc14-S081

McGivern, J. G., & Worley, J. F. (2007). Ion Channels – Voltage Gated. In J. B. T. J. Triggle (Ed.), *Comprehensive Medicinal Chemistry II* (2nd ed). 827–875. Elsevier. https://doi.org/10.1016/b0-08-045044-x/00066-3

Meftahi, G. H., Bahari, Z., Zarei Mahmoudabadi, A., Iman, M., & Jangravi, Z. (2021). Applications of western blot technique: From bench to bedside. *Biochemistry and Molecular Biology Education*, *49*(4), 509–517. https://doi.org/10.1002/BMB.21516

Mirza, M., Marston, S., Willott, R., Ashley, C., Mogensen, J., McKenna, W., Robinson, P., Redwood, C., & Watkins, H. (2005). Dilated cardiomyopathy mutations in three thin filament regulatory proteins result in a common functional phenotype. *Journal of Biological Chemistry*, *280*(31), 28498–28506. https://doi.org/10.1074/jbc.M412281200

Sherman-Gold, R., & H. Maertz, W. (2012). *The Axon Guide: electrophysiology and biophysics laboratory techniques*. Third edition. Molecular Devices.

Mori, S., Spicer, D. E., & Anderson, R. H. (2016). Revisiting the Anatomy of the Living Heart. *Circulation Journal*, *80*(1), 24–33. https://doi.org/10.1253/circj.CJ-15-1147

Mortuza, R., & Chakrabarti, S. (2014). Glucose-induced cell signaling in the pathogenesis of diabetic cardiomyopathy. *Heart Failure Reviews*, *19*(1), 75–86. https://doi.org/10.1007/s10741-013-9381-z

Mourmoura, E., Vial, G., Laillet, B., Rigaudière, J.-P., Hininger-Favier, I., Dubouchaud, H., Morio, B., & Demaison, L. (2013). Preserved endothelium-dependent dilatation of the coronary microvasculature at the early phase of diabetes mellitus despite the increased oxidative stress and depressed cardiac mechanical function ex vivo. *Cardiovascular Diabetology*, *12*(1), 49–66. https://doi.org/10.1186/1475-2840-12-49

Murarka, S., & Movahed, M. R. (2010). Diabetic Cardiomyopathy. *Journal of Cardiac Failure*, *16*(12), 971–979. https://doi.org/10.1016/J.CARDFAIL.2010.07.249

Nam, S. M., Kim, Y. N., Yoo, D. Y., Yi, S. S., Choi, J. H., Hwang, I. K., Seong, J. K., & Yoon, Y. S. (2013). Hypothyroidism affects astrocyte and microglial morphology in type 2 diabetes. *Neural Regeneration Research*, *8*(26), 2458–2467. https://doi.org/10.3969/J.ISSN.1673-5374.2013.26.007

National Center for Biotechnology Information (2022). PubChem Compound Summary for CID 5807, Isoproterenol hydrochloride. Retrieved from https://pubchem.ncbi.nlm.nih.gov/compound/Isoproterenol-hydrochloride. Accessed on April 23, 2022

Neill, U. S. (2013). A conversation with Jeffrey M. Friedman. *Journal of Clinical Investigation*, *123*(2), 529–530. https://doi.org/10.1172/JCI68394

Nguyen, A., & Wahed, A. (2013). Sources of Errors in Hematology and Coagulation Testing. *Accurate Results in the Clinical Laboratory: A Guide to Error Detection and Correction*, 305–314. https://doi.org/10.1016/B978-0-12-415783-5.00019-0

NHLBI Obesity Education Initiative Expert Panel. National Institutes of Health. National Heart Lung and Blood Institute. (n.d.). The Practical Guide: Identification, Evaluation, and Treatment of Overweight and Obesity in Adults. *NIH Publication*, No. 00-4084.

Noda, N., Hayashi, H., Satoh, H., Terada, H., Hirano, M., Kobayashi, A., & Yamazaki, N. (1993). Ca2+ transients and cell shortening in diabetic rat ventricular myocytes. *Japanese Circulation Journal*, *57*(5), 449–457. https://doi.org/10.1253/jcj.57.449

Nowakowski, A. B., Wobig, W. J., & Petering, D. H. (2014). Native SDS-PAGE: High Resolution Electrophoretic Separation of Proteins With Retention of Native Properties Including Bound Metal Ions. *Metallomics : Integrated Biometal Science*, *6*(5), 1068. https://doi.org/10.1039/C4MT00033A

Nygren, A., Olson, M. L., Chen, K. Y., Emmett, T., Kargacin, G., & Shimoni, Y. (2007). Propagation of the cardiac impulse in the diabetic rat heart: Reduced conduction reserve. *Journal of Physiology*, *580*(2), 543–560. https://doi.org/10.1113/jphysiol.2006.123729

Obayashi, M., Xiao, B., Stuyvers, B. D., Davidoff, A. W., Mei, J., Chen, S. R. W., & Ter Keurs, H. E. D. J. (2006). Spontaneous diastolic contractions and phosphorylation of the cardiac ryanodine receptor at serine-2808 in congestive heart failure in rat. *Cardiovascular Research*, *69*(1), 140–151. https://doi.org/10.1016/J.CARDIORES.2005.07.010

Okruhlicova, L., Tribulova, N., Weismann, P., & Sotnikova, R. (2005). Ultrastructure and histochemistry of rat myocardial capillary endothelial cells in response to diabetes and hypertension. *Cell Research 2005 15:7*, *15*(7), 532–538. https://doi.org/10.1038/sj.cr.7290322

Onal, B., Gratz, D., & Hund, T. J. (2017). Ca2+/calmodulin-dependent kinase II-dependent regulation of atrial myocyte late Na+ current, Ca2+ cycling, and excitability: a mathematical modeling study. *American Journal of Physiology. Heart and Circulatory Physiology*, *313*(6), H1227–H1239. https://doi.org/10.1152/ajpheart.00185.2017

Pavlović, D., McLatchie, L. M., & Shattock, M. J. (2010). The rate of loss of T-tubules in cultured adult ventricular myocytes is species dependent. *Experimental Physiology*, *95*(4), 518–527. https://doi.org/10.1113/EXPPHYSIOL.2009.052126

Pennycook, S. J., Lupini, A. R., Varela, M., Borisevich, A., Peng, Y., Oxley, M. P., Van Benthem, K., & Chisholm, M. F. (2006). Scanning Transmission Electron Microscopy for Nanostructure Characterization. In *Scanning Microscopy for Nanotechnology: Techniques and Applications*. 152–191. Springer, New York, NY. https://doi.org/10.1007/978-0-387-39620-0_6

Pereira, L., Matthes, J., Schuster, I., Valdivia, H. H., Herzig, S., Richard, S., & Gómez, A. M. (2006). Mechanisms of [Ca2+]i transient decrease in cardiomyopathy of db/db type 2 diabetic mice. *Diabetes*, *55*(3), 608–615. https://doi.org/10.2337/diabetes.55.03.06.db05-1284

Pfeiffer, E. R., Tangney, J. R., Omens, J. H., & McCulloch, A. D. (2014). Biomechanics of cardiac electromechanical coupling and mechanoelectric feedback. *J Biomech Eng*, *136*(2), 021007–021018. https://doi.org/10.1115/1.4026221

Pinnell, J., Turner, S., & Howell, S. (2007). Cardiac muscle physiology. *Continuing Education in Anaesthesia, Critical Care and Pain*, *7*(3), 85–88. https://doi.org/10.1093/bjaceaccp/mkm013

Ploug, T., Braunstein, T. H., Olsen, K. B., Holstein-Rathlou, N.-H., Axelsen, L. N., Sørensen, C. M., Nielsen, M. S., & Andersen, C. B. (2013). Myocardial impulse propagation is impaired in right ventricular tissue of Zucker Diabetic Fatty (ZDF) rats. *Cardiovascular Diabetology*, *12*(1), 19–30. https://doi.org/10.1186/1475-2840-12-19

Posner, B. I. (2017). Insulin Signalling: The Inside Story. *Canadian Journal of Diabetes*, *41*(1), 108–113. https://doi.org/10.1016/j.jcjd.2016.07.002

Qadota, H., & Benian, G. M. (2010). Molecular Structure of Sarcomere-to-Membrane Attachment at M-Lines in C. elegans Muscle. *Journal of Biomedicine and Biotechnology*, *2010*, 1–9. https://doi.org/10.1155/2010/864749

Radovits, T., Korkmaz, S., Mátyás, C., Oláh, A., Németh, B. T., Páli, S., Hirschberg, K., Zubarevich, A., Gwanmesia, P. N., Li, S., Loganathan, S., Barnucz, E., Merkely, B., & Szabó, G. (2015). An Altered Pattern of Myocardial Histopathological and Molecular Changes Underlies the Different Characteristics of Type-1 and Type-2 Diabetic Cardiac Dysfunction. *Journal of Diabetes Research*, *2015*, 728741–728753. https://doi.org/10.1155/2015/728741

Rao, A. C. A., Ng, A. C. C., Sy, R. W., Chia, K. K. M., Hansen, P. S., Chiha, J., Kilian, J., & Kanagaratnam, L. B. (2021). Electrocardiographic QRS duration is influenced by body mass index and sex. *International Journal of Cardiology. Heart & Vasculature*, *37*, 100884. https://doi.org/10.1016/j.ijcha.2021.100884

Raza, H., John, A., & Howarth, F. C. (2012). Alterations in Glutathione Redox Metabolism, Oxidative Stress, and Mitochondrial Function in the Left Ventricle of Elderly Zucker Diabetic Fatty Rat Heart. *International Journal of Molecular Sciences*, *13*(12), 16241–16254. https://doi.org/10.3390/ijms131216241

Reaven, G. M. (1988). Role of insulin resistance in human disease. *Diabetes*, *37*(12), 1595–1607. https://doi.org/10.2337/diab.37.12.1595

Relling, D. P., Esberg, L. B., Fang, C. X., Johnson, W. T., Murphy, E. J., Carlson, E. C., Saari, J. T., & Ren, J. (2006). High-fat diet-induced juvenile obesity leads to cardiomyocyte dysfunction and upregulation of Foxo3a transcription factor independent of lipotoxicity and apoptosis. *Journal of Hypertension*, *24*(3), 549–561. https://doi.org/10.1097/01.HJH.0000203846.34314.94

Reuter, H., Grönke, S., Adam, C., Ribati, M., Brabender, J., Zobel, C., Frank, K. F., Wippermann, J., Schwinger, R. H. G., Brixius, K., & Müller-Ehmsen, J. (2008). Sarcoplasmic Ca2+ release is prolonged in nonfailing myocardium of diabetic patients. *Molecular and Cellular Biochemistry*, *308*(1–2), 141–149. https://doi.org/10.1007/s11010-007-9622-3

Ricci, E., Smallwood, S., Chouabe, C., Mertani, H. C., Raccurt, M., Morel, G., & Bonvallet, R. (2006). Electrophysiological characterization of left ventricular myocytes from obese Srague-Dwley rat. *Obesity*, *14*(5), 778–786. https://doi.org/10.1038/oby.2006.90

Rowan, W. H., Campen, M. J., Wichers, L. B., & Watkinson, W. P. (2007). Heart rate variability in rodents: uses and caveats in toxicological studies. *Cardiovascular Toxicology*, *7*(1), 28–51. https://doi.org/10.1007/S12012-007-0004-6

Sahraoui, A., Dewachter, C., De Medina, G., Naeije, R., Bouguerra, S. A., & Dewachter, L. (2016). Myocardial structural and biological anomalies induced by high fat diet in Psammomys obesus gerbils. *PLoS ONE*, *11*(2), 1–16. https://doi.org/10.1371/journal.pone.0148117

Sakakibara, M., Hirashiki, A., Cheng, X. W., Bando, Y., Ohshima, K., Okumura, T., Funahashi, H., Ohshima, S., & Murohara, T. (2011). Association of diabetes mellitus with myocardial collagen accumulation and relaxation impairment in patients with dilated cardiomyopathy. *Diabetes Research and Clinical Practice*, *92*(3), 348–355. https://doi.org/10.1016/J.DIABRES.2011.02.023

Sanyal, S. N., Arita, M., & Ono, K. (2002). Inhomogeneous derangement of cardiac autonomic nerve control in diabetic rats. *Circulation Journal : Official Journal of the Japanese Circulation Society*, *66*(3), 283–288. https://doi.org/10.1253/CIRCJ.66.283

Sárközy, M., Zvara, Á., Gyémánt, N., Fekete, V., Kocsis, G. F., Pipis, J., Szucs, G., Csonka, C., Puskás, L. G., Ferdinandy, P., & Csont, T. (2013). Metabolic syndrome influences cardiac gene expression pattern at the transcript level in male ZDF rats. *Cardiovascular Diabetology*, *12*(1), 16. https://doi.org/10.1186/1475-2840-12-16

Schach, C., Resch, M., Schmid, P. M., Riegger, G. A., & Endemann, D. H. (2014). Type 2 diabetes: increased expression and contribution of IK Ca channels to vasodilation in small mesenteric arteries of ZDF rats. *American Journal of Physiology-Heart and Circulatory Physiology*, *307*(8), H1093–H1102. https://doi.org/10.1152/ajpheart.00240.2013

Schaffer, S. W. (1991). Cardiomyopathy associated with noninsulin-dependent diabetes. *Molecular and Cellular Biochemistry*, *107*(1), 1–20. https://doi.org/10.1007/BF02424571

Schneider, C. A., Rasband, W. S., & Eliceiri, K. W. (2012). NIH Image to ImageJ: 25 years of Image Analysis. *Nature Methods*, *9*(7), 671. https://doi.org/10.1038/NMETH.2089

Sequeira, V., Wijnker, P. J. M., Nijenkamp, L. L. A. M., Kuster, D. W. D., Najafi, A., Witjas-Paalberends, E. R., Regan, J. A., Boontje, N., Ten Cate, F. J., Germans, T., Carrier, L., Sadayappan, S., Van Slegtenhorst, M. A., Zaremba, R., Foster, D. B., Murphy, A. M., Poggesi, C., Dos Remedios, C., Stienen, G. J. M., … Van Der Velden, J. (2013). Perturbed length-dependent activation in human hypertrophic cardiomyopathy with missense sarcomeric gene mutations. *Circulation Research*, *112*(11), 1491–1505. https://doi.org/10.1161/CIRCRESAHA.111.300436

Shao, C. H., Rozanski, G. J., Patel, K. P., & Bidasee, K. R. (2007). Dyssynchronous (non-uniform) Ca2+ release in myocytes from streptozotocin-induced diabetic rats. *Journal of Molecular and Cellular Cardiology*, *42*(1), 234–246. https://doi.org/10.1016/j.yjmcc.2006.08.018

Sheu, S. S., Sharma, V. K., & Banerjee, S. P. (1984). Measurement of cytosolic free calcium concentration in isolated rat ventricular myocytes with Quin 2. *Circulation Research*, *55*(6), 830–834. https://doi.org/10.1161/01.RES.55.6.830

Shih, H.-T. T. (1994). Anatomy of the Action Potential in the Heart. *Texas Heart Institute*, *21*(1), 30–41.

Silverthorn, D. U., Ober, W. C., Garrison, C. W., Silverthorn, A. C., & Johnson, B. R. (2007). *Human physiology: an integrated approach* (5th ed.). Pearson Education Inc/Benjamin Cummings.

Simonds, S. E., Pryor, J. T., Ravussin, E., Greenway, F. L., Dileone, R., Allen, A. M., Bassi, J., Elmquist, J. K., Keogh, J. M., Henning, E., Myers, M. G., Licinio, J., Brown, R. D., Enriori, P. J., O'Rahilly, S., Sternson, S. M., Grove, K. L., Spanswick, D. C., Farooqi, I. S., & Cowley, M. A. (2014). Leptin mediates the increase in blood pressure associated with obesity. *Cell*, *159*(6), 1404–1416. https://doi.org/10.1016/j.cell.2014.10.058

Sista, A. K., O'Connell, M. K., Hinohara, T., Oommen, S. S., Fenster, B. E., Glassford, A. J., Schwartz, E. A., Taylor, C. A., Reaven, G. M., & Tsao, P. S. (2005). Increased aortic stiffness in the insulin-resistant Zucker fa/fa rat. *Am J Physiol Heart Circ Physiol*, *289*(2), H845–H851. https://doi.org/10.1152/ajpheart.00134.2005

Smail, M., Al Kury, L., Qureshi, M. A., Shmygol, A., Oz, M., Singh, J., & Howarth, F. C. (2018). Cell shortening and calcium dynamics in epicardial and endocardial myocytes from the left ventricle of Goto-Kakizaki type 2 diabetic rats. *Experimental Physiology*, *103*(4), 502–511. https://doi.org/10.1113/EP086542

Smail, M. M. A., Qureshi, M. A., Shmygol, A., Oz, M., Singh, J., Sydorenko, V., Arabi, A., Howarth, F. C., & Al Kury, L. (2016). Regional effects of streptozotocin-induced diabetes on shortening and calcium transport in epicardial and endocardial myocytes from rat left ventricle. *Physiological Reports*, *4*(22), e13034. https://doi.org/10.14814/phy2.13034

Snyders, D. J. (1999). Structure and function of cardiac potassium channels. *Cardiovascular Research*, *42*(2), 377–390. https://doi.org/10.1016/S0008-6363(99)00071-1

Solaro, R. J., & Rarick, H. M. (1998). Troponin and tropomyosin: proteins that switch on and tune in the activity of cardiac myofilaments. *Circulation Research*, *83*(5), 471–480. https://doi.org/10.1161/01.RES.83.5.471

Spurgeon, H. A., duBell, W. H., Stern, M. D., Sollott, S. J., Ziman, B. D., Silverman, H. S., Capogrossi, M. C., Talo, A., & Lakatta, E. G. (1992). Cytosolic calcium and myofilaments in single rat cardiac myocytes achieve a dynamic equilibrium during twitch relaxation. *The Journal of Physiology*, *447*(1), 83–102. https://doi.org/10.1113/JPHYSIOL.1992.SP018992

Stølen, T. O., Høydal, M. A., Kemi, O. J., Catalucci, D., Ceci, M., Aasum, E., Larsen, T., Rolim, N., Condorelli, G., Smith, G. L., & Wisløff, U. (2009). Interval training normalizes cardiomyocyte function, diastolic Ca 2+ control, and SR Ca2+ release synchronicity In a mouse model of diabetic cardiomyopathy. *Circulation Research*, *105*(6), 527–536. https://doi.org/10.1161/CIRCRESAHA.109.199810

Sultan, A., Jacobson, M., Adeghate, E., Oulhaj, A., Shafiullah, M., Qureshi, A., & Howarth, F. C. (2021). Effects of obesity and diabesity on heart rhythm in the Zucker rat. *Clinical and Experimental Pharmacology and Physiology*, *48*(5), 735–747. https://doi.org/10.1111/1440-1681.13473

Swinburn, B. A., Kraak, V. I., Allender, S., Atkins, V. J., Baker, P. I., Bogard, J. R., Brinsden, H., Calvillo, A., De Schutter, O., Devarajan, R., Ezzati, M., Friel, S., Goenka, S., Hammond, R. A., Hastings, G., Hawkes, C., Herrero, M., Hovmand, P. S., Howden, M., … Dietz, W. H. (2019). The Global Syndemic of Obesity, Undernutrition, and Climate Change: The Lancet Commission report. *The Lancet*, *393*(10173), 791–846. https://doi.org/10.1016/S0140-6736(18)32822-8

Taegtmeyer, H., McNulty, P., & Young, M. E. (2002). Adaptation and maladaptation of the heart in diabetes: Part I: general concepts. *Circulation*, *105*(14), 1727–1733. https://doi.org/10.1161/01.CIR.0000012466.50373.E8

Takaya, K., Ogawa, Y., Isse, N., Okazaki, T., Satoh, N., Masuzaki, H., Mori, K., Tamura, N., Hosoda, K., & Nakao, K. (1996). Molecular cloning of rat leptin receptor isoform complementary DNAs-identification of a missense mutation in Zucker fatty (fa/fa) rats. *Biochemical and Biophysical Research Communications*, *225*(1), 75–83. https://doi.org/10.1006/bbrc.1996.1133

Task Force. (1996). Heart rate variability: standards of measurement, physiological interpretation and clinical use. Task Force of the European Society of Cardiology and the North American Society of Pacing and Electrophysiology. *Eur. Heart J.*, *17*(17), 354–381. https://doi.org/10.1161/01.CIR.93.5.1043

ter Keurs, H. E. D. J., Shinozaki, T., Zhang, Y. M., Zhang, M. L., Wakayama, Y., Sugai, Y., Kagaya, Y., Miura, M., Boyden, P. A., Stuyvers, B. D. M., & Landesberg, A. (2008). Sarcomere mechanics in uniform and non-uniform cardiac muscle: A link between pump function and arrhythmias. *Progress in Biophysics and Molecular Biology*, *97*(2–3), 312–331. https://doi.org/10.1016/j.pbiomolbio.2008.02.013

Teunissen, B. E. J., & Bierhuizen, M. F. A. (2004). Transcriptional control of myocardial connexins. *Cardiovascular Research*, *62*(2), 246–255. https://doi.org/10.1016/j.cardiores.2003.12.011

Thaung, H. P. A., Baldi, J. C., Wang, H. Y., Hughes, G., Cook, R. F., Bussey, C. T., Sheard, P. W., Bahn, A., Jones, P. P., Schwenke, D. O., & Lamberts, R. R. (2015). Increased Efferent Cardiac Sympathetic Nerve Activity and Defective Intrinsic Heart Rate Regulation in Type 2 Diabetes. *Diabetes*, *64*(8), 2944–2956. https://doi.org/10.2337/DB14-0955

Thomas D. Pollard, William C. Earnshaw, Jennifer Lippincott-Schwartz, & Graham T. Johnson. (2017). Introduction to Cells. In Cell Biology (3rd ed) . 3–14. https://www-clinicalkey-com.uaeu.idm.oclc.org/student/content/book/3-s2.0-B9780323341264000013. Elsevier

Tomlinson, D. R., & Yusof, A. P. M. (1983). Autonomic neuropathy in the alloxan-diabetic rat. *Journal of Autonomic Pharmacology*, *3*(4), 257–263. https://doi.org/10.1111/J.1474-8673.1983.TB00543.X

Turpie, A. G. G., Bauer, K. A., Eriksson, B. I., & Lassen, M. R. (2002). Overweight and obesity as determinants of cardiovascular risk: The Framingham experience. *Archives of Internal Medicine*, *162*(16), 1867–1872. https://doi.org/10.1001/archinte.162.16.1867

VanHoose, L., Sawers, Y., Loganathan, R., Vacek, J. L., Stehno-Bittel, L., Novikova, L., Al-Jarrah, M., & Smirnova, I. V. (2010). Electrocardiographic changes with the onset of diabetes and the impact of aerobic exercise training in the Zucker Diabetic Fatty (ZDF) rat. *Cardiovascular Diabetology*, *9*, 56–66. https://doi.org/10.1186/1475-2840-9-56

Vasanji, Z., Dhalla, N. S., & Netticadan, T. (2004). Increased inhibition of SERCA2 by phospholamban in the type I diabetic heart. *Molecular and Cellular Biochemistry*, *261*(1), 245–249. https://doi.org/10.1023/B:MCBI.0000028762.97754.26

Wang, B., Chandrasekera, P. C., & Pippin, J. J. (2014). Leptin- and Leptin Receptor-Deficient Rodent Models: Relevance for Human Type 2 Diabetes. *Current Diabetes Reviews*, *10*(2), 131–145. https://doi.org/10.2174/1573399810666140508121012

Wang, P., Zeng, H., Lloyd, S. G., Bonen, A., & Chatham, J. C. (2004). Impact of altered substrate utilization on cardiac function in isolated hearts from Zucker diabetic fatty rats. *American Journal of Physiology-Heart and Circulatory Physiology*, *288*(5), H2102–H2110. https://doi.org/10.1152/ajpheart.00935.2004

Weyer, C., Funahashi, T., Tanaka, S., Hotta, K., Matsuzawa, Y., Pratley, R. E., & Tataranni, P. A. (2001). Hypoadiponectinemia in Obesity and Type 2 Diabetes: Close Association with Insulin Resistance and Hyperinsulinemia. *The Journal of Clinical Endocrinology & Metabolism*, *86*(5), 1930–1935. https://doi.org/10.1210/jcem.86.5.7463

World Health Organization. (2018). Fact Sheets. Obesity and overweight. WHO. Retreived from https://www.who.int/en/news-room/fact-sheets/detail/obesity-and-overweight. Accessed on February 14, 2020

Wu, Y., Ding, Y., Tanaka, Y., & Zhang, W. (2014). Risk factors contributing to type 2 diabetes and recent advances in the treatment and prevention. *International Journal of Medical Sciences*, *11*(11), 1185–1200. https://doi.org/10.7150/ijms.10001

Yaras, N., Ugur, M., Ozdemir, S., Gurdal, H., Purali, N., Lacampagne, A., Vassort, G., & Turan, B. (2005). Effects of diabetes on ryanodine receptor Ca release channel (RyR2) and Ca2+ homeostasis in rat heart. *Diabetes*, *54*(11), 3082–3088. https://doi.org/10.2337/DIABETES.54.11.3082

Yokoi, N., Hoshino, M., Hidaka, S., Yoshida, E., Beppu, M., Hoshikawa, R., Sudo, K., Kawada, A., Takagi, S., & Seino, S. (2013). A Novel Rat Model of Type 2 Diabetes: The Zucker Fatty Diabetes Mellitus ZFDM Rat. *Journal of Diabetes Research*, *2013*, 103731–103740. https://doi.org/10.1155/2013/103731

Zhang, Y., Wang, Y., Yanni, J., Qureshi, M. A., Logantha, S. J. R. J., Kassab, S., Boyett, M. R., Gardiner, N. J., Sun, H., Howarth, F. C., & Dobrzynski, H. (2019). Electrical Conduction System Remodeling in Streptozotocin-Induced Diabetes Mellitus Rat Heart. *Frontiers in Physiology*, *10*. https://doi.org/10.3389/FPHYS.2019.00826

Zhou, B. Q., Hu, S. J., & Wang, G. Bin. (2006). The analysis of ultrastructure and gene expression of sarco/endoplasmic reticulum calcium handling proteins in alloxan-induced diabetic rat myocardium. *Acta Cardiologica*, *61*(1), 21–27. https://doi.org/10.2143/AC.61.1.2005136

Zimmet, P., Alberti, K. G. M. M., & Shaw, J. (2001). Global and societal implications of the diabetes epidemic. *Nature*, *414*(6865), 782–787. https://doi.org/10.1038/414782a

List of Publications

Sultan, A., Adeghate, E., Emerald, B. S., Qureshi, M. A., Minhas, S. T., & Howarth, F. C. (2022). Effects of Obesity and Diabesity on Ventricular Muscle Structure and Function in the Zucker Rat. *Life, 12*(8), 1221. https://doi.org/10.3390/LIFE12081221

Sultan, A., Jacobson, M., Adeghate, E., Oulhaj, A., Shafiullah, M., Qureshi, A., & Howarth, F. C. (2021). Effects of obesity and diabesity on heart rhythm in the Zucker rat. *Clinical and Experimental Pharmacology and Physiology, 48*(5), 735–747. https://doi.org/10.1111/1440-1681.13473

Sultan, A., Qureshi, M. A., & Howarth, F. C. (2022). Effects of Isoprenaline on ventricular myocyte shortening and Ca2+ transport in the Zucker rat. *European Journal of Pharmacology, 933*, 175263. https://doi.org/10.1016/J.EJPHAR.2022.175263

Sultan, A., Singh, J., & Howarth, F. C. (2019). Mechanisms underlying electro-mechanical dysfunction in the Zucker diabetic fatty rat heart: a model of obesity and type 2 diabetes. *Heart Failure Reviews*, 1–14. https://doi.org/10.1007/s10741-019-09872-4

Sultan, A., Singh, J., & Howarth, F. C. (2021). Cellular and Molecular Effects of Obesity on the Heart. In P. S. Tappia, B. Ramjiawan, & N. S. Dhalla (Eds.), Cellular and Biochemical Mechanisms of Obesity (pp. 167–183). *Springer International Publishing*. https://doi.org/10.1007/978-3-030-84763-0_8

UAEU جامعة الإمارات العربية المتحدة
United Arab Emirates University

UAE UNIVERSITY DOCTORATE DISSERTATION NO. 2022:16

This dissertation describes the molecular basis of Diabetic Cardiomyopathy. DCM is a complex disease with many factors influencing the disease progression and outcome. Our research demonstrates that ageing and prolonged exposure to diabetic risk factors would lead to worsened scenarios. It is important to target and implement strategies that will prevent disease progression such as exercise training and therapeutic interventions.

Ahmed Salaheldin Sultan received his PhD from the Department of Physiology, College of Medicine & Health Sciences at UAE University, UAE. He received his Masters of Medical Sciences track Pharmacology and Toxicology from the College of Medicine & Health Sciences at UAE University, UAE. He received his Bachelor of Pharmacy degree from University of Sharjah, UAE.

www.uaeu.ac.ae